

Storage-Discharge Characteristics of Headwaters by Tracer Analysis:

A Case Study in the Vallon de Nant over the Recession Period 2022

Master thesis
Faculty of Science, University of Bern

handed in by
Sabina Kurmann

2023

Supervisors
Prof. Dr. Bettina Schaefli
Dr. Natalie Ceperley

Abstract

Mountains store and release water at different timepoints in the year, but due to climate change the seasonal water storage-release pattern is expected to be changed, particularly the discharge in summer is assumed to decrease, which, nonetheless, may have severe consequences for the water supply in lower lying regions. In hydrological research a series of tracers has been used in order to identify the origin of streamwater and thus, particularly to gain an understanding of the contribution of groundwater to the stream discharge, while, however, the question of how groundwater storages can moderate the discharge pattern, altered by climate change, in the summer months is still part of research and has rarely been investigated in-depth at springs. So, the key objective of the Master thesis is to investigate how hydrochemical as well as isotopic tracers can be related to differences in storage and discharge of springs in the Vallon de Nant catchment during the summer recession period from June until October 2022. In order to gain an understanding of the storage-discharge pattern at the springs, the research process was divided into water quality and water quantity analysis. In the water quantity part, the spatial as well as temporal variation of the discharge, determined by salt dilution measurements during seven sampling campaigns, as well as the recession constants are presented, and in the water quality analysis the ion concentration as well as the isotopic composition of the collected water samples are spatially as well as temporally discussed; additionally, the ions are put into context with the measured discharge and finally, proportion of rain as well as snow is isotopically determined for each sampling station. The investigations have showed that a low depletion of heavy isotopes, giving indication of a high proportion of rain, as well as high electrical conductivity values, highlighting a long residence time of water in the subsurface, and low discharge rates indicate a shallow water flowing path; additionally, warm temperatures and a comparably high concentration of calcium and nitrate, but a low sodium concentration are characteristic for a shallow water storage-discharge pattern, which is also expressed in low recession constants. Overall, it can be concluded that at most of the monitored springs the results of the water quality and of the water quantity analysis are coherent and suggest the same storage-discharge pattern, but there are also cases where the identified tracers do not accurately correspond to the results of the recession analysis due to reasons such as influences of an artificial water catchment or in case of a tributary, due to several different contributing water origins, in which cases more specific and profound research is essential.

Contents

A. List of Tables.....	IV
B. List of Figures.....	VII
C. List of Equations	XIII
1 Introduction.....	1
1.1 State of Research.....	2
1.2 Research Objectives	4
2 Study Site and Time	6
2.1 Vallon de Nant.....	6
2.2 Meteorological Conditions in Switzerland	8
2.3 Measurement Sites	10
3 Data and Methods.....	12
3.1 Supplementary Data.....	12
3.2 Data Acquisition	14
3.3 Water Quantity Variables.....	17
3.4 Water Quality Variables	19
3.5 Data Analysis	25
3.6 RStudio	29
4 Results	30
4.1 Overview Meteorological Conditions in the Catchment.....	30
4.2 Water Quantity Variables.....	34
4.3 Water Quality Variables	46
4.4 Data Analysis	84
5 Discussion	97
5.1 Discussion of Meteorological Conditions in the Catchment.....	97
5.2 Discussion of Water Quantity Variables.....	99
5.3 Discussion of Water Quality Variables	103
5.4 Synthesis.....	116
5.5 Limitations.....	121
6 Conclusion	123
7 References.....	125
Acknowledgements.....	131
Annex A - Pictures and Coordinates of Sampling Stations	132
Annex B – Data Acquisition	136

Annex C - Additional Results 140

A. List of Tables

Table 1: Metadata to the measurement stations in Figure 4. In his table the sampling stations and their corresponding abbreviations, coordinates and elevation levels are listed (Swisstopo, 2023; Mächler et al., 2021).	10
Table 2: Supplementary Data. Meteorological, in particular precipitation and temperature data of both local (Weather Station Network Vallon de Nant) as well as nearby official stations (MeteoSwiss), and discharge data of the outlet of the Avançon de Nant are listed. In addition, the corresponding coordinates and elevation level of these stations as well the time resolution of the data and its time range are illustrated.	12
Table 3: Dates of sampling campaigns in 2022. The measurements were taken during seven sampling campaigns, while each sampling campaign lasted 2 days.....	14
Table 4: Variables used for principal component analysis. Since a condition for performing principal component analysis is a complete dataset, not all variables are considered, but only those that have a value per sampling date.	28
Table 5: Streamflow periods of the Avançon de Nant of 2016-2018 and 2022. The streamflow periods of the year 2016-2018 of the study, performed by Michelon et al., 2023, as well as the streamflow periods of 2022 are visually determined, while for the former period Figure 1 was considered and for the latter Figure 8.	33
Table 6: Results of the statistical significance test of the discharge at the springs. The p-values of the discharge between the different pairs of sampling stations are determined by the Tukey Honest Significance Differences (Tukey HSD) test.....	35
Table 7: Summary of spring and mainstream discharge pattern during a sampling campaign. The discharge pattern of the springs, of the mainstream as well as of the mainstream baseflow is assessed during a sampling campaign, while a discharge decrease (D) is illustrated in orange, a discharge increase in blue and an equivalent discharge (E) in yellow. Then, it is calculated how often the overall discharge as well as the baseflow of the mainstream were mimicked per sampling station (ST) and per sampling campaign (SC).....	42
Table 8: Recession constants of the mainstream baseflow per subperiod. The recession constants are defined by $1/\alpha$, while α corresponds to the slope of the equation, which is the result of linear regression of the discharge data.	45
Table 9: Recession constants of the springs for the first recession subperiod. The recession constants are defined by $1/\alpha$, while α corresponds to the slope of the equation, which is the result of linear regression of the discharge data.	46
Table 10: Results of the statistical significance test of the electrical conductivity. The p-values of the electrical conductivity between the different pairs of sampling stations are determined by the Tukey Honest Significant Differences (Tukey HSD) test.....	48
Table 11: Results of the statistical significance test of the temperature. The p-values of the temperature between the different pairs of sampling stations are determined by the Tukey Honest Significant Differences (Tukey HSD) test.	50
Table 12: Results of the statistical significance test of the pH value. The p-values of the pH values between the different pairs of sampling stations are determined by the Tukey Honest Significant Differences (Tukey HSD) test.....	53

Table 13: Results of the statistical significance test of the nitrate concentration. The p-values of the nitrate concentration between the different pairs of sampling stations are determined by the Tukey Honest Significant Differences (Tukey HSD) test.....	59
Table 14: Results of the statistical significance test of the sulphate concentration. The p-values of the sulphate concentration between the different pairs of sampling stations are determined by the Tukey Honest Significant Differences (Tukey HSD) test.	63
Table 15: Results of the statistical significance test of the calcium concentration. The p-values of the calcium concentration between the different pairs of sampling stations are determined by the Tukey Honest Significant Differences (Tukey HSD) test.....	67
Table 16: Results of the statistical significance test of the potassium concentration. The p-values of the potassium concentration between the different pairs of sampling stations are determined by the Tukey Honest Significant Differences (Tukey HSD) test.	69
Table 17: Results of the statistical significance test of the magnesium concentration. The p-values of the magnesium concentration between the different pairs of sampling stations are determined by the Tukey Honest Significant Differences (Tukey HSD) test.....	71
Table 18: Results of the statistical significance test of the deuterium content. The p-values of the deuterium content between the different pairs of sampling stations are determined by the Tukey Honest Significant Differences (Tukey HSD) test.....	75
Table 19: Results of statistical significance test of the $\delta^{18}\text{O}$ content. The p-values of the $\delta^{18}\text{O}$ content between the different pairs of sampling stations are determined by the Tukey Honest Significant Differences (Tukey HSD) test.....	78
Table 20: Results of the statistical significance test of the deuterium excess (d-excess). The p-values of the deuterium excess (d-excess) between the different pairs of sampling stations are determined by the Tukey Honest Significant Differences (Tukey HSD) test.	80
Table 21: Summary of Water Quality Variables. The extent of the spatial as well as the temporal variations of the water quality variables as well as some key processes, which set a context, are summarized. 81	81
Table 22: Normality check of temperature, pH, electrical conductivity (EC) and discharge. These parameters are checked for normality by means of a Shapiro Wilk test.....	84
Table 23: Results of statistical significance test for the time-of-day analysis. It was checked by means of a Wilcoxon significance test, if the time-of-day has a significant impact on the values of the temperature, pH, electrical conductivity (EC) and the discharge.	84
Table 24: Results of concentration-discharge analysis of the first recession subperiod at the sampling stations. There are three different concentration-discharge patterns: dilution (red), mobilization (blue) and chemostasis (green), determined by plotting the mainstream data and the spring discharge respectively against the solute concentration. When the solute concentration decreases with increasing discharge, dilution happens; mobilization describes the relationship of increasing solute concentration with increasing discharge and when the solute concentration hardly changes with altered discharge rates, chemostasis occurs (Knapp et al., 2020).	89
Table 25: Results of the statistical significance test of the proportion of rain. The p-values of the proportion of rain between the different pairs of sampling stations are determined by the Tukey Honest Significant Differences (Tukey HSD) test.....	91

Table 26: Summary of significantly correlated water variables. In order to evaluate whether the water variables are significantly linearly related among each other, the water variables were tested for their significance level.94

Table 27: Origin of ions in the Vallon de Nant (VdN) and the Erlenbach catchment (Erlenbach C.). The ions are attributed to their corresponding input, while it is differentiated between geological, atmospheric and biological input and based on these inputs the origin of the ions is defined, namely bedrock, atmosphere or soil.110

B. List of Figures

Figure 1: Streamflow Periods. Baseflow Period (B), Early Melt Period (E), Melt Period (M) and Seasonal Recession Period (R) of the Avançon de Nant in the Vallon de Nant catchment are illustrated over the research period 2016 until 2018 as well as the water temperature at several springs (reprinted by Michelin et al., 2023).....	2
Figure 2: Map of Switzerland with the Vallon the Nant (red point). The Vallon de Nant catchment is located in the Vaudois Alps in the south-western part of Switzerland (reprinted from Michelin et al.,2023).....	6
Figure 3: Hydrological units in the Vallon de Nant Catchment. In the southern part there is the glacier, followed by the moraine unit. In the western part hillslopes and in the eastern part steep rock slopes can be located, followed by the talus and finally the riparian area (reprinted from Michelin et al., 2021b).....	7
Figure 4: Map of the measurement stations in the Vallon de Nant. In this map the springs are illustrated by orange circles, the stations along the mainstream by blue stars and the tributary by a red triangular (Swisstopo, 2023).	11
Figure 5: Precipitation data of Sorniot-Lac Inférieur and La Chaux over 2022. The precipitation, recorded at the MeteoSwiss weather station Sorniot-Lac Inférieur (top), at the local weather station La Chaux (middle), measured by a 24GHz Doppler radar sensor (WS400-UMB; G. Lufft Mess- und Regeltechnik GmbH, Fellbach, Germany) and the combination of both stations (bottom) is illustrated.	13
Figure 6: Discharge curve of a hypothetical measurement (reprinted from Wernli, 2007). After the salt was induced into the stream, the electrical conductivity should be approximately 100 $\mu\text{S}/\text{cm}$ over the background electrical conductivity within the first 4 minutes in order to generate a valuable discharge measurement and the measurement lasts as long as the background electrical conductivity is reached again.	16
Figure 7: Concentration discharge relationship (reprinted from Knapp et al., 2020). Examples of dilution (a), chemostasis (b) and mobilization (b) patterns in the Erlenbach catchment, while dilution explains an increasing concentration with decreasing discharge, mobilization decreasing concentration with decreasing discharge and chemostatis unchanged concentration behavior with decreasing discharge.	27
Figure 8: Overview of meteorological conditions of 2022 in the Vallon de Nant catchment and discharge of the Avançon de Nant, measured at the outlet. The daily precipitation amount, determined for both, the La Chaux and the Sorniot-Lac Inférieur, weather stations, as well as the mean daily discharge, recorded at the outlet of the Avançon de Nant, are illustrated over 2022 (top). Then, the mean daily temperature, measured at La Chaux, is presented (bottom). Furthermore, the visits of the Vallon de Nant catchment for performing the measurements are indicated.	32
Figure 9: Definition of recession period of 2022 for the Vallon de Nant catchment. The daily amount of precipitation, recorded at both, the La Chaux as well as at the Sorniot-Lac Inférieur, weather stations and the mean daily discharge, measured at the outlet of the Avançon de Nant, over 2022 are illustrated.....	33
Figure 10: Mean discharge of the monitored springs per sampling campaign over research period of 2022. The discharge of the springs was determined by salt dilution measurements and then the mean discharge of both sampling days during a sampling campaign was calculated.	34

Figure 11: Boxplots of discharge per spring. The discharge, measured during the research period from early July until early October 2022 by salt dilution measurements, is illustrated per sampling station, located in the Vallon de Nant catchment.....	35
Figure 12: Comparison of discharge between Black-Blue Pipe Spring and Mainstream. The discharge at the Black-Blue Pipe Spring is illustrated over the research period (top), determined by salt dilution measurements, the overall discharge as well as the baseflow of the mainstream and, additionally, the daily amount of precipitation measured at both, the La Chaux and the Sorniot-Lac Inférieur, weather stations over the research period (bottom) are illustrated.	36
Figure 13: Comparison of discharge between Grass Spring and Mainstream. The discharge at the Grass Spring is illustrated over the research period (top), determined by salt dilution measurements, the overall discharge as well as the baseflow of the mainstream and, additionally, the daily amount of precipitation measured at both, the La Chaux and the Sorniot-Lac Inférieur, weather stations over the research period (bottom) are illustrated.....	37
Figure 14: Comparison of discharge between Bridge Spring and Mainstream. The discharge at the Bridge Spring is illustrated over the research period (top), determined by salt dilution measurements, the overall discharge as well as the baseflow of the mainstream and, additionally, the daily amount of precipitation measured at both, the La Chaux and the Sorniot-Lac Inférieur, weather stations over the research period (bottom) are illustrated.....	38
Figure 15: Comparison of discharge between La Chaux Spring and Mainstream. The discharge at the La Chaux Spring is illustrated over the research period (top), determined by salt dilution measurements, the overall discharge as well as the baseflow of the mainstream and, additionally, the daily amount of precipitation measured at both, the La Chaux and the Sorniot-Lac Inférieur, weather stations over the research period (bottom) are illustrated.	39
Figure 16: Comparison of discharge between La Chaux Meander and Mainstream. The discharge at the La Chaux Meander is illustrated over the research period (top), determined by salt dilution measurements, the overall discharge as well as the baseflow of the mainstream and, additionally, the daily amount of precipitation measured at both, the La Chaux and the Sorniot-Lac Inférieur, weather stations over the research period (bottom) are illustrated.	40
Figure 17: Springs' fraction of mainstream baseflow over research period. The proportion of the discharge of all the monitored springs to the baseflow of the mainstream is determined by adding up all the discharges of the springs per sampling date and then calculating the percentage of the baseflow.	43
Figure 18: Baseflow of the Avançon de Nant over research period. Four subperiods are defined over the research period by analysing the evolution of the mainstream baseflow data.	44
Figure 19: Mean spring discharge of a sampling campaign per sampling station in the corresponding subperiod. The mean discharge of a sampling campaign was calculated per spring and additionally, the recession subperiod boundaries, which were defined by the analysis of the evolution of the mainstream baseflow, are illustrated.	45
Figure 20: Electrical conductivity (EC) over research period. The EC, measured at the different sampling stations in the Vallon de Nant catchment, is illustrated over the research period from early July until early October 2022.....	46

Figure 21: Boxplots of electrical conductivity (EC) per sampling station. The EC, measured during the research period from early July until early October 2022, is illustrated per sampling station in the Vallon de Nant catchment.....	47
Figure 22: Temperature over research period. The temperature, measured at the different sampling stations in the Vallon de Nant catchment, is illustrated over the research period from early July until early October 2022.....	48
Figure 23: Boxplots of temperature per sampling station. The temperature, measured during the research period from early July until early October 2022, is illustrated per sampling station in the Vallon de Nant catchment.....	49
Figure 24: Continuous temperature measurement at the springs over research period. The temperature was continuously measured by temperature logger (HOBO Pendant Temperature/Light 64K Data Loggers; Onset, Bourne, United States) at all the monitored springs in the Vallon de Nant catchment over the research period from early July until early October 2022.....	51
Figure 25: pH value over research period. The pH value, measured at the different sampling stations in the Vallon de Nant catchment, is illustrated over the research period from early July until early October 2022.....	52
Figure 26: Boxplots of pH value per sampling station. The pH value, measured during the research period from early July until early October 2022, is illustrated per sampling station in the Vallon de Nant catchment.....	52
Figure 27: Fluoride concentration over research period. The fluoride concentration, determined by ion chromatography, is illustrated per sampling station in the Vallon de Nant catchment over the research period from early July until early October 2022.	54
Figure 28: Boxplots of fluoride concentration per sampling station. The fluoride concentration, determined by ion chromatography for all the collected water samples during the research period from early July until early October 2022, is illustrated per sampling station in the Vallon de Nant catchment.	54
Figure 29: Chloride concentration over research period. The chloride concentration, determined by ion chromatography, is illustrated per sampling station in the Vallon de Nant catchment over the research period from early July until early October 2022.	55
Figure 30: Boxplots of chloride concentration per sampling station. The chloride concentration, determined by ion chromatography for all the collected water samples during the research period from early July until early October 2022, is illustrated per sampling station in the Vallon de Nant catchment.	56
Figure 31: Nitrite concentration over research period. The nitrite concentration, determined by ion chromatography, is illustrated per sampling station in the Vallon de Nant catchment over the research period from early July until early October 2022.	56
Figure 32: Boxplots of nitrite concentration per sampling station. The nitrite concentration, determined by ion chromatography for all the collected water samples during the research period from early July until early October 2022, is illustrated per sampling station in the Vallon de Nant catchment.	57
Figure 33: Nitrate concentration over research period. The nitrate concentration, determined by ion chromatography, is illustrated per sampling station in the Vallon de Nant catchment over the research period from early July until early October 2022.	58

Figure 34: Boxplots of nitrate concentration per sampling station. The nitrate concentration, determined by ion chromatography for all the collected water samples during the research period from early July until early October 2022, is illustrated per sampling station in the Vallon de Nant catchment.	58
Figure 35: Phosphate concentration over research period. The phosphate concentration, determined by ion chromatography, is illustrated per sampling station in the Vallon de Nant catchment over the research period from early July until early October 2022.....	60
Figure 36: Boxplots of phosphate concentration per sampling station. The phosphate concentration, determined by ion chromatography for all the collected water samples during the research period from early July until early October 2022, is illustrated per sampling station in the Vallon de Nant catchment.	60
Figure 37: Sulphate concentration over research period. The sulphate concentration, determined by ion chromatography, is illustrated per sampling station in the Vallon de Nant catchment over the research period from early July until early October 2022.....	61
Figure 38: Boxplots of sulphate concentration per sampling station. The sulphate concentration, determined by ion chromatography for all the collected water samples during the research period from early July until early October 2022, is illustrated per sampling station in the Vallon de Nant catchment.	62
Figure 39: Ammonium concentration over research period. The ammonium concentration, determined by ion chromatography, is illustrated per sampling station in the Vallon de Nant catchment over the research period from early July until early October 2022.....	64
Figure 40: Boxplots of ammonium concentration per sampling station. The ammonium concentration, determined by ion chromatography for all the collected water samples during the research period from early July until early October 2022, is illustrated per sampling station in the Vallon de Nant catchment.	64
Figure 41: Calcium concentration over research period. The calcium concentration, determined by ion chromatography, is illustrated per sampling station in the Vallon de Nant catchment over the research period from early July until early October 2022.	66
Figure 42: Boxplots of calcium concentration per sampling station. The calcium concentration, determined by ion chromatography for all the collected water samples during the research period from early July until early October 2022, is illustrated per sampling station in the Vallon de Nant catchment.	66
Figure 43: Potassium concentration over research period. The potassium concentration, determined by ion chromatography, is illustrated per sampling station in the Vallon de Nant catchment over the research period from early July until early October 2022.....	68
Figure 44: Boxplots of potassium concentration per sampling station. The potassium concentration, determined by ion chromatography for all the collected water samples during the research period from early July until early October 2022, is illustrated per sampling station in the Vallon de Nant catchment.	68
Figure 45: Magnesium concentration over research period. The magnesium concentration, determined by ion chromatography, is illustrated per sampling station in the Vallon de Nant catchment over the research period from early July until early October 2022.	70

Figure 46: Boxplots of magnesium concentration per sampling station. The magnesium concentration, determined by ion chromatography for all the collected water samples during the research period from early July until early October 2022, is illustrated per sampling station in the Vallon de Nant catchment	70
Figure 47: Sodium concentration over research period. The sodium concentration, determined by ion chromatography, is illustrated per sampling station in the Vallon de Nant catchment over the research period from early July until early October 2022. Temporal Variation	72
Figure 48: Boxplots of sodium concentration per sampling station. The sodium concentration, determined by ion chromatography for all the collected water samples during the research period from early July until early October 2022, is illustrated per sampling station in the Vallon de Nant catchment.	72
Figure 49: Deuterium content over research period. The deuterium content, determined by the L2140-I Isotope and Gas Concentration Analyzer (Picarro, Inc.; Santa Clara, California, USA), is illustrated per sampling station in the Vallon de Nant catchment over the research period from early July until early October 2022.....	73
Figure 50: Boxplots of deuterium content per sampling station. The deuterium content, determined by the L2140-I Isotope and Gas Concentration Analyzer (Picarro, Inc.; Santa Clara, California, USA), for all the collected water samples during the research period from early July until early October 2022, is illustrated per sampling station in the Vallon de Nant catchment.	74
Figure 51: $\delta^{18}\text{O}$ content over research period. The $\delta^{18}\text{O}$ content, determined by the L2140-I Isotope and Gas Concentration Analyzer (Picarro, Inc.; Santa Clara, California, USA), is illustrated per sampling station in the Vallon de Nant catchment over the research period from early July until early October 2022.....	76
Figure 52: Boxplots of $\delta^{18}\text{O}$ content per sampling station. The $\delta^{18}\text{O}$ content, determined by the L2140-I Isotope and Gas Concentration Analyzer (Picarro, Inc.; Santa Clara, California, USA) for all the collected water samples during the research period from early July until early October 2022, is illustrated per sampling station in the Vallon de Nant catchment.	77
Figure 53: Relationship between $\delta^2\text{H}$ and $\delta^{18}\text{O}$ per sampling station. The determined $\delta^2\text{H}$ and $\delta^{18}\text{O}$ contents per sampling station are plotted against each other and the Global Meteoric Water Line (GMWL) as well as the Local Meteoric Water Line (LMWL) of the Vallon de Nant catchment, which was defined by Mächler et al. (2021), are illustrated.....	78
Figure 54: Deuterium excess (d-excess) values over research period. The deuterium excess (d-excess) values are illustrated per sampling station in the Vallon de Nant catchment over the research period from early July until early October 2022.	79
Figure 55: Boxplots of deuterium excess (d-excess) values per sampling station. The deuterium excess (d-excess) values for all the collected water samples during the research period from early July until early October 2022, are illustrated per sampling station in the Vallon de Nant catchment.	80
Figure 56: Time-of-day analysis of electrical conductivity (EC). The electrical conductivity, measured in the morning, is plotted against the electrical conductivity, determined in the afternoon (top), and in the boxplots, the electrical conductivity values are illustrated per time-of-day (bottom).....	85
Figure 57: Time-of-day analysis of pH values. The pH values, measured in the morning, are plotted against the pH values, determined in the afternoon (top), and in the boxplots, the pH values are illustrated per time-of-day (bottom).....	86

Figure 58: Time-of-day analysis of temperature. The temperature, measured in the morning, is plotted against the temperature, determined in the afternoon (top), and in the boxplots, the temperature is illustrated per time-of-day (bottom).....	87
Figure 59: Time-of-day analysis of discharge. The discharge, measured in the morning, is plotted against the discharge, determined in the afternoon (top), and in the boxplots, the discharge values are illustrated per time-of-day (bottom).....	88
Figure 60: Boxplots of proportion of rain per sampling site over research period. The proportion of rain, determined by the isotopic mixing model (MixSIAR), during the research period from early July until early October 2022, is illustrated per sampling site in the Vallon de Nant catchment.	90
Figure 61: Proportion of rain per sampling date over research period in the Vallon de Nant catchment. The proportion of rain, determined by the isotopic mixing model (MixSIAR), is illustrated per sampling date over the research period from early July until early October 2022.....	91
Figure 62: Correlation plot of water variables. In order to evaluate whether the water variables are linearly related among each other, correlation coefficients were determined in RStudio, while blue indicates positive correlations and red describes negative correlations.	92
Figure 63: Correlation plot of water variables under consideration of significance level. In order to evaluate whether the water variables are significantly linearly related among each other, the water variables were tested for their significance level, while blue indicates positive correlations, red describes negative correlations and the cross highlights no significant correlations.....	93
Figure 64: Principal Component 1 (PC 1) versus Principal Component 2 (PC 2) with sampling dates and sampling stations. The dimensionality is reduced by principal component analysis and thus, principal components, that contain the core information, are calculated by means of linear combinations of the original variables (Abdi and Williams, 2010).....	94
Figure 65: Principal Component 3 (PC 3) versus Principal Component 4 (PC 4) with sampling dates and sampling stations. The dimensionality is reduced by principal component analysis and thus, principal components, that contain the core information, are calculated by means of linear combinations of the original variables (Abdi and Williams, 2010).....	96

C. List of Equations

Equation 1: Calculation of the discharge by considering the flow velocity (Hendriks, 2010).....	15
Equation 2: Calculation of the mixing section (Gees et al., 1995).	15
Equation 3: Calculation of the mean and net electrical conductivity (Wernli, 2011).	17
Equation 4: Calculation of the n^{th} concentration in the calibration process (Wernli, 2011).	17
Equation 5: Calculation of the slope in the calibration process (Wernli, 2011).	17
Equation 6: Calculation of the calibration factor (Wernli, 2011).	18
Equation 7: Calculation of the mean concentration (Wernli, 2011).	18
Equation 8: Calculation of the total discharge (Wernli, 2011).....	18
Equation 9: Definition of recession constant (Müller et al., 2022).....	19
Equation 10: Baseflow Recession Equation defined by Boussinesq in 1903 (McMahon and Nathan, 2021).....	19
Equation 11: Logarithmic Transformation of Equation 10 (McMahon and Nathan, 2021).....	19
Equation 12: Definition of the pH value (Berner and Berner, 1987).	20
Equation 13: Definition of the isotopic composition of a water sample (Galewsky et al., 2016).....	24
Equation 14: Definition of Global Meteoric Water Line (GMWL) (Araguás-Araguás et al., 2000).	25
Equation 15: Definition of Local Meteoric Water Line (LMWL) (Mächler et al., 2021).	25
Equation 16: Definition of deuterium excess (d-excess) (Araguás-Araguás et al., 2000).	25
Equation 17: Definition of the correlation coefficient (Rogerson, 2015).....	27

1 Introduction

Mountains contribute to about 32% of the global discharge, which is the reason why they are situated as the “water towers” for lower lying regions (Cochand et al., 2019; Viviroli et al., 2007, Meybeck et al., 2001). Due to seasonal air temperature variations, mountains store and release water at different timepoints in the year. So, water is stored in winter in form of snow or ice and then released under warmer conditions in spring and early summer by snowmelt, providing water to the warmer and drier lowland (Cochand et al., 2019). However, Mächler et al. (2021) mention that current observations indicate that this storage-release pattern is changing in the context of climate change due to increasing temperature and increasingly early snow melt, the rising position of the snow line as well as the shrinking of glaciers. They highlight that a severe consequence of such alterations might be a drastically reduced streamwater discharge in summer as well as in autumn. So, there is rising importance considering the role of groundwater’s storage-release characteristics in catchments whose discharge is strongly influenced by snowmelt (Cochand et al., 2019). But according to Cochand et al. (2019), it is still quite unclear how groundwater storages can buffer by climate change induced alterations in discharge as well as storage behavior, since hydrological processes are often under-investigated in Alpine catchments particularly of headwaters, as explained by Mächler et al. (2021). Aside from the open question of how groundwater storage in Alpine regions could alleviate the consequences of droughts, there is still no clear understanding of how different Alpine catchments respond to earlier snowmelt due to climate change (Mächler et al., 2021; Cochand et al., 2019).

Müller et al. (2022) emphasize that both the streamflow regime and the seasonal water supply are altered in glaciated catchments owing to climate change. But Müller et al. (2022) highlight that though climate change induced alterations in the cryosphere are already well investigated, the impact of groundwater on the hydrological dynamics of the catchment have not been considered enough in the past, motivating their hydrological research in Alpine glaciated catchments. But according to Müller et al. (2022), the field has been changing lately and the impact of groundwater on hydrological processes at the catchment scale as well as in depth consideration of how hydrological dynamics are influenced by specific landforms has been more present in research in order to gain an understanding of how groundwater is stored and thus contributes to the baseflow. Furthermore, they emphasize that without investigating the subsurface of hydrological processes one cannot make any conclusions about how water is stored and released to the streamflow and thus, they strongly highlight the importance of devoting the necessary attention to the analysis of groundwater.

So, it is key for understanding hydrological as well as ecological dynamics to investigate the sources of the streamwater and thus analyze the main contributors such as snowmelt, rain and baseflow (Mächler et al., 2021). But performing studies in Alpine regions is demanding since the environment is highly diverse and the nature can differ dramatically according to increasing elevation or with a changed exposition (Cochand et al., 2019). Nevertheless, since many hydrological processes are hard to investigate because they happen below the surface, Mächler et al. (2021) explain that tracers can be used as a tool to determine the different origins of the streamwater and, therefore, define the proportion of snowmelt, soil water or groundwater in the stream.

Investigating the storage-release rates of aquifer’s headwaters in Alpine catchments, which have so far poorly been studied, and assessing how they contribute to streamflow during the summer and fall is of high research significance, also under consideration that, according to Mächler et al. (2021), high elevation areas are expected to be specifically affected by climate change.

1.1 State of Research

There is a remarkable variation in amount of discharge over the course of a year in Alpine regions (Cochand et al. 2019). Hayashi (2020) writes that a short high-flow period during spring as a consequence of snowmelt can be defined, while its length heavily depends on the amount of snow mass as well as on the timing of snowmelt. After this high-flow period, there is a relatively long low-flow period, the recession period, mainly maintained by groundwater discharge of headwaters (Hayashi, 2020). Michelin et al. (2023) explain the annual discharge variation in more details by defining several streamflow periods such as baseflow (B), early melt (E), melt (M) and seasonal recession (R) period for the Avançon de Nant in the Vallon de Nant catchment over the study period 2016 to 2018 (see Figure 1). They elaborate that the baseflow period usually lasts from the end of September to mid-March or to the beginning of April. Characteristic for this baseflow period is that the streamflow weakly declines over time, but it does not exclude discharge peaks, which happen due to strong precipitation events or short-term temperature increases (Michelon et al., 2023). The early melt period occurs before the main melt period, which can also be situated, according to Frisbee et al. (2011), as snowmelt freshet. Michelin et al. (2023) explain that in the main melt period a strong rise of the streamflow is measurable, while an early melt period may not be observed in years where the temperature rises fast. Frisbee et al. (2011) mention that in addition to the snowmelt, groundwater also significantly contributes to the stream discharge during the snowmelt freshet, particularly in their study, which was performed in the Rocky Mountains of Colorado, groundwater has a proportion of the stream discharge in the range of 14% up to 44% during the snowmelt freshet, which lasts in their study period from April until July. Finally, in the seasonal recession period, streamflow is dominated by groundwater contribution and additionally, evaporation increases during that period (Michelon et al., 2023).

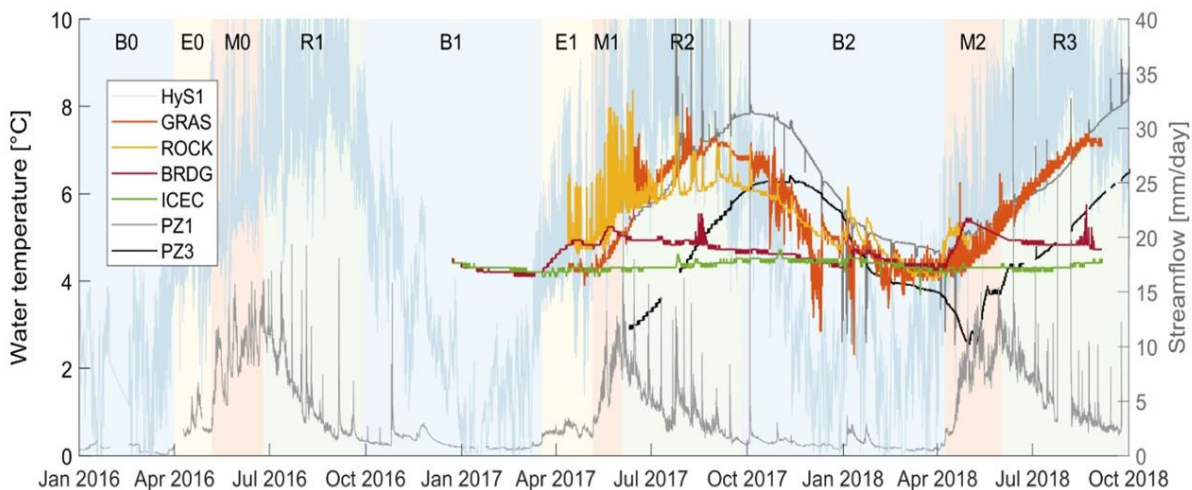


Figure 1: Streamflow Periods. Baseflow Period (B), Early Melt Period (E), Melt Period (M) and Seasonal Recession Period (R) of the Avançon de Nant in the Vallon de Nant catchment are illustrated over the research period 2016 until 2018 as well as the water temperature at several springs (reprinted by Michelin et al., 2023).

Mächler et al. (2021) mention in their paper that the measuring of a change in discharge (dq/dt) at the mainstream's outlet can be applied as an indicator for stream network contraction or expansion. Such analysis of change in discharge over time is widely applied in the hydrological research field in order to define hydrological characteristics, specifically the amount of storage and rate of release, of a catchment (Jachens et al., 2020). If dq/dt is negative during a recession period, stored water heavily contributes to the streamflow, which then predominantly consists of the baseflow (Mächler et al., 2021). Recession can, according to Tallaksen (1995), be particularly observed in time periods without

precipitation. Conversely, Mächler et al. (2021) used positive values of dq/dt as a proxy for network expansion, for example after a rainfall or snow melt event. However, recession has a long history (Brutsaert and Lopez, 1998; Zecharias and Brutsaert, 1988) and with time passing the methods evolved and the application field extended, but recession analysis is, nevertheless, still rarely applied to springs.

Müller et al. (2022) explain that when analyzing the recession curve, that illustrates the decline in discharge after the snowmelt process, as well as when determining the recession constants, which indicate the storage-release rate of an aquifer's compartment, storage contributors to the baseflow can be defined. In addition, they explain that analyzing the recession constants gives an understanding of the recession timescales. However, Müller et al. (2022) show in their study that factors such as slope, aquifer flowpath and sediment structure have an impact on the storage-discharge relationship of a catchment and thus, need to be considered when determining the recession constant of a specific landform or an aquifer's compartment. Müller et al. (2022) performed their study at the base of the Otemma glacier (Switzerland) and determined the recession constants for several geomorphological landforms such as for the talus, steep lateral moraines or an outwash plain. They found in their study that specifically flat aquifers have recession constants that indicate water release in a time span of more than weeks. As a further matter, bedrocks with large slopes lose more water and thus, flat aquifers can store more water. In addition, Müller et al. (2022) conclude based on their study that surface-near landforms rarely have recession constants longer than a few days due to factors such as steep slopes but also due to their high hydraulic conductivity.

So, in order to assess storage-discharge characteristics of headwaters in Alpine catchments, investigation should focus on the period after the snowmelt and thus, in the recession period, when the measured discharge predominantly consists of groundwater release. Tracers such as stable isotopes, ion concentration as well as electrical conductivity or the temperature are widely applied in the hydrological research field in order to understand hydrological dynamics of a catchment (Kiewiet et al., 2019). Kiewiet et al. (2019) explain that the analysis of how chemical tracers of groundwater vary in a catchment allows, for instance, figuring out which specific contributing areas of a catchment influence streamflow, since it is known that topography or geomorphological characteristics of a landscape influence how water is stored and released. So, in the following paragraphs some studies, which applied these tracers in order to understand such storage-release relationships in a high-elevation catchment, are elaborated.

Mächler et al. (2021) determined the source of streamwater (glacier, snow or soil) of the Vallon de Nant catchment (Switzerland) inter alia by the electrical conductivity, the temperature as well as the isotopic composition of water. The electrical conductivity, for instance, differentiates between snowmelt and groundwater, since the latter is richer in solutes due to more exchange with the bedrock and soil than the former (Mächler et al., 2021). However, water temperature is not a very precise tracer for making conclusions about the sources of the stream, since the water temperature can vary rapidly due to changed exposition (Mächler et al., 2021; Constantz, 1998). Nevertheless, Mächler et al. (2021) highlight that the temperature can give indication whether there is an inflow from subsurface water. Besides, they mention that stable isotopes of water can be used to identify precipitation inputs and flow paths.

In addition, different groundwater types as well as individual areas of a catchment that have an impact on the streamflow are determined by groundwater chemistry, as the research project of Kiewiet et al. (2019) shows. They derived the chemical composition of groundwater from analysing water samples of the baseflow. Bedrock and soil characteristics, biological processes and contact time with the soil heavily influence the hydrochemical characteristics of groundwater and consequently of the stream.

So, groundwater has an important impact on the chemical composition of the stream, since it transports solutes, which are accumulated while the water flows below the surface (Kiewiet et al., 2019).

Beria et al. (2018) explain that a series of different research projects used stable isotopes as tracers in order to determine the origins of groundwater recharge, in particular to define the proportion of snow and of rain in groundwater. They highlight that the concept behind this tracer is that snow and snowmelt are isotopically more depleted than rain since the cloud condensation temperature, which correlates with the air temperature, is lower in the formation of snow than it is in case of rain. So, according to Beria et al. (2018), these studies come to the same result, namely that snowmelt contributes in high elevation catchments to a larger extent to groundwater recharge than rain does, which can be observed in recharge areas all over the world such as, for instance, in the United States, in Chile, in the Himalayas as well as in Italy. Based on such isotopic analysis Beria et al. (2018) therefore conclude that snowmelt during spring is particularly responsible for the groundwater recharge in temperate areas and in the context of global warming the proportion of rain is expected to increase in contrast to the proportion of snow.

The analysis of how the streamflow chemistry varies with altered discharge rates supports the understanding of the catchment's storage-discharge characteristics. Knapp et al. (2020) investigated concentration-discharge (cQ) relationships in the Erlenbach catchment (Switzerland) by means of streamflow chemistry. In particular, they analysed ion concentrations in the stream and set it into relation with the streamwater discharge in order to collect information of the water flowing path but also to gain an understanding of dilution or mobilization processes as well as of other chemical reactions that happen in the catchment. They explain that changes in discharge are mirrored by solute concentration and thus, such concentration-discharge relationships allow to understand how water and solute are stored or released in a catchment. Dilution behavior of a solute is, noticed by Knapp et al. (2020), when its concentration becomes lower with increasing flow and mobilization behavior, when the solute concentration becomes higher with increasing flow. As a further matter, they highlight that there is also a process where no change in the ion concentration can be observed with an altered discharge; this concentration-discharge behavior is then called chemostasis.

Based on these studies, it can be seen that such tracers are widely used to determine the origins of streamwater (Mächler et al., 2021; Kiewiet et al., 2019), to gain an understanding of storage-discharge characteristics by, for instance, analyzing storage-discharge relationships (Knapp et al., 2020) or to determine the origins of groundwater recharge (Beria et al., 2018). However, these studies have a strong focus on applying tracers on either streamwater or its baseflow, but hardly any analysis specifically of groundwater is performed. So, the goal of my research is to particularly apply tracers to groundwater and small alpine streams in order to determine storage-discharge characteristics at springs.

1.2 Research Objectives

Based on the identified research gaps, I defined the core objective of my Master thesis, namely to investigate how the storage-discharge characteristics of different springs and a tributary in the Vallon de Nant vary over the time period from July until October. My research particularly used hydrochemical and isotopic approaches as well as salt dilution measurements in order to investigate the following overarching research question and subsequent subquestions:

How can hydrochemical and isotopic tracers be related to differences in storage and discharge of headwaters in the Vallon de Nant over the summer recession period?

To answer the main research question, the research process was divided into two parts, water quantity and water quality analysis and thus, a series of subquestions was defined for each part. The results of

the subquestions concerning the water quantity analysis are elaborated in chapter 4.2 and those concerning the water quality analysis in chapter 4.3.

Water Quantity Analysis

i) *When does the summer recession period start and end in the Vallon de Nant in 2022?*

In order to define the summer recession period, the discharge recorded at the outlet of the Avançon de Nant was analyzed and ultimately, based on the discharge analysis of the mainstream, the summer recession period for the Vallon de Nant catchment was defined.

ii) *How much does the amount of water flowing in these springs and the tributary change over the recession period?*

In order to reply to this subquestion, salt discharge measurement was performed in the field at different springs and a tributary over the whole research period. The idea behind this investigation was to identify any temporal and spatial variations over the defined recession period and between the springs.

iii) *How is the mainstream's discharge pattern mimicked by the springs' and the tributary's discharge over the recession period?*

By comparing the springs' as well as the tributary's discharge to the mainstream's overall discharge as well as to its baseflow, an understanding of how the springs are connected to the mainstream is gained.

iv) *What are the recession timescales at the springs as well as at the tributary?*

The recession timescales were determined at the springs and at the tributary by means of the calculation of the recession constants and thus, give an understanding of the storage-release relationship of the springs and the tributary over the recession period.

v) *What is the spatial and temporal variation of the pH value, the electrical conductivity as well as of the temperature at the springs, the tributary and at some stations along the mainstream in the Vallon de Nant over the summer recession period?*

The values of these variables were determined in the field and they were measured twice per sampling campaign, once in the morning and once in the afternoon in order to investigate whether there exist any diurnal variations.

vi) *What is the spatial and temporal variation of some anion and cation concentrations of water samples collected at the springs, the tributary and at some stations along the mainstream in the Vallon de Nant over the summer recession period?*

Water samples were collected in the field in duplicate and then the ion concentration was determined by means of ion chromatography in the lab.

vii) *What is the spatial and temporal variation of heavy isotope compositions of water samples collected at the springs, the tributary and at some stations along the mainstream in the Vallon de Nant over the summer recession period?*

Similarly, to subquestion vi), water samples were collected in the field in duplicate and their isotopic composition was determined by means of an isotope and gas concentration analyzer in the lab.

Finally, the results of the water quantity and water quality analysis were synthesized in order to answer the main research question.

2 Study Site and Time

An overview of the study site including information about the geographic location, the geological conditions and in particular about the hydrological background is given in this section. In addition, my study case interest is highlighted and a general overview of the meteorological conditions in Switzerland over the year 2022 and some climate projections for Switzerland in the context of climate change are given. The meteorological conditions of the Vallon de Nant during the course of the study are part of the data analysis and thus, they are elaborated in details in chapter 4.1. Finally, the measurement stations in the Vallon de Nant are defined.

2.1 Vallon de Nant

Research for this Master project was performed in the Vallon de Nant headwater catchment, which lies in the Vaudois Alps in the south-western part of Switzerland (see red point in Figure 2). The Vallon de Nant catchment has an area of 13.4 km², is oriented from south to north and its mainstream is called Avançon de Nant (Michelon et al., 2023). The lowest point of the catchment is at 1200 meters above sea level (m.a.s.l.), which corresponds to the gauging station at the outlet of the Avançon de Nant, 46.25301°N, 7.10954°E (WGS84), and its highest point is defined at 3051 m.a.s.l., which matches the height of Le Grand Muveran (Michelon et al., 2023; Mächler et al., 2021).

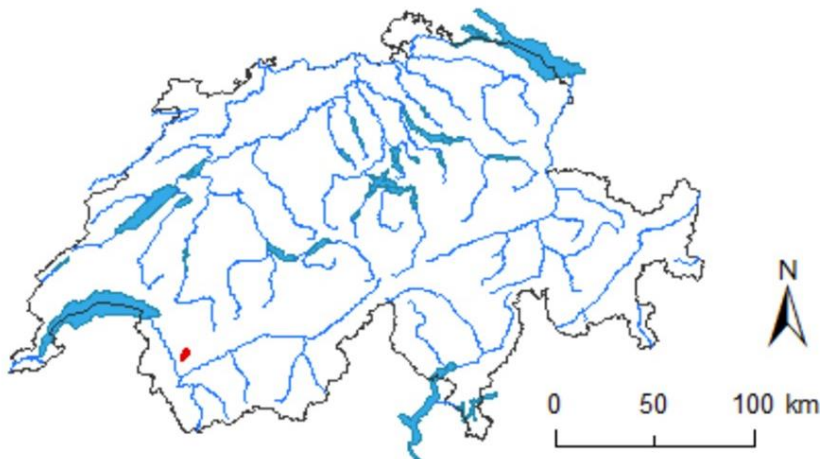


Figure 2: Map of Switzerland with the Vallon the Nant (red point). The Vallon de Nant catchment is located in the Vaudois Alps in the south-western part of Switzerland (reprinted from Michelon et al.,2023).

Geology

Thornton et al. (2018) mention that the Vallon de Nant is situated in the north-western part of the Nappe de Morcles and it particularly has its origin in the inverse zone of the Nappe de Morcles. There are limestone layers below the valley floor from the Lower Cretaceous, which are again situated on flysch, a soft rock, which inter alia contains marls, sandstone and shales (Michelon et al., 2023). A more in-depth discussion about the Vallon de Nant can be found in the paper “A 3D geological model of a structurally complex Alpine region as a basis for interdisciplinary research” of Thornton et al. (2018).

Hydrology

Figure 3 shows a map of the Vallon de Nant catchment illustrating different hydrological units. It can be observed that the hydrological unit on the western part of the catchment is primarily determined by hillslopes. In this pasture-dominated area the soils are of large depths and have high water storage capacities (Michelon et al., 2021a). The northwards exposition of the Vallon de Nant makes it possible,

according to Michelon et al. (2021a), that the small Glacier des Martinets, which is situated on the south side of the valley but in the northern shadow of the Dent de Morcles, can exist at a quite low elevation level. However, its contribution to the streamflow of the catchment must be limited according to Michelon et al. (2023), since the glacier is small, has a strong northwards exposition and since it is heavily shielded with debris, but its exact contribution has not been studied yet (Mächler et al., 2021). Michelon et al. (2021a) highlight that there are steep rock faces on the east side of the valley, where in case of rainfall the water drains fast since the soils are quite shallow. Furthermore, they add that there are immense scree cones in the talus region, on the bottom of the rock faces. Nevertheless, they explain that the bottom of the Vallon de Nant consists primarily of fine alluvial deposits, where large water storage capacities can be observed and the riparian area consists of rough alluvial deposits which indicate high hydraulic conductivity and thus, the riparian area allows, according to Thornton et al. (2018), to store water.

Investigating in detail the presence of the springs, Michelon et al. (2023) could observe a connection between low slopes and the occurrence of springs. Therefore, they highlight that most springs are located on the west side of the catchment, in the hillslope unit as well as on the right side of the main-stream. Similarly, tributaries do not exist at locations where the slopes are steep and where hydraulic conductivity is high, which is the case in the north-western part of the Vallon de Nant (Michelon et al., 2023).

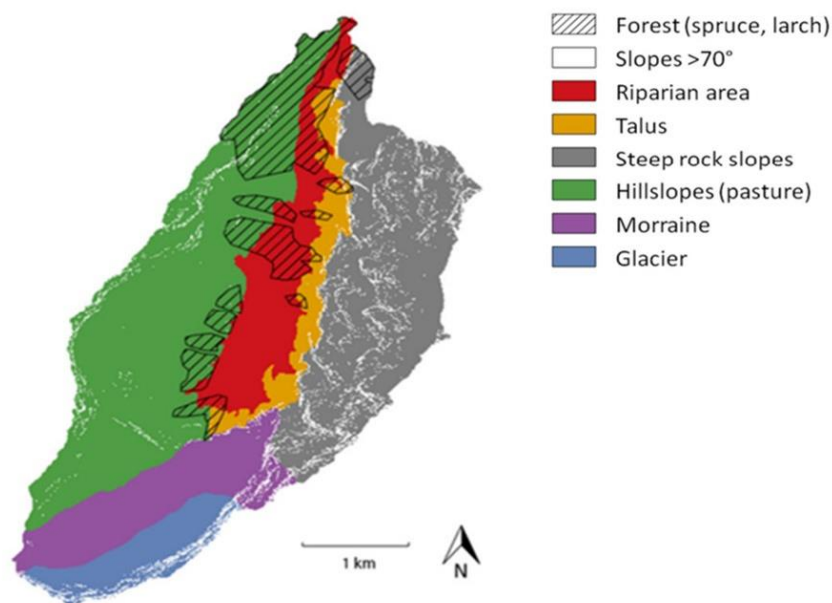


Figure 3: Hydrological units in the Vallon de Nant Catchment. In the southern part there is the glacier, followed by the moraine unit. In the western part hillslopes and in the eastern part steep rock slopes can be located, followed by the talus and finally the riparian area (reprinted from Michelon et al., 2021b).

When analysing the streamflow network, Mächler et al. (2021) explain that snow has a major impact on the streamflow of the Avançon de Nant and thus they define the streamflow regime as nivo-pluvial. They emphasize that the water flowing is low in winter but higher in spring as well as in early summer and usually has its highest rate in June. So, the consequence of this differing water flowing rate is that the length of the Avançon de Nant shows seasonal variations. Michelon et al. (2023) observed based on the Swiss digital elevation model that in early summer, in the melting period, the river has a length of about 6 km and in winter time, outside the melting period and thus, in the snow accumulation period, its length is reduced by 2.95 km since the water begins flowing at a lower elevation.

To sum up, the snow melting and soil as well as groundwater drainages primarily have an impact on stream network (Mächler et al., 2021; Michelon et al., 2023). Mächler et al. (2021) highlight that the extent to which permafrost and the melt water of the glacier contribute to stream network remains to be seen. Additionally, they explain that the streams in the Vallon de Nant can be classified, based on the classification by Schaffner et al. (2013), into either low ($<0.05 \text{ m}^3\text{s}^{-1}$) or medium ($0.05 \text{ m}^3\text{s}^{-1} - 1 \text{ m}^3\text{s}^{-1}$) discharge amount, corresponding to tributaries and to mainstreams respectively. When considering the mainstream at the outlet of the Avançon de Nant, a minimum mean daily discharge of about $0.0927 \text{ m}^3\text{s}^{-1}$ in early February and a maximum mean daily discharge of about $2.2862 \text{ m}^3\text{s}^{-1}$ in early October can be measured in 2022.

Case Study Interest

Of particular appeal for the subject of the Master thesis is the fact that the Vallon de Nant is a region, which is minimally affected by human activities as it has been under protection since 1969 and is part of the Natural Reserve of the Muveran. Furthermore, the Vallon de Nant is a well accessible headwater catchment, which has been well studied, and therefore making it an experimental research catchment with greater potential for interdisciplinary exchange and data sharing. Additionally, it allows my research project to both build on previous work and lay the foundation for future work.

2.2 Meteorological Conditions in Switzerland

The following summary of the meteorological conditions in Switzerland of 2022 are based on the Klimabulletin 2022 (MeteoSwiss, 2023). The year 2022 was the warmest year since temperature measurements started in 1864. The mean annual temperature over all of Switzerland was 7.4°C , which is $+1.6^\circ\text{C}$ degrees over the MeteoSwiss norm period of 1991-2020. In some regions, especially in the western part of Switzerland and in the canton of Wallis, the temperature values were between 1.9°C and 2.1°C over the norm. Average country-wide precipitation was 70% to 90% of the norm although in some places the year 2022 was the driest year since the beginning of measurements in 1864.

The temperature in winter 2022 and spring 2022 was mild, particularly in February, March and May respectively. In February, the temperature was 1.1°C and in May even 2.6°C over the norm 1991-2020. As a further matter, it was a very dry winter, especially on the south side of the Swiss Alps, which in general leads to a smaller snowpack storage in comparison to wet winters and thus consequences in a reduced discharge as well as groundwater recharge (MeteoSwiss, 2023; Doummar et al., 2018; Beria et al., 2018). The amount of precipitation measured in May and March was also small. Specifically, in the western part of Switzerland, May 2022 was the May with the smallest amount of precipitation since the beginning of measurements. The summer 2022 was the second warmest summer since the beginning of measurements in 1864 and showed three heat periods. It was the second hottest June, the fourth hottest July and the third warmest August since 1864. The mean temperature averaged over the whole country was 2.3°C over the norm, whereas the warmest summer since the beginning of measurements in 2003 showed a mean temperature that was 3°C over the norm period of 1991-2020. The amount of precipitation measured over the whole country in summer 2022 corresponds to 60% up to 80% of the norm. However, in the western part of Switzerland the precipitation amounted less than 60% of the norm, whilst in the eastern part of Switzerland and in the Swiss Plateau more than 80% of the norm was measured. In June the amount of precipitation was between 80% and 120% of the norm, in July at some places less than 30% and in August, between 40% and 70% of the norm. In some regions of the south-western part of Switzerland July 2022 was the July with the lowest amount of precipitation for the last 50 years. Correspondingly, high level of evaporation, relative to the low amount of precipitation, led to severe dryness in that region. Autumn 2022 was, according to MeteoSwiss (2023), the third warmest autumn since the beginning of measurements and corresponds to

3.8°C over the norm. Concerning precipitation, autumn 2022 was wet, particularly the western part of Switzerland and the central Swiss Plateau, where values over 130% over the norm 1991-2020 were measured.

Climate Projections for Switzerland

Muelchi et al. (2021) investigated, using the Swiss Climate Change Scenarios of the CH2018 framework (National Centre for Climate Services, 2018), how the river runoff in Switzerland is being altered by climate change. The CH2018 framework contains Swiss climate scenarios, which are in particular climate change projections that are defined by means of the EURO-CORDEX ensemble of regional climate simulations. It includes climate change projections according to the three Representative Concentration Pathways (RCPs), which deal with the anthropogenic driving of climate change differently. RCP8.5 presumes that no mitigation actions are taken, whereas RCP2.6 assumes that the global temperature increase is below 2°C and finally, RCP4.5 takes into account that mitigation actions are taken but nevertheless, the 2°C objective is missed.

Regardless which RCP scenario was considered, all temperature projections indicate a rise in temperature with climate change independent of the time of the year and of the geographic region of Switzerland (National Centre for Climate Services, 2018). Especially the mean temperature in summer and the temperature at higher elevation levels are expected to increase more heavily. In case where no mitigation actions are taken, thus, according to RCP8.5, the temperature is assumed to rise in a range between 3.1°C and 5.5°C. So, according to RCP8.5, the mean temperature is expected to increase of about 4.5°C in summer and of approximately 3.8°C in winter in the north-eastern part of Switzerland, whereas the increase in temperature is of about 5.5°C in the eastern and western Alps in summer and of around 3.9°C in winter. The change of the autumn temperature is expected to be comparable to the changes in winter temperature, whilst the projections of the spring temperature show a smaller increase than the changes in winter temperature (National Centre for Climate Services, 2018). Such a temperature rise leads inter alia to changes in hydrological dynamics such as to more precipitation in form of rain than snow as well as to altered seasonal amounts of precipitation, which is supposed to rise with climate change in winter, to decline in summer, but showing little alterations in spring and autumn (Muelchi et al., 2021; BAFU, 2021). Accompanying climate change longer dry periods in the summer months, increased evapotranspiration as well as more strong precipitation events over the whole year are expected (BAFU, 2021).

Finally, these changed meteorological conditions consequence in an altered runoff regime (Muelchi et al., 2021). The results of Muelchi et al.'s (2021) research show that the runoff in winter is expected to rise in the context of climate change due to higher temperature and amounts of precipitation. They explain that when the temperature increases in winter, there will be an increasing amount of precipitation in form of rain instead of snow, which therefore has an impact on winter runoff. In higher-lying catchments, according to Muelchi et al. (2021), a stronger runoff is expected with climate change in spring due to an enhanced melting of snow, whereas the runoff in catchments on lower elevations is expected to be smaller in spring since these regions have less snow in winter times and thus, a much smaller amount of snowmelt. According to Muelchi et al. (2021), the runoff in summer will decline, but when elaborating an explanation, they differentiate between catchments on lower and higher elevation levels. In the former case, runoff decreases due to enhanced evapotranspiration and smaller amounts of precipitation, while in the latter case, the lower accumulation of snow contributes to this reduction in runoff. Additionally, in autumn Muelchi et al. (2021) expect smaller runoff rates with climate change owing to reasons such as lower amounts of precipitation, more evapotranspiration and in case of higher lying catchments due to a reduced contribution of snow and glacier melt. Muelchi et al. (2021) conclude that the annual mean runoff is expected to decrease in most of the catchments

that were investigated in their research, but they highlight that catchments on lower elevation levels show with climate change more moderate reactions in runoff than catchments on higher elevation levels. In addition, they highlight that the seasonal availability of water from the rivers will be changed, specifically stronger runoff in winter but lower runoff in summer. Besides, when considering the different RCP scenarios the same results are expected but to a different extent (Muelchi et al., 2021).

2.3 Measurement Sites

Eight locations on various elevation levels over the whole catchment were chosen. Samples and measurements were taken at four different springs, at one tributary and at three stations along the mainstream (see Table 1, Figure 4, Annex A). The measurement methods applied are discussed in chapter 3.2. The choice of those locations was based on previously performed studies in the Vallon the Nant, in particular, by the paper of Mächler et al. (2021). Other criteria that were taken into account, especially regarding the springs, are good accessibility and a clearly visible separation from other springs or tributaries. As a further matter, these springs span an elevation gradient from 1190m.a.s.l. to 1780m.a.s.l., providing the opportunity to study elevation-driven processes.

Table 1: Metadata to the measurement stations in Figure 4. In his table the sampling stations and their corresponding abbreviations, coordinates and elevation levels are listed (Swisstopo, 2023; Mächler et al., 2021).

Sampling Station	Type	Abbreviation	Coordinates (WGS84)	Elevation Level [m.a.s.l.]
Black-Blue Pipe Spring	spring	S1	46.24828, 7.10664	1268
Grass Spring	spring	S2	46.24760, 7.10642	1281
Bridge Spring	spring	S3	46.23167, 7.10235	1465
La Chaux Spring	spring	S4	46.22194, 7.09238	1730
La Chaux Meander	tributary	T1	46.22565, 7.09163	1780
Mainstream 1/ Outlet	mainstream	R1	46.25301, 7.10954	1190
Mainstream 2	mainstream	R2	46.23171, 7.10231	1461
Mainstream 3	mainstream	R3	46.22332, 7.09756	1554

The **Black-Blue Pipe Spring** is situated close to the mainstream and it is the lowest spring. The spring's outflow is captured in a pipe and the water flows in a stony, quite equally wide streambed into the mainstream. Furthermore, the Black-Blue Pipe Spring is situated close to a pasture, where cows graze. The surrounding is shady, with trees enclosing the spring and thus, not fully exposed to the sun. The **Grass Spring** is a capped spring and located in the middle of the pasture, where cows graze. Its outflow is hidden behind trees and thus, situated in the shadow. Shortly after the outflow, there is no clearly visible path of the water flowing and consequently, the pasture is muddy around the spring's outflow. With greater distance to the outflow of the springs, the water flows in a tiny and narrow streambed. The **Bridge Spring** is situated in the forest and on an elevation, where already some larches can be found. Its flow path is short, since it is located close to the mainstream. In its surroundings there are diverse other small springs and tributaries. As its name expresses, the Bridge Spring originates close to the bridge, which crosses the Avançon de Nant, and which is currently the only one on the hiking trail from the Auberge de Pont de Nant to the hiking destination La Chaux. The **La Chaux Spring** is the

highest investigated spring in the thesis. The outflow is located below a rock and thus, it is not exposed to the sun. The streambed of the spring is rocky and steep. The La Chaux Spring is situated in a vegetational surrounding of bushes, grass and mosses. It crosses the hiking path and keeps on flowing on a steep path down until it reaches the mainstream. The **La Chaux Meander** is a tributary close to a plateau, where cows graze. The flowing path of the La Chaux Meander is not clearly visible, since the area is quite overgrown by bushes and grass. Additionally, there are many rocks, which make it difficult to recognize the meandering of the water. The width of the streambed varies distinctively and so does the subsoil. At some spots it is rocky and at others the water flows through the grass, which makes the water flowing path muddy. In addition, measurements are taken at three different elevation levels: **Mainstream 1** is the outlet, where measurements for other hydrological research projects have been taken and additionally, where diverse instruments are permanently installed. The sampling station **Mainstream 2** is close to the bridge and thus to the Bridge Spring. **Mainstream 3** is the highest sampling station and located outside the forest. There are several tributaries entering the mainstream in the surrounding of that sampling station.

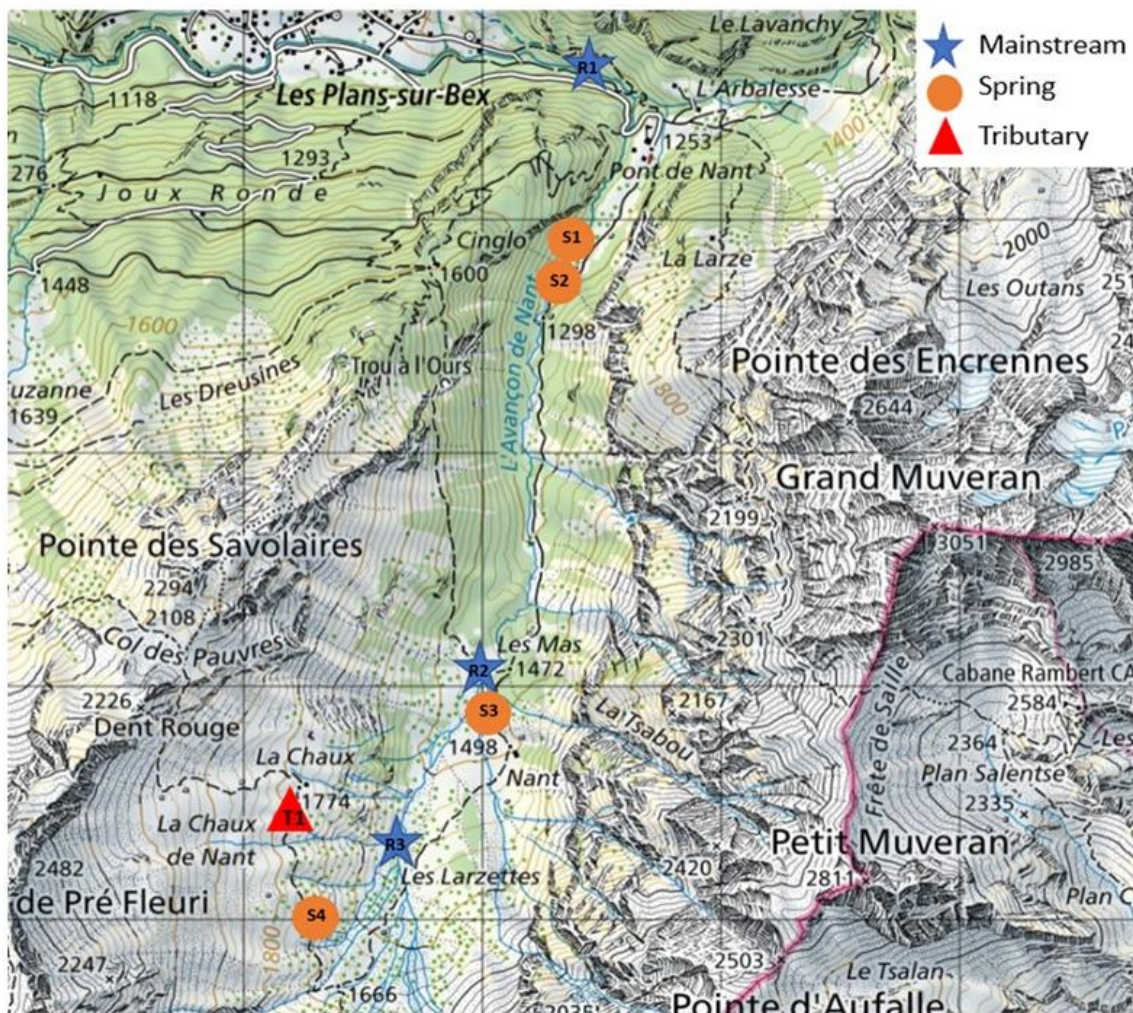


Figure 4: Map of the measurement stations in the Vallon de Nant. In this map the springs are illustrated by orange circles, the stations along the mainstream by blue stars and the tributary by a red triangular (Swisstopo, 2023).

3 Data and Methods

In this chapter, the supplementary data, which I used for my analysis, as well as the methods for analysing the collected data are presented. I initiated my research process with field studies, which is explained in detail in chapter 3.2. Then, the analysis of the investigated water variables is divided into chapter 3.3, water quantity variables, including the methods behind the discharge measurement as well as recession analysis, and chapter 3.4, water quality variables, considering the parameters such as pH value, electrical conductivity, temperature, ions and isotopes. Finally, in the data analysis section, chapter 3.5, the methods used to perform the multivariate data analysis are presented.

3.1 Supplementary Data

In this chapter, the data, which is additionally needed for the analysis part, is discussed (see Table 2). Since hydrological processes are inter alia driven by precipitation and temperature, it was essential to measure these parameters. Unfortunately, this study came at a moment of transition of the installed weather stations, so both local (Weather Station Network Vallon de Nant) stations, which were installed and are maintained by the University of Lausanne, and nearby official (MeteoSwiss) stations were used to compose a continual time series of both temperature and precipitation for the analysis and interpretation of the hydrologic data. Additionally, at the outlet discharge, temperature, opacity and electrical conductivity were continually measured at a 1-minute resolution (WSL and UNIL).

Table 2: Supplementary Data. Meteorological, in particular precipitation and temperature data of both local (Weather Station Network Vallon de Nant) as well as nearby official stations (MeteoSwiss), and discharge data of the outlet of the Avançon de Nant are listed. In addition, the corresponding coordinates and elevation level of these stations as well the time resolution of the data and its time range are illustrated.

Variable	Time Resolution	Station and Coordinates (WGS84)	Elevation [m.a.s.l.]	Data Source	Time Range
precipitation	daily	Sorniot-Lac Inférieur (VSSOR) 46.10, 7.06	1990	MeteoSwiss	1 January 2022 to 31 December 2022
precipitation	daily	La Chauz 46.23, 7.09	1780	Weather Station Network Vallon de Nant	1 January 2022 to 31 December 2022
temperature	daily	La Chauz 46.23,7.09	1780	Weather Station Network Vallon de Nant	1 January 2022 to 31 December 2022
discharge	daily	outlet 46.25,7.10	1200	WSL (Forschungsanstalt für Wald, Schnee und Landschaft)	1 January 2022 to 31 December 2022

Precipitation Data

Whenever possible, the precipitation data of the weather station at La Chauz, which was measured by a 24GHz Doppler radar sensor (WS400-UMB; G. Lufft Mess- und Regeltechnik GmbH, Fellbach, Germany), was used (Michelon et al., 2023). However, since the weather station at La Chauz in the Vallon de Nant was temporarily out of order, precipitation could not be continuously measured over the year

2022. As a consequence, publicly available precipitation data of the MeteoSwiss weather station at Sorniot-Lac Inférieur was considered as well, in order to know when and how much precipitation occurred. Filling gaps in local data with data from the MeteoSwiss weather station at Sorniot-Lac Inférieur was necessary given the gaps in the local time series, but it would have been preferable to use all locally collected data. The precipitation data of Sorniot-Lac Inférieur was used since this MeteoSwiss weather station is located on a similar elevation level as the weather station of La Chaux in the Vallon de Nant. For the further analysis, the third precipitation plot of Figure 5, illustrating both the precipitation at La Chaux, including its gaps, and the precipitation recorded at Sorniot-Lac Inférieur, is considered. Finally, the idea was to illustrate the precipitation amount of the two stations beside each other in order to show the precipitation amount at the simultaneous timepoint.

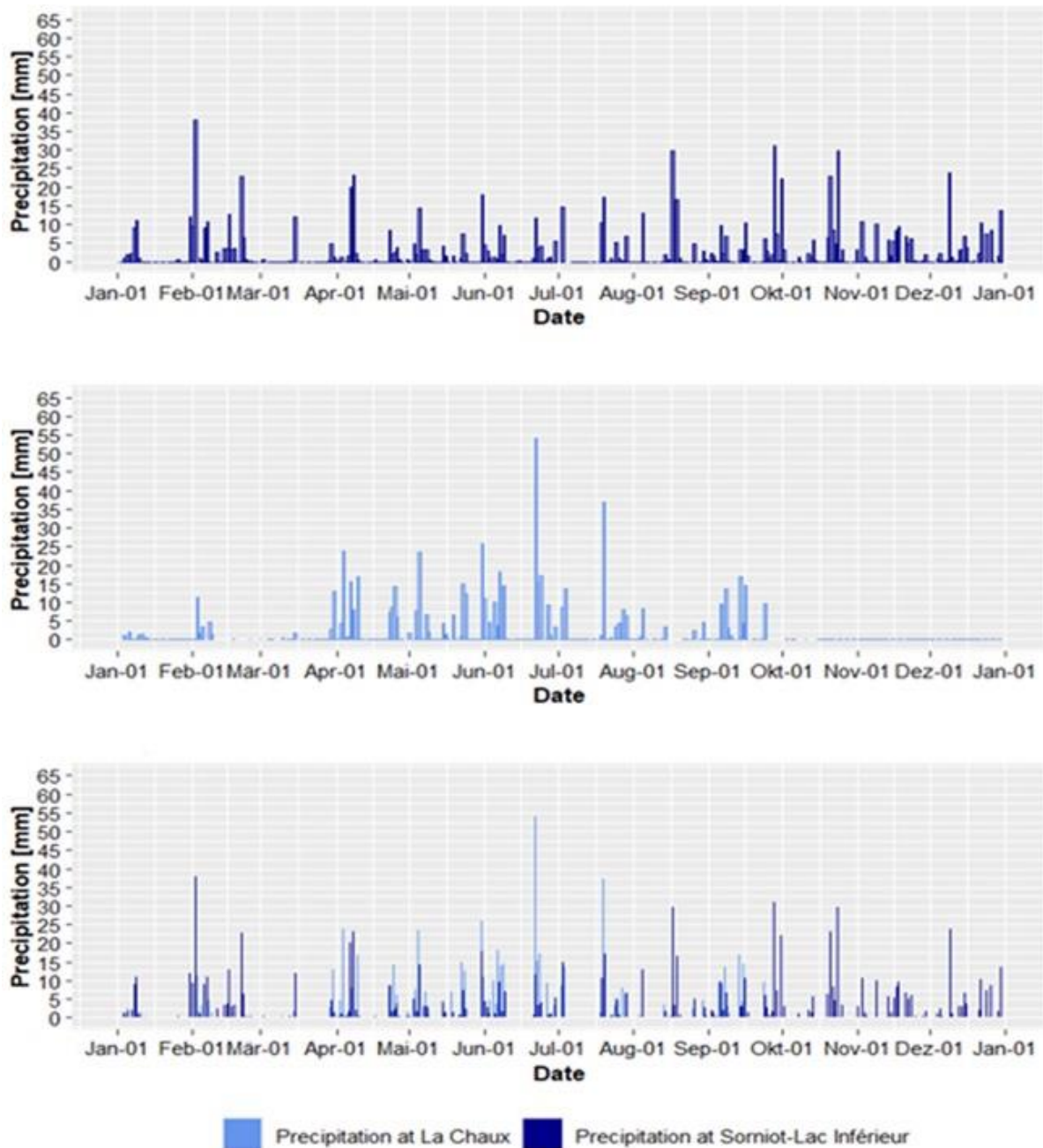


Figure 5: Precipitation data of Sorniot-Lac Inférieur and La Chaux over 2022. The precipitation, recorded at the MeteoSwiss weather station Sorniot-Lac Inférieur (top), at the local weather station La Chaux (middle), measured by a 24GHz Doppler radar sensor (WS400-UMB; G. Luftt Mess- und Regeltechnik GmbH, Fellbach, Germany) and the combination of both stations (bottom) is illustrated.

Air Temperature

The air temperature was recorded with an air temperature sensor (WS300-UMB; G. Luft Mess- und Regeltechnik GmbH, Fellbach, Germany) at the La Chaux weather station (Michelon et al., 2023), which is part of the Weather Station Network Vallon de Nant. As a further matter, in this paper the air temperature is indicated by the daily mean value.

Discharge Data

The discharge of the Avançon de Nant at the outlet was considered, while the discharge of the mainstream was determined by means of an optical height gauge (VEGAPULS WL 61 optical height gauge; VEGA Grieshaber KG, Schiltach, Germany). Then, the height of the water was transformed into stream-flow quantities by means of a rating curve (Ceperley et al., 2018; Michelon et al., 2023).

Geographic Data

In order to illustrate the measurement stations with a map, elevation and coordinates were determined by referencing features on the map (Swisstopo, 2023). The elevation is indicated in meter above sea level (m.a.s.l.) and WGS84 is used as a reference coordinate system.

Isotopic Data

In the context of the isotopic analysis, data from Michelon et al. (2022) was used as the source input for a Bayesian mixing model (MixSIR) (Stock et al., 2018) in order to determine the proportion of rain and snow of the collected water samples.

3.2 Data Acquisition

In this section, the data acquisition process in the field is discussed and the applied methods are explained. Over the course of my research period, I went to the Vallon de Nant seven times for two days each (see Table 3) in order to collect the water samples, to take the measurements of specific water quality parameters at all the measurement stations as well as to measure the discharge of the four springs and the tributary.

Table 3: Dates of sampling campaigns in 2022. The measurements were taken during seven sampling campaigns, while each sampling campaign lasted 2 days.

Sampling Campaign	Date
1	5/6 July
2	17/18 July
3	6/7 August
4	13/14 August
5	27/28 August
6	13/14 September
7	7/8 October

Collection of Water Samples

Water samples from eight different locations were taken in duplicate, in particular at four springs, one tributary and at three different stations along the mainstream (see Annex B). 20ml vials made of LDPE were used. Hydrochemical and isotopic analysis was performed on these samples immediately after the field work in the laboratory at the Institute of Geography at the University of Bern (GIUB).

Electrical Conductivity, pH and Temperature Measurement

The pH value was measured with the pH-meter (WTW pH330i; Xylem Inc., Washington DC, United States) at all eight sampling stations. Furthermore, the water temperature and the electrical

conductivity were determined by the WTW Portable Conductivity meter (ProfiLine Cond 3310; Xylem Inc., Washington DC, United States) at each location (see Annex B).

Salt Dilution Method

The salt dilution method was performed according to the instructions of Wernli (2007; 2011), Gees et al. (1995) and Hendriks (2010).

As a first step, the discharge of the springs was estimated by means of the velocity-area method (see Equation 1). A [m²] corresponds to the cross-sectional flow area, v [m/s] to the flow velocity, h [m] to the height of the water level, w [m] to the width of the streambed, whereas Q [m³/s] to the discharge (Hendriks, 2010).

$$Q = A * v$$

$$Q = w * h * v$$

Equation 1: Calculation of the discharge by considering the flow velocity (Hendriks, 2010).

As a next step, the amount of salt was determined (see Annex B) and the mixing section was calculated. Wernli (2007) suggests to use approximately 4-5kg NaCl per m³ of water and to previously dilute the NaCl in streamwater. As a further matter, Gees et al. (1995) highlight to calculate the mixing section according to Equation 2, whilst w [m] indicates the width at the least wide location of the spring. The factor **20** is used for springs with large turbulences and high roughness, while the factor **50** is used for springs with little turbulences and small roughness (Gees et al., 1995).

$$20 * w$$

$$50 * w$$

Equation 2: Calculation of the mixing section (Gees et al., 1995).

Four kilograms of NaCl per m³ of water were used since the estimated discharge was small. The short distance between some springs and the mainstream channel limits the length of the mixing section. Then, the probe of the WTW-Portable Conductivity meter (ProfiLine Cond 3310; Xylem Inc., Washington DC, United States) was installed according to the calculated mixing section (see Annex B). Only one probe was placed as the cross-sectional areas of the springs are small. Before starting the measurement, the background electrical conductivity was determined. Then, the previously diluted NaCl was added to the spring and the electrical conductivity measurements were started, while the current electrical conductivity was recorded in a time interval of 1 second.

Gees et al. (1995) highlight that, when doing salt dilution measurements, an electrical conductivity peak of approximately 100 μ S/cm over the background electrical conductivity within the first 4 minutes should be observed. After the peak is achieved, Wernli (2007) explains that the measurement runs until the background electrical conductivity is reached again and only then the measurement can be stopped. Thus, he highlights that the discharge curve should have the shape as illustrated in Figure 6 and he additionally adds, that for validation reasons, the procedure with the exact same amount of salt and the identical measurement distance needs to be performed twice.

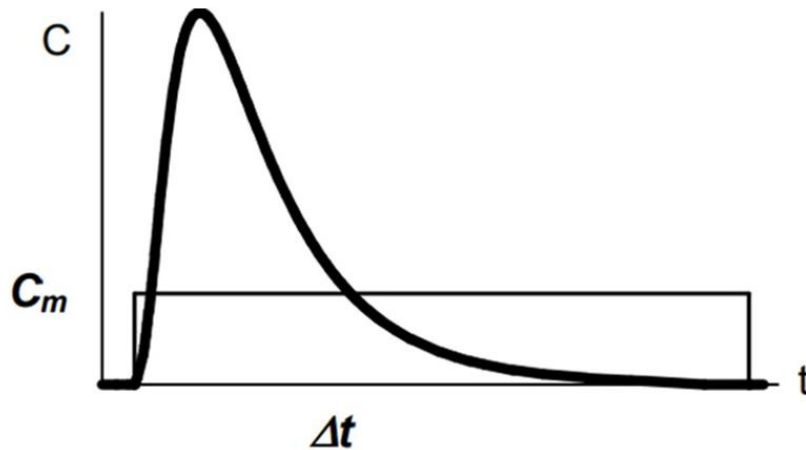


Figure 6: Discharge curve of a hypothetical measurement (reprinted from Wernli, 2007). After the salt was induced into the stream, the electrical conductivity should be approximately $100 \mu\text{S}/\text{cm}$ over the background electrical conductivity within the first 4 minutes in order to generate a valuable discharge measurement and the measurement lasts as long as the background electrical conductivity is reached again.

Long Term Water Temperature Measurements

In order to measure the water temperature over the whole research period, temperature loggers (HOBO Pendant Temperature/Light 64K Data Loggers; Onset, Bourne, United States) were installed. These loggers are stored in a waterproof housing and are battery driven of the battery type CR2032 (Onset, 2023). They measure the water temperature and the light intensity, though the latter parameter is not considered in my thesis. They have, according to the Onset company (2023), an accuracy of $\pm 0.53^\circ\text{C}$ and their measurement range is between -20°C and 70°C . In addition, the Onset company (2023) highlights that they have a memory capacity of 64K bytes.

In total, six temperature loggers were installed at six different locations of the Vallon de Nant catchment, in particular, at the four springs, the tributary and at the Mainstream 3, while the latter got lost (see Annex B). The measurements of the water temperature started at the beginning of the research period, on 1 July 2022, and finished at the end of the research period, on 7 October 2022. A measurement interval of 10 minutes was chosen. At the end of the research period, the data of the temperature loggers was transferred by means of the HOBO software in the field.

Water Quality Measurements by the EXO2 Sonde

The EXO2 Sonde (EXO2 Multiparameter Sonde; Xylem, Yellow Springs, United States) is an instrument that measures a series of different water quality variables simultaneously and also records the values over a defined time span (Xylem, 2020). For taking measurements, the instrument is put into the water (see Annex B) and then the values are measured for the predefined time span, which was in my case 120 seconds. This instrument is newly acquired by the Institute of Geography at the University of Bern and since there was a delivery delay, I could only use it during the last sampling campaign. Therefore, no data was collected by the EXO2 Sonde over the whole research time. However, by means of this instrument one can determine water quality variables such as Cl^- , NH_3 , NH_4^+ , electrical conductivity, salinity, total dissolved solutes, turbidity, pH or temperature (Xylem, 2020). For my paper the pH values measured during the last sampling campaign are used, since the pH meter I previously used broke during the last sampling campaign. However, in Annex C a comparison of the electrical conductivity and temperature values, measured by the EXO2 Sonde as well as by the WTW tool of the last sampling campaign is included. Finally, using the EXO2 Sonde is a further experience to make field work and determine some water quality variables, but the collected data is not very valuable for my research since the data is incomplete over the research period.

3.3 Water Quantity Variables

In this chapter, the methods for calculating the discharge of the springs, the baseflow of the main-stream as well as the recession constants are presented.

Discharge Calculations

In the field, the electrical conductivity was measured by means of the WTW-Portable Conductivity meter (ProfiLine Cond 3310; Xylem Inc., Washington DC, United States) in a time interval of 1 second until the timepoint when the background electrical conductivity was reached again. However, in order to determine the discharge, concentration values are needed. These concentration values are gained, according to Wernli (2011), by converting the electrical conductivity values into concentration values. But he highlights that before this conversion the net electrical conductivity, EC_{net} , has to be determined by subtracting the background electrical conductivity, EC_{base} , from the mean electrical conductivity, EC_{mean} , whilst the electrical conductivity is measured in $\mu\text{S}/\text{cm}$ and the EC_k corresponds to the measured electrical conductivity at timepoint k and n to the number of electrical conductivity values (see Equation 3).

$$EC_{mean} = \sum_{k=0}^n \frac{EC_k}{n}$$

$$EC_{net} = EC_{mean} - EC_{base}$$

Equation 3: Calculation of the mean and net electrical conductivity (Wernli, 2011).

Then, the net electrical conductivity value was converted into a concentration value by multiplying the net electrical conductivity value with the calibration factor, which was determined, according to Wernli (2011), as follows: A calibration solution (10g NaCl per 1l deionized water) was made. Afterwards the amount of 0.5ml from this calibration solution was added to 500ml of stream water 10 times, whilst the electrical conductivity value was measured after each addition. Then, their concentration values were calculated (see Equation 4), while n describes the number of already performed additions, V_n [l] the volume after the n^{th} addition of the calibration solution and C_n [mg/l] the concentration after the n^{th} addition of the calibration solution. This calibration process needs to be performed at every water source at the right temperature, since temperature as well as the background solutes have an impact on the calibration.

$$C_n = \frac{n * 0.0005L}{V_n} * \frac{10g}{L} * 1000$$

Equation 4: Calculation of the n^{th} concentration in the calibration process (Wernli, 2011).

Then, Wernli (2011) highlights that the slope, m , between the concentration, C_n [mg/l], and the electrical conductivity value, EC_n [$\mu\text{S}/\text{cm}$], needs to be determined (see Equation 5).

$$EC_n = m * C_n + q$$

Equation 5: Calculation of the slope in the calibration process (Wernli, 2011).

So, the calibration factor, E [(mg/l)/($\mu\text{S}/\text{cm}$)], corresponds to the inverse value of the slope (see Equation 6) (Wernli, 2011).

$$E = \frac{1}{m}$$

Equation 6: Calculation of the calibration factor (Wernli, 2011).

After having determined the mean electrical conductivity, EC_{mean} [$\mu\text{S}/\text{cm}$], the mean concentration, C_{mean} [mg/L], can be determined by means of the calibration factor, E [$(\text{mg}/\text{l})/(\mu\text{S}/\text{cm})$] (Wernli, 2011).

$$C_{mean} = EC_{mean} * E$$

Equation 7: Calculation of the mean concentration (Wernli, 2011).

Finally, the total discharge Q_{total} [m^3/s] can be calculated (see Equation 8), while M [mg] corresponds to the mass of inserted salt, C_{mean} [mg/m^3] to the mean concentration and Δt [s] to the time period (Wernli, 2011).

$$Q_{total} = \frac{M}{C_{mean} * \Delta t}$$

Equation 8: Calculation of the total discharge (Wernli, 2011).

Calculation of Baseflow

When doing recession analysis, McMahon and Nathan (2021) mention that only discharge values, recorded on days without precipitation, should be used. Thus, in order to exclude precipitation inputs to the overall discharge, the baseflow needs to be considered. As a result, the baseflow of the mainstream is calculated by centring the minimum recorded discharge value over a time period of 7 days, measured at the outlet, to midday of the reported day (Michelon et al., 2023). In this Master thesis, the baseflow of the springs is defined as being equal to its overall discharge. Since there are no continuous discharge measurements at the springs, there is too little discharge data of the springs in order to exclude potential precipitation inputs.

Calculation of Recession Constant

In order to analyse the storage-release characteristics of the springs, in particular to gain an understanding of the recession timescale of the springs, the methods behind the calculation of the recession constants are explained based on theoretical inputs by Müller et al. (2022) and McMahon and Nathan (2021).

As a first step, the baseflow of the mainstream over the previously defined recession period was plotted in order to identify some baseflow variations and thus, to potentially define some recession sub-periods similarly to the study performed in the Pescadero Creek, close to San Francisco (Hornberger et al., 1998). In this case study, two different slopes for the discharge values over the recession period were defined, indicating that different stores of water release water at different rates as well as at different timepoints. So, in order to analyse whether there are also different storages in the Vallon de Nant catchment that may release water to the mainstream at different timepoints, four different sub-periods were defined based on baseflow variations of the mainstream over the whole research period (see chapter 4.2). Then, the mean values of the spring discharge were calculated per sampling campaign in order to check whether the sub-periods, which were defined by the mainstream baseflow variation, correspond to the spring discharge evolution over the research time.

As a next step, the recession constants, k , were calculated (see Equation 9) for every single subperiod as well as for the spring discharge with the aim of determining the recession time scale of the mainstream as well as of the springs (Müller et al., 2022). Müller et al. (2022) explain that the α corresponds to alpha, which is a parameter, that includes information about the characteristics of the aquifer such as the hydraulic conductivity, the porosity or the thickness as well as the length of the aquifer and additionally, this parameter is defined by means of linear approximations. Such a recession constant, indicated in days, describes, according to Müller et al. (2022), the rate of water release of the aquifer, but this recession constant is a specific and individual measure for each storage compartment of an aquifer.

$$k = 1/\alpha$$

Equation 9: Definition of recession constant (Müller et al., 2022).

Based on this background, the original baseflow recession equation (see Equation 10), defined by Boussinesq in 1903, was considered in order to determine alpha and ultimately the recession constant, while Q_t corresponds to the discharge at time t and Q_0 to the discharge at $t=0$ (McMahon and Nathan, 2021). In this paper, the recession constant was determined for the baseflow at the mainstream as well as for the spring discharge per subperiod.

$$Q_t = Q_{t_0} e^{-\alpha(t-t_0)}$$

Equation 10: Baseflow Recession Equation defined by Boussinesq in 1903 (McMahon and Nathan, 2021).

In order to fit the measured discharge data as well as the baseflow of the mainstream to the baseflow recession equation, and thus, to calculate α , the logarithmic of equation 10 was taken (see Equation 11) and a linear regression was performed (McMahon and Nathan, 2021). These calculations were made per subperiod with the mainstream baseflow as well as per spring discharge.

$$\ln(Q_t) = -\alpha(t - t_0) + \ln(Q_{t_0})$$

Equation 11: Logarithmic Transformation of Equation 10 (McMahon and Nathan, 2021).

Finally, the recession constants were calculated per subperiod and spring (see Equation 9), which then indicate the recession time scale in days.

3.4 Water Quality Variables

In this section, some background information about the water quality variables is given, in particular about the pH value, the temperature, the electrical conductivity as well as about some ions and some stable water isotopes.

pH value

In order to measure the acidity of the water in the springs and the mainstream, the pH value, defined as the negative logarithm of the hydrogen ion concentration (see Equation 12) (Berner and Berner, 1987), was determined. Solutions, which have pH values larger than 7, are, according to Berner and Berner (1987), basic and those, which indicate pH values smaller than 7, are acidic. In addition, they highlight that pure water, which means that it does not contain any dissolved minerals, has a pH value of 7 and is thus neutral.

$$pH = -\log[H^+]$$

Equation 12: Definition of the pH value (Berner and Berner, 1987).

The pH value of rain is acidic, which is the product from the reaction of water and CO₂, resulting in carbonic acid (H₂CO₃) and under the assumption that the CO₂ level is about the same all over the world, the pH value of rain can be defined as approximately 5.7, as explained by Berner and Berner (1987). They highlight that higher pH values are measured, for instance, in arid areas, where dust, containing abundant CaCO₃, is dissolved and as a result, the acidity is reduced since the hydrogen ions are used and Ca²⁺ as well as HCO₃⁻ ions are produced. So, Berner and Berner (1987) emphasize that Ca²⁺ ions in the rain provide information about a potential interplay between rain and CaCO₃ dust. They also elaborate that the pH value of rain might also be higher than 5.7 when a reaction with ammonia can be observed, which is particularly the case in regions with high agricultural activity. Rain is considered acid when its pH is below 5.7, which is the result of reactions between rain and acidic gases except CO₂ such as SO₂ or NO₂ as well as due to the absence of CaCO₃ or NH₃ that can lower the acidity (Berner and Berner, 1987). In addition, acidic rain can influence the pH value of the surface waters, but also the pH value of the soil and thus, acidic rain may have an impact on the biodiversity, since it can lead to a limitation of certain nutrients such as, for instance, calcium and magnesium (Likens and Butler, 2019). However, rain in Europe has, according to Prakash et al. (2023), a pH value in the range of 4.19 and 5.82 and additionally, they highlight that the overall pH value increased of about 10% over the last 20 years. Fuss et al. (2015) explain that there may happen episodic acidification of surface water in particular in the snow melting period, but also after strong precipitation events, since then the originally accumulated atmospheric depositions in the snow enter the surface water.

Depending on the pH of the groundwater, some elements are soluble or biologically accessible and therefore Gunarathna et al. (2016) explain that the pH value is also a commonly applied indicator for groundwater quality assessment. Besides, Nelson (2002) writes that the higher the number of H⁺ ions is, the lower is the pH value and the higher is the amount of total dissolved solids since a high H⁺ concentration accelerates weathering processes.

Temperature

Heat is a common hydrologic tracer since its robustness is, according to Rau et al. (2014), high and additionally, the measurement methods are quite straightforward and inexpensive. Since the temperature of groundwater and surface water is different, Rau et al. (2014) highlight that one can investigate by means of temperature variations, for instance, whether groundwater discharge or recharge happens. Particularly, the temperature of groundwater shows, according to Rau et al. (2014), hardly any fluctuations on a yearly scale, whereas the temperature of streamwater can show distinctive daily and seasonally variations. Anderson (2005) sums up that by means of measuring the temperature, the pathways of the water can be understood or conclusions of the consequences of surface warming can be drawn.

Nelson (2002) adds that the higher the temperature is, the higher is the amount of total dissolved solids. In addition, he highlights that seasonal temperature variations are at groundwater levels lower than 50 to 75 feet around 1°C, whereas at shallow groundwater a seasonal temperature range of about 5 to 10 degrees can be recorded. As a result of the temperature variation in the shallow groundwater, the amount of the total dissolved solids also changes with the season, according to Nelson (2002). Finally, he explains that the water inflow from the surface during strong precipitation events can also lead to alteration of the groundwater temperature.

Electrical Conductivity

Pellerin et al. (2008) explain that the electrical conductivity is a parameter which is used to trace the flowing route of water, since, while the water is flowing, it interplays with the geological surrounding, which then is reflected in the mineral composition of water. Tutmez et al. (2006) highlight that the electrical conductivity is an essential tracer when evaluating the quality of groundwater, as it is a direct indicator of the ion concentration of water. Thus, according to Tutmez et al. (2006) almost pure water with very low ion concentration has a much lower electrical conductivity than water with higher ion concentration. Therefore, they explain that there is a direct relationship between the water composition of the total dissolved solids and the water's electrical conductance. In addition, Hayashi (2004) explains that the electrical conductivity is applied to differentiate between groundwater, surface water or precipitation inputs in hydrograph, when precipitation usually contains the lowest number of solids, followed by the surface water and finally, by the groundwater, which indicates the highest amount of total dissolved solids and thus, higher electrical conductivity values.

Ions

The chemical composition of water that reaches the surface in form of rain is altered, since as soon as the water is on the surface, it can take one of several different pathways. Thus, no matter which path the water follows, it encounters different surroundings and consequently is part of a chemical, biological or physical reaction, which finally leads to a modification of the water composition (Berner and Berner, 1987). Throughfall, for instance, is the pathway, where water is caught by vegetation and then reaches the ground as drops, as explained by Berner and Berner (1987). They also mention that water can directly enter the soil (soil water) or flow into surface water (surface runoff), while the water, caught in the soil is either absorbed by the vegetation and then eventually transpired by the plants' leaves (transpiration) or it may flow further down, reach the saturated zone, where the pores of the bedrock are full of water. The water in that saturated zone below the water table is called groundwater, which can be stored in the ground or move to the point where the water table crosses the surface and then gets part of the surface water, including inter alia springs and rivers (Berner and Berner, 1987). Groundwater can continuously feed the rivers, while this constant groundwater input to rivers is, according to Berner and Berner (1987), called baseflow and exists due to the hydrostatic head that is maintained by new rainwater entering the saturated zone.

Berner and Berner (1987) explain that on these pathways, several different weathering processes may occur. For instance, chemical weathering can occur, when water comes upon rocks and a reaction between the water and the minerals of the rocks is caused. Such dissolution processes are particularly accelerated and reinforced by acids, which are products of biological weathering processes. Physical weathering processes in particular separating big rocks into smaller ones is another weathering process which may support chemical weathering since new surfaces are now accessible to water. So, when analysing the ions contained in the groundwater, studying chemical weathering processes are fundamental, since these reactions lead to alterations of the chemical composition of groundwater. Nevertheless, there is a close connection between chemical, physical and biological weathering processes, which do favour each other.

Based on this information, the water samples that were collected in the field, were analyzed on their ion concentration in the lab at the Institute of Geography at the University of Bern (GIUB) by means of ion chromatography (Dionex Aquion Ion Chromatography System; Thermos Fisher Scientific, Waltham, United States) (see Annex B). The ion concentration of the following anions and cations are determined: sodium (Na^+), potassium (K^+), calcium (Ca^{2+}), magnesium (Mg^{2+}), phosphate (PO_4^{3-}), sulphate (SO_4^{2-}), chloride (Cl^-), ammonium (NH_4^+), nitrate (NO_3^-), nitrite (NO_2^-), fluoride (F^-). The focus of the

following paragraphs is to explain how these ions end in the groundwater and finally in the stream-water.

Sodium (Na^+), an alkali metal, is strongly abundant in silicate rocks and it accumulates, according to Berner and Berner (1987), in groundwater due to weathering of silicate minerals such as plagioclase or feldspar. Besides, they highlight that the weathering of halite, which is a key component of sedimentary rocks, also leads to sodium accumulation. When analyzing sodium concentrations of rivers, Berner and Berner (1987) add that contributors such as sea salt and pollution need to be considered.

The origin of **potassium (K^+)**, an alkali metal, in groundwater is particularly the weathering process of silicate minerals, specifically of potassium feldspar, biotite or clay minerals, which are contained in sediments but also in igneous and metamorphic rocks (Berner and Berner, 1987). Saha et al. (2019) highlight that potassium is also a product of the chemical weathering of KCl. As a further matter, since potassium is specifically part of primary minerals, the dissolution of potassium in groundwater is, according to Saha et al. (2019), not very efficient and thus, its weathering is much slower than the one of sodium. When analysing surface water, pollution, cyclic salt and the vegetation need, according to Berner and Berner (1987), to be considered as potential contributors. In addition, they highlight that potassium is a major component of the flora, since plants need it for their growing process in summer and thus, potassium concentrations tend then to be lower, whereas in autumn potassium is released again by the plants, which may lead to an increase of potassium. Furthermore, Berner and Berner (1987) highlight that a connection between the rise of the potassium abundance as well as of increased discharge can be observed, which can explain that after strong precipitation events potassium is washed from the vegetation into the stream.

The weathering process of carbonate rocks such as limestones and dolomites that include calcite is inter alia the origin of **calcium (Ca^{2+})** in groundwater (Berner and Berner, 1987). Saha et al. (2019) explain that the dissolution of minerals such as calcic-plagioclase feldspars as well as of pyroxenes contribute to the calcium concentration in the groundwater. Furthermore, they highlight that sedimentary rocks contain a large amount of calcium and thus, the weathering of such sedimentary rocks explains why calcium is overall the element with the highest concentration in surface water.

The origin of **magnesium (Mg^{2+})** in groundwater is the weathering process of silica rocks, especially the ones that contain minerals such as amphiboles, biotite or olivine (Berner and Berner, 1987). Saha et al. (2019) add that magnesium is also included in chlorite or serpentine. Furthermore, pollution and sea salt play, according to Berner and Berner (1987), a very small role when investigating the origin of magnesium in the water.

Phosphate (PO_4^{3-}) is dissolved phosphorus and in an inorganic but soluble form (Berner and Berner, 1987). Berner and Berner (1987) explain that phosphorus, which is contained in rocks and sediments, has a low solubility and is often embodied as phosphate in calcium-phosphate minerals such as the apatite. Other sources of phosphate are, according to Berner and Berner (1987), precipitation, but it is a minor contributor to the phosphate concentration in the water and pollution processes.

The origin of **sulphate (SO_4^{2-})** in groundwater is often due to weathering processes of sedimentary rocks like organic shale that particularly contain minerals such as pyrite, gypsum or anhydrite (Berner and Berner, 1987). Saha et al. (2019) add that sulphate in groundwater is also a result of oxidation processes of sulphate within igneous rocks. Furthermore, when analysing surface water, contributors such as cyclic salt as well as pollution need to be considered (Berner and Berner, 1987). Another contributor of sulphate are the biogenic sulphur emissions in the atmosphere, which have partly natural, partly artificial origin (Aneja and Cooper, 1989).

A major source of **chloride (Cl⁻)** in groundwater is the dissolution of salts such as halite or sodium chloride, potassium, calcium or magnesium chloride as well as the weathering of soils and rocks (New Zealand Government, 2023). In addition, if chloride is correlated with sodium or potassium, the main source of chloride is halite or sylvite (New Zealand Government, 2023). When analysing streamwater, sea salt as well as pollution such as sewage are other contributors need to be considered according to Berner and Berner (1987).

The upper crust of the earth contains **fluoride (F⁻)**, which can be resolved in water and thus, according to Qian et al. (1999), fluoride can be found in surface water as well as in groundwater. However, they add that the fluoride concentration in groundwater is variable depending on the geology as well as on the chemical conditions in the aquifer, but it quite often just occurs as a trace element in the water. However, Podgorski and Berg (2022) explain that high fluoride abundance is specifically attributed to acidic areas where magmatic rocks can be found or to regions where sediments and metamorphic rocks are located in basic conditions and where the temperature is higher and low calcium concentrations can be observed. Thus, they explain that arid regions, which have little precipitation rates, high temperature and higher pH values tend to have higher fluoride concentrations in groundwater. In addition, they highlight that fertilizers or rainfall can also contribute to an enriched fluoride concentration in the groundwater.

When having a closer look at the products of the nitrogen cycle, it can be noticed that **ammonium (NH₄⁺)** is the product of nitrogen fixation as well as of nitrogen mineralization, whilst in the former case, nitrogen is fixed by microorganisms and then transformed into ammonium, and in the latter case, ammonium is the product of the decomposition process (Schilling, 2002). But according to Lingle (2013), the amount of ammonium as the product of the nitrogen mineralization, or also called ammonification, is small since the amount of organic matter that can be decomposed is restricted in the subsurface. In addition, Harrison (2003) explains that environmental factors such as temperature as well as pH value have an impact on the height of the ammonium concentration, in particular for higher ammonium abundances the pH value of the water should be neutral or acidic and the temperature warm.

A source of **nitrate (NO₃⁻)** is the nitrification, which is the reaction when ammonium is transformed to nitrate by bacteria (Lingle, 2013). As a further matter, nitrate can aside from ammonium also be formed by nitrogen fixation processes, but nitrate is in contrast to ammonium negatively charged and thus, it can be easily washed out, since it cannot be attached to the negatively charged clay particles in the soil and consequently, nitrate can accumulate in groundwater or in streamwater (Harrison, 2003; Lingle, 2013). Other origins of nitrate as well as of ammonium are precipitation events and dry depositions (Berner and Berner, 1987).

Nitrite (NO₂⁻) often appears as an intermediate product in the nitrogen cycle (Lingle, 2013). Lingle (2013) mentions, for instance, that nitrite is the intermediate of the nitrification process, where ammonium is oxidized to nitrate as well as an intermediate product of the denitrification process, where nitrate is reduced to nitrogen.

Isotopes

Stable isotopes of hydrogen as well as of oxygen exist in the environment and in case of oxygen, there are ¹⁶O, ¹⁷O and ¹⁸O and when considering hydrogen, one can observe ¹H and ²H, whereas the latter hydrogen isotope is also called deuterium (Galewsky et al., 2016). Two hydrogen isotopes and one oxygen isotope build together stable water isotopes. In total there are nine different water isotopes, while H₂¹⁶O is the most commonly measured water isotope in nature and H₂¹⁸O, H₂¹⁷O as well as HD¹⁶O are the least frequently recorded ones (Yoshimura, 2014; Galewsky et al., 2016). Besides, Galewsky et

al. (2016) write that the lighter an isotope is, the more abundant it is, such as for example ^1H or ^{16}O , whereas heavy isotopes like deuterium (^2H) or the oxygen isotopes such as ^{18}O and ^{17}O occur more rarely in nature, since they vary in their chemical as well as physical characteristics. Beria et al. (2018) highlight that the heavy isotopes, especially ^2H as well as ^{18}O , are often used as isotopic tracers in hydrology and so are they in this paper. Thus, the isotopic composition of the collected water samples was determined in the lab at the Institute of Geography at the University of Bern (GIUB) by means of the L2140-I Isotope and Gas Concentration Analyzer (Picarro, Inc.; Santa Clara, California, USA) (see Annex B).

It is common to indicate the deuterium and oxygen isotopic composition of a water sample by the Vienna Standard Mean Ocean Water, V-SMOW, which is an international standard (Araguás-Araguás et al., 2000). Araguás-Araguás et al. (2000) write that in case of hydrogen isotopes one defined $^2\text{H}/^1\text{H} = (155.95 \pm 0.08) \times 10^{-6}$ and when considering the oxygen isotopes $^{18}\text{O}/^{16}\text{O} = (200.5 \pm 0.45) \times 10^{-6}$ was determined. Furthermore, the number of heavy isotopes in a water sample is usually indicated by a delta value, defining to which per mil it is different from the standard (see Equation 13), while R_{sample} corresponds to the isotope ratio of the sample ($^2\text{H}/^1\text{H}$ or $^{18}\text{O}/^{16}\text{O}$) and R_{standard} to the isotope ratio of the standard ($^2\text{H}/^1\text{H}$ or $^{18}\text{O}/^{16}\text{O}$) (Galewsky et al., 2016). The more negative a delta value is, the smaller is the number of heavy isotopes and thus, one talks about a higher depletion in heavy isotopes, whilst water samples with less negative delta values are more enriched with heavy isotopes (Araguás-Araguás et al., 2000; Galewsky et al., 2016).

$$\delta = \left[\frac{R_{\text{sample}} - R_{\text{standard}}}{R_{\text{standard}}} \right] \times 1000$$

Equation 13: Definition of the isotopic composition of a water sample (Galewsky et al., 2016).

Some variations in the chemical and physical characteristics among the different water isotopes can be identified. They, for instance, do not need the same amount of latent energy for fractionation processes, which occur when the isotopes change the aggregate state such as in processes like condensation or evaporation and thus, it is differed between equilibrium and kinetic fractionation processes, while condensation happens in contrast to evaporation, which is an example of kinetic fractionation, under equilibrium conditions (Beria et al., 2018). The result of fractionation is an altered composition of stable isotopes in the corresponding aggregate state. So, Araguás-Araguás et al. (2000) explain that despite the fact that condensation is an equilibrium process, the heavy isotopes are more abundant in the liquid phase, while the gaseous phase consequently has a smaller abundance of heavy isotopes. In addition, they add that evaporation is a non-equilibrium reaction, which means that the heavy isotopes tend to enter the liquid phase and thus, the water vapour is more depleted in stable isotopes. They add that in such a kinetic process the $\delta^2\text{H}$ values vary more between the two phases than the $\delta^{18}\text{O}$ values do, since the HD^{16}O isotopes show a lower weight than the H_2^{18}O water isotopes. Finally, such differing isotopic compositions allow to draw conclusions about evaporation or precipitation processes as well as about the origin of the water isotopes (Araguás-Araguás et al., 2000; Aaron et al., 2021; Yoshimura, 2014; Beria et al., 2018).

Globally as well as locally collected $\delta^2\text{H}$ and $\delta^{18}\text{O}$ data has showed that $\delta^2\text{H}$ and $\delta^{18}\text{O}$ values are strongly related, which is defined by equation 14. The resulting line, that specifically expresses the linear relationship between $\delta^2\text{H}$ and $\delta^{18}\text{O}$, is called Global Meteoric Water Line (GMWL). (Araguás-Araguás et al., 2000)

$$\delta^2H = 8 \delta^{18}O + 10$$

Equation 14: Definition of Global Meteoric Water Line (GMWL) (Araguás-Araguás et al., 2000).

However, since the environmental conditions are not globally the same, a Local Meteoric Water Line (LMWL) can be defined, which then also considers local characteristics such as seasonal variations in precipitation and evaporation (Araguás-Araguás et al., 2000). In this paper, the Local Meteoric Water Line (LMWL) equation (see Equation 15) is the same as the one from the paper of Mächler et al. (2021), who also performed isotopic analysis of data collected in the Vallon de Nant and then defined the LMWL of the Vallon de Nant based on a large amount of data.

$$\delta^2H = 7.82\delta^{18}O + 10.47$$

Equation 15: Definition of Local Meteoric Water Line (LMWL) (Mächler et al., 2021).

The deuterium excess (d-excess), corresponding to the intercept of the GMWL or of the LMWL is another method to express the relationship between δ^2H and $\delta^{18}O$ (Araguás-Araguás et al., 2000).

$$d = \delta^2H - 8\delta^{18}O$$

Equation 16: Definition of deuterium excess (d-excess) (Araguás-Araguás et al., 2000).

On balance, the stable isotopes δ^2H and $\delta^{18}O$ are determined by means of the L2140-I Isotope and Gas Concentration Analyzer (Picarro, Inc.; Santa Clara, California, USA), the d-excess values are calculated by Equation 16 and the local meteoric water line of this paper corresponds to the one defined by Mächler et al. (2021).

3.5 Data Analysis

In this section, the methods for the linking of variables with other factors as well as with each other are explained in order to answer the main research question, namely to gain an understanding of the storage-discharge characteristics of the springs. In particular, it is explained how it is determined whether the values of some parameters vary depending on the time of the day. In addition, the idea behind concentration-discharge analysis is elaborated and finally, it is explained how the variables are checked for potential correlations as well as light is thrown on the steps behind principal component analysis.

Statistical Significance Testing of Water Quality Variables

In order to check whether the means of a water quality variable are significantly different between all the sampling stations, a one-way ANOVA (analysis of variance) test with a significance level of 0.05 was performed per water quality variable (Kassambara, 2023).

H0: The means of all the sampling stations are the same.

H1: The mean value of at least one station is not equal to the mean values of the other stations.

When the p-value is smaller than 0.05, H0 is rejected and thus, the means are not the same at all the sampling stations. But, when the p-value is larger than 0.05, the H0 is failed to reject and therefore, the mean value of a water quality variable is the same at all the sampling stations.

However, the one-way ANOVA only indicates whether the mean of a water quality variable is different between the sampling stations or not, but it does not indicate between which stations, in case of a

significant p-value, such a statistically significant difference exists. Therefore, a further statistical test is performed, namely the Tukey HSD (Tukey Honest Significant Differences), in order to evaluate between which sampling stations a statistically significant difference in their means exists. Identically as above-elaborated in context of the one-way ANOVA, if the p-value is larger than 0.05, the mean values are not significantly different, while a p-value smaller than 0.05 highlights a significant difference of the mean values between two sampling stations.

Time-of-Day Analysis

In order to assess whether any diurnal variations such as, for instance, diurnal heating, which then might be related to diurnal cycles of melt, have an impact on the discharge, the discharge measurements were determined once in the morning and once in the afternoon during a sampling campaign. In addition, the pH values, the temperature and the electrical conductivity were also measured once in the morning and once in the afternoon. But in order to perform any further statistical analysis, it is important to check the data for normality first, which is therefore performed in R by the Shapiro Wilk normality test with a significance level of 0.05.

H0: The values are normally distributed.

H1: The values are not normally distributed.

When the p-value is smaller than 0.05, H0 is rejected and thus, the values are not normally distributed. But, when the p-value is larger than 0.05, the H0 is failed to reject and therefore, the values are normally distributed.

Then, in order to analyse if the parameters vary with the time of the day, the following hypothesis was tested: Is there a significant difference between the median of the early measured variable and the median of the late measured variable?

H0: The medians of the two populations are not significantly different.

H1: The medians of the two populations are significantly different.

When the p-value is smaller than 0.05, H0 is rejected. Thus, there is a significant difference between measuring the variable in the morning and in the afternoon. But when the p-value is larger than 0.05, H0 is failed to be rejected. Thus, there is no significant difference depending on the time of the day.

Concentration-Discharge Relationship

The concentration-discharge analysis, which is performed in this thesis, is based on the paper of Knapp et al. (2020), who performed concentration-discharge analysis of various solutes in the Erlenbach catchment. They differ between three different concentration-discharge relationships: dilution, mobilization and chemostasis (see Figure 7). When the solute concentration decreases with increasing discharge, according to Knapp et al. (2020), dilution happens, indicating that during the recession period the solute concentration increases. In contrast to dilution, they highlight that mobilization describes the relationship of increasing solute concentration with increasing discharge. In the recession period, mobilization can be identified, according to Knapp et al. (2020), when the solute concentration decreases over time. When the solute concentration hardly changes with altered discharge rates, Knapp et al. (2020) explain that chemostasis occurs. They emphasize that, while mobilization is often observed when the solutes are washed out from the soil, dilution arises, for instance, when the occurrence of the solutes is restricted or when the solutes are already strongly diluted with the stream and finally, chemostasis is noticed when the source of the solute is unlimited.

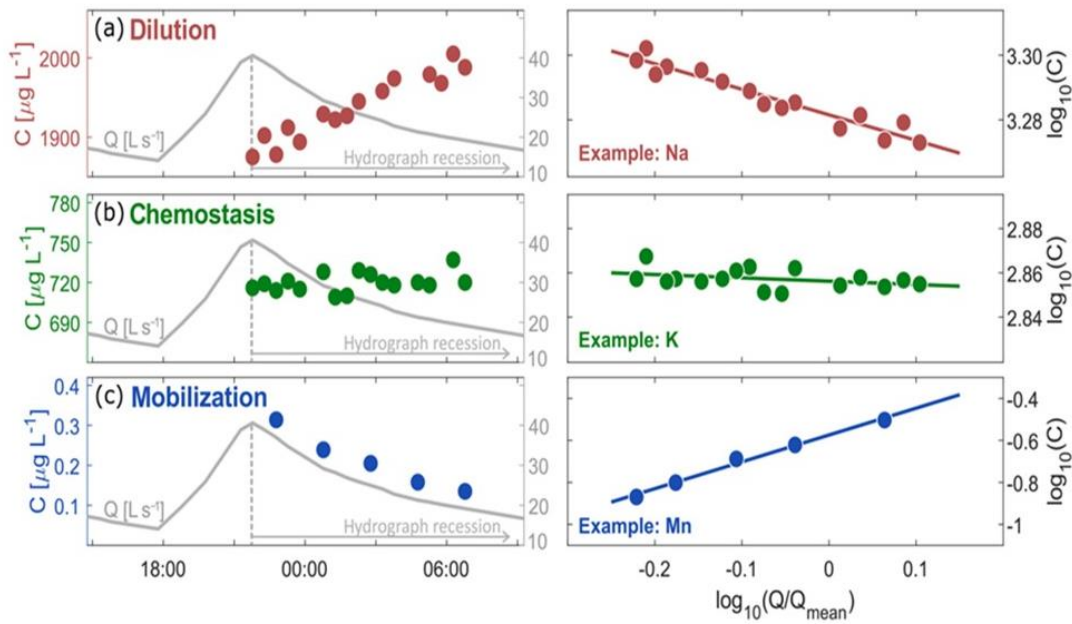


Figure 7: Concentration discharge relationship (reprinted from Knapp et al., 2020). Examples of dilution (a), chemostasis (b) and mobilization (c) patterns in the Erlenbach catchment, while dilution explains an increasing concentration with decreasing discharge, mobilization decreasing concentration with decreasing discharge and chemostatis unchanged concentration behavior with decreasing discharge.

In order to define the concentration-discharge relationship for all the ions in the Vallon de Nant catchment, the baseflow data and the spring discharge was used as discharge data. Besides, since there is too little data at the springs for determining the concentration-discharge for every subperiod over the whole recession period, it was only determined for the first subperiod of the recession period.

Correlation Analysis

In order to evaluate whether the variables are linearly related among each other, correlation analysis was performed. The concept behind correlation analysis is to determine a correlation coefficient which indicates the extent of correlation. This correlation coefficient, r , was calculated by determining the standardized covariance between two variables (see Equation 17), while s_x corresponds to the standard deviation of variable x , s_y to the standard deviation of variable y and n to the sample size (Rogerson, 2015). However, Rogerson (2015) highlights that such a correlation coefficient only indicates to which extent two variables follow a positive or a negative linear relationship, but in case of a correlation between two variables it does not necessarily mean that there is a causality between those two variables.

$$r = \frac{\sum_{i=1}^n (x_i - \bar{x})(y_i - \bar{y})}{(n-1)s_x s_y}$$

Equation 17: Definition of the correlation coefficient (Rogerson, 2015).

The correlation between the variables and the resulting correlation coefficients from -1 to 1 are calculated in RStudio. Strong correlations show high correlation coefficients, while weak correlations are indicated by low correlation coefficients. Finally, in order to support finding the core correlations among all the variables, a correlation matrix with p-values at a significance level of 0.05 was calculated in R.

Principal Component Analysis

In this paper, there are several different variables investigated, which are all correlated with each other, but to a different extent. So, in order to collect the key information of all these variables, the dimensionality was reduced by means of principal component analysis. This multivariate statistical method was used to define new variables, so called principal components, that contain the core information and are calculated by means of linear combinations of the original variables (Abdi and Williams, 2010). Abdi and Williams (2010) highlight that these principal components are defined in a way that they describe most of the variation, but keep the information loss on a low level. In addition, they add that principal component analysis is also a clustering method that illustrates similar observations closely and different observations more distantly.

An important condition before performing principal component analysis is to have a complete dataset, which means that there is a value per variable and per sampling date recorded. Unfortunately, there are some variables which are incomplete over time and thus, not part of the principal component analysis and for the considered variables refer to table 4.

Table 4: Variables used for principal component analysis. Since a condition for performing principal component analysis is a complete dataset, not all variables are considered, but only those that have a value per sampling date.

Variable
temperature
pH
electrical conductivity
chloride
nitrate
sulphate
sodium
potassium
magnesium
calcium
detex
$\delta^{18}\text{O}$
$\delta^2\text{H}$

As a first step, the data was standardized, since all the variables were measured in different scales. Then, the eigenvalues were determined, in order to examine how many principal components should be considered. These eigenvalues indicate how much of the total variation is described by a principal component. Since there is no general rule about how much all the considered principal components need to explain, one can individually set the limits. So, for my analysis I set the limit at 75%, meaning that I considered as many principal components as necessary to explain at least 75% of the total variation. Then, the variables were illustrated by means of arrows on a variable contribution plot, where the first principal component is on the x-axis and the second principal component is on the y-axis. The coordinates of these variables were determined by the extent of correlation between the variable and the principal component and the length of the arrow indicates how large the variance of a variable is. So, long arrows indicate large variance (Kohler and Luniak, 2005). When considering the angle between the variables, Kohler and Luniak (2005) explain that angles which are close to 90° or to 270° respectively, indicate low correlation, whereas angles which are close to 0° or 180° show a correlation close to 1 or -1. In addition, a scatterplot of the observations, in particular of the values of the variables at a specific date and location, is defined and overlaid with the variable contribution plot.

3.6 RStudio

The data visualization as well as the statistical analysis including hypotheses testing, correlation and principal component analysis were performed in RStudio of the version 4.2.2 (R Core Team, 2022). Additionally, the MixSIAR model framework from R (Stock and Semmens, 2016) was applied for the isotopic analysis. In the following paragraphs the applied key packages as well as the concept behind the framework MixSIAR are presented.

The dplyr package (Wickham et al., 2023) is used for generally handling the data and the rstatix package for statistical significance analysis (Kassambara, 2023). FactoMineR package (Le et al., 2008) for principal component analysis. As a further matter, the key package I used in order to visualize the data in R is the ggplot2 package (Wickham, 2016), but several other packages such as RColorBrewer (Neuwirth, 2022), scales (Wickham and Seidel, 2022) and lubridate (Grolemund and Wickham, 2011) were used in order to illustrate the data in a clear way. Furthermore, in order to ensure that the data is readable for colour blind people the colorBlindness package (Ou, 2021) was applied.

MixSIAR Model

The investigation of the isotopic composition of the collected water samples allows us to define the proportion of snow and rain. This analysis was performed in R by means of the MixSIAR package which defines a Bayesian mixing model that then determines the share of rain and snow of each of the individual water samples (Stock and Semmens, 2016). But before running the model, the following terms need, according to Stock and Semmens (2016) to be defined in order to get a valuable output: Mixture, Sources and Discrimination. As *source* data, the most recent isotopic composition of snow and rain from 2707 water samples in the Vallon de Nant, analysed by Michelon et al. (2022), was chosen. The $\delta^2\text{H}$ and the $\delta^{18}\text{O}$ values of the collected water samples per sampling campaign or per measurement station over the research period 2022, determined by L2140-I Isotope and Gas Concentration Analyzer (Picarro, Inc.; Santa Clara, California, USA), were attributed to *mixture*. Finally, the distinction of the water into the categories snow and rain, corresponding to the water distinction in the source section, was ascribed to *discrimination*. Based on these inputs, the proportion of rain and snow in the mixture were calculated by using the stable isotopes as tracers. Since there is a particular interest in spatial and temporal variation between the different sampling stations, the proportions are calculated per sampling station, per sampling campaign as well as per sampling date.

4 Results

This chapter begins with an overview of the meteorological conditions of the research water catchment over the year 2022. Streamflow periods for 2022 are defined based on those of Michelon et al. (2023). Then, the results of the salt discharge measurements as well as of the recession analysis are presented in the water quantity section. Furthermore, the temporal as well as the spatial variation of the water quality variables are discussed. And at last, in the data analysis subchapter, the results of the time-of-day analysis, of the concentration-discharge analysis as well as of the correlation and principal component analysis are explained.

4.1 Overview Meteorological Conditions in the Catchment

In this section, the meteorological conditions of the Vallon de Nant catchment of the year 2022 as well as the discharge of the Avançon de Nant, recorded at the outlet, are presented. Then, based on the evolution of these variables over the year and by inputs of Michelon et al. (2023), the different streamflow periods of 2022 are defined for the Vallon de Nant catchment. Finally, the specific meteorological conditions that occur during the sampling campaign are highlighted.

Overview of the Temperature in the Vallon de Nant

The temperature range of the Vallon de Nant, recorded at the La Chaux weather station, is from -9°C in mid-December to about 21°C in mid-July. Days with mean temperature below zero could be measured until mid-April and then again from early November on.

The year 2022 started with positive daily temperature, then the temperature decreased below zero to about -9°C (see Figure 8). Afterwards, it continued fluctuating between positive and negative temperature through January, February and March. At the end of March as well as at the beginning of April, a cold spell could be notified, when a temperature of about -7°C was recorded. Towards mid-April the temperature increased again before it decreased in the second half of April as well as towards the beginning of May. Towards mid-May a strong temperature increase up to 17°C was measured, but then a quick decline could be noticed. June started warm and the temperature reached about 20°C , but afterwards it decreased again and then stayed on a level between 10°C and 15°C . At the beginning of July, a temperature rise up to 15°C was recorded, but it fell shortly afterwards again. However, the temperature increased again and remained within the range of approximately 17°C and 19°C before the downfall at the end of July. August started with a temperature of about 20°C and before the temperature reached 12°C at the end of the month, the temperature fluctuated between 14°C and 17°C . The first half of September showed a temperature between 12°C and 18°C , which is in contrast to the second half, when a temperature between 1°C and 10°C was recorded. Towards October, the temperature increased up to 13°C and then showed a strong decline. November started cold but then temperature increased to around 10°C . However, in the second half of November and during the whole December the temperature fluctuated between low positive and negative values. In mid-December the lowest temperature of 2022 of almost -10°C was measured at the La Chaux weather station.

Overview of the Precipitation in the Vallon de Nant

Since the precipitation data of the weather station at La Chaux is incomplete over the whole year of 2022, precipitation data of Sorniot Lac-Inférieur is additionally considered (see chapter 3.1).

January started dry, while at the beginning of February, a prominent precipitation event of about 38 mm, indicated as the sum of the daily precipitation amount, was recorded at Sorniot Lac-Inférieur (see Figure 8). It can be perceived that March was dry in contrast to April, which showed a series of precipitation events through the whole month. In May, one could identify rainfall through the whole month,

but at the beginning of May a distinctive precipitation event of about 23 mm was clearly observed and another one of about 25 mm at the end of May. June started and ended wet and it included the strongest precipitation event of about 54 mm ever recorded at the La Chaux weather station in 2022. The beginning of July was dry, but in mid-month there was another prominent precipitation event of about 37 mm recorded at La Chaux. The start of August was quite dry but towards mid-month a remarkable precipitation event of about 29 mm was recorded at Sorniot Lac-Inférieur. In September several precipitation events with the strongest event of an amount of 31 mm on 28th September 2022 were observed. October started with a precipitation amount of about 22 mm, but otherwise the first half of October was dry in contrast to the second half. In November a series of modest precipitation events were recorded. Ultimately, December was regarding precipitation events similar to November, but two remarkable precipitation events of about 23 mm and 65 mm were recorded in early and mid-December at Sorniot Lac-Inférieur.

Overview Discharge of the Avançon de Nant

The lowest discharge was recorded in early February at the outlet and the highest in early October (see Figure 8). The discharge increased from mid-March towards mid-May, then there were some discharge fluctuations visible from mid-May till mid-June. From the end of June until the end of September a decrease of discharge was observed. In early October, a peak of discharge, corresponding to the yearly maximum, and another high discharge were identified in mid-October. And, from mid-October until the end of December the discharge decreased again, but then towards the end of 2022 another discharge peak was recorded.

Sampling Campaigns

The dashed lines in Figure 8 show the visits, when the measurements were taken and the corresponding metadata is explained in Annex C. The sampling days were dry except on 14th August and on 14th September. As a further matter, the temperature increased towards the second sampling campaign up to almost 20°C. In August, it varied between 12°C and 16°C, whereas in September a temperature of about 18.24°C was recorded and finally, the temperature of the last sampling campaign was the lowest over the research period.

In order to lay a foundation for the interpretation of any discharge patterns at the springs, the discharge at the outlet needs to be considered, since it is the sampling station, where continuous discharge data is available. At the outlet, we see a decrease in discharge between the first and the second sampling campaign, so we can imagine that at the springs the discharge decreases as well. A slight discharge increase towards 28th August was manifested at the outlet, but then it decreased again towards the second last campaign in September. Finally, there was an increased discharge recorded at the outlet in the last sampling campaign, so we can imagine that such an increase is also regarded at the springs.

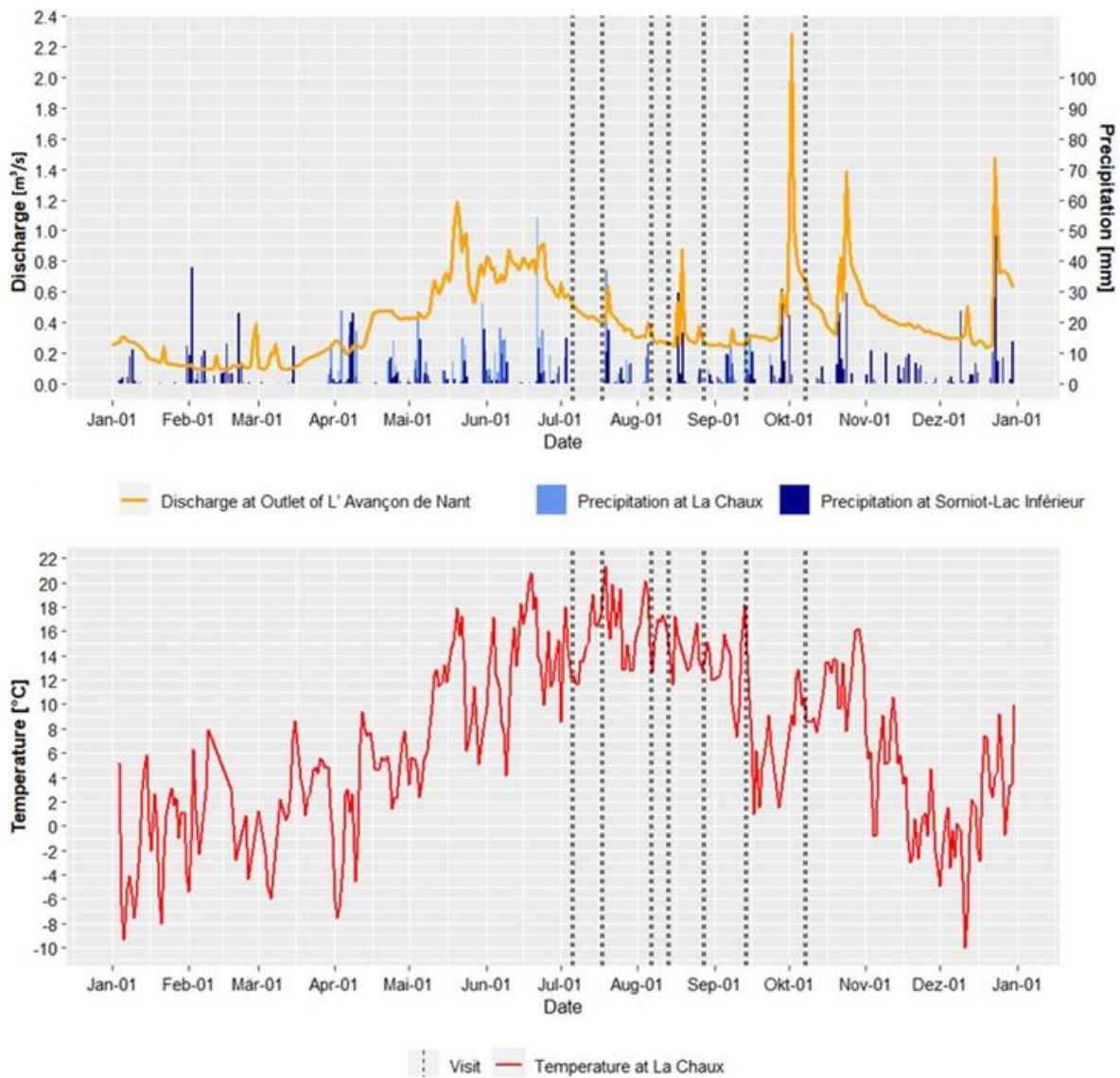


Figure 8: Overview of meteorological conditions of 2022 in the Vallon de Nant catchment and discharge of the Avançon de Nant, measured at the outlet. The daily precipitation amount, determined for both, the La Chau and the Sorniot-Lac Inférieur, weather stations, as well as the mean daily discharge, recorded at the outlet of the Avançon de Nant, are illustrated over 2022 (top). Then, the mean daily temperature, measured at La Chau, is presented (bottom). Furthermore, the visits of the Vallon de Nant catchment for performing the measurements are indicated.

Definition of Streamflow Periods

The streamflow periods (see Table 5) are visually determined by means of the streamflow curve by Michelin et al. (2023) (see Figure 1) as well as by the discharge curve of the Avançon de Nant from 2022 (see Figure 8) in order to set a context for the streamflow periods of 2022, which are discussed in chapter 5.1.

The baseflow period measured in 2022 lasted a similar length of time to that of 2017, which also lasted until mid-March, whereas the early melt period was rather long in 2022 in comparison to corresponding observations of Michelin et al. (2023) (see Figure 1). The melt period of 2022 was similar to the one of 2016. The seasonal recession period of 2022 was similar to the one of 2016 and ended before the substantial increase of streamflow at the beginning of October, when the next baseflow period started. More details about the definition of the recession period 2022 is given below.

Table 5: Streamflow periods of the Avançon de Nant of 2016-2018 and 2022. The streamflow periods of the year 2016-2018 of the study, performed by Michelin et al., 2023, as well as the streamflow periods of 2022 are visually determined, while for the former period Figure 1 was considered and for the latter Figure 8.

Streamflow Period	2016	2017	2018	2022
Baseflow Period (B)	- end of March (2016)	end September (2016) - mid March (2017)	end September (2018) - beginning of April (2018)	-mid March
Early Melt Period (E)	April	mid-March - end of April	-	mid-March – beginning of May
Melt Period (M)	May until end of June	May	early April – end of May	beginning of May – end-June
Seasonal Recession Period (R)	end of June until end of September	beginning of June until end of September	beginning of June until end of September	end-June until end of September

Definition of Recession Period

In this Master thesis, the definition of the recession period is based on the classification of the streamflow periods according to Michelin et al. (2023) and thus, elaborated by means of the discharge data measured at the outlet of the catchment. When considering the evolution of the discharge at the outlet of the Avançon de Nant in the Vallon de Nant catchment (see Figure 9), the discharge decreases from the end of June (24 June 2022) towards the end of September (30 September 2022) before the discharge increases again at the beginning of October. So, this time period (see grey part in Figure 9) is defined as the recession period of 2022 for the Vallon de Nant catchment.

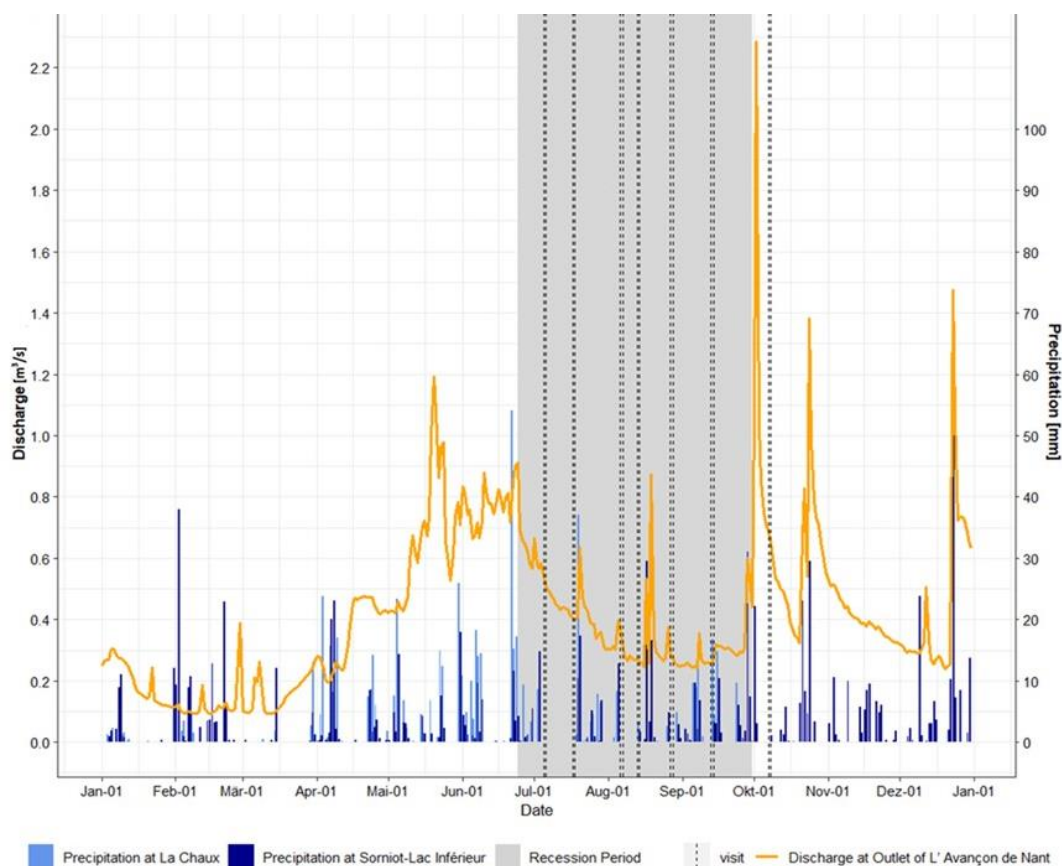


Figure 9: Definition of recession period of 2022 for the Vallon de Nant catchment. The daily amount of precipitation, recorded at both, the La Chau as well as at the Sorniot-Lac Inférieur, weather stations and the mean daily discharge, measured at the outlet of the Avançon de Nant, over 2022 are illustrated.

4.2 Water Quantity Variables

In this subchapter, the recorded discharge data of the springs is discussed, specifically, the spatial variation between the springs and the temporal variation over the research period are analysed. As a further matter, the discharge pattern between the springs and the mainstream as well as the recession constants are determined in order to gain an understanding of the storage-discharge characteristics of the springs.

Discharge Analysis

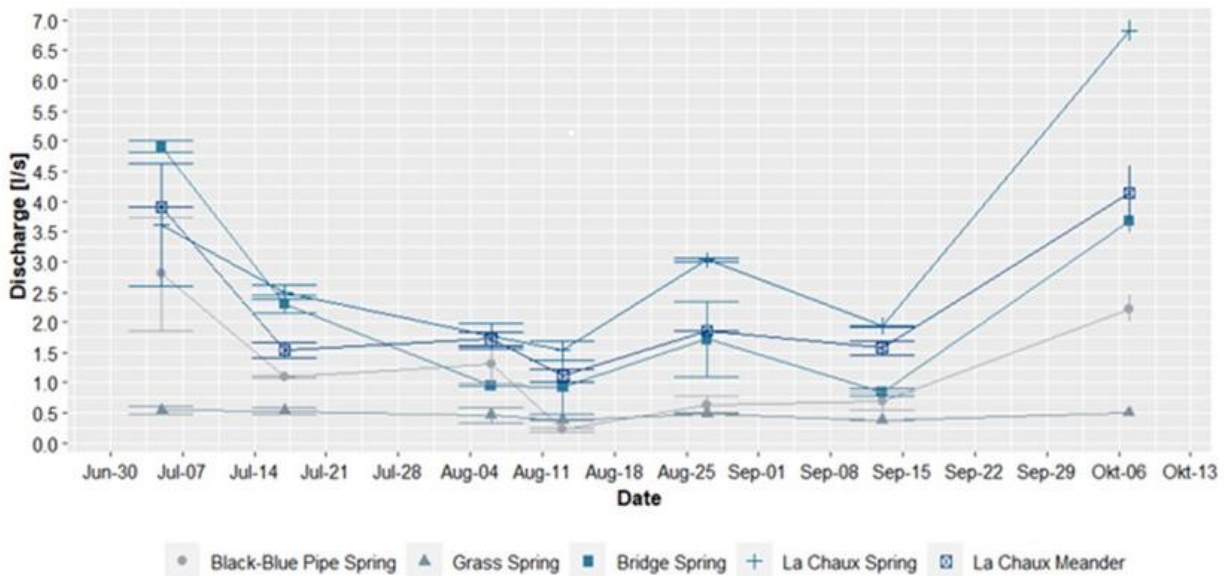


Figure 10: Mean discharge of the monitored springs per sampling campaign over research period of 2022. The discharge of the springs was determined by salt dilution measurements and then the mean discharge of both sampling days during a sampling campaign was calculated.

Temporal Variation

Over time, there are two drops in discharge over the observation period: The first is noticeable from early July until mid-August and the second decline from end-August until mid-September. In between, there is an increase of discharge from mid-August towards end-August and the discharge value of the last sampling campaign in October shows again a much higher value compared to the one in September. Aside from the Grass Spring, which shows small temporal discharge variations, all other springs and the tributary as well follow that trend except that the discharge of the Black-Blue Pipe Spring and the La Chaux Meander increases again slightly towards the beginning of August and that there is quite a strong increase in discharge compared to the other sampling stations at the La Chaux Spring in October.

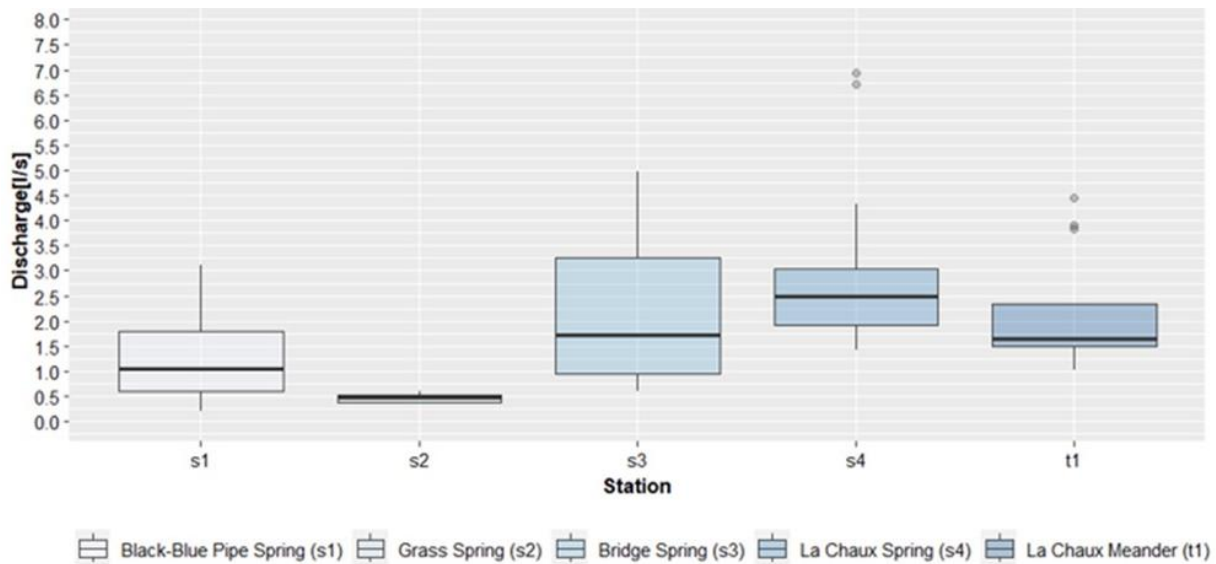


Figure 11: Boxplots of discharge per spring. The discharge, measured during the research period from early July until early October 2022 by salt dilution measurements, is illustrated per sampling station, located in the Vallon de Nant catchment

Spatial Variation

A variation in space is clearly visible when considering the median discharge of the springs. The La Chaux Spring has the highest median discharge of approximately 2.5l/s, while the Grass Spring has the lowest median discharge of about 0.5l/s, followed by the Black-Blue Pipe Spring, which has a median discharge of about 1l/s. The median discharge of the Bridge Spring as well as of the La Chaux Meander is almost identical and approximately 1.75l/s.

Outliers

There are three outliers recorded at the La Chaux Meander, which show discharge values between 3.75l/s and 4.5l/s. They can be attributed to the first and to the last sampling campaign.

Results of Statistical Significance Test

The results of the statistical significance test (Tukey HSD), assessing between which sampling stations a significant difference in the mean values of the discharge variable exists, indicate that there is no significant difference in the mean discharge between all the pairs of the stations apart from the pair La Chaux Spring/Grass Spring.

Table 6: Results of the statistical significance test of the discharge at the springs. The p-values of the discharge between the different pairs of sampling stations are determined by the Tukey Honest Significance Differences (Tukey HSD) test.

	s1	s2	s3	s4	t1
Black-Blue Pipe Spring (s1)					
Grass Spring (s2)	not significant				
Bridge Spring (s3)	not significant	not significant			
La Chaux Spring (s4)	not significant	not significant	p<0.001		
La Chaux Meander (t1)	not significant	not significant	not significant	not significant	

Comparison of the Discharge Pattern between Springs and Mainstream

In this section, the focus is on analyzing if the discharge at the springs mimics the discharge at the outlet over the recession period, which therefore requests comparing the spring discharge within the sampling campaign to the temporarily equivalent overall discharge and baseflow of the mainstream.

This comparison includes the assessment of whether there is a decrease of the spring discharge, an increase or no change within a sampling campaign (see Figures 12 to 16). As a further matter, it is analyzed how precipitation events are reflected in the spring discharge.

Discharge Black-Blue Pipe Spring vs Mainstream

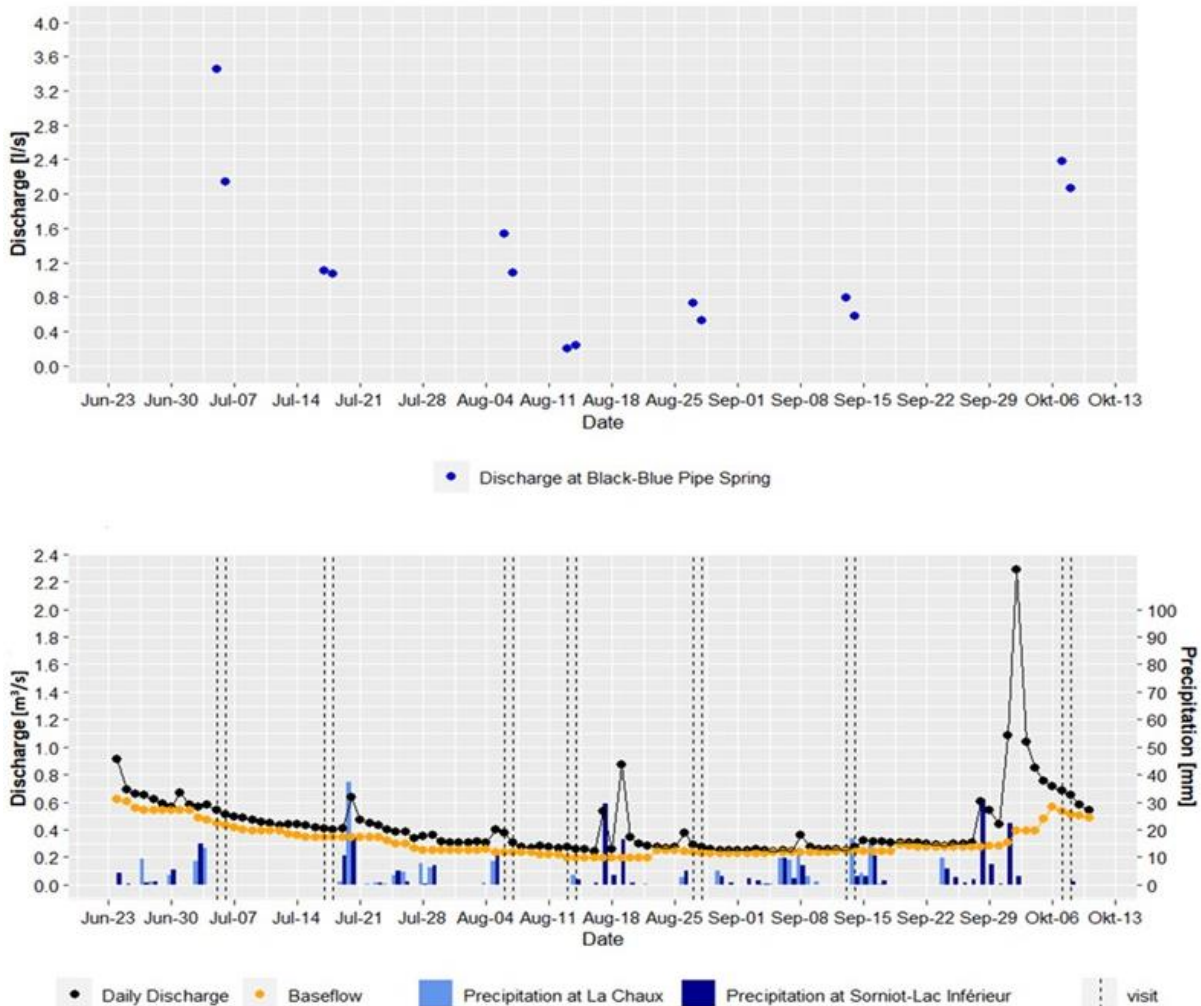


Figure 12: Comparison of discharge between Black-Blue Pipe Spring and Mainstream. The discharge at the Black-Blue Pipe Spring is illustrated over the research period (top), determined by salt dilution measurements, the overall discharge as well as the baseflow of the mainstream and, additionally, the daily amount of precipitation measured at both, the La Chaux and the Somriot-Lac Inférieur, weather stations over the research period (bottom) are illustrated.

The mainstream baseflow and its overall discharge are perfectly mimicked by the **Black-Blue Pipe Spring** during the first, second and the last sampling campaign. However, the spring discharge decrease within the third sampling campaign cannot be mirrored in the mainstream baseflow but in its overall discharge. Exploring in more details the precipitation amount around the third sampling campaign, rainfall can be observed the days before, which must have had an impact on the spring discharge amount. Besides, there is an increase in the spring discharge during the fourth sampling campaign, whereas this increase is noticed neither in the mainstream baseflow nor in its overall discharge. Considering precipitation, there was a small precipitation event on the second day within this fourth sampling campaign. When taking the fifth and the sixth sampling campaign into consideration, a discharge decrease at the Black-Blue Pipe Spring is noticed, but neither one in the mainstream discharge nor in its baseflow. In the former case, precipitation occurred the days before, whereas in the latter case no previous precipitation events were recorded, but on the second sampling day one could record precipitation.

Discharge Grass Spring vs Mainstream

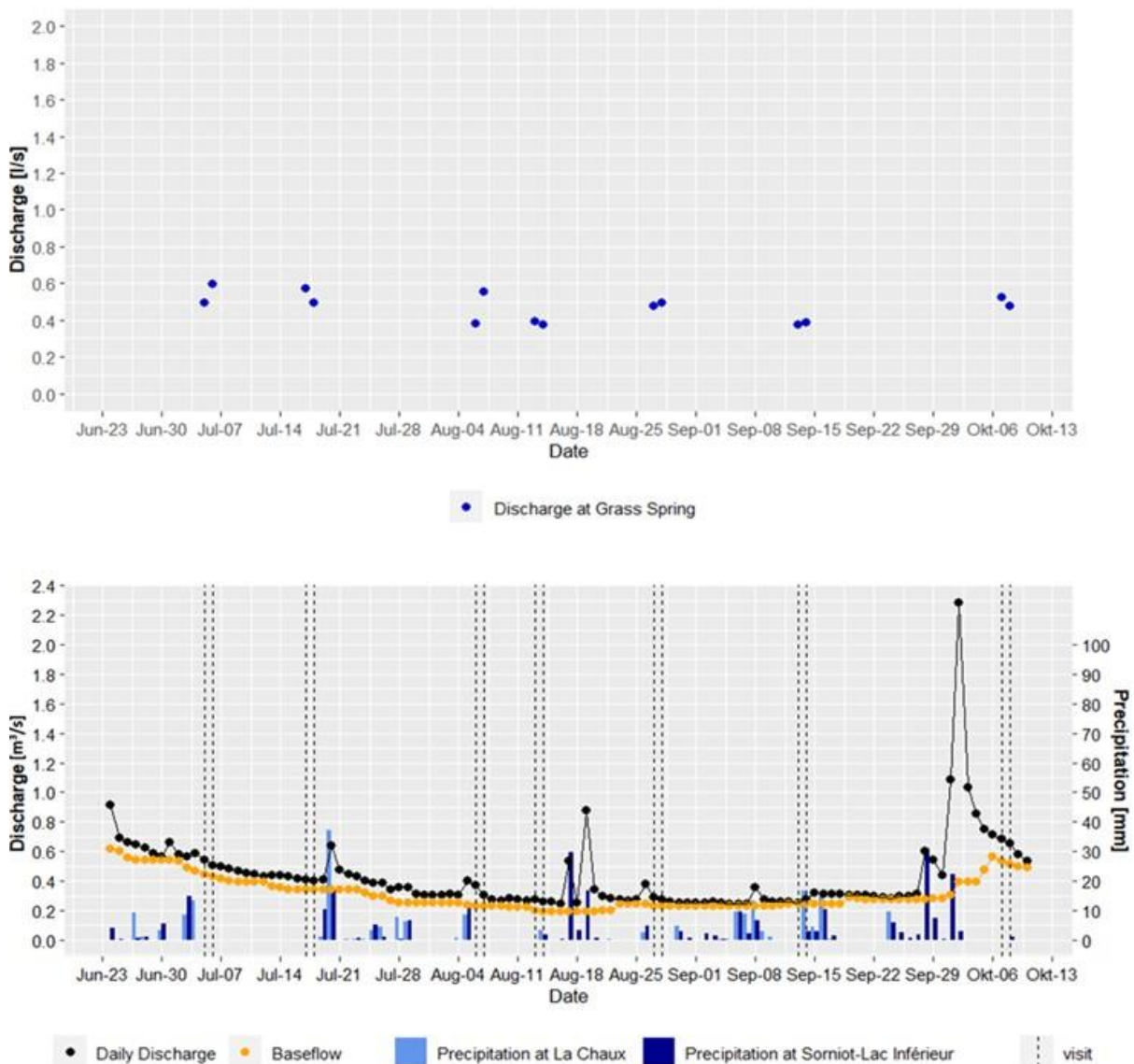


Figure 13: Comparison of discharge between Grass Spring and Mainstream. The discharge at the Grass Spring is illustrated over the research period (top), determined by salt dilution measurements, the overall discharge as well as the baseflow of the mainstream and, additionally, the daily amount of precipitation measured at both, the La Chau and the Sorniot-Lac Inférieur, weather stations over the research period (bottom) are illustrated.

The discharge of the **Grass Spring** corresponds during the fourth, fifth and last sampling campaign to both the mainstream discharge and its baseflow, whereas the discharge of the Grass Spring follows the equivalent pattern of the mainstream baseflow during the sixth sampling campaign. As opposed to the behavior of the mainstream, the discharge rises during the first sampling campaign as well as during the third one, but decreases during the second one.

Discharge Bridge Spring vs Mainstream

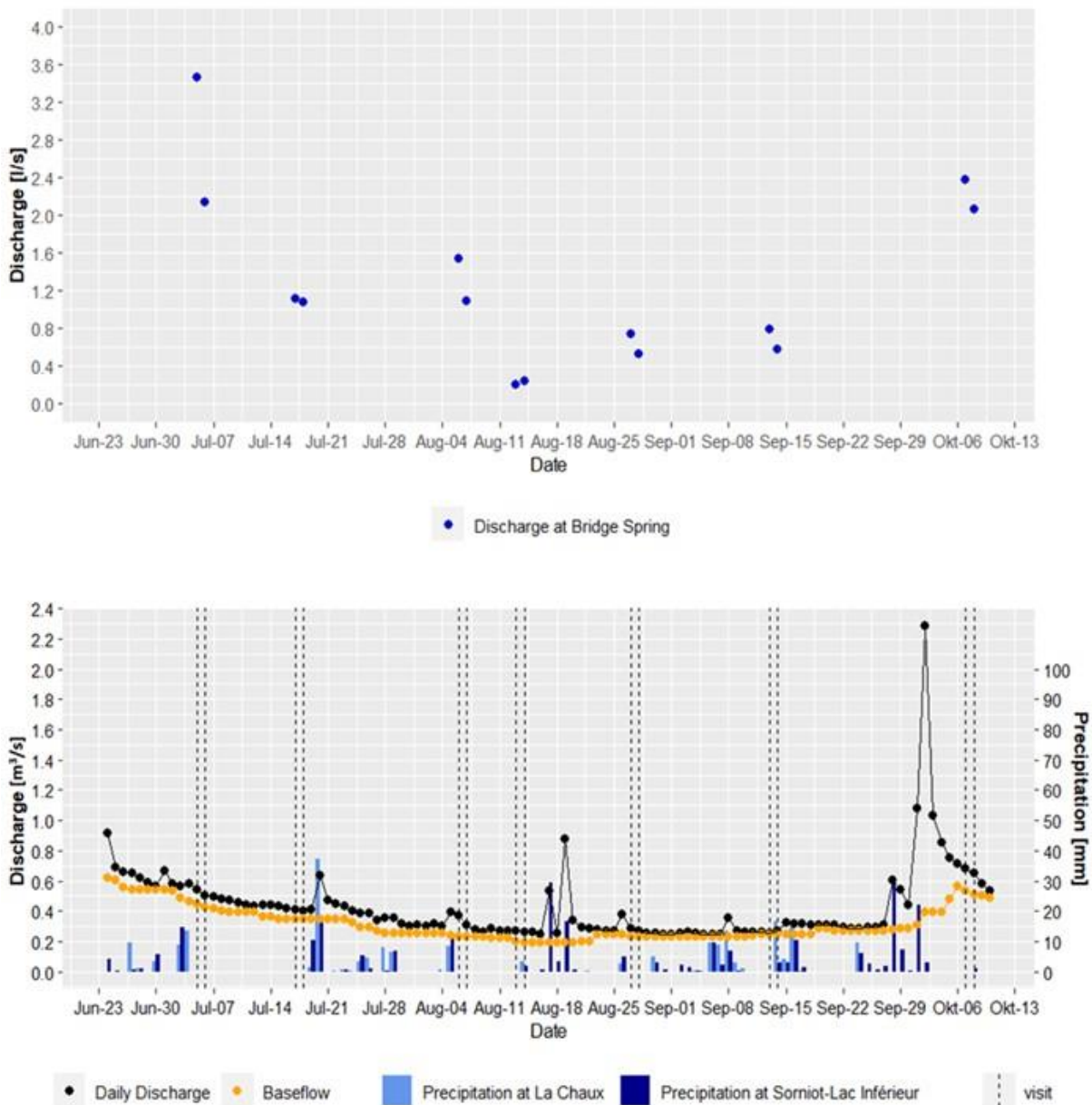


Figure 14: Comparison of discharge between Bridge Spring and Mainstream. The discharge at the Bridge Spring is illustrated over the research period (top), determined by salt dilution measurements, the overall discharge as well as the baseflow of the mainstream and, additionally, the daily amount of precipitation measured at both, the La Chau and the Sorniot-Lac Inférieur, weather stations over the research period (bottom) are illustrated.

The **Bridge Spring** mimics the mainstream baseflow and its overall discharge during the first and the last sampling campaign, whereas the spring discharge mirrors only the mainstream baseflow during the third sampling campaign. Additionally, no reaction to the previously occurred precipitation events are showed by the spring discharge during the third sampling campaign. The increase of the spring discharge during the sixth sampling campaign is reflected in the overall mainstream discharge but not in its baseflow, whereas the spring discharge increase in the fourth sampling campaign is neither reflected in the mainstream discharge nor in its baseflow. Considering precipitation, within the fourth sampling campaign precipitation was recorded on the second sampling day. As already observed at the Black-Blue Pipe Spring, there is a discharge decrease at the Bridge spring during the fifth sampling campaign, but which is neither mirrored in the mainstream discharge nor in its baseflow. However, a precipitation event was recorded just the day before the measurement. Ultimately, an increase of

discharge is measured at the Bridge Spring in the second sampling campaign, which is not recorded by the mainstream and furthermore, no previous precipitation events occurred.

Discharge La Chaux Spring vs Mainstream

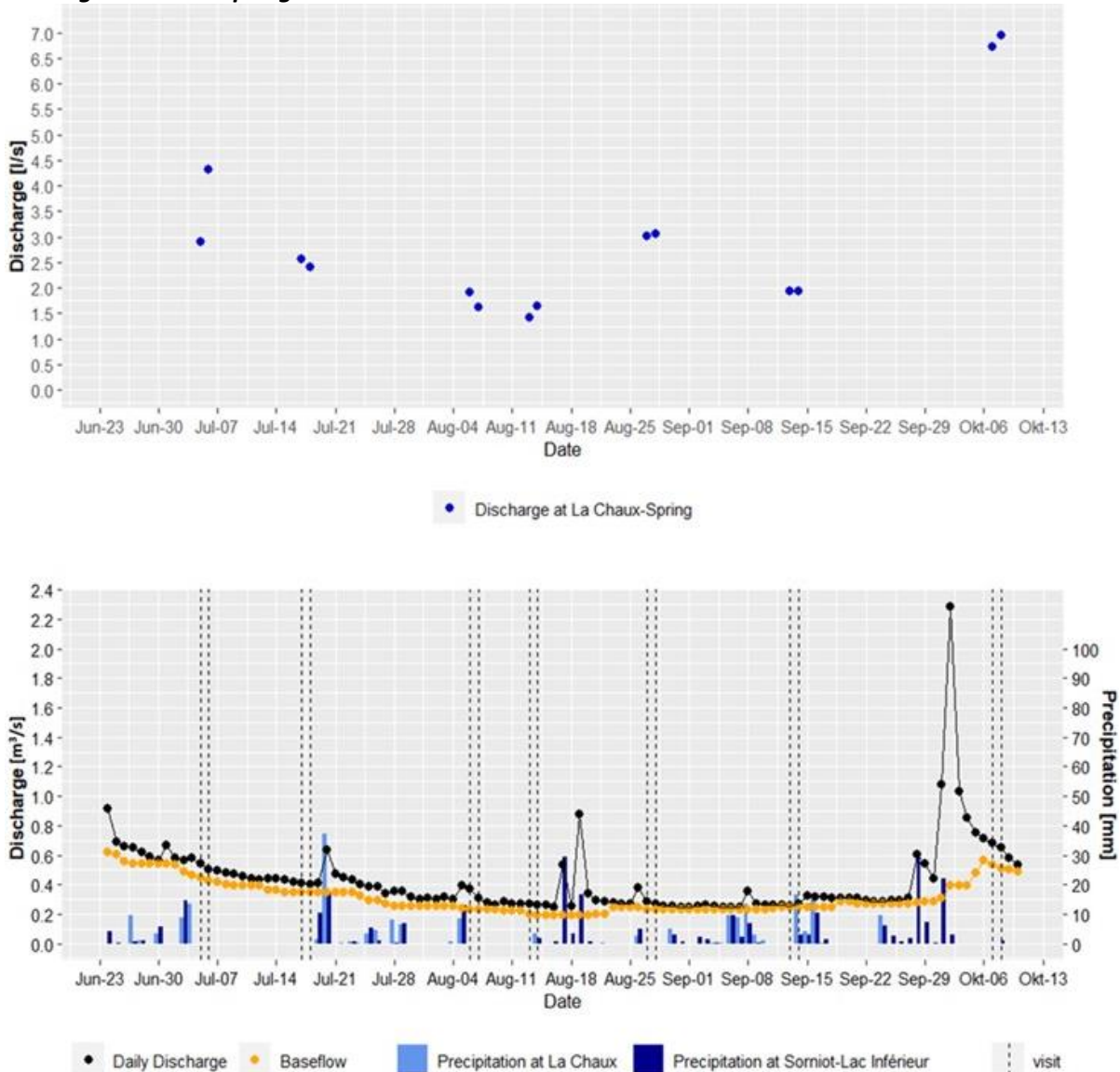


Figure 15: Comparison of discharge between La Chaux Spring and Mainstream. The discharge at the La Chaux Spring is illustrated over the research period (top), determined by salt dilution measurements, the overall discharge as well as the baseflow of the mainstream and, additionally, the daily amount of precipitation measured at both, the La Chaux and the Sorniot-Lac Inférieur, weather stations over the research period (bottom) are illustrated.

The **La Chaux Spring** mimics the mainstream discharge and its baseflow during the fifth sampling campaign, when hardly any changes can be identified. In contrast to the mainstream, an increase of discharge at the La Chaux Spring is observed during the first and last sampling campaign. Identically to the other springs, there is an increase of discharge during the fourth sampling campaign. Finally, the spring discharge decreases during the second and third sampling campaign, which corresponds in the latter case to the mainstream discharge but not to the mainstream baseflow. During the sixth sampling campaign, equal conditions of the spring discharge within the campaign can be noticed, which, however, is in contrast to the mainstream overall discharge, but it corresponds to the baseflow behavior.

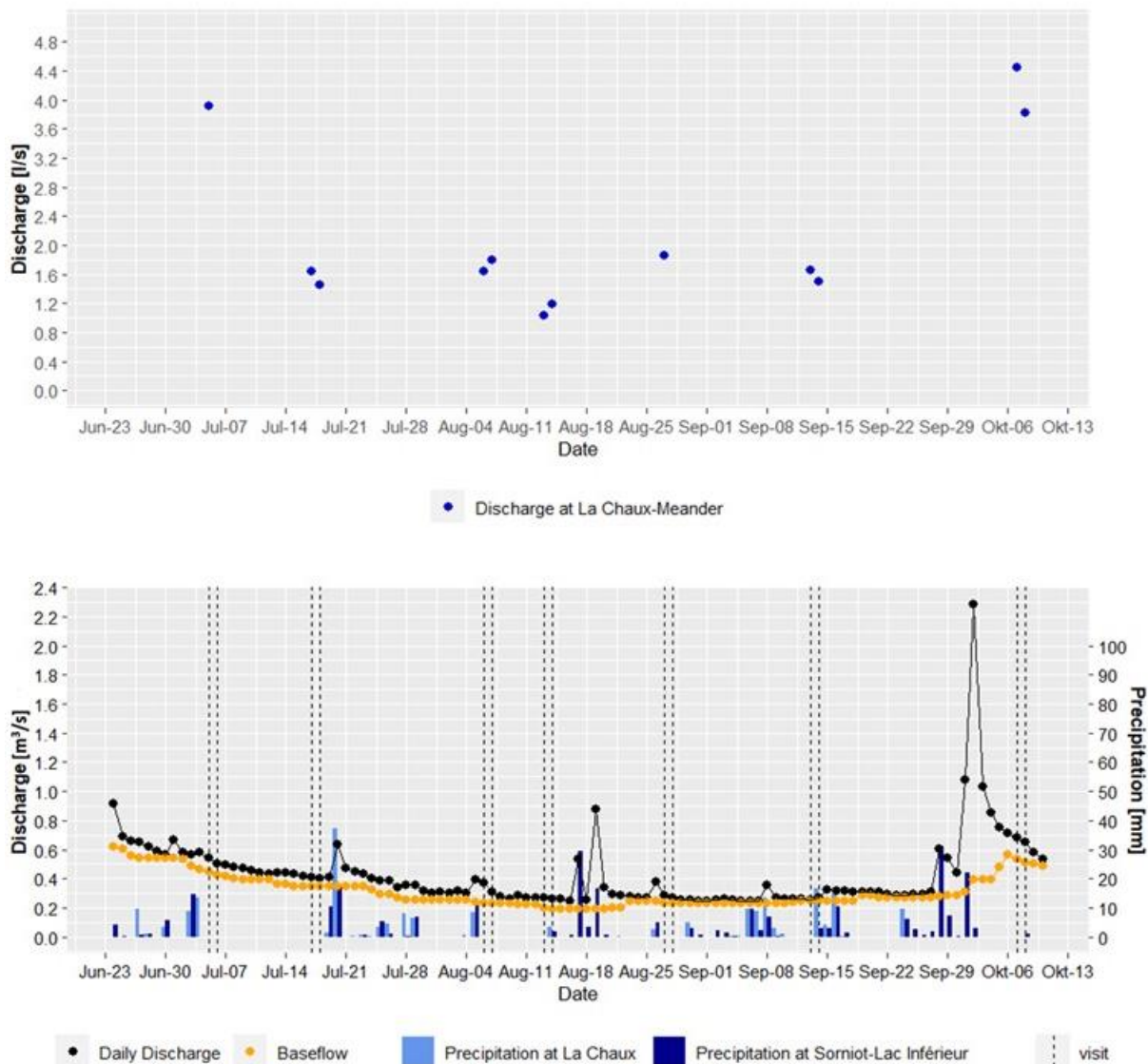
Discharge La Chaux Meander vs Mainstream

Figure 16: Comparison of discharge between La Chaux Meander and Mainstream. The discharge at the La Chaux Meander is illustrated over the research period (top), determined by salt dilution measurements, the overall discharge as well as the baseflow of the mainstream and, additionally, the daily amount of precipitation measured at both, the La Chaux and the Sorniot-Lac Inférieur, weather stations over the research period (bottom) are illustrated.

The discharge at the **La Chaux Meander** mimics the mainstream discharge and baseflow during the last sampling campaign. The discharge at the spring increases during the third and fourth campaign, which is in contrast to the mainstream behavior, since the mainstream discharge decreases during the third campaign and during the fourth it remains equal. However, there was a precipitation event on the second day of the fourth sampling campaign and the days before the third sampling campaign precipitation events were recorded. Finally, there is a decline of discharge during the second and sixth sampling campaign, which is neither reflected in the mainstream discharge nor in its baseflow.

To sum up, the impact of precipitation on the spring discharge pattern varies depending on the sampling station. All springs, except the Grass Spring, reacted with a discharge increase to a precipitation event that happened on the second sampling day during the fourth sampling campaign, but the mainstream did then not show any changes in discharge. Additionally, when a series of precipitation events was recorded before the sampling campaigns, a discharge decrease at the Black-Blue Pipe Spring and at the Bridge Spring can be seen, corresponding to the discharge decrease of the mainstream.

However, one the La Chaux Spring, Grass Spring and the La Chaux Meander react differently to precipitation events that occurred previously to the sampling dates, since they show a discharge increase, while the discharge of the mainstream is still decreasing or no changes could be identified. What can also be observed is that the discharge at the La Chaux Spring and the La Chaux Meander shows a decrease despite the fact that no precipitation events were recorded before.

Ultimately, the analysis of the above-explained discharge pattern of a sampling station within a sampling campaign is summarized in Table 7 and it is also highlighted in how many cases the springs mimic the overall discharge and the baseflow of the mainstream per sampling campaign as well as per sampling station.

When considering the number of sampling campaigns (SC) in which the springs mimic the overall discharge or the baseflow of the mainstream, spatial differences are noticed (see Table 7, last two rows). The discharge pattern of the Black-Blue Pipe Spring as well as of the Grass Spring corresponds in 4 out of 7 sampling campaigns in case of the Black-Blue Pipe Spring to the overall discharge and in case of the Grass Spring to the baseflow of the mainstream. Then, the discharge pattern of the Bridge Spring corresponds in 3 out of 7 sampling campaigns to the overall discharge as well as to the baseflow of the mainstream. In contrast to those springs, the discharge pattern of the La Chaux Spring only corresponds in 2 out of 7 sampling campaigns to the overall discharge as well as to the baseflow of the mainstream. Additionally, the discharge pattern of the La Chaux Meander corresponds in only one out of five sampling campaigns to the overall discharge as well as to the baseflow of the mainstream, while it needs to be highlighted that the discharge pattern could only be analysed during five sampling campaigns, since during two sampling campaigns only one discharge value was determined. Temporal differences between the sampling campaigns are noticed when analysing the results of by how many sampling stations (ST) the discharge or the baseflow pattern of the mainstream was mimicked (see Table 7, last two columns). During some campaigns the overall discharge as well as the baseflow pattern of the mainstream are mimicked by the springs to a large extent such as during the last sampling campaign, whereas during other sampling campaigns the analysed discharge situations only mimic the mainstream discharge pattern to a moderate or even little extent, such as, for instance, during the second, fourth or fifth sampling campaign. In addition, during the sixth sampling campaign the discharge of the baseflow is mimicked to a larger extent than the mainstream overall discharge, whereas during the other sampling campaigns no differences between mainstream and baseflow are noticed.

Table 7: Summary of spring and mainstream discharge pattern during a sampling campaign. The discharge pattern of the springs, of the mainstream as well as of the mainstream baseflow is assessed during a sampling campaign, while a discharge decrease (D) is illustrated in orange, a discharge increase in blue and an equivalent discharge (E) in yellow. Then, it is calculated how often the overall discharge as well as the baseflow of the mainstream were mimicked per sampling station (ST) and per sampling campaign (SC).

	Black-Blue Pipe Spring	Grass Spring	Bridge Spring	La Chaux Spring	La Chaux Me-ander	River Discharge	River Baseflow	Mimicry of River Dis-charge per SC	Mimicry of River Baseflow per SC
5/6 July	D	I	D	I	NA	D	D	2/4	2/4
17/18 July	E	D	I	D	D	E	E	1/5	1/5
6/7 August	D	I	E	D	I	D	E	2/5	1/5
13/14 August	I	E	I	I	I	E	E	1/5	1/5
27/28 August	D	E	D	E	NA	E	E	2/4	2/4
13/14 September	D	E	I	E	D	I	E	1/5	2/5
7/8 October	D	D	D	I	D	D	D	4/5	4/5
Mimicry of River Discharge per ST	4/7	3/7 SC	3/7 SC	2/7 SC	1/5 SC				
Mimicry of River Baseflow per ST	3/7 SC	4/7 SC	3/7 SC	2/7 SC	1/7 SC				

According to the definition of the baseflow, its amount corresponds to the sum of the discharge of all springs, since it reflects the amount of groundwater. Thus, in Figure 17 the percentage to which extent all the monitored springs contribute to the mainstream baseflow is illustrated. Overall, the springs contribute to a small amount to the mainstream baseflow. As a further matter, the springs contribute to a different extent to the mainstream baseflow during the sampling campaigns as well as over the whole research period. In addition, the contribution of the springs to the baseflow decreases from early July towards mid-July, then increases towards early August before it decreases again towards mid-August. Then, it increases again towards end-August and declines towards September before it finally increases towards October. When comparing the contributions of the individual sampling campaigns over the research period, the contributions in the range of about 3.25% and 3.5% are the highest, determined during the first sampling campaign in early July, during the fifth at the end of August as well as during the last sampling campaign in October. Finally, the lowest contribution of a bit more than 1.75% is determined during the fourth sampling campaign.

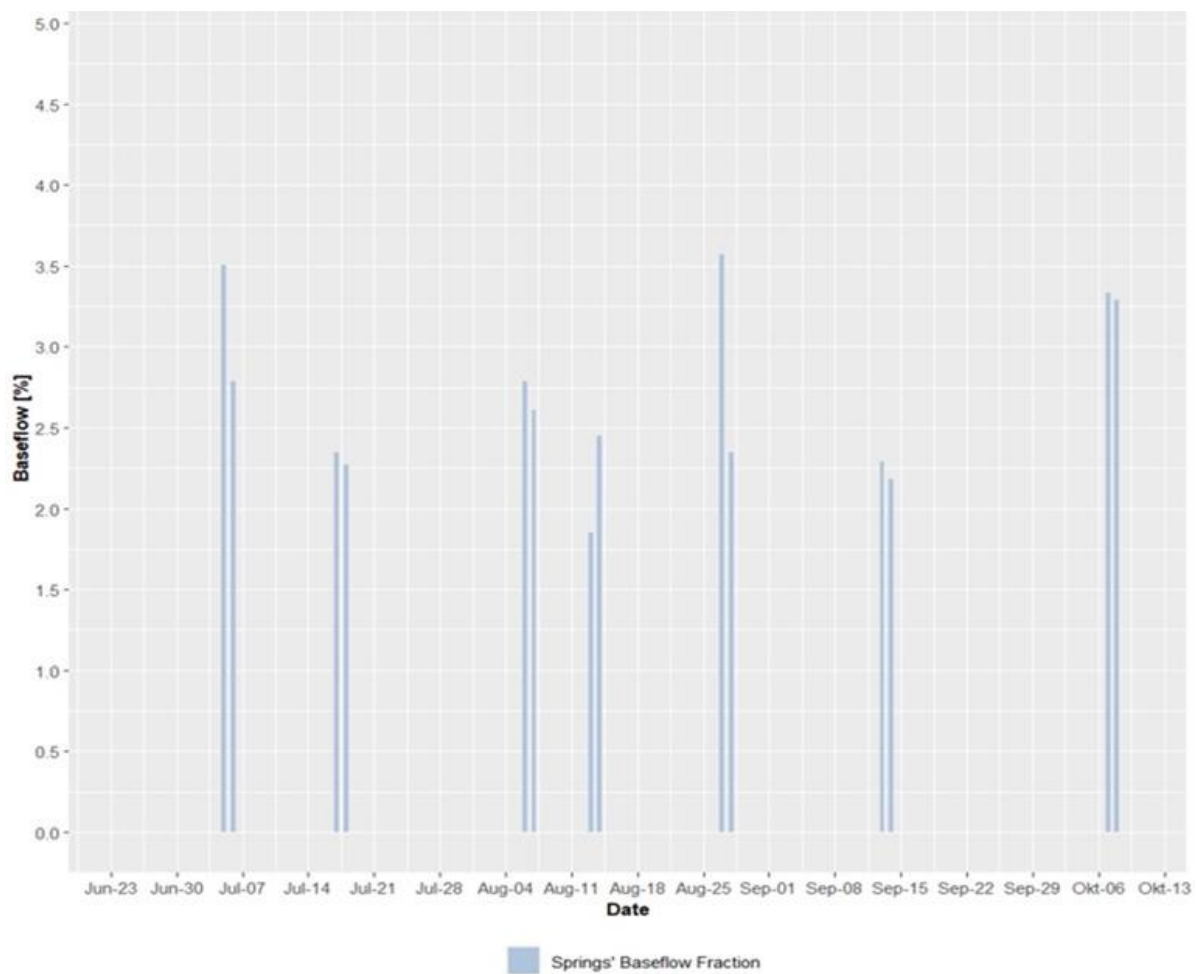


Figure 17: Springs' fraction of mainstream baseflow over research period. The proportion of the discharge of all the monitored springs to the baseflow of the mainstream is determined by adding up all the discharges of the springs per sampling date and then calculating the percentage of the baseflow.

Results of Calculation of Recession Constants

When considering the plot where the logarithmic discharge over the research period is illustrated (see Figure 18), the mainstream baseflow is identified not to continuously decrease over the recession period. Thus, this is an indication that several storages in the catchment contribute to the mainstream baseflow. As a consequence, four subperiods are defined (see Figure 18) based on the evolution of the mainstream baseflow, similarly to the recession study in the Pescadero Creek (see chapter 3.3), in order to gain an understanding of the different storage contributions. Particularly, the baseflow decreases from the beginning of the recession period, from 24th June towards 2nd August, which corresponds to the first subperiod and which is also the longest defined subperiod. The second subperiod starts on 23th August and ends on 4th September before the baseflow starts increasing from 5th September towards 18th September, which in fact corresponds to a baseflow expansion. The last recession subperiod lasts from 19th September until 28th September.

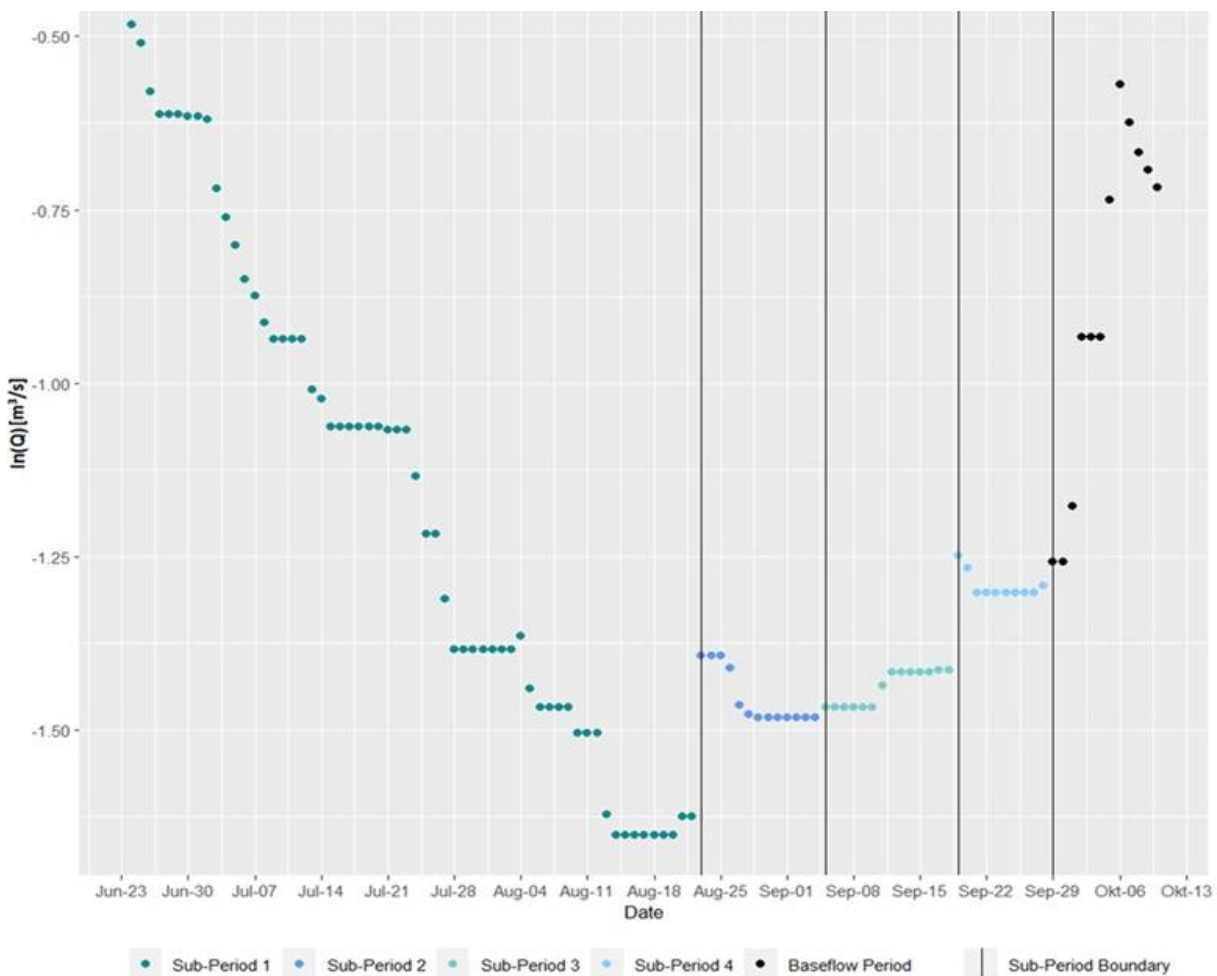


Figure 18: Baseflow of the Avançon de Nant over research period. Four subperiods are defined over the research period by analysing the evolution of the mainstream baseflow data.

Table 8 illustrates the equations, resulting from linear regression, and additionally, the corresponding recession constants. The R^2 values, indicating how well the model fits the data, are listed. The linear model fit is quite accurate for the first, second as well as for the third subperiods, whereas it is low for the last subperiod. The recession constants reflect the rate of decrease over discharge of the corresponding period. Thus, the first period has the lowest recession constant and the last the highest (see Figure 18). However, the positive alpha in the third period highlights that there is an expansion happening within the overall recession period and thus, no recession constant was calculated.

Table 8: Recession constants of the mainstream baseflow per subperiod. The recession constants are defined by $1/\alpha$, while α corresponds to the slope of the equation, which is the result of linear regression of the discharge data.

Subperiod	Equation	R ²	Alpha	Recession Constant 1/alpha [d]
subperiod 1	$y = -0.0203x + 908.63$	0.9744	-0.0203	49.26
subperiod 2	$y = -0.0087x + 389.71$	0.7205	-0.0087	114.94
subperiod 3	$y = 0.0056x - 250.38$	0.8132	0.0056	-
subperiod 4	$y = -0.0039x + 173.93$	0.3883	-0.0039	256.41

Figure 19 shows which springs follow the temporal pattern of the subperiods, based on the evolution of the mainstream baseflow over the recession period. The Bridge, the Grass and the La Chaux Springs show in the first subperiod recession as well, whereas the Black-Blue Pipe Spring and the La Chaux Meander show two recessions within the first subperiod. The following subperiods are meaningless for the recession constant analysis of the springs since there is only one sampling campaign per subperiod and thus, no discharge evolution within a period is assessed.

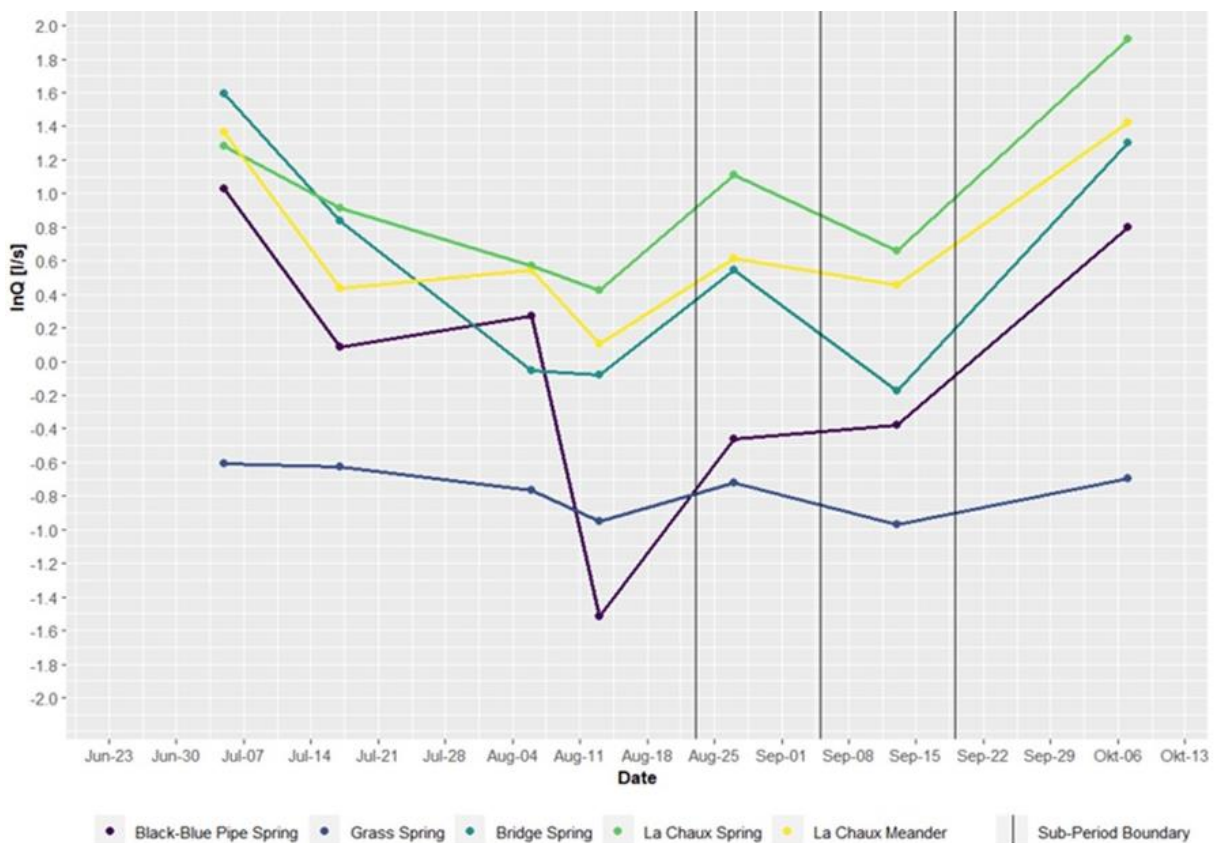


Figure 19: Mean spring discharge of a sampling campaign per sampling station in the corresponding subperiod. The mean discharge of a sampling campaign was calculated per spring and additionally, the recession subperiod boundaries, which were defined by the analysis of the evolution of the mainstream baseflow, are illustrated.

Table 9 illustrates the equations, resulting from linear regression, of the first subperiod per spring and the corresponding recession constants. The R² values, indicating how well the model fits the data, are listed. The linear model fit is quite accurate for all the springs, where a R² value exists, but in some cases the R² value corresponds to NA, since it was only a model fit between two points. When considering the recession constants of the springs, the Black-Blue Pipe Spring shows the lowest recession constant, followed by the La Chaux Meander. The Bridge Spring has a recession constant of 22.78 days, while the recession constant of the La Chaux Spring is more than the double of the one of the Bridge

Spring. Finally, the Grass Spring has a recession constant of almost 122 days and thus, it shows by far the largest recession constant.

Table 9: Recession constants of the springs for the first recession subperiod. The recession constants are defined by $1/\alpha$, while α corresponds to the slope of the equation, which is the result of linear regression of the discharge data.

Spring	Equation	R ²	Alpha	Recession Constant 1/alpha [d]
Black-Blue Pipe Spring	$y = -0.142x + 6358.7$	NA	-0.142	7.04
	$y = -0.1558x + 6977.2$	NA	-0.1558	6.42
Grass Spring	$Y = -0.0082x + 366.04$	0.8521	-0.0082	121.95
Bridge Spring	$Y = -0.0439x + 1964.3$	0.9659	-0.0439	22.78
La Chaux Spring	$Y = -0.0211x + 946.44$	0.9834	-0.0211	47.39
La Chaux Meander	$Y = -0.0775x + 3467.5$	NA	$a = -0.0775$	12.90
	$Y = -0.0622x + 2785.9$	NA	$a = -0.0622$	16.08

4.3 Water Quality Variables

In this subchapter, the spatial variation between the measurement stations in the Vallon de Nant and the temporal variation of the water quality variables such as of the electrical conductivity, the temperature, the pH values as well as of some ions and stable isotopes are presented.

Electrical Conductivity (EC)

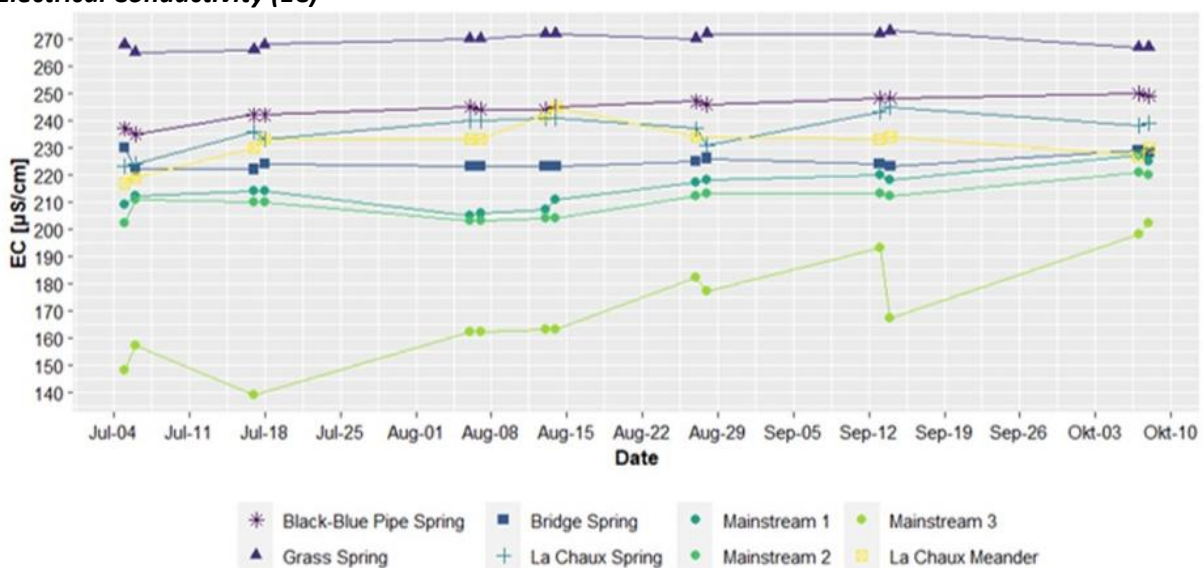


Figure 20: Electrical conductivity (EC) over research period. The EC, measured at the different sampling stations in the Vallon de Nant catchment, is illustrated over the research period from early July until early October 2022.

Temporal Variation

Overall, the temporal variation (see Figure 20) of the EC is lower at the springs than it is in the mainstream, whereas in the latter case it depends on the measurement station. There is much more temporal variation recorded at the top station along the mainstream than at the lowest station. Regarding the EC values of the mainstream, the values recorded at the Mainstream 1 and the Mainstream 2 decrease towards mid-August and then continue increasing towards October, whilst the EC values at the Mainstream 3 are then constant.

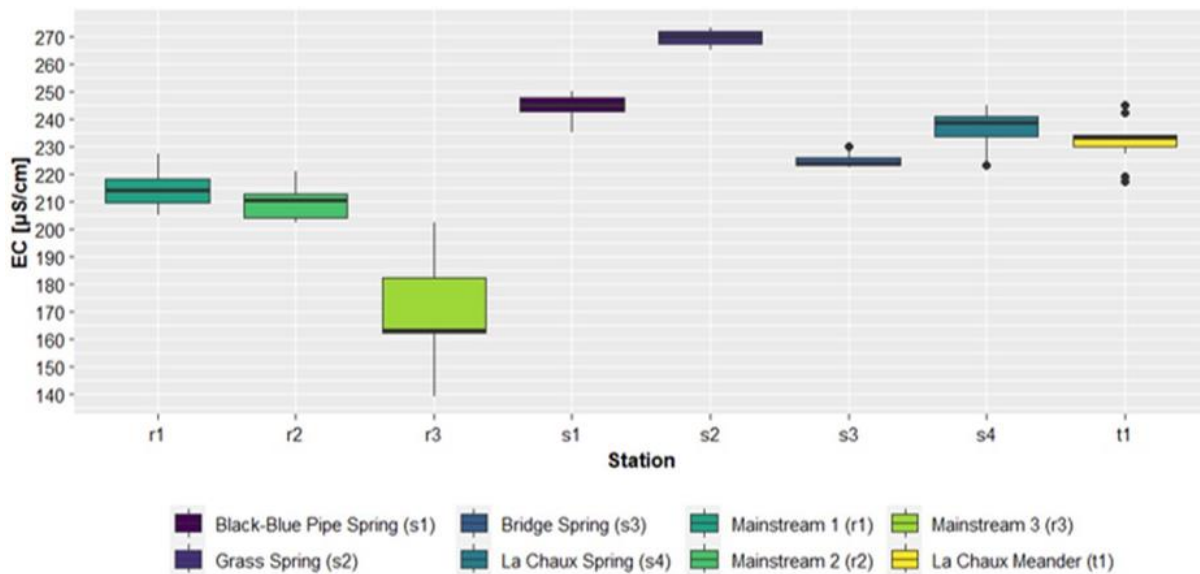


Figure 21: Boxplots of electrical conductivity (EC) per sampling station. The EC, measured during the research period from early July until early October 2022, is illustrated per sampling station in the Vallon de Nant catchment.

Spatial Variation

At the springs as well as at the tributary higher median EC values are measured than at the stations along the mainstream (see Figure 21). The Grass Spring shows the highest median EC value, followed by the Black Blue Pipe Spring. The La Chau Meander as well as the La Chau Spring have similar median values. The Bridge Spring has the lowest median EC among the springs. When considering the median EC values measured along the mainstream, the EC is the lowest at the top station and then the EC increases with decreasing elevation.

Outliers

There is an outlier at the Bridge Spring as well as the La Chau Spring, at the former of about 230 µS/cm and at the latter of about 223 µS/cm. Both values are recorded on 5th July 2022. Besides, there are several outliers at the La Chau Meander of about 217 µS/cm and 219 µS/cm measured on 5th and 6th July 2022 and of 242 µS/cm and 245 µS/cm recorded on 13th and 14th August 2022.

Results of Statistical Significance Test

The results of the statistical significance test (Tukey HSD), assessing between which sampling stations a significant difference in the mean values of the electrical conductivity variable exists, indicate that there are significant differences between almost all pairs of sampling stations, apart from the following pairs: Mainstream 1/Mainstream 2, La Chau Spring/Black-Blue Pipe Spring, La Chau Meander/Bridge Spring and La Chau Meander/La Chau Spring.

Table 10: Results of the statistical significance test of the electrical conductivity. The p-values of the electrical conductivity between the different pairs of sampling stations are determined by the Tukey Honest Significant Differences (Tukey HSD) test.

Mainstream 1 (r1)								
Mainstream 2 (r2)	not significant							
Mainstream 3 (r3)	p<0.001	p<0.001						
Black-Blue Pipe Spring (s1)	p<0.001	p<0.001	p<0.001					
Grass Spring (s2)	p<0.001	p<0.001	p<0.001	p<0.001				
Bridge Spring (s3)	p<0.05	p<0.001	p<0.001	p<0.001	p<0.001			
La Chaux Spring (s4)	p<0.001	p<0.001	p<0.001	not significant	p<0.05	p<0.05		
La Chaux Meander (t1)	p<0.001	p<0.001	p<0.001	p<0.05	p<0.001	not significant	not significant	
	r1	r2	r3	s1	s2	s3	s4	t1

Temperature

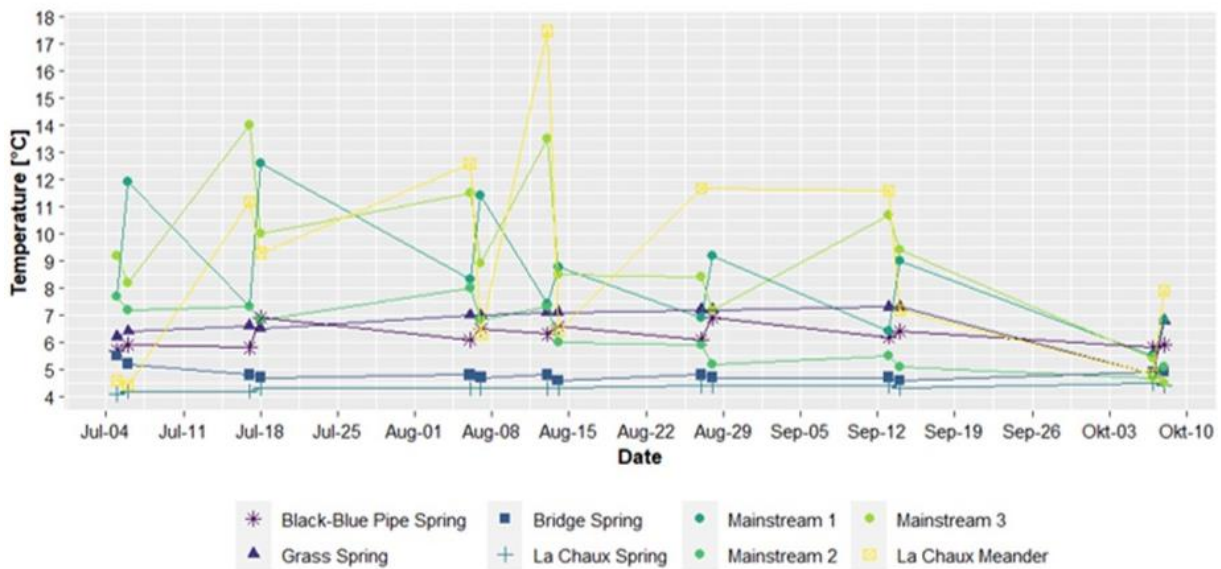


Figure 22: Temperature over research period. The temperature, measured at the different sampling stations in the Vallon de Nant catchment, is illustrated over the research period from early July until early October 2022.

Temporal Variation

The temporal variation of the temperature (see Figure 22) is much lower at the springs than it is at the tributary and at the stations along the mainstream, while in the latter case the extent of variation also depends on the station. There is much more temporal variation recorded at the second and the third station along the mainstream than at the lowest station. During a sampling campaign the temperature is measured once in the afternoon and once in the morning in order to identify any diurnal changes. When considering the temperature values of the mainstream as well as of the tributary some time-of-day variations are observed. While the temperature of the springs is rather constant over time, the temperature of the mainstream decreases from early July until early October, whereas in between some increases are visible.

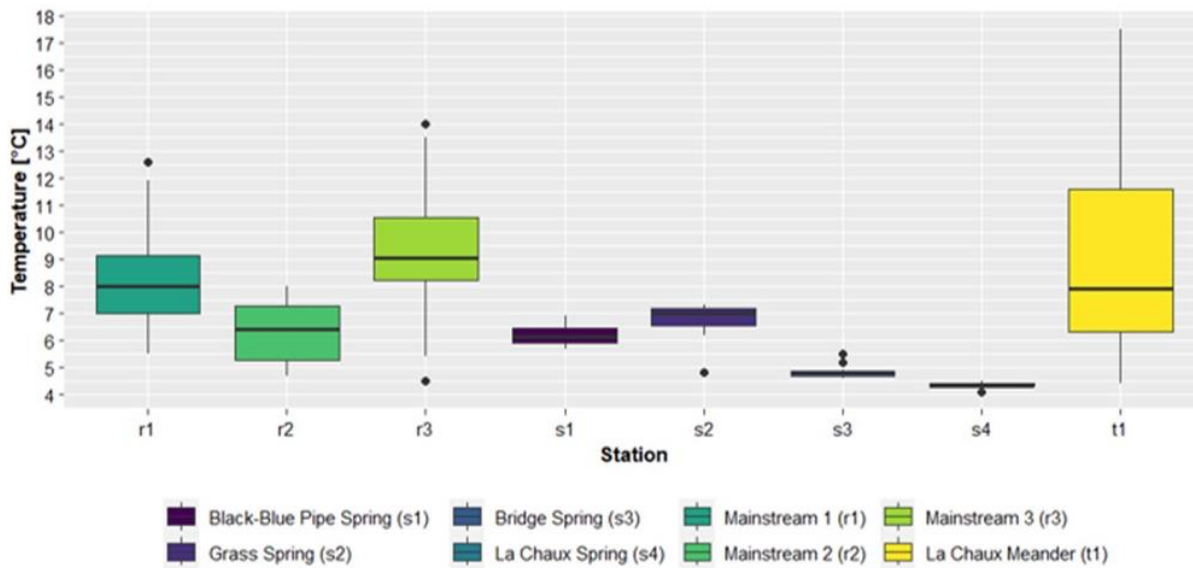


Figure 23: Boxplots of temperature per sampling station. The temperature, measured during the research period from early July until early October 2022, is illustrated per sampling station in the Vallon de Nant catchment.

Spatial Variation

The La Chau Spring, followed by the Bridge Spring, shows the lowest median temperature (see Figure 23), while the median of the Black-Blue Pipe as well as of the Grass Spring almost corresponds to the one of the Mainstream 2. The highest median temperature is measured at the Mainstream 3, whilst the temperature of the La Chau Meander almost corresponds to the Mainstream 1.

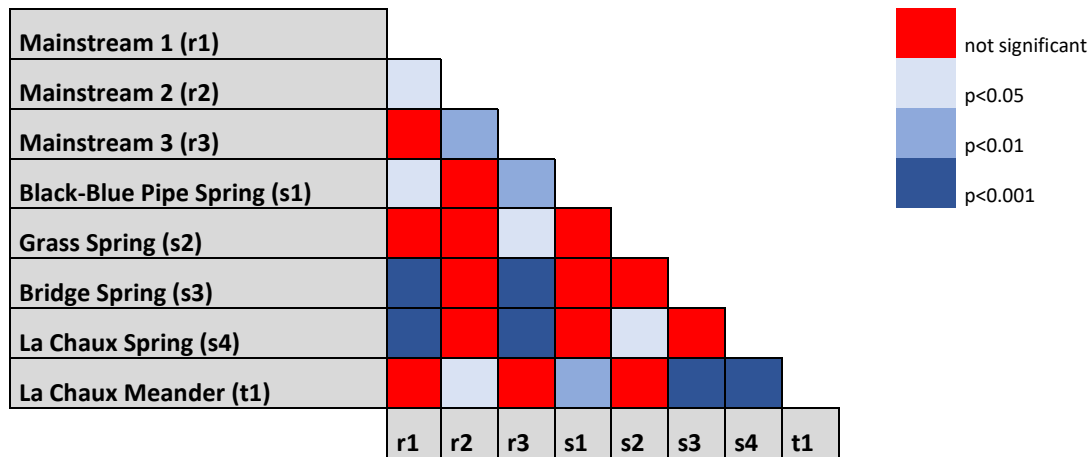
Outlier

The temperature of 12.5°C, measured at the Mainstream 1 on 6th July 2022, is an outlier. In addition, a temperature of 4.5°C and of 14°C is recorded at the Mainstream 3 on 8th October 2022 and on 13th August 2022 respectively. Referring to the outliers at the springs, there is one of 4.8°C recorded at the Grass Spring on 7th October 2022; one of 5.5°C and of 5.2°C at the Bridge Spring measured on 5th and 6th July 2022 and at last, another outlier of 4.5°C at the La Chau Spring on 7th October 2022.

Results of Statistical Significance Test

The results of the statistical significance test (Tukey HSD), assessing between which sampling stations a significant difference in the mean values of the temperature variable exists, indicate that there are significant differences between the springs and the Mainstream 1 as well as the Mainstream 3, while the mean temperature of the Mainstream 2 is not significantly different from the springs, but from the La Chau Meander and the Mainstream 3. In addition, the mean temperature values of all springs, apart from the Grass Spring, are significantly different from the La Chau Meander.

Table 11: Results of the statistical significance test of the temperature. The p-values of the temperature between the different pairs of sampling stations are determined by the Tukey Honest Significant Differences (Tukey HSD) test.



Long-Term Temperature Measurement

Whilst the temperature values in the Figures 22 and 23 reflect the water temperature at a specific time, the temperature below (see Figure 24) illustrates the water temperature over the whole research period. However, the continuous temperature measurements confirm the above-described observations of the temperature evolution over the recession period. The temperature at the springs shows little variation in comparison to the temperature recorded at the La Chaux Meander. The temperature curves of the springs are even slightly concave, indicating a light increase towards mid-August and then decrease towards October. At the La Chaux Meander the temperature increases towards mid-August and then, aside from the abrupt decline at the end of August, it gradually decreases towards October. Nonetheless, noise is observed, particularly, at the La Chaux Spring between mid-July and early August, which is explained in details in chapter 5.3.

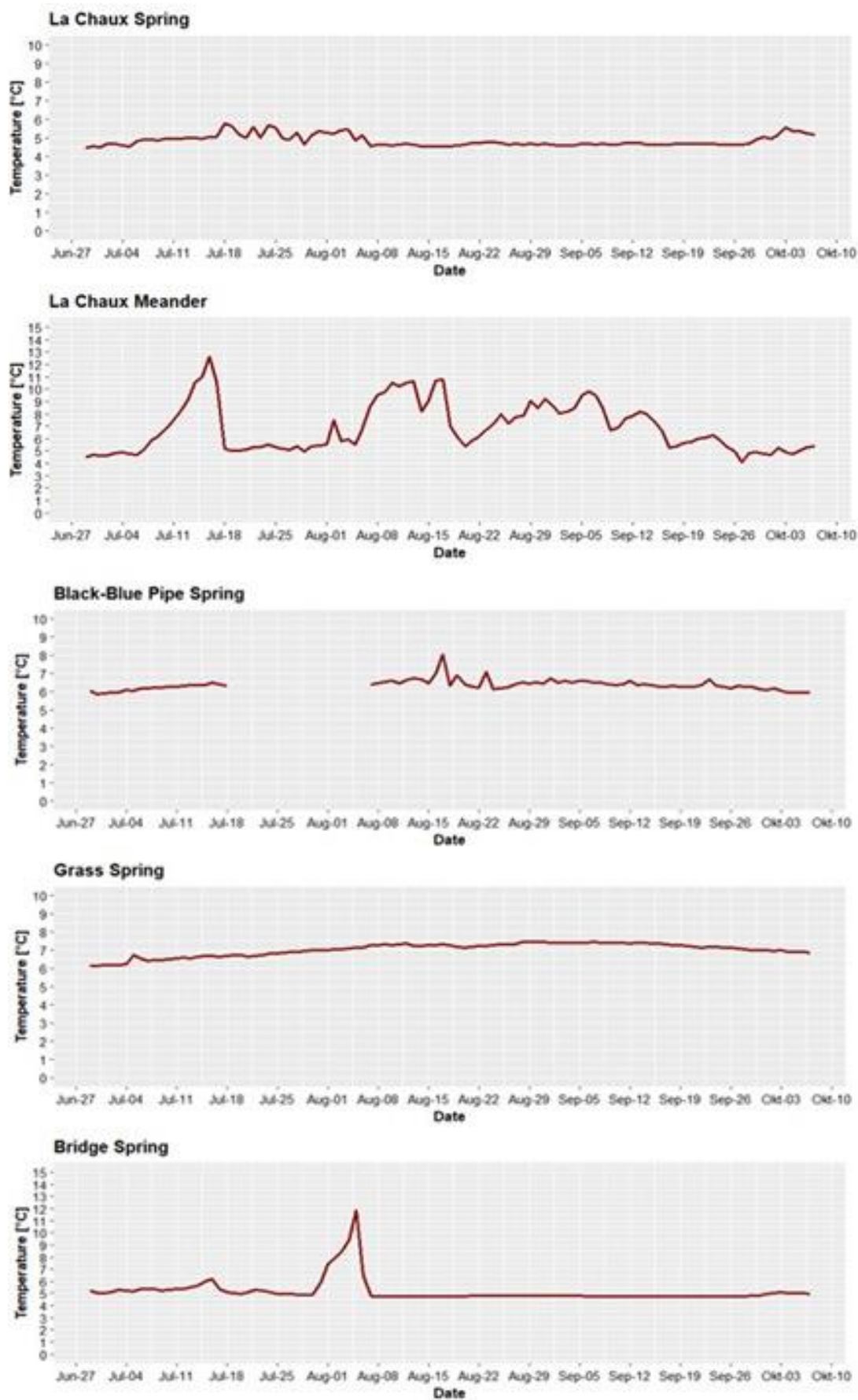


Figure 24: Continuous temperature measurement at the springs over research period. The temperature was continuously measured by temperature logger (HOBO Pendant Temperature/Light 64K Data Loggers; Onset, Bourne, United States) at all the monitored springs in the Vallon de Nant catchment over the research period from early July until early October 2022

pH Value

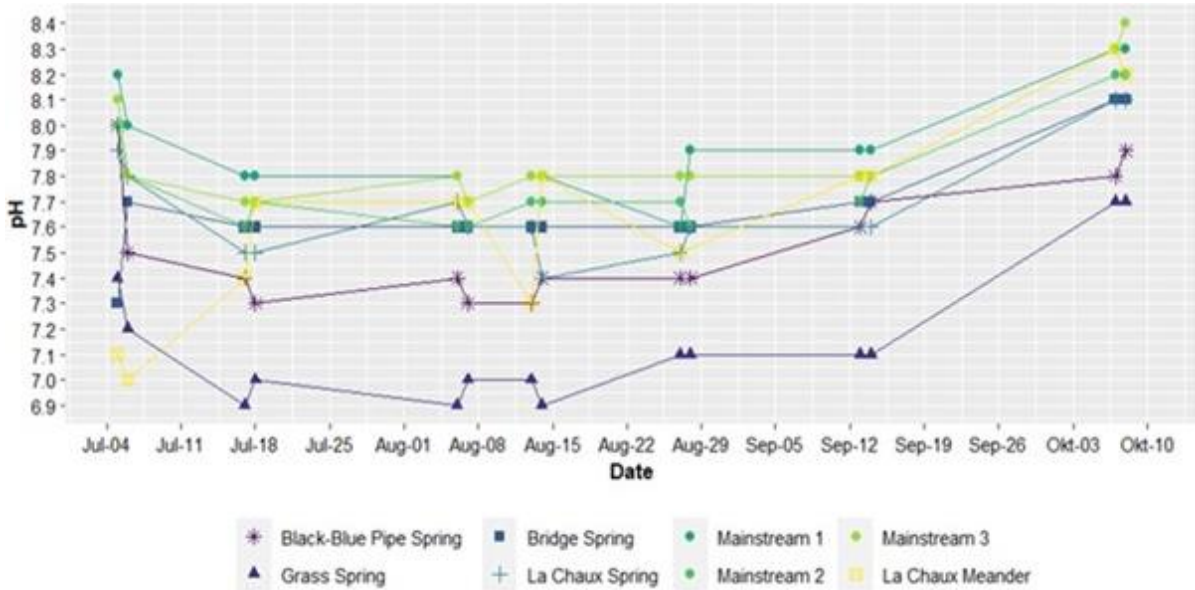


Figure 25: pH value over research period. The pH value, measured at the different sampling stations in the Vallon de Nant catchment, is illustrated over the research period from early July until early October 2022.

Temporal Variation

Regarding the temporal variation (see Figure 25) the pH value decreases towards the second sampling campaign and then it is more or less constant before it increases again towards October. However, the La Chaux Meander, the La Chaux and the Black-Blue Pipe Spring vary more than the Bridge or the Grass Spring. When considering the values recorded from the mainstream, some temporal variations at the Mainstream 1 and at the Mainstream 2 are identified, whereas at the Mainstream 3, each value that differs from 7.8 is recorded as an outlier.

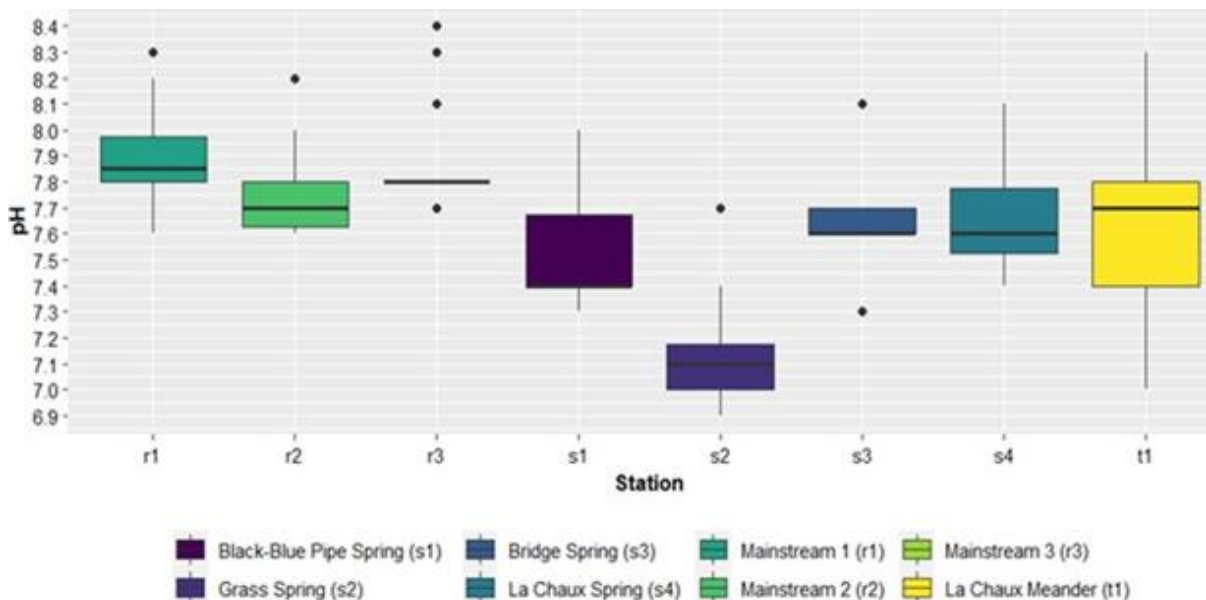


Figure 26: Boxplots of pH value per sampling station. The pH value, measured during the research period from early July until early October 2022, is illustrated per sampling station in the Vallon de Nant catchment.

Spatial Variation

There is little spatial variation among all the measurement stations (see Figure 26) since they all have median pH values between 7.6 and 7.8, aside from that of the Black-Blue Pipe and the Grass Spring. A median value of about 7.4 is determined at the Black-Blue Pipe Spring and at the Grass Spring of about 7.1. Additionally, the stations along the mainstream tend to have higher values than the springs.

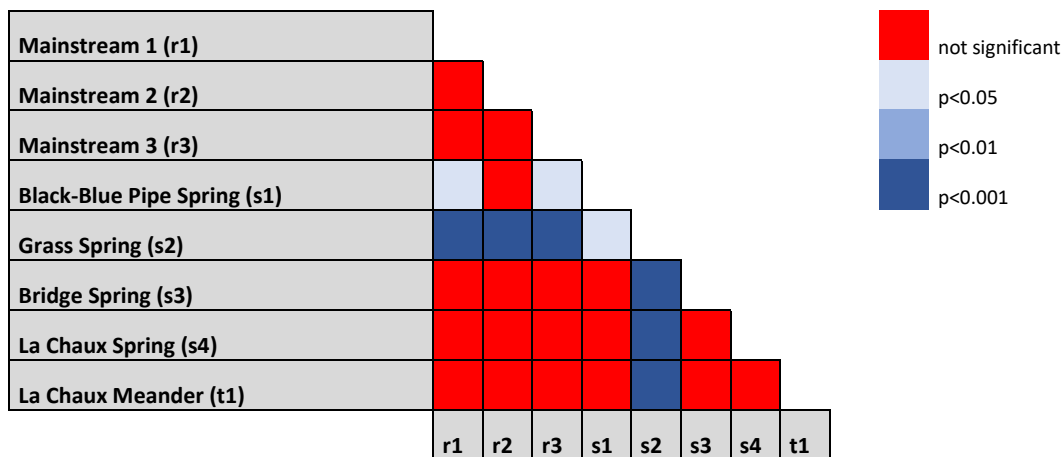
Outliers

Most outliers are recorded during the last sampling campaign: 8.3 at the Mainstream 1, 8.2 at the Mainstream 2, 8.3 and 8.4 at the Mainstream 3, 7.7 at the Grass Spring. In addition, there are several outliers recorded at the Mainstream 3, in particular, each value that differs from 7.8 is considered as an outlier, which is the case on 5th of July 2022, when a value of 8.1 is recorded, on 17th and 18th July 2022 as well as on 7th August 2022, when a pH value of 7.7 is measured.

Results of Statistical Significance Test

The results of the statistical significance test (Tukey HSD), assessing between which sampling stations a significant difference in the mean values of the pH variable exists, indicate that there are particularly significant differences between the Grass Spring and all the other sampling stations as well as between the following pairs: Mainstream 1/Black-Blue Pipe Spring and Mainstream 3/ Black-Blue Pipe Spring.

Table 12: Results of the statistical significance test of the pH value. The p-values of the pH values between the different pairs of sampling stations are determined by the Tukey Honest Significant Differences (Tukey HSD) test.



Anion – Fluoride

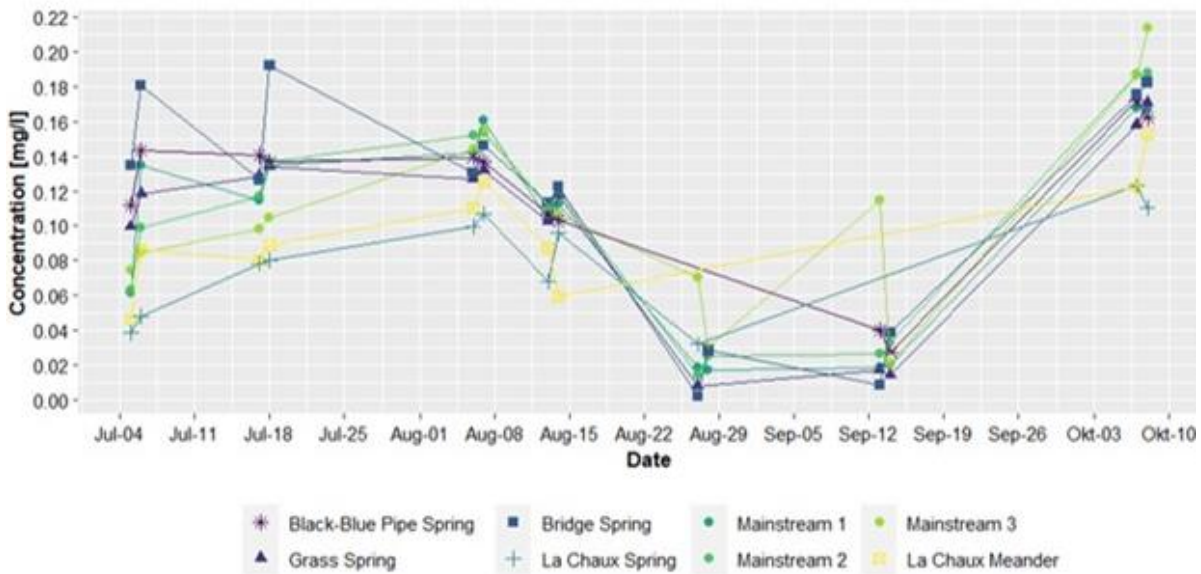


Figure 27: Fluoride concentration over research period. The fluoride concentration, determined by ion chromatography, is illustrated per sampling station in the Vallon de Nant catchment over the research period from early July until early October 2022.

Temporal Variation

The temporal variation (see Figure 27) is more pronounced than the spatial variation. There is a weak increase towards the beginning of August, then a strong decrease from end-August until mid-September and ultimately, another rise in concentration is recorded during the last sampling campaign. The fluoride concentrations vary stronger in the mainstream than at the springs apart from the Bridge Spring. Additionally, the fluoride concentration varies with the time of the day, which can be identified, for instance, at the Bridge Spring during the first and second sampling campaign or at the Mainstream 3 in September.

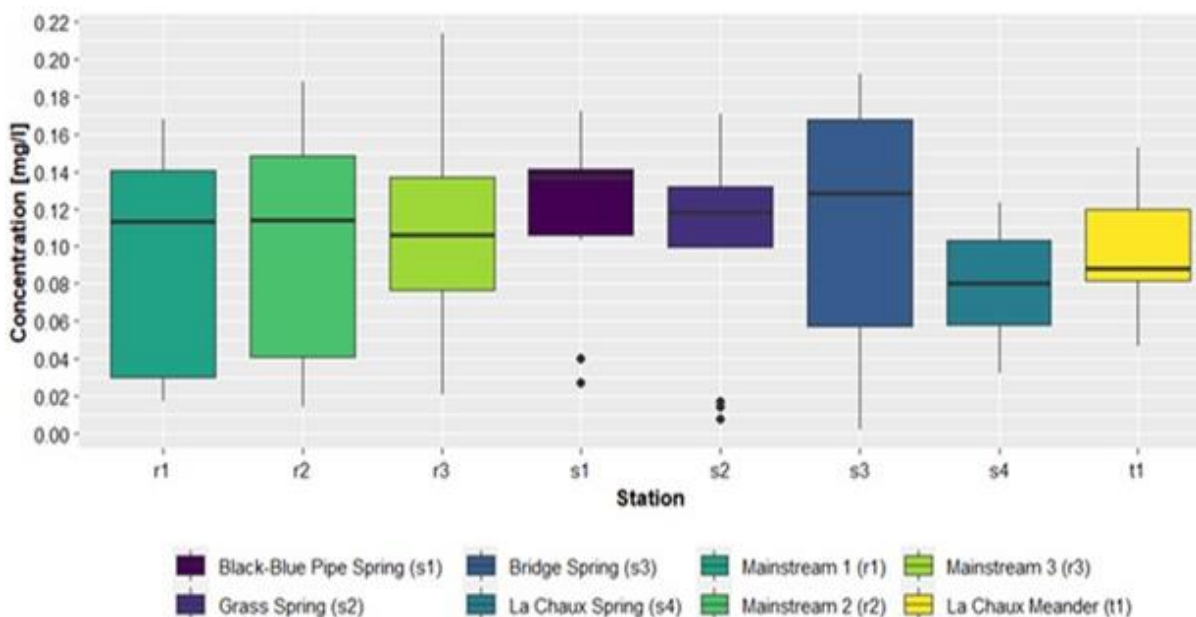


Figure 28: Boxplots of fluoride concentration per sampling station. The fluoride concentration, determined by ion chromatography for all the collected water samples during the research period from early July until early October 2022, is illustrated per sampling station in the Vallon de Nant catchment.

Spatial Variation

The median concentration of fluoride (see Figure 28) varies less among the stations along the mainstream than among the springs. The Black-Blue Pipe Spring shows the highest median concentration of about 0.14mg/l, followed by the Bridge and the Grass Spring, while at the La Chaux Spring the lowest concentration of about 0.08m/l is measured, which is slightly lower than the one of the La Chaux Meander.

Outlier

Outliers are recorded at the Black-Blue Pipe Spring on 13th and 14th September 2022 of 0.04 mg/l and 0.03 mg/l as well as at the Grass Spring on 27th August 2022 of 0.01mg/l and on 13th and 14th September 2022 of about 0.02mg/l.

Results of Statistical Significance Test

Sine the p-value of the one-way ANOVA test was larger than 0.05, no statistically significant difference of the fluoride mean concentrations between the sampling stations can be noticed.

Anion – Chloride

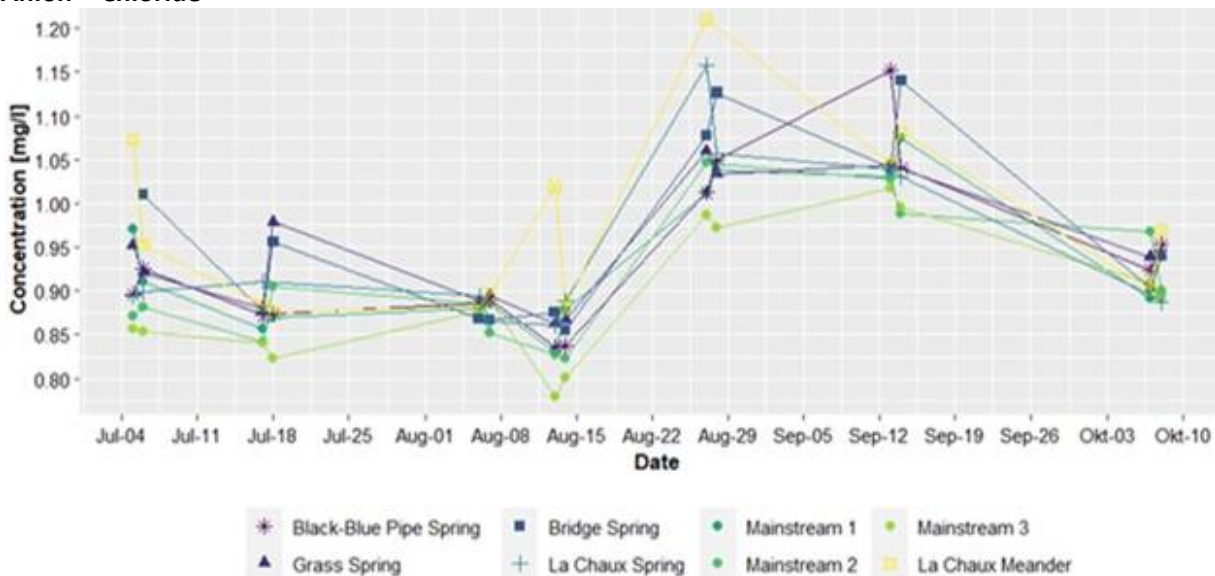


Figure 29: Chloride concentration over research period. The chloride concentration, determined by ion chromatography, is illustrated per sampling station in the Vallon de Nant catchment over the research period from early July until early October 2022.

Temporal Variation

The temporal variation (see Figure 29) is truly similar among all the sampling stations. The general pattern is that the chloride concentration decreases slightly towards mid-August and it increases again at the end of August before it decreases towards October. Occasionally, there are distinct variations during a sampling campaign and thus, depending on the time of the day.

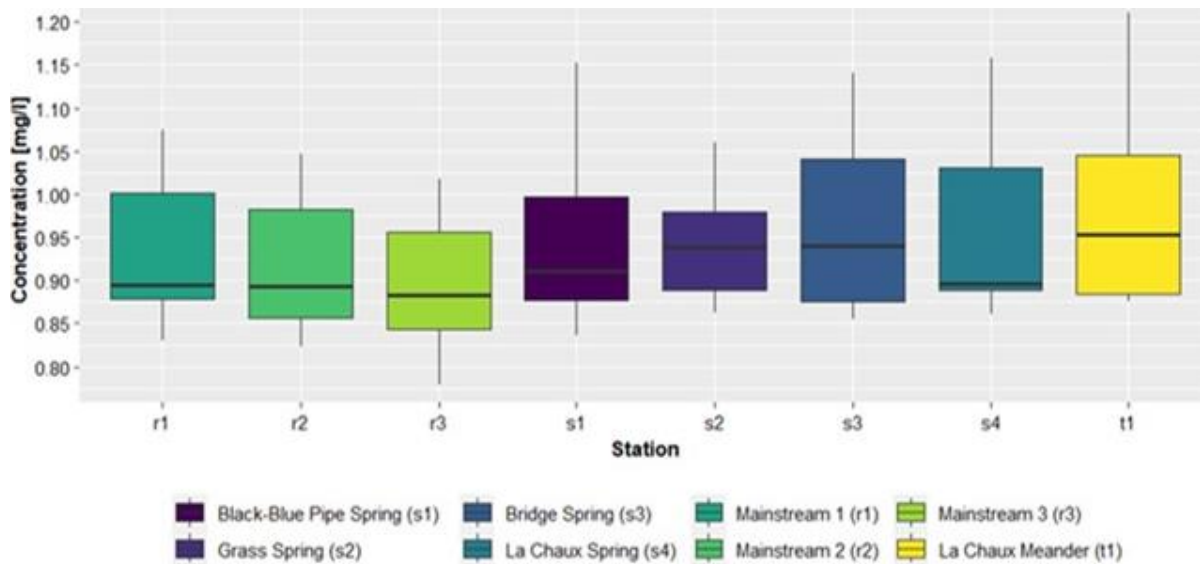


Figure 30: Boxplots of chloride concentration per sampling station. The chloride concentration, determined by ion chromatography for all the collected water samples during the research period from early July until early October 2022, is illustrated per sampling station in the Vallon de Nant catchment.

Spatial Variation

There is a very small spatial variation of the chloride concentration (see Figure 30) among the sampling stations. The median chloride concentrations of the stations along the mainstream are slightly lower than the ones of the springs apart from the La Chaux Spring, which shows a similar median concentration as the one of the Mainstream 1 and the Mainstream 2.

Results of Statistical Significance Test

Sine the p-value of the one-way ANOVA test was larger than 0.05, no statistically significant difference of the chloride mean concentrations between the sampling stations can be noticed.

Anion – Nitrite

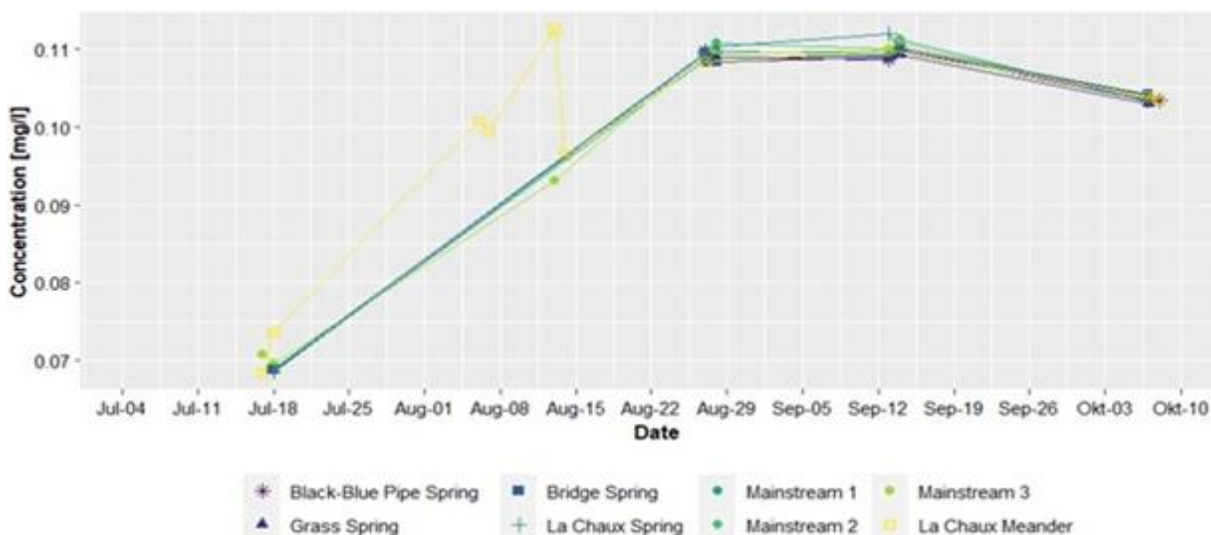


Figure 31: Nitrite concentration over research period. The nitrite concentration, determined by ion chromatography, is illustrated per sampling station in the Vallon de Nant catchment over the research period from early July until early October 2022.

Temporal Variation

There is a strong increase of the nitrite concentration from end-July towards end-August and from mid-September a slight decrease towards early October is noticeable (see Figure 31) Variations during a sampling campaign are not observable, apart from a small extent at the La Chaux Meander.

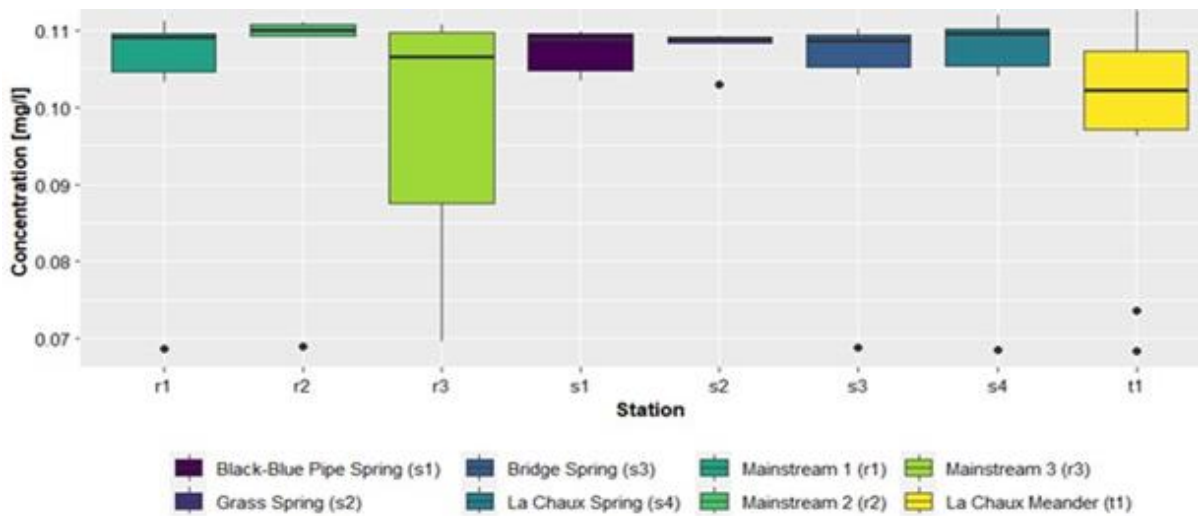


Figure 32: Boxplots of nitrite concentration per sampling station. The nitrite concentration, determined by ion chromatography for all the collected water samples during the research period from early July until early October 2022, is illustrated per sampling station in the Vallon de Nant catchment.

Spatial Variation

There is hardly any spatial variation (see Figure 32) of the nitrite concentration visible. All median nitrite concentrations are within the range of 0.105mg/l and 0.11mg/l apart from the one of the La Chaux Meander, which is slightly lower. In addition, not at all stations nitrite is measured during every sampling campaign, but at the La Chaux Meander and at the Mainstream 3 nitrite is observed more regularly than at the other stations.

Outliers

Outliers, which are recorded at the Mainstream 1, the Mainstream 2, the Bridge Spring and at the La Chaux Meander during the second sampling campaign, correspond to a smaller concentration than 0.07mg/l. Another outlier of about 0.1025mg/l is determined at the Grass Spring on 7th October 2022.

Results of Statistical Significance Test

Sine the p-value of the one-way ANOVA test was larger than 0.05, no statistically significant difference of the nitrite mean concentrations between the sampling stations can be noticed.

Anion - Nitrate

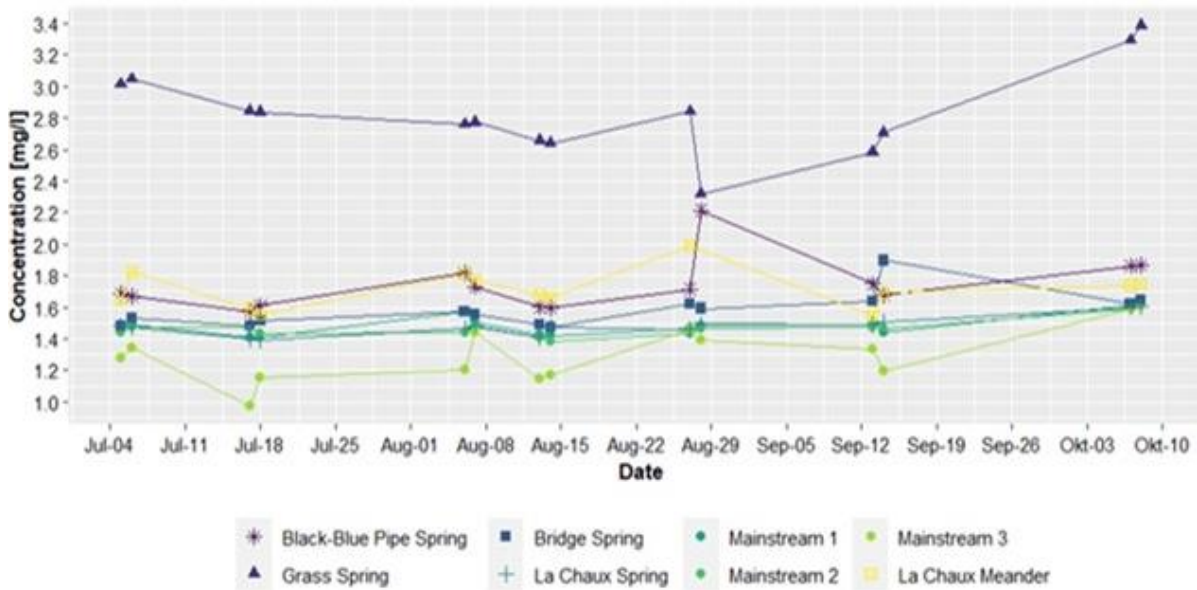


Figure 33: Nitrate concentration over research period. The nitrate concentration, determined by ion chromatography, is illustrated per sampling station in the Vallon de Nant catchment over the research period from early July until early October 2022.

Temporal Variation

The nitrate concentration is rather constant over time (see Figure 33), but the temporal variation is more pronounced at the Mainstream 3, the Black-Blue Pipe and the Grass Spring. There, the nitrate concentration increases towards October. Concentration variations, such as the decrease towards mid-August, can be noticed at all stations. Variations during a sampling campaign are occasionally visible, such as at the Grass and at the Black-Blue Pipe Spring at the end of August.

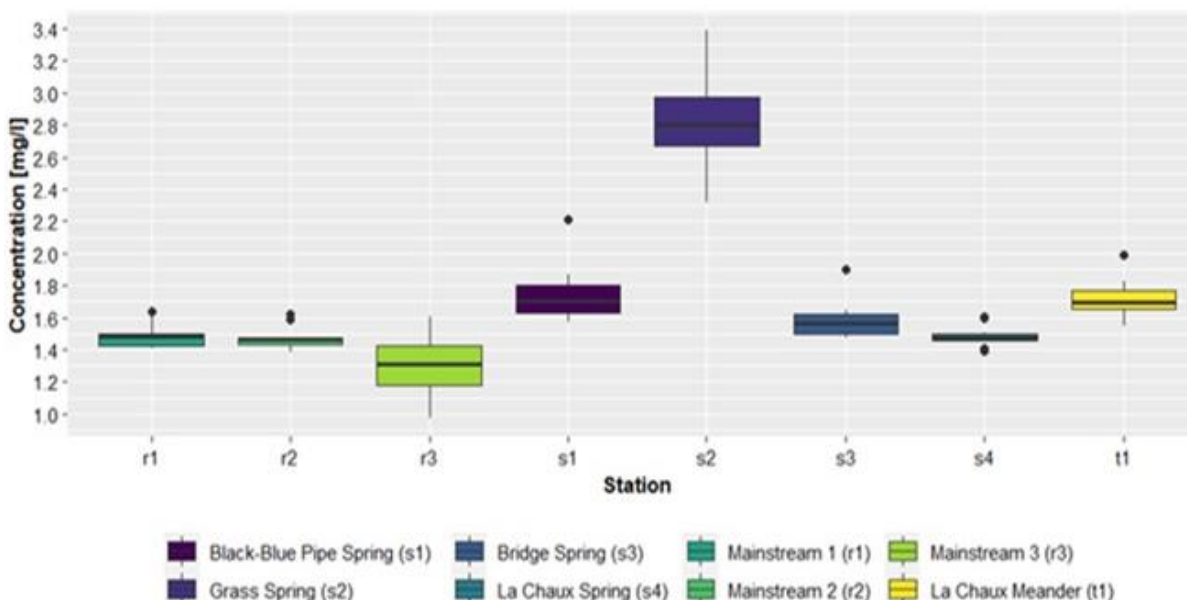


Figure 34: Boxplots of nitrate concentration per sampling station. The nitrate concentration, determined by ion chromatography for all the collected water samples during the research period from early July until early October 2022, is illustrated per sampling station in the Vallon de Nant catchment.

Spatial Variation

The spatial variation is limited among the sampling stations (see Figure 34). The median nitrate concentrations are lower at the stations along the mainstream than at the springs. However, the Grass Spring has the highest median nitrate concentration of about 2.8mg/l, followed by the Black-Blue Pipe Spring, while the lowest one is recorded at the Mainstream 3 of about 1.3mg/l.

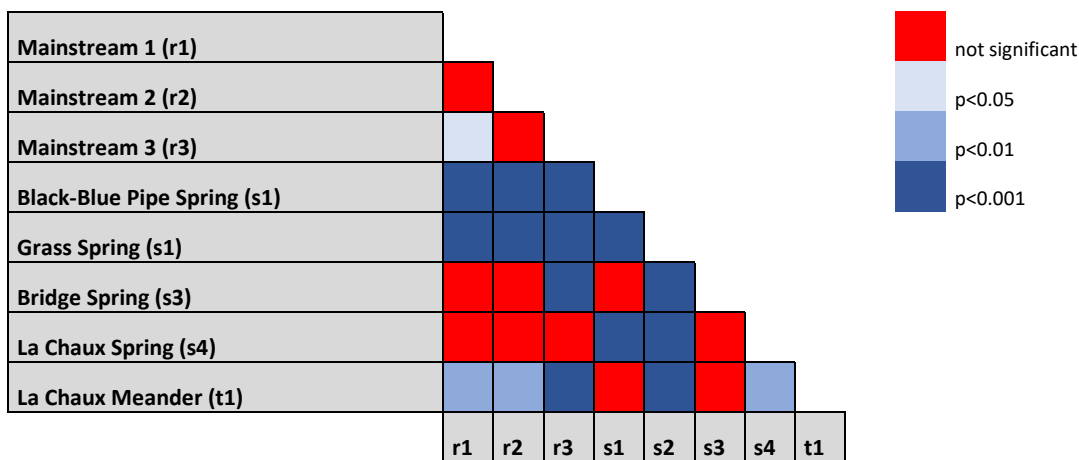
Outliers

The outliers at the stations along the mainstream are all about 1.6mg/l and are recorded in October. The outlier at the Black-Blue Pipe Spring of about 2.2mg/l is measured on 28th August 2022, while the outlier of about 2 mg/l can be attributed to the La Chaux Meander on 27th August 2022. At the Bridge Spring an outlier of 1.9 mg/l is measured and at the Bridge Spring several outliers are identified such as one of about 1.4 mg/l in mid-July and one of 1.6 mg/l in October.

Results of Statistical Significance Test

The results of the statistical significance test (Tukey HSD), assessing whether between two sampling stations a significant difference in the mean values of the nitrate concentration exists, indicate that the Bridge Spring as well as the La Chaux Spring are not significantly different from almost all stations along the mainstream. In addition, the nitrate concentration of the La Chaux Spring and the La Chaux Meander is not significantly different from the Bridge Spring.

Table 13: Results of the statistical significance test of the nitrate concentration. The p-values of the nitrate concentration between the different pairs of sampling stations are determined by the Tukey Honest Significant Differences (Tukey HSD) test.



Anion - Phosphate

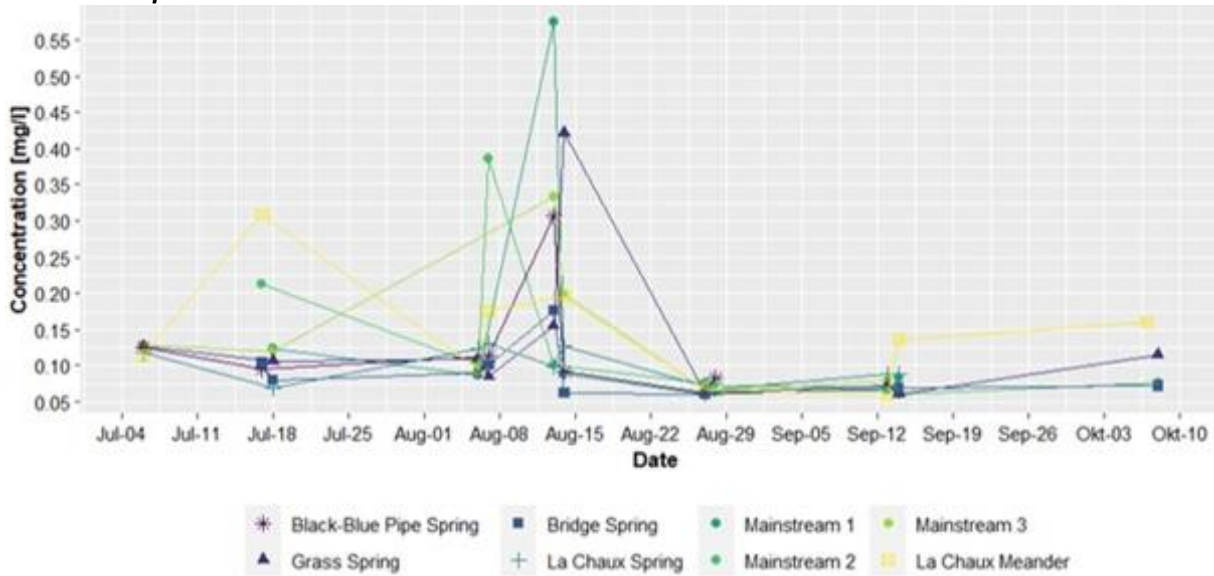


Figure 35: Phosphate concentration over research period. The phosphate concentration, determined by ion chromatography, is illustrated per sampling station in the Vallon de Nant catchment over the research period from early July until early October 2022.

Temporal Variation

The phosphate concentration is constant until early August (see Figure 35), when it strongly increases before it decreases again towards end-August and finally, remains more or less on the same level. The extent of concentration increase in early August varies depending on the station. It is particularly pronounced at the stations along the mainstream and at the Black-Blue Pipe and the Grass Spring, while the increase is lower at the Bridge and the La Chaux Spring as well as at the La Chaux Meander. Variations during a sampling campaign can hardly be identified.

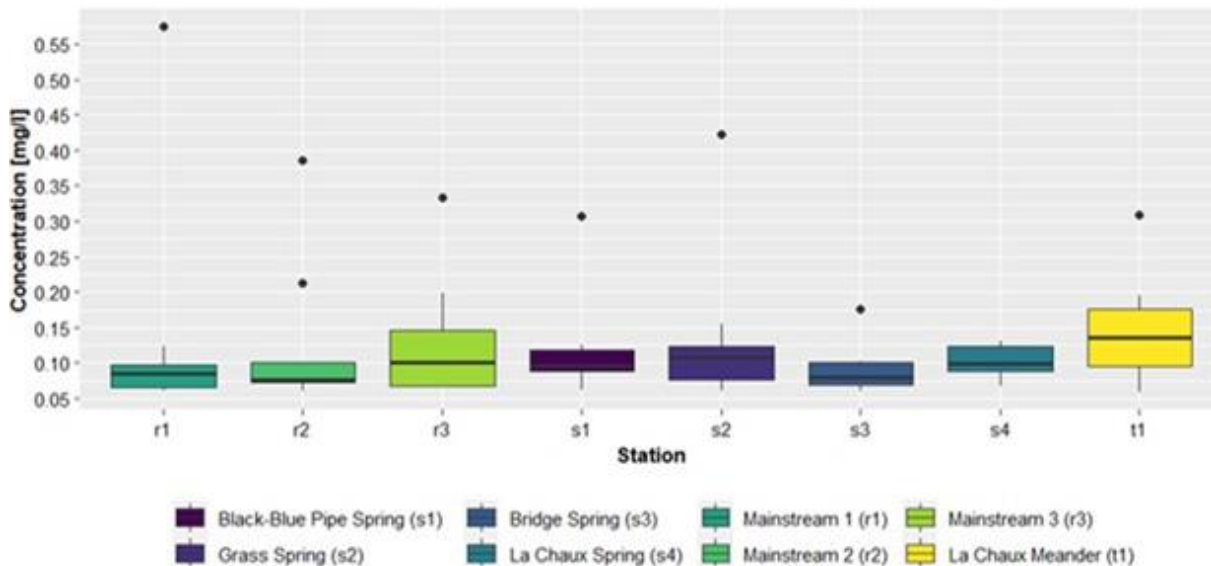


Figure 36: Boxplots of phosphate concentration per sampling station. The phosphate concentration, determined by ion chromatography for all the collected water samples during the research period from early July until early October 2022, is illustrated per sampling station in the Vallon de Nant catchment.

Spatial Variation

There is hardly any spatial variation (see Figure 36) visible among the different sampling stations. The median phosphate concentrations of all the sampling stations range within 0.075mg/l and 0.1mg/l with

the exception of the La Chaux Meander that has a median phosphate concentration slightly lower than 0.15mg/l. Besides, not at every station and not on each sampling date a phosphate concentration is determined.

Outliers

In mid-July outliers of about 0.12mg/l at the Mainstream 3, of 0.31mg/l at the La Chaux Meander and of 0.21mg/l at the Mainstream 2 are recorded. At the Mainstream 2 another outlier of about 0.39 mg/l is manifested in early August. At the Mainstream 1 a concentration of 0.57mg/l, at the Black-Blue Pipe Spring of 0.31mg/l, at the Grass Spring of 0.42mg/l and at the Bridge Spring of about 0.18mg/l is measured in mid-August.

Results of Statistical Significance Test

Sine the p-value of the one-way ANOVA test was larger than 0.05, no statistically significant difference of the phosphate mean concentrations between the sampling stations can be noticed.

Anion – Sulphate

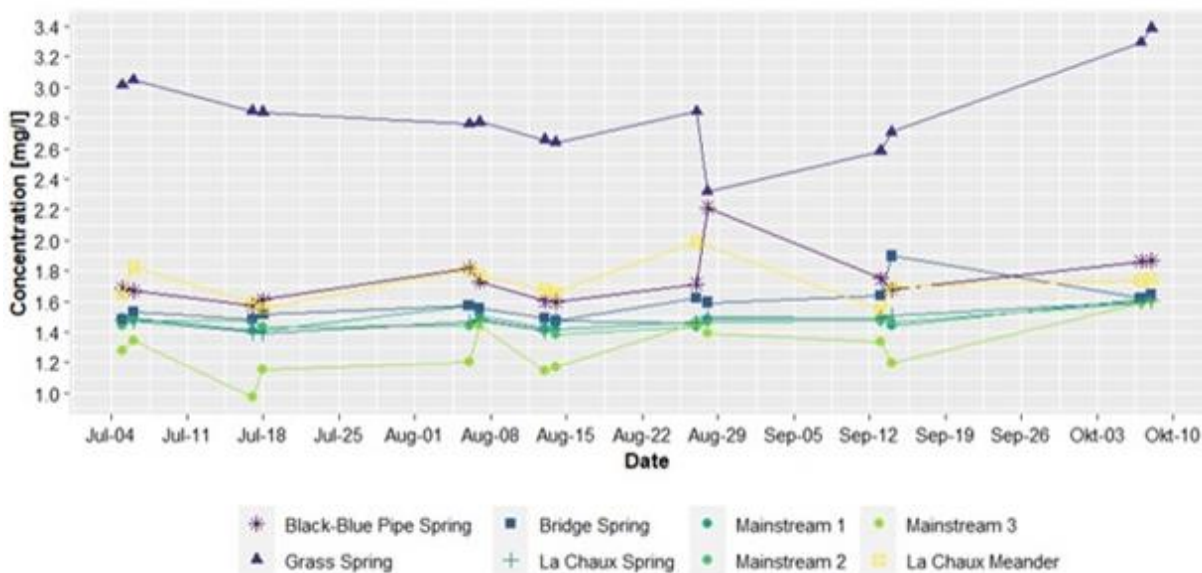


Figure 37: Sulphate concentration over research period. The sulphate concentration, determined by ion chromatography, is illustrated per sampling station in the Vallon de Nant catchment over the research period from early July until early October 2022.

Temporal Variation

An increase in sulphate concentration over the research period at most of the stations (see Figure 37) can be observed. However, at the Grass Spring, the La Chaux Spring and at the La Chaux Meander the sulphate concentration decreases towards October. Variations depending on the time of the day is noticed at the Mainstream 3 as well as at the Grass Spring during the fifth sampling campaign.

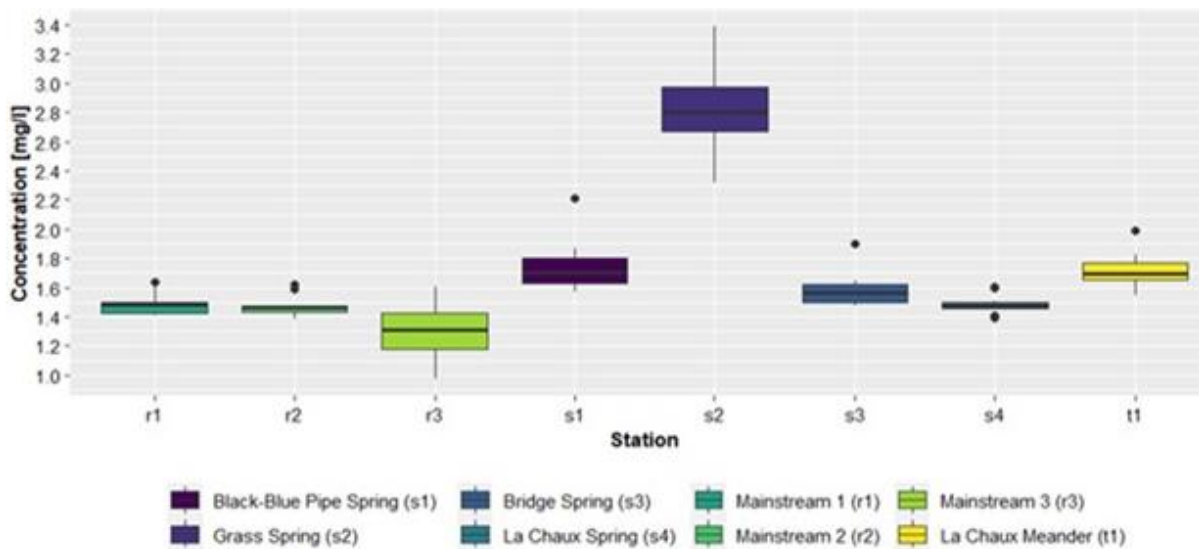


Figure 38: Boxplots of sulphate concentration per sampling station. The sulphate concentration, determined by ion chromatography for all the collected water samples during the research period from early July until early October 2022, is illustrated per sampling station in the Vallon de Nant catchment.

Spatial Variation

A spatial variation among the sampling stations is visible (see Figure 38), while the spatial variation of the median sulphate concentration is smaller among the stations along the mainstream than among the springs. The Black-Blue Pipe Spring has the highest median sulphate concentration of about 21mg/l, whereas the La Chaux Meander has the lowest of about 9.5mg/l. The Bridge, the La Chaux and the Grass Spring have similar median concentrations. Furthermore, the median concentration of the Mainstream 1 and the Mainstream 2 are almost equivalent, namely approximately 15.5mg/l, whereas the median of the Mainstream 3 is about 17mg/l.

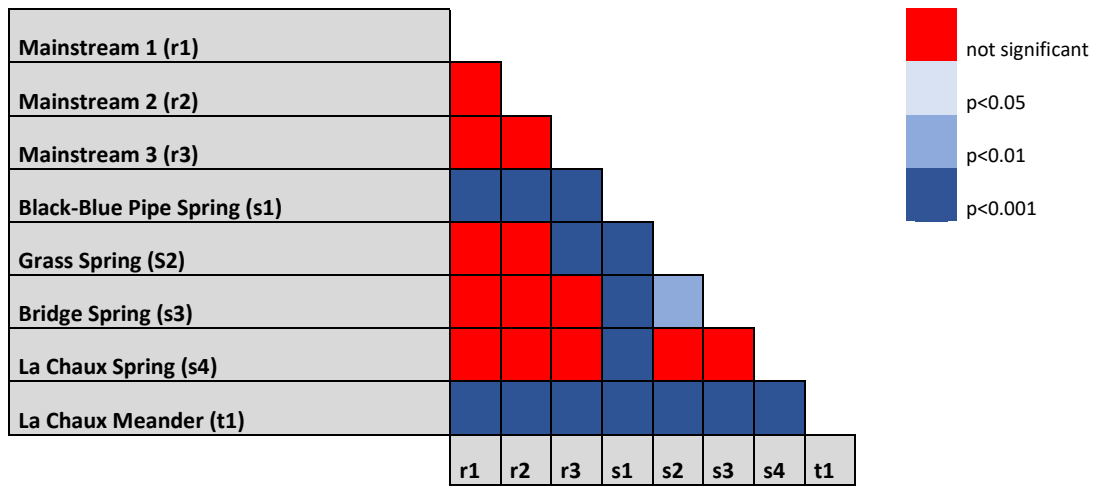
Outliers

Two outliers can be manifested, one at the Mainstream 2, which has a value of about 12.5mg/l and is recorded on 5th July 2022, and one at the Black-Blue Pipe Spring of about 17mg/l on 28th August 2022.

Results of Statistical Significance Test

The results of the statistical significance test (Tukey HSD), assessing whether between two sampling stations a significant difference in the mean values of the sulphate concentration exists, indicate that the La Chaux Meander as well as the Black-Blue Pipe Spring show significantly different sulphate concentrations from all the other sampling stations. In addition, the following pairs show significant differences: Grass Spring/Bridge Spring, Grass Spring/Mainstream 3.

Table 14: Results of the statistical significance test of the sulphate concentration. The p-values of the sulphate concentration between the different pairs of sampling stations are determined by the Tukey Honest Significant Differences (Tukey HSD) test.



Cation - Ammonium

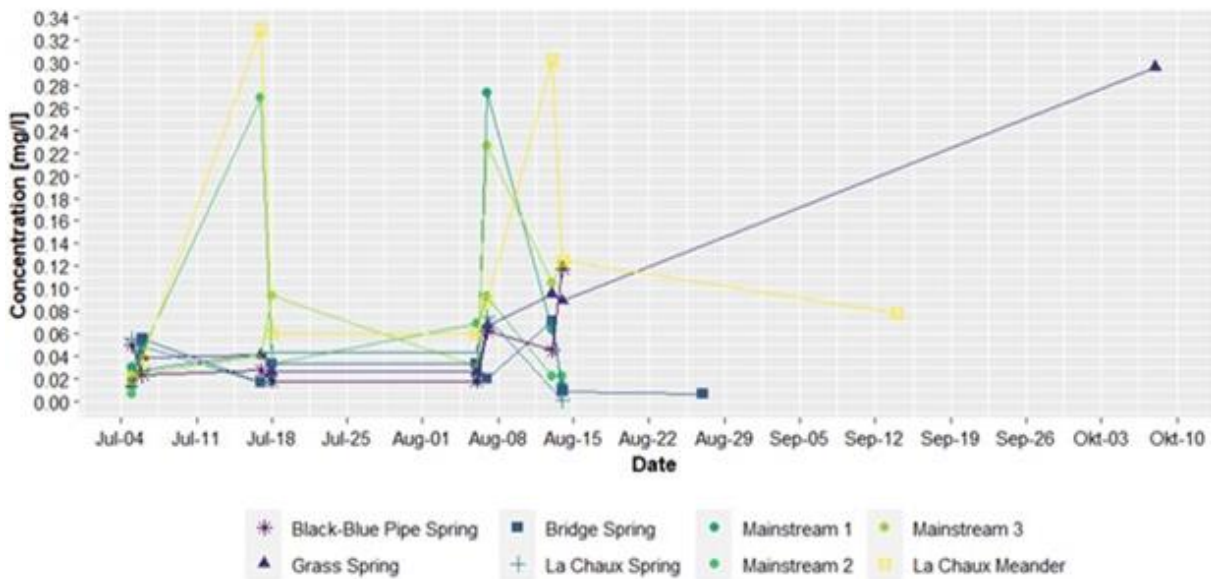


Figure 39: Ammonium concentration over research period. The ammonium concentration, determined by ion chromatography, is illustrated per sampling station in the Vallon de Nant catchment over the research period from early July until early October 2022.

Temporal Variation

The ammonium concentration is on a constant level until early August and then it starts increasing to a different extent depending on the station, but it decreases again towards end-August (see Figure 39). Before the increase in early August, the concentration at the La Chaux Meander, the Mainstream 2 and the Mainstream 3 strongly rises. During the third sampling campaign in early August a variation in the ammonium concentration is visible. In case of the La Chaux Meander also a strong variation during the fourth campaign is observed. However, the ammonium occurrence is irregular over the research period. During the fifth sampling campaign only at the Bridge Spring, during the sixth only at the La Chaux Meander and during the last sampling campaign only at the Grass Spring ammonium is measured.

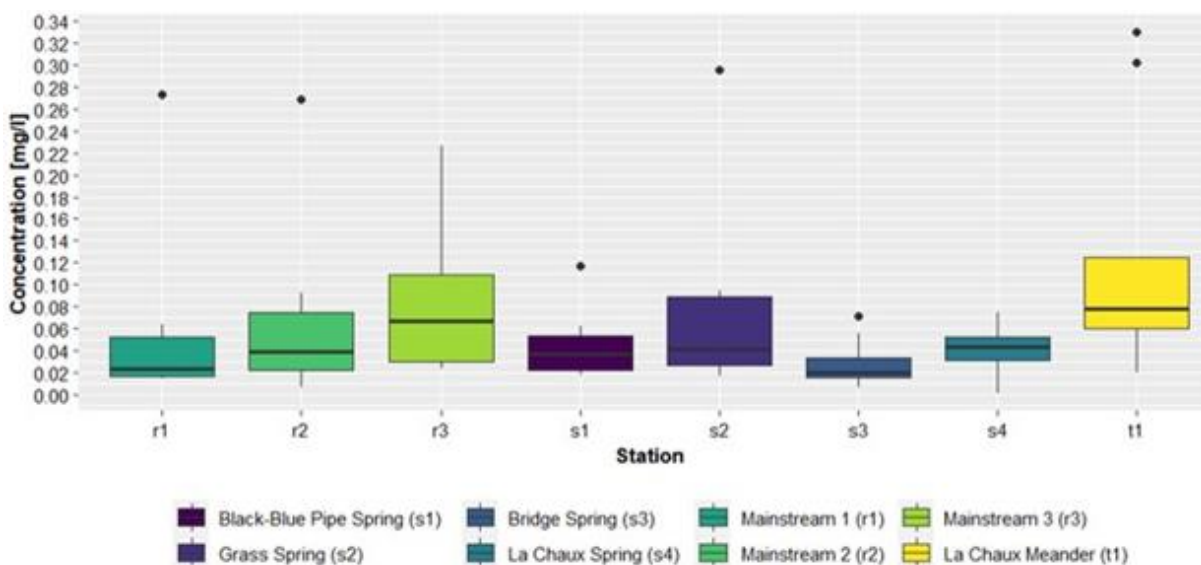


Figure 40: Boxplots of ammonium concentration per sampling station. The ammonium concentration, determined by ion chromatography for all the collected water samples during the research period from early July until early October 2022, is illustrated per sampling station in the Vallon de Nant catchment.

Spatial Variation

The spatial variation of the median ammonium concentration is small (see Figure 40). The median concentration of the La Chaux Meander with a value of 0.08 mg/l is the highest, followed by the Mainstream 3, whilst the ammonium concentration at the Bridge Spring with a value of 0.02mg/l is the lowest and the one at the Mainstream 1 the second lowest.

Outliers

At the Mainstream 1 a value of 0.27mg/l on 7th August 2022, at the Mainstream 2 one of 0.27mg/l on 17th July 2022 and at the Black-Blue Pipe Spring a concentration of 0.12mg/ on 14th August 2022 is measured. In addition, a concentration of 0.29 mg/l at the Grass Spring on 8th August 2022, one of 0.07mg/l at the Bridge Spring on 13th August 2022 and values of 0.3mg/l and 0.32 mg/l at the La Chaux Meander on 17th July and 18th August 2022 are determined.

Results of Statistical Significance Test

Sine the p-value of the one-way ANOVA test was larger than 0.05, no statistically significant difference of the ammonium mean concentrations between the sampling stations can be noticed.

Cation - Calcium

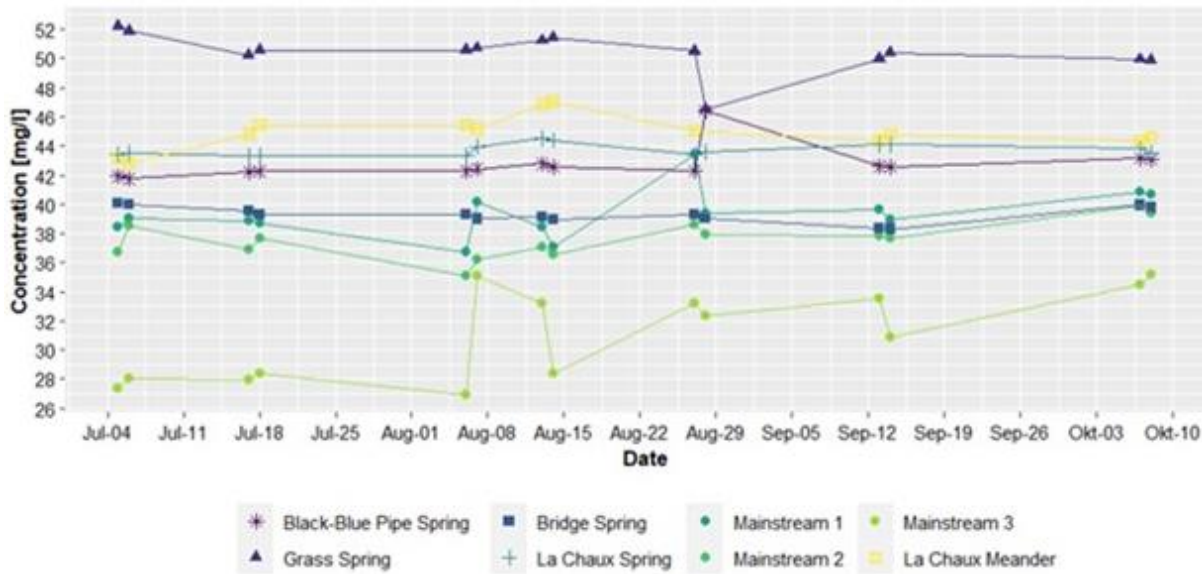


Figure 41: Calcium concentration over research period. The calcium concentration, determined by ion chromatography, is illustrated per sampling station in the Vallon de Nant catchment over the research period from early July until early October 2022.

Temporal Variation

The calcium concentration changes little over the research period (see Figure 41). But the calcium concentration increases from early August towards mid-August before it declines towards the original concentration level. The mainstream shows in contrast to the springs more variations during the sampling campaigns with the exception of the Black-Blue Pipe as well as the Grass Spring, which show variations during the fifth sampling campaign.

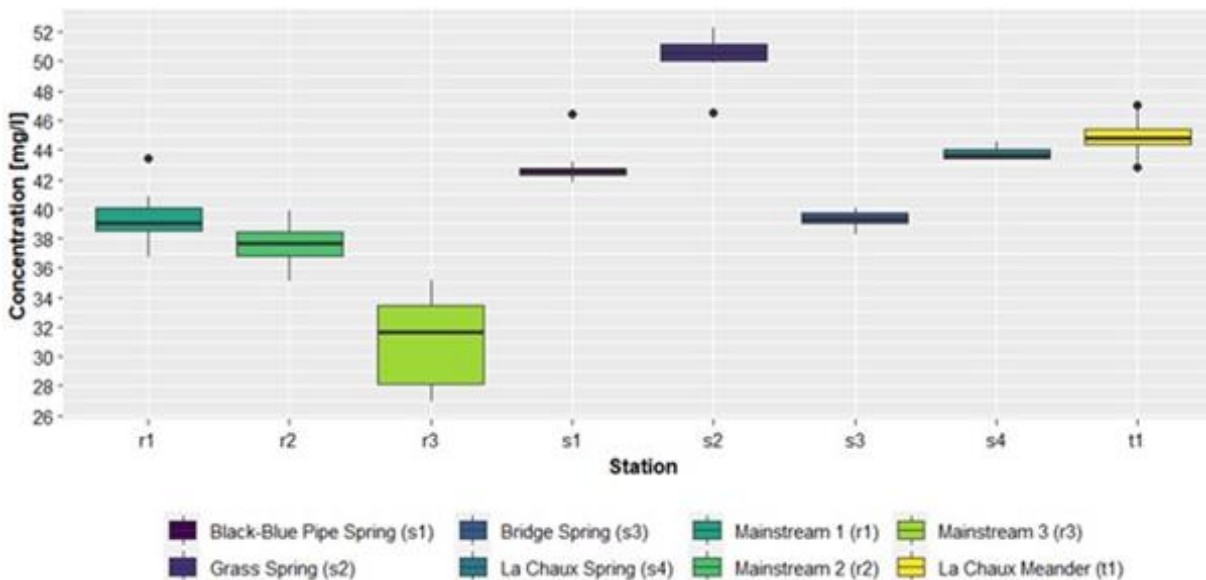


Figure 42: Boxplots of calcium concentration per sampling station. The calcium concentration, determined by ion chromatography for all the collected water samples during the research period from early July until early October 2022, is illustrated per sampling station in the Vallon de Nant catchment.

Spatial Variation

There is quite a spatial variation of the calcium concentration discernible (see Figure 42), while the mainstream shows lower median calcium concentrations than the springs do. The lowest median

calcium concentration of about 32mg/l is observed at the Mainstream 3, followed by the Mainstream 2 and the Mainstream 1, whilst the highest calcium concentrations are measured at the Grass Spring of approximately 50.5mg/l, followed by the La Chaux Meander and the La Chaux Spring. Finally, the Black-Blue Pipe Spring has a median calcium concentration of about 42.5mg/l and the Bridge Spring of about 39mg/l.

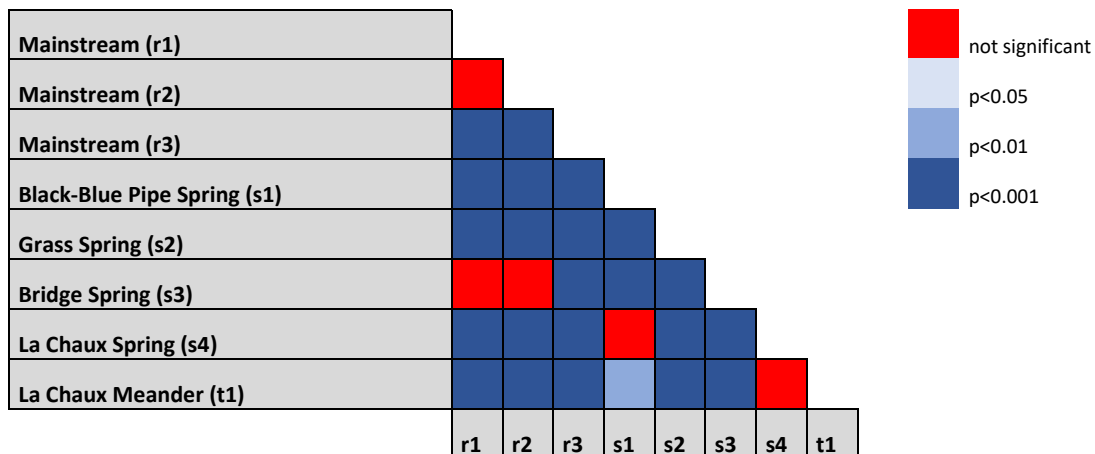
Outlier

The outliers at the Mainstream 1, the Black-Blue Pipe and the Grass Spring occur during the fifth sampling campaign and have concentrations of 43mg/l and 46mg/l. Whereas the ones at the La Chaux Meander are recorded on 5th July 2022 and 14th August 2022 with values of 43mg/l and 47mg/l.

Results of Statistical Significance Test

The results of the statistical significance test (Tukey HSD), assessing whether between two sampling stations a significant difference in the mean values of the calcium concentration exists, indicate that there are significantly different calcium concentrations between almost all possible pairs of sampling stations apart from the following ones: Mainstream 1/Mainstream 2, Mainstream 1/Bridge Spring, Mainstream 2/Bridge Spring, Black-Blue Pipe Spring/La Chaux Spring, La Chaux Spring/La Chaux Meander.

Table 15: Results of the statistical significance test of the calcium concentration. The p-values of the calcium concentration between the different pairs of sampling stations are determined by the Tukey Honest Significant Differences (Tukey HSD) test.



Cations – Potassium

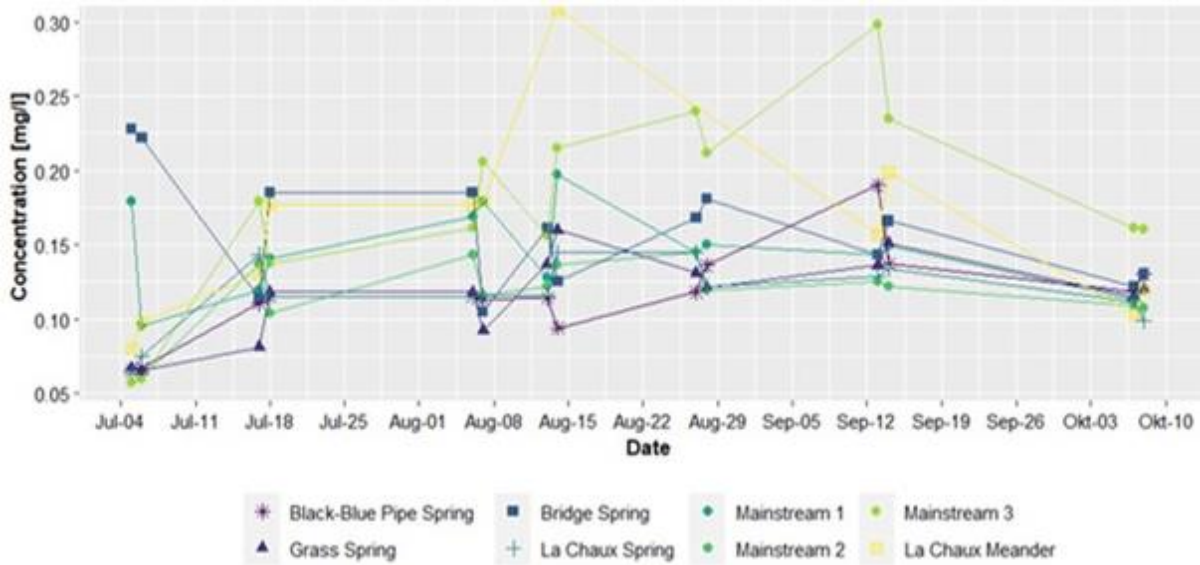


Figure 43: Potassium concentration over research period. The potassium concentration, determined by ion chromatography, is illustrated per sampling station in the Vallon de Nant catchment over the research period from early July until early October 2022.

Temporal Variation

The potassium concentration increases slightly towards October (see Figure 43), but there are variations within that time period. Especially the Mainstream 3, the Bridge Spring and the La Chaux Meander show stronger temporal variations than the other stations. The concentration at the La Chaux Meander increases towards mid-August before it decreases again. Similarly at the Mainstream 2, but there the increase is manifested towards mid-September. The potassium concentration, measured at the Bridge Spring, declines towards mid-July, then it remains constant before showing another increase at end-August and then decreases towards October. Variations during a sampling campaign cannot be identified except slightly at the Mainstream 2 during the fourth sampling campaign.

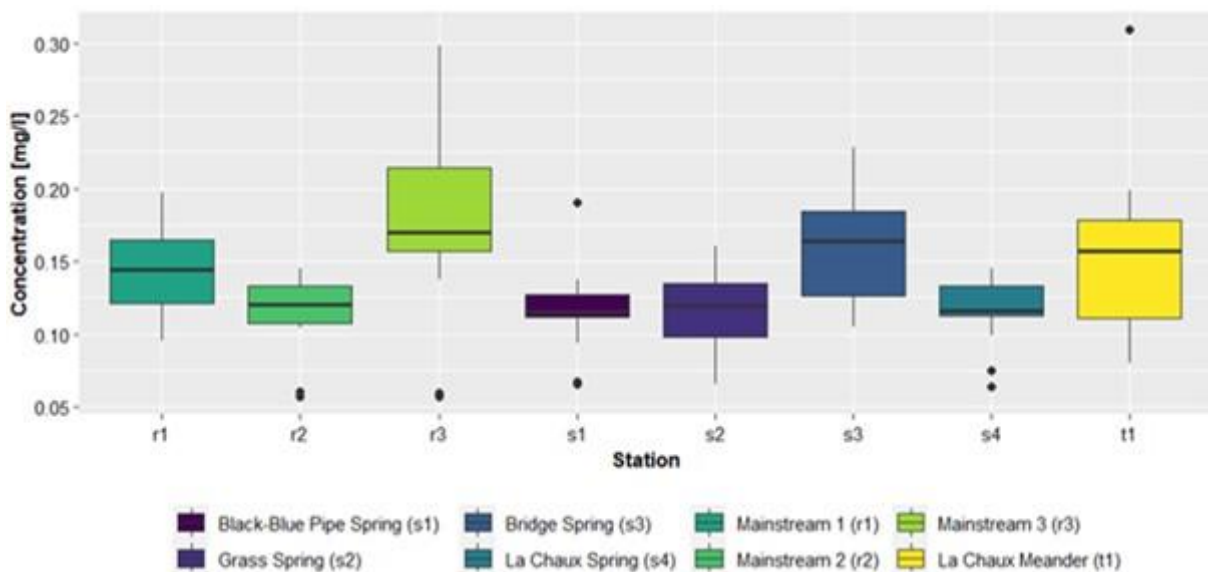


Figure 44: Boxplots of potassium concentration per sampling station. The potassium concentration, determined by ion chromatography for all the collected water samples during the research period from early July until early October 2022, is illustrated per sampling station in the Vallon de Nant catchment.

Spatial Variation

The potassium concentration varies to a limited extent among the sampling stations (see Figure 44). The Mainstream 2, the Black-Blue Pipe, the Grass and the La Chaux Spring have all median potassium concentrations of about 0.12mg/l, whereas the Mainstream 3, the Bridge Spring as well as the La Chaux Meander have a median concentration of around 0.17mg/l.

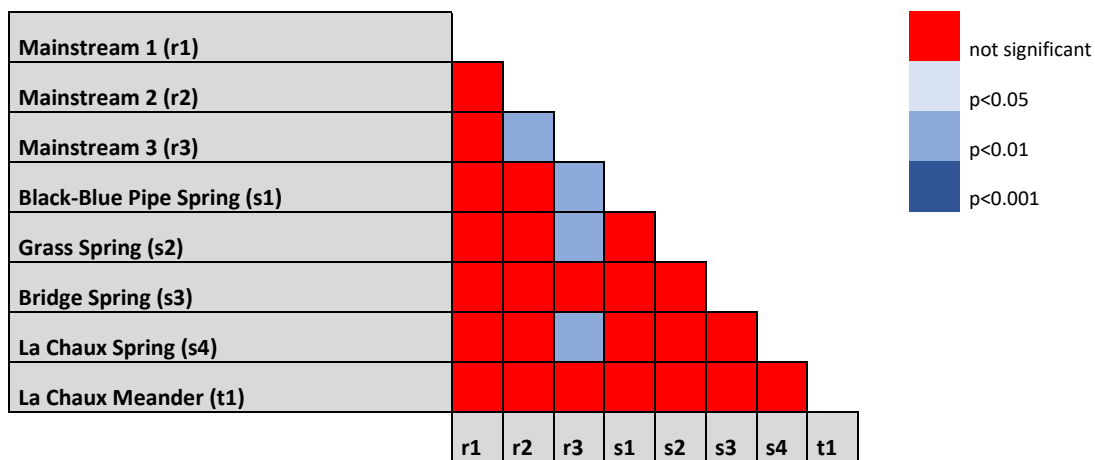
Outliers

In early July outliers of about 0.06mg/l at the Mainstream 2 as well as at the Mainstream 3, one of 0.07mg/l at the Black-Blue Pipe and at the La Chaux Spring are recorded. At the La Chaux Spring another outlier of about 0.8 mg/l is measured in early July. At the Black-Blue Pipe Spring an outlier of about 0.13mg/l occurs in mid-September. At last, an outlier of about 0.32mg/l is observed at the La Chaux Meander on 14th August 2022.

Results of Statistical Significance Test

The results of the statistical significance test (Tukey HSD), assessing whether between two sampling stations a significant difference in the mean values of the potassium concentration exists, indicate that there are no significantly different potassium concentrations between almost all possible pairs of sampling stations, apart from the following ones: Mainstream 3/Mainstream 2, Mainstream 3/Black-Blue Pipe Spring, Mainstream 3/Grass Spring, Mainstream 3/La Chaux Spring.

Table 16: Results of the statistical significance test of the potassium concentration. The p-values of the potassium concentration between the different pairs of sampling stations are determined by the Tukey Honest Significant Differences (Tukey HSD) test.



Cations – Magnesium

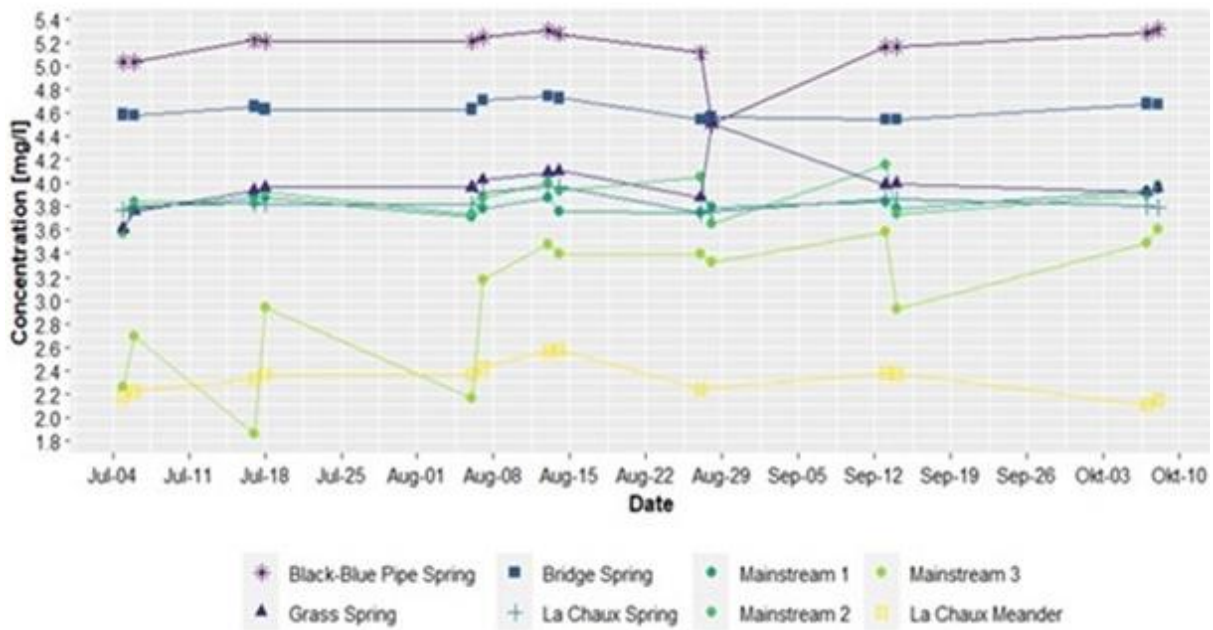


Figure 45: Magnesium concentration over research period. The magnesium concentration, determined by ion chromatography, is illustrated per sampling station in the Vallon de Nant catchment over the research period from early July until early October 2022.

Temporal Variation

The magnesium concentrations vary little at most of the sampling stations over the research period apart from the Mainstream 2 (see Figure 45). But the concentration slightly increases from the beginning of August towards mid-August at all sampling stations and then decreases again at the end of August before levelling off. Variations during the sampling campaign are particularly identified at the Mainstream 2, whereas at the other stations they are much less pronounced.

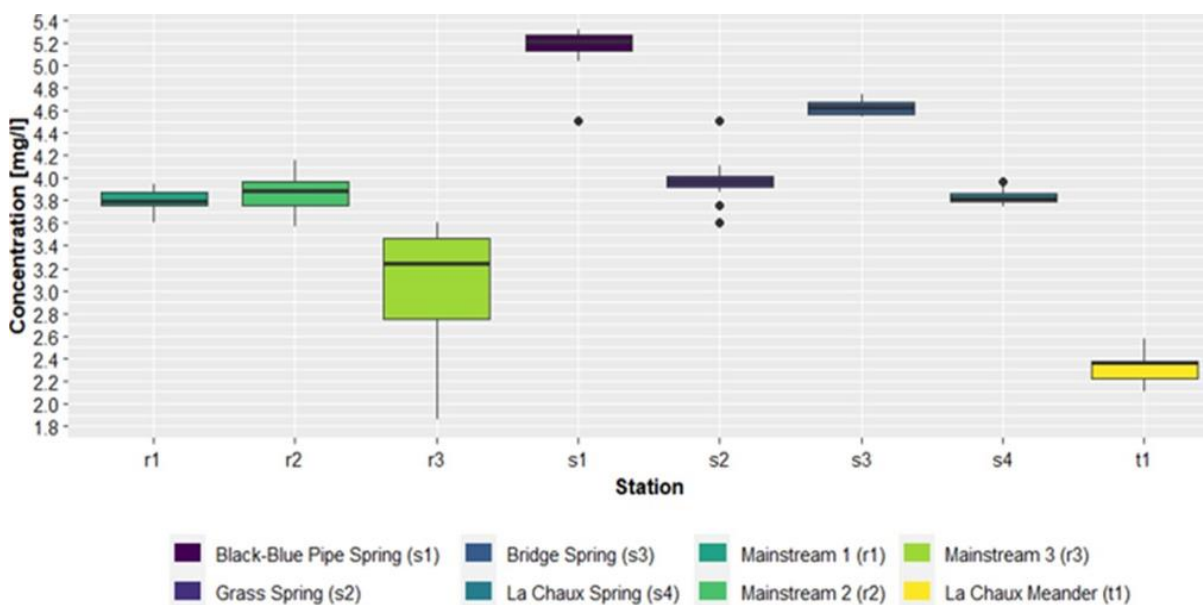


Figure 46: Boxplots of magnesium concentration per sampling station. The magnesium concentration, determined by ion chromatography for all the collected water samples during the research period from early July until early October 2022, is illustrated per sampling station in the Vallon de Nant catchment

Spatial Variation

There is a clear spatial variation among the sampling stations visible (see Figure 46). The La Chaux Meander has the lowest median magnesium concentration of about 2.4mg/l, followed by the Bridge Spring, whereas the Black-Blue Pipe Spring shows the highest median concentration of approximately 5.2mg/l. As a further matter, the spatial variation at the stations along the mainstream is smaller than it is among the springs. The median magnesium concentration of the Mainstream 3 of about 3.3mg/l is much lower than the concentration of the Mainstream 1 and the Mainstream 2.

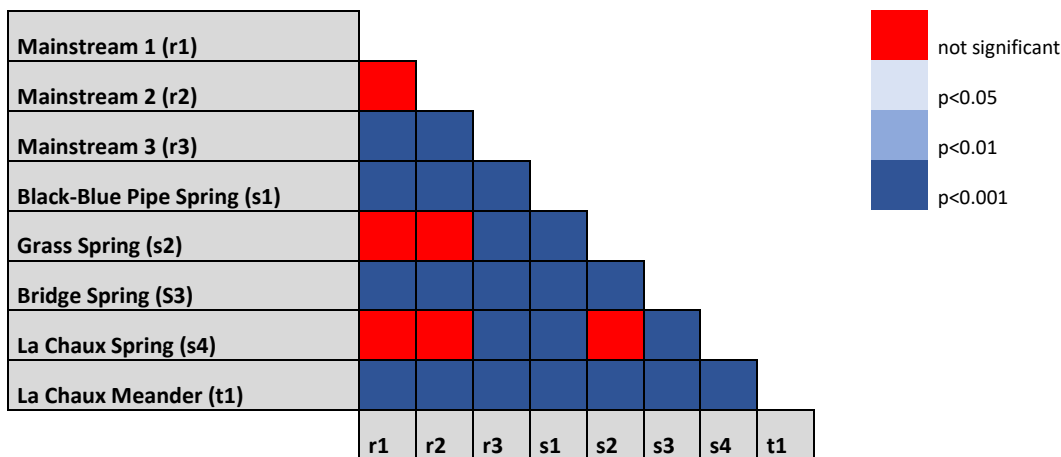
Outliers

At the Grass Spring outliers of about 3.6 mg/l and 3.7mg/l during the first sampling campaign and one of 4.5mg/l on 28th August 2022 are recorded. At the Black-Blue Pipe Spring a value of 4.5mg/l on 28th August 2022 and one of 3.9mg/l at the La Chaux Spring on 14th August 2022 are measured.

Results of Statistical Significance Test

The results of the statistical significance test (Tukey HSD), assessing whether between two sampling stations a significant difference in the mean values of the magnesium concentration exists, indicate that there are significantly different magnesium concentrations between almost all possible pairs of sampling stations apart from the following pairs: Mainstream 1/Mainstream 2, Mainstream 1/La Chaux Spring, Mainstream 1/Grass Spring, Mainstream 2/Grass Spring, Mainstream 2/La Chaux Spring, Grass Spring/La Chaux Spring.

Table 17: Results of the statistical significance test of the magnesium concentration. The p-values of the magnesium concentration between the different pairs of sampling stations are determined by the Tukey Honest Significant Differences (Tukey HSD) test.



Cations – Sodium

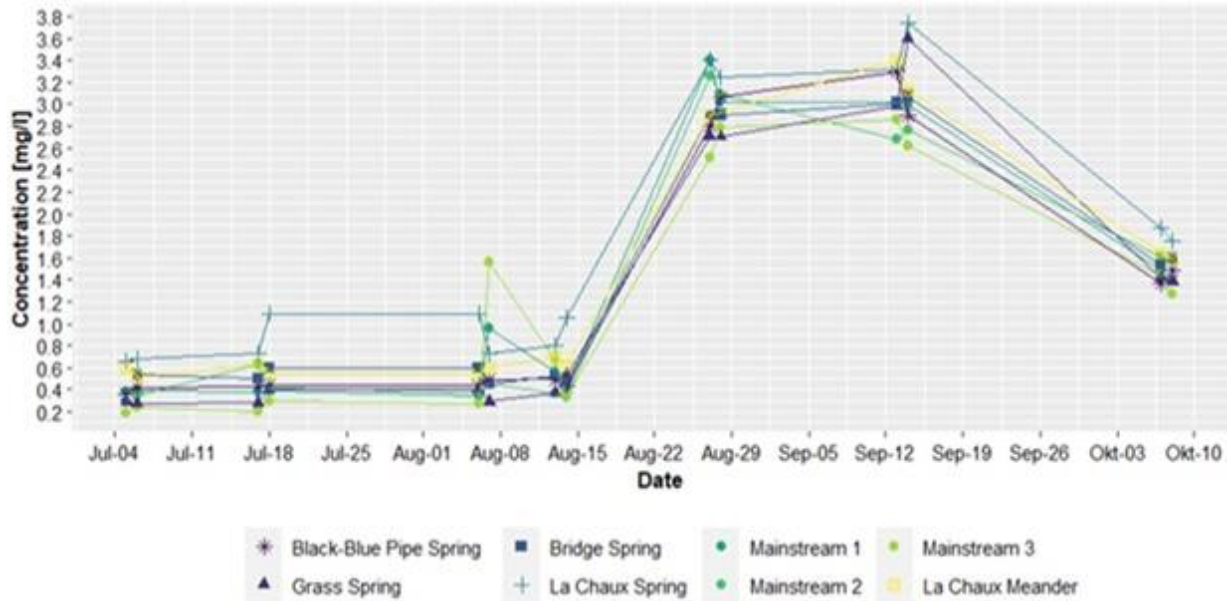


Figure 47: Sodium concentration over research period. The sodium concentration, determined by ion chromatography, is illustrated per sampling station in the Vallon de Nant catchment over the research period from early July until early October 2022. Temporal Variation

The temporal variation is quite pronounced (see Figure 47). The sodium concentration is more or less constant until early August, then it starts increasing towards end-August and levels off, before it decreases again towards October. At the La Chaux Spring an increase of can be noticed in mid-July. At last, variations during a sampling campaign are hardly observable.

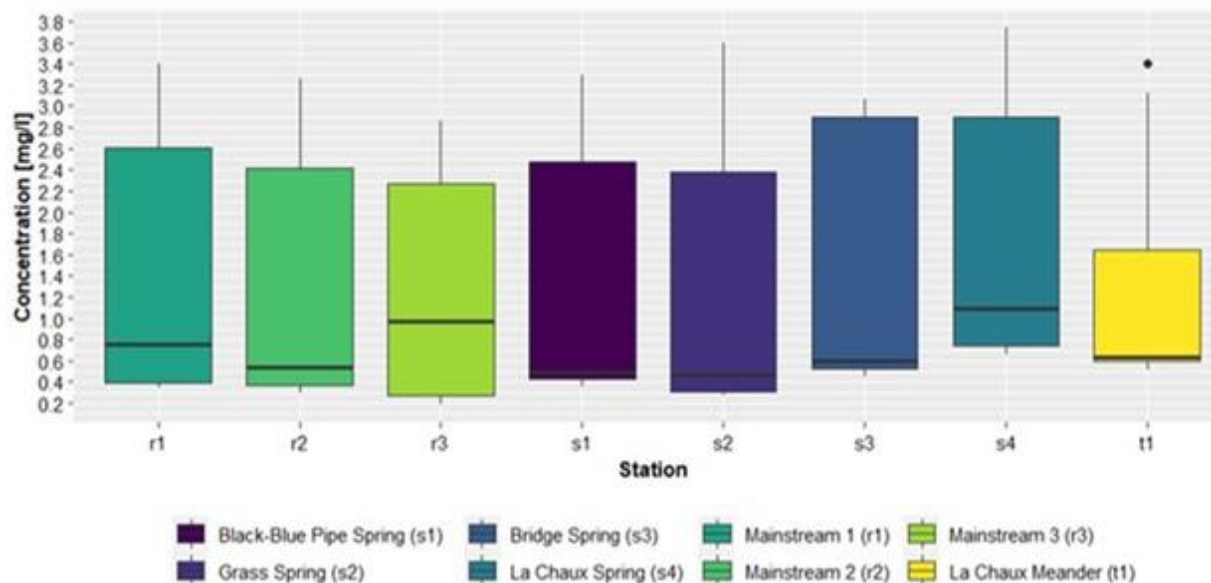


Figure 48: Boxplots of sodium concentration per sampling station. The sodium concentration, determined by ion chromatography for all the collected water samples during the research period from early July until early October 2022, is illustrated per sampling station in the Vallon de Nant catchment.

Spatial Variation

The spatial variation of the sodium concentration is limited (see Figure 48). The La Chaux Spring has the highest median concentration, followed by the Mainstream 3, while a concentration of about 0.5mg/l is measured at the Black-Blue Pipe, the Grass Spring as well as at the Mainstream 2. The

median sodium concentrations of the Bridge Spring and the La Chaux Meander are almost identical, namely approximately 0.6mg/l and the one of the Mainstream 1 is about 0.7mg/l.

Outliers

One outlier of about 3.4 mg/l is recorded at the La Chaux Meander on 13th September 2022.

Results of Statistical Significance Test

Sine the p-value of the one-way ANOVA test was larger than 0.05, no statistically significant difference of the sodium mean concentrations between the sampling stations can be noticed.

Isotopes – Deuterium ($\delta^2\text{H}$)

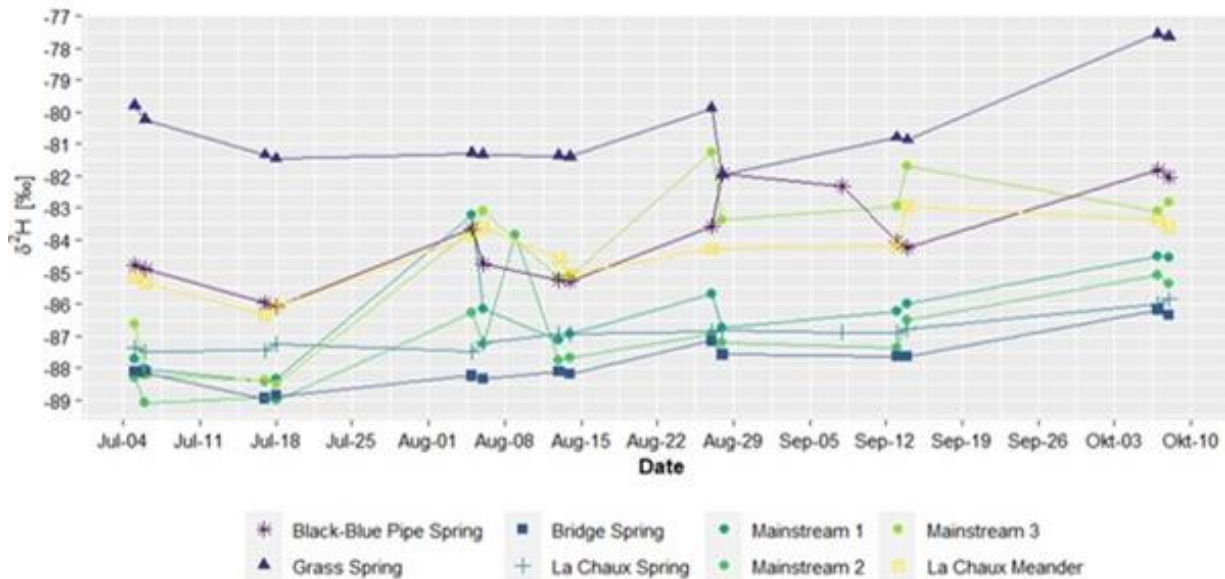


Figure 49: Deuterium content over research period. The deuterium content, determined by the L2140-I Isotope and Gas Concentration Analyzer (Picarro, Inc.; Santa Clara, California, USA), is illustrated per sampling station in the Vallon de Nant catchment over the research period from early July until early October 2022.

Temporal Variation

An increase in the $\delta^2\text{H}$ composition is noticed over time (see Figure 49). At the beginning of August, the $\delta^2\text{H}$ content at the La Chaux Meander, the Black-Blue Pipe Spring and at all the stations along the mainstream decreases. In addition, there is a clear increase visible at all the stations from mid-August towards end-August, then it decreases before rising again towards October. However, not all stations show temporal variations to the same extent. The Mainstream 3 as well as the Black-Blue Pipe Spring show stronger temporal variation, while the $\delta^2\text{H}$ composition varies less at the Bridge and the La Chaux Spring. Ultimately, variations of the $\delta^2\text{H}$ content during a sampling campaign can be identified to some extent but are more pronounced in the mainstream.

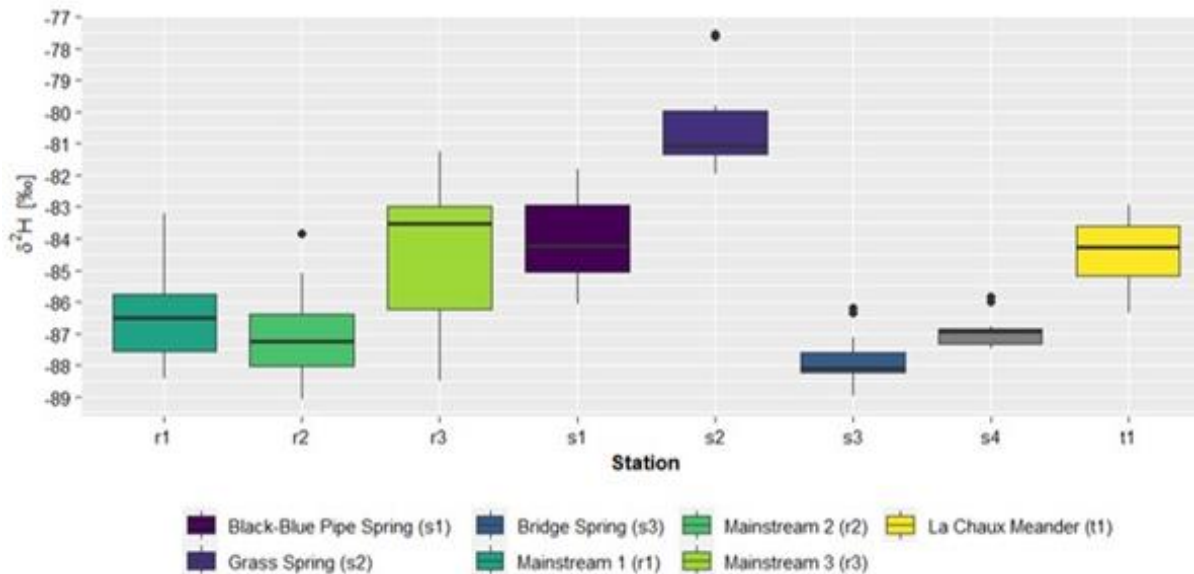


Figure 50: Boxplots of deuterium content per sampling station. The deuterium content, determined by the L2140-I Isotope and Gas Concentration Analyzer (Picarro, Inc.; Santa Clara, California, USA), for all the collected water samples during the research period from early July until early October 2022, is illustrated per sampling station in the Vallon de Nant catchment.

Spatial Variation

When considering the median $\delta^2\text{H}$ content spatial variation is observed (see Figure 50). The smallest median $\delta^2\text{H}$ content is identified at the Bridge Spring with a median of about -88.5‰ , followed by the Mainstream 2 and the La Chaux Spring, whereas the largest one at the Grass Spring, with an amount of -81‰ . The median $\delta^2\text{H}$ content of the La Chaux Meander and the Black-Blue Pipe Spring is similar, namely about -84.5‰ . The Mainstream 3 with a value of -83.5‰ shows the highest median $\delta^2\text{H}$ amount among the stations along the mainstream, followed by the Mainstream 2.

Outliers

Most of the outliers are attributed to the last sampling campaign: Grass Spring with a value of about -78‰ , Bridge Spring with values of around -86.5‰ , La Chaux Spring with a $\delta^2\text{H}$ content of about -86‰ . The outlier at the Mainstream 2 occurred on 8th September 2022 and has a $\delta^2\text{H}$ content of about -84‰ .

Results of Statistical Significance Test

The results of the statistical significance test (Tukey HSD), assessing whether between two sampling stations a significant difference in the mean values of the deuterium content exists, indicate that there are significantly different deuterium contents between almost all possible pairs of sampling stations. However, the Mainstream 1 and Mainstream 2 are not significantly different in their deuterium content from the Bridge and the La Chaux Spring. Other pairs without any significant difference in the deuterium content are the following: La Chaux Meander/Mainstream 3, La Chaux Meander/Black-Blue Pipe Spring, Mainstream 3/Black-Blue Pipe Spring, Mainstream 1/Mainstream 2, Bridge Spring/La Chaux Spring.

Table 18: Results of the statistical significance test of the deuterium content. The p-values of the deuterium content between the different pairs of sampling stations are determined by the Tukey Honest Significant Differences (Tukey HSD) test.

Mainstream 1 (r1)								
Mainstream 2(r2)	not significant							
Mainstream 3 (r3)	p<0.05	p<0.01						
Black-Blue Pipe Spring (s1)	p<0.01	p<0.01	not significant					
Grass Spring (s2)	p<0.01	p<0.01	p<0.01	p<0.01				
Bridge Spring (s3)	not significant	not significant	p<0.01	p<0.01	p<0.01			
La Chaux Spring (s4)	not significant	not significant	p<0.01	p<0.01	p<0.01	not significant		
La Chaux Meander (t1)	p<0.05	p<0.01	not significant	not significant	p<0.01	p<0.01	p<0.01	
	r1	r2	r3	s1	s2	s3	s4	t1

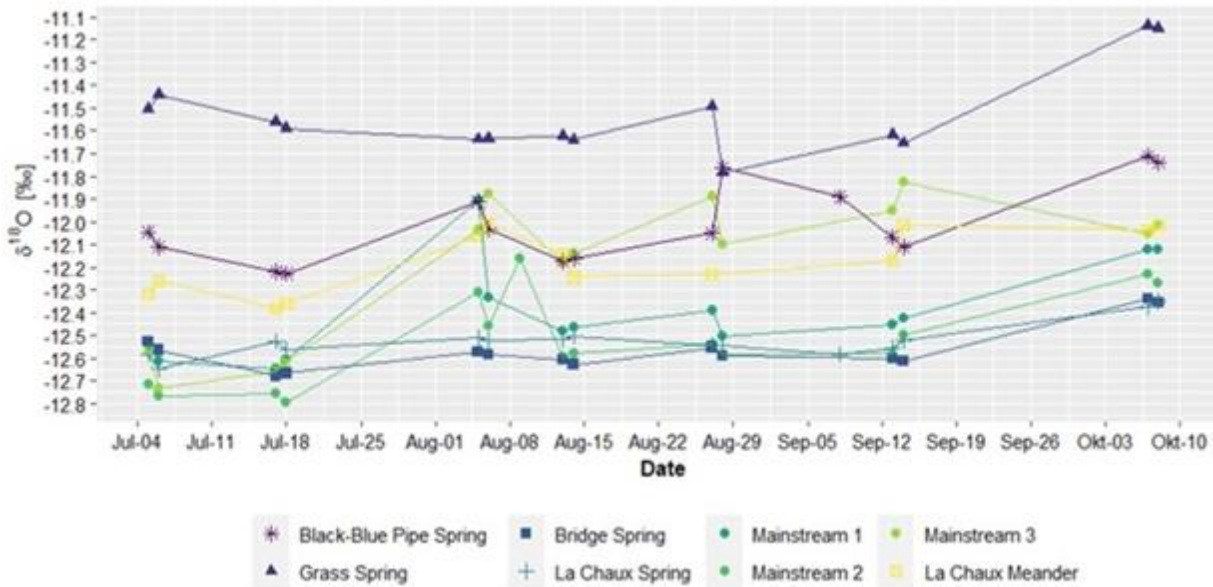
Isotopes – $\delta^{18}\text{O}$ 

Figure 51: $\delta^{18}\text{O}$ content over research period. The $\delta^{18}\text{O}$ content, determined by the L2140-I Isotope and Gas Concentration Analyzer (Picarro, Inc.; Santa Clara, California, USA), is illustrated per sampling station in the Vallon de Nant catchment over the research period from early July until early October 2022.

Temporal Variation

An increase of the $\delta^{18}\text{O}$ values is observed over the whole research period (see Figure 51). However, not all stations vary to the same extent. For instance, there is little variation at the Bridge and the La Chaux Spring and thus, their composition is more or less constant before the increase from mid-September towards early October, while more variations are observed at the other stations. For example, the Black-Blue Pipe, the Grass and the Bridge Spring as well as the La Chaux Meander show a decrease from early July until mid-July before the $\delta^{18}\text{O}$ content rises at all the mentioned stations except at the Grass Spring again towards early August. The growth from mid-July until early August is observed at the stations along the mainstream. Then, there is another decline in the $\delta^{18}\text{O}$ content towards mid-August before the $\delta^{18}\text{O}$ content either increases or remains on the same level until mid-September, which is observed at most stations, except at the Mainstream 3, showing a decrease and at the La Chaux Meander, where it levels off. At last, variations during a sampling campaign are particularly noticed at the stations along the mainstream and at the Black-Blue Pipe and the Grass Spring at the end of August.

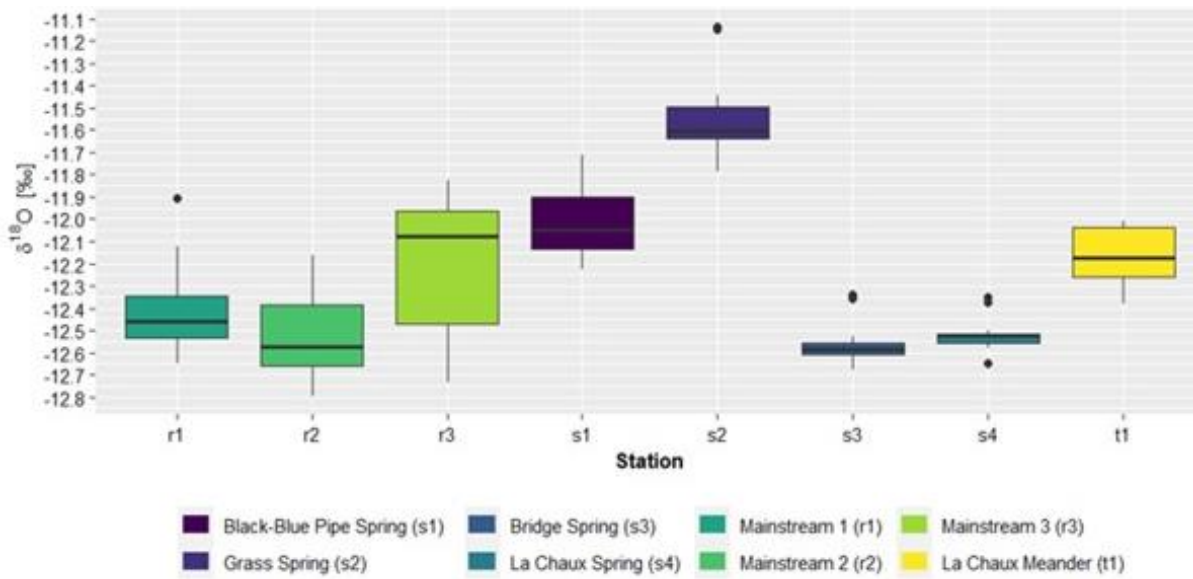


Figure 52: Boxplots of $\delta^{18}\text{O}$ content per sampling station. The $\delta^{18}\text{O}$ content, determined by the L2140-I Isotope and Gas Concentration Analyzer (Picarro, Inc.; Santa Clara, California, USA) for all the collected water samples during the research period from early July until early October 2022, is illustrated per sampling station in the Vallon de Nant catchment.

Spatial Variation

The $\delta^{18}\text{O}$ content varies spatially (see Figure 52). The smallest median $\delta^{18}\text{O}$ content is manifested at the Bridge Spring as well as at the Mainstream 2 with a median amount of approximately -12.55 ‰, followed by the La Chaux Spring, whilst the largest at the Grass Spring, with an amount of -11.6 ‰. The median $\delta^{18}\text{O}$ content of the Mainstream 3 and the Black-Blue Pipe Spring is similar. A slightly lower median $\delta^{18}\text{O}$ content is measured at the La Chaux Meander.

Outlier

Most outliers are recorded during the last sampling campaign such as at the Grass Spring with a $\delta^{18}\text{O}$ content of -11.15‰, at the Bridge Spring with a $\delta^{18}\text{O}$ content of around 12.35 ‰ as well as at the La Chaux Spring with a $\delta^{18}\text{O}$ content of approximately 12.25 ‰, while in the latter case another outlier of about 12.65 ‰ is recorded on 6th July 2022.

Results of Statistical Significance Test

The results of the statistical significance test (Tukey HSD), assessing whether between two sampling stations a significant difference in the mean values of the $\delta^{18}\text{O}$ content exists, indicate that there are significantly different $\delta^{18}\text{O}$ contents between almost all possible pairs of sampling stations. However, the Mainstream 1 and the Mainstream 2 are not significantly different in their $\delta^{18}\text{O}$ content from the Bridge and the La Chaux Spring. Other pairs without any significant difference in the $\delta^{18}\text{O}$ content are the following ones: La Chaux Meander/Mainstream 3, La Chaux Meander/Black-Blue Pipe Spring, Mainstream 3/Black-Blue Pipe Spring, Mainstream 1/Mainstream 2, Bridge Spring/La Chaux Spring, Mainstream 1/Mainstream 3.

Table 19: Results of statistical significance test of the $\delta^{18}\text{O}$ content. The p-values of the $\delta^{18}\text{O}$ content between the different pairs of sampling stations are determined by the Tukey Honest Significant Differences (Tukey HSD) test.

	r1	r2	r3	s1	s2	s3	s4	t1
Mainstream 1 (r1)								
Mainstream 2 (r2)	not significant							
Mainstream 3 (r3)	not significant	$p < 0.001$						
Black-Blue Pipe Spring (s1)	$p < 0.001$	$p < 0.001$	not significant					
Grass Spring (s2)	$p < 0.001$	$p < 0.001$	$p < 0.001$					
Bridge Spring (s3)	not significant	not significant	$p < 0.001$	$p < 0.001$				
La Chaux Spring (s4)	not significant	not significant	$p < 0.001$	$p < 0.001$	$p < 0.001$	not significant		
La Chaux Meander (t1)	$p < 0.05$	$p < 0.001$	not significant	not significant	$p < 0.001$	$p < 0.001$	$p < 0.001$	

Relationship between $\delta^2\text{H}$ and $\delta^{18}\text{O}$ per Sampling Station

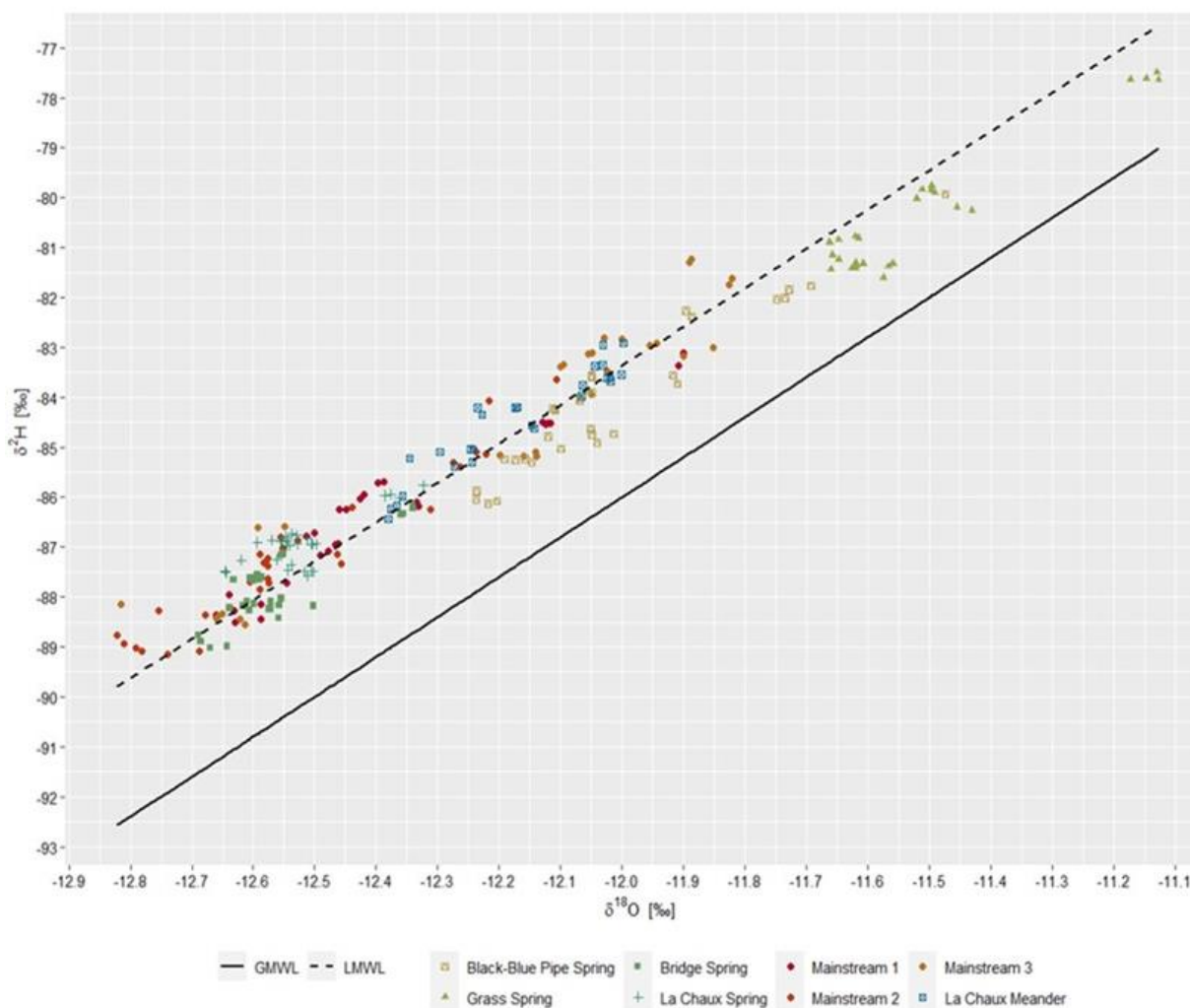


Figure 53: Relationship between $\delta^2\text{H}$ and $\delta^{18}\text{O}$ per sampling station. The determined $\delta^2\text{H}$ and $\delta^{18}\text{O}$ contents per sampling station are plotted against each other and the Global Meteoric Water Line (GMWL) as well as the Local Meteoric Water Line (LMWL) of the Vallon de Nant catchment, which was defined by Mächler et al. (2021), are illustrated.

The determined isotope compositions follow the Local Meteoric Water Line (LMWL) more or less accurately (see Figure 53). As a further matter, a spatial variation among the sampling stations is noticed. While the isotopic composition of the samples, that were collected at stations along the mainstream, are widely spread along the LMWL, the isotopic values at the springs are more clustered. The Grass Spring, for instance, is less depleted in heavy isotopes than the La Chaux Spring or the Bridge Spring, whilst the Black-Blue Pipe Spring as well as the La Chaux Meander show values that are more widely spread along the LMWL.

Among the springs, no clear elevation pattern can be identified, except that the two lower lying springs are more depleted than the other ones, but the Bridge Spring, which is the most depleted one, is lower lying than the La Chaux Spring as well as the La Chaux Meander. When considering the stations along the mainstream, the Mainstream 3, which is the highest lying station along the mainstream, is more enriched than the two lower lying stations along the mainstream. But there are still values recorded at the Mainstream 3 that show similar isotopic compositions than the values of the Mainstream 1 and the Mainstream 2.

Isotopes – Deuterium Excess (*d-excess*)

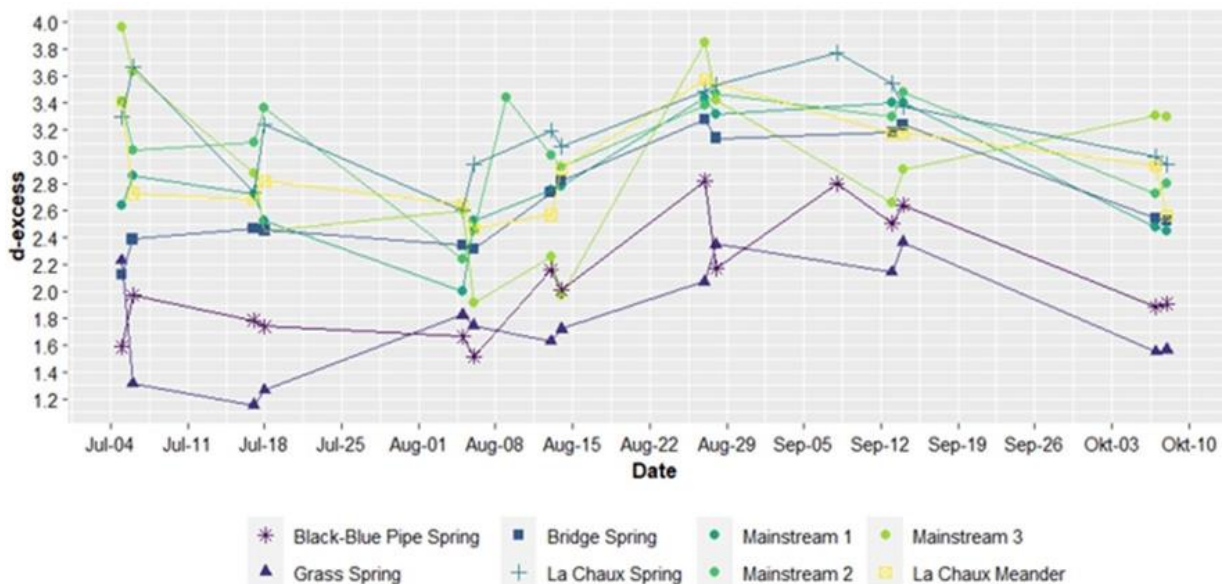


Figure 54: Deuterium excess (*d-excess*) values over research period. The deuterium excess (*d-excess*) values are illustrated per sampling station in the Vallon de Nant catchment over the research period from early July until early October 2022.

Temporal Variation

From an overall perspective, the *d-excess* value increases at most of the stations from early August towards mid-August before it decreases again towards October (see Figure 54). However, the Mainstream 2 shows after the increase towards mid-August a decline towards mid-September and then a final increase towards October. The temporal pattern from early July until early August varies depending on the station. The Bridge Spring, for instance, shows little variation, the Black-Blue Pipe and the La Chaux Spring and the stations along the mainstream show a decrease, but the Grass Spring an increase of the *d-excess* values from early July until early August. Variations during a sampling campaign are noticed at all sampling stations, less pronounced at the Bridge and the Grass Spring.

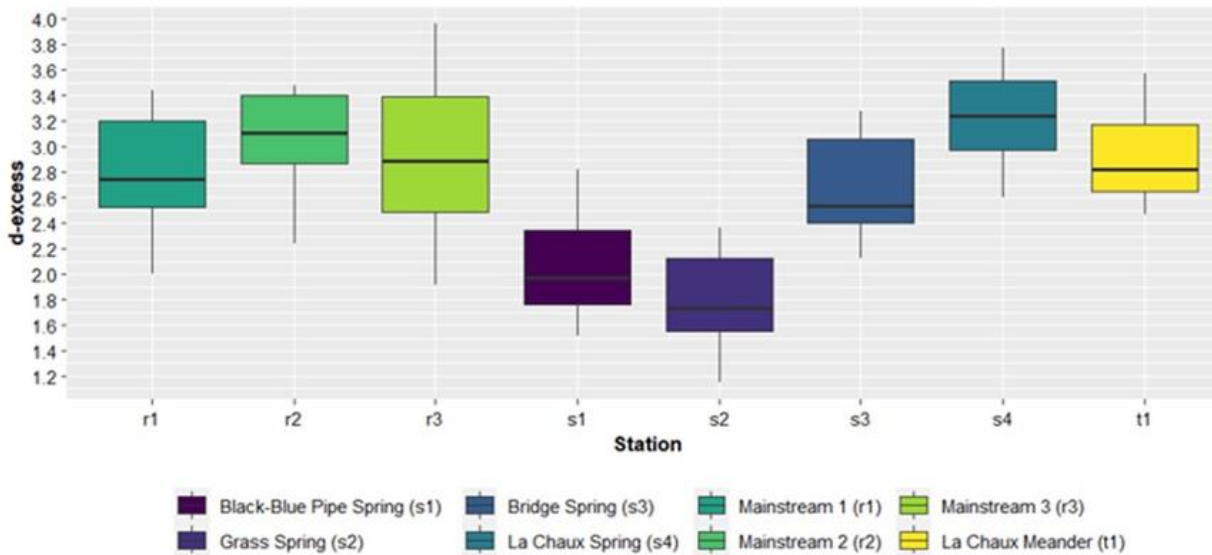


Figure 55: Boxplots of deuterium excess (d-excess) values per sampling station. The deuterium excess (d-excess) values for all the collected water samples during the research period from early July until early October 2022, are illustrated per sampling station in the Vallon de Nant catchment.

Spatial Variation

The spatial variation of the d-excess values is more pronounced among the springs and the tributary than among the stations along the mainstream (see Figure 55). The lowest median d-excess value of about 1.7 is recorded at the Grass Spring, followed by the Black-Blue Pipe Spring with a value of 2, whereas the highest median of about 3.2 is determined at the La Chaux Spring and the second highest of approximately 3.1 at the Mainstream 2, a bit higher than the median d-excess of 2.8 at the La Chaux Meander. Finally, the d-excess value of the Mainstream 1 and the Mainstream 3 is about 2,7 and 2.9 respectively and the one of the Bridge Spring is slightly lower at about 2.5.

Results of Statistical Significance Test

The results of the statistical significance test (Tukey HSD), assessing whether between two sampling stations a significant difference in the mean values of the deuterium excess exists, indicate that there are significantly different deuterium excess values between all the stations and the Black-Blue Pipe as well as the Grass Spring. In addition, the deuterium excess value of the Bridge Spring is significantly different from the La Chaux Spring.

Table 20: Results of the statistical significance test of the deuterium excess (d-excess). The p-values of the deuterium excess (d-excess) between the different pairs of sampling stations are determined by the Tukey Honest Significant Differences (Tukey HSD) test.

	r1	r2	r3	s1	s2	s3	s4	t1
Mainstream 1 (r1)	not significant							
Mainstream 2 (r2)	not significant	not significant						
Mainstream 3 (r3)	not significant	not significant	not significant					
Black-Blue Pipe Spring (s1)	p<0.001	p<0.001	p<0.001	not significant				
Grass Spring (s2)	p<0.001	p<0.001	p<0.001	p<0.001	not significant			
Bridge Spring (s3)	p<0.001	p<0.001	p<0.001	p<0.001	p<0.001	not significant		
La Chaux Spring (s4)	p<0.001	p<0.001	p<0.001	p<0.001	p<0.001	p<0.001	not significant	
La Chaux Meander (t1)	p<0.001	not significant						

The following table sums up the above-elaborated results of the water quality variables and additionally, sets a context by elaborating some processes, but the analysis of these water quality variables is more profoundly discussed in chapter 5.3.

Table 21: Summary of Water Quality Variables. The extent of the spatial as well as the temporal variations of the water quality variables as well as some key processes, which set a context, are summarized.

Variable	Spatial Variation	Temporal Variation	Comment	Context
electrical conductivity (EC)	yes	no	The highest median electrical conductivity was measured at the Grass Spring. The stations along the mainstream show temporal variation.	indication of the flowing route of water; the higher the EC, the higher the water mineral composition (Pellerin et al., 2008; Tutmez et al., 2006; Hayashi, 2004)
temperature	yes	no	The stations along the mainstream and the La Chaux Meander show temporal variation.	Indication of water inflow from surface in groundwater; the higher the temperature, the higher the amount of total dissolved solids (Rau et al., 2014; Anderson, 2005; Nelson, 2002)
pH	no	yes	The Grass Spring has the lowest median pH value.	Average pH of rain is 5.7. Rain input can have an impact on the pH of surface water. low pH, more dissolved H ⁺ , higher amount of total dissolved solids (Berner and Berner, 1987; Nelson, 2002; Gunarathna et al. 2016)
fluoride	yes	yes	Spatial variation is stronger than temporal variation. A strong decrease of the fluoride concentration was recorded towards the end of August until mid-September.	part of the upper crust; naturally found in low concentration; high fluoride concentrations under acidic areas in magmatic rocks and under basic conditions in sedimentary and metamorphic rocks (Qian et al., 1999; Podgorski and Berg, 2022)

Variable	Spatial Variation	Temporal Variation	Comment	Context
chloride	no	yes	There is a strong increase towards the end of August at all stations.	accumulation due to dissolution of salts; weathering of soils, rocks; halite main source if correlated with sodium; sylvite main source if correlated with potassium (Berner and Berner, 1987; Saha et al., 2019; GOVZ.nz, 2023)
nitrite	no	yes	There is a strong increase towards the end of August at all stations.	accumulates as a consequence of the nitrification or denitrification process; often intermediate product (Lingle, 2013)
nitrate	no	no	The Grass Spring has remarkably higher values than the other stations.	accumulates as a consequence of nitrification or nitrogen fixation processes; easily washed out (Harrison, 2003; Berner and Berner, 1987; Lingle, 2013)
phosphate	no	no	There is a strong increase at the beginning of August at most of the stations.	accumulation due to weathering of phosphate minerals such as apatite; precipitation inputs (Berner and Berner, 1987)
sulphate	yes	yes	Spatial variation is stronger among springs than among the stations along the mainstream.	accumulation due to weathering of sedimentary rocks including minerals such as pyrite, gypsum, anhydrite; oxidation processes within igneous rocks (Berner and Berner, 1987; Saha et al., 2019; Aneja and Cooper, 1989)
ammonium	no	yes	There is an increase in mid-July and one at the beginning of August. Data could not be recorded over the whole research period.	accumulates as a consequence of nitrogen fixation and nitrogen mineralization processes; high concentrations under acidic or neutral pH and warm temperature (Berner and Berner, 1987; Harrison 2003, Lingle, 2013)

Variable	Spatial Variation	Temporal Variation	Comment	Context
calcium	yes	no	The Grass Spring has the highest amount of calcium. Spatial variation is stronger among springs than among the stations along the mainstream.	accumulation due to weathering of sedimentary rocks, in particular, carbonate rocks such as limestones or dolomites; weathering of minerals such as calcic-plagioclase feldspars or pyroxene (Saha et al., 2019; Berner and Berner, 1987)
potassium	no	no	No remarkable spatial or temporal variation can be identified.	accumulation due to weathering of silicate minerals such as potassium feldspar, biotite and clay minerals; weathering of potassium chloride; organic inputs (Berner and Berner, 1987; Saha et al., 2019)
magnesium	yes	no	Spatial variation is stronger among springs than among the stations along the mainstream. The Black-Blue Pipe and the Bridge Spring have the highest and the La Chaux Meander the lowest concentration.	accumulation of magnesium due to weathering of silicate minerals such as amphiboles, biotite, olivine, chlorite (Berner and Berner, 1987; Saha et al., 2019)
sodium	no	yes	There is an increase towards the end of August until mid-September.	accumulation due to weathering of silicate minerals such as plagioclase or feldspar; weathering of halite (Saha et al., 2019; Berner and Berner, 1987)
$\delta^2\text{H}$	yes	yes	The Grass Spring has the highest values. All stations show temporal variation, while the Bridge and La Chaux Spring show temporal variation to a smaller extent.	kinetic fractionation (evaporation) under non-equilibrium conditions (Beria et al., 2018)
$\delta^{18}\text{O}$	Yes	yes	The Grass Spring has the highest values. All stations show temporal variation, while the Bridge and the La Chaux Spring show temporal variation to a smaller extent.	kinetic fractionation (evaporation) under non-equilibrium conditions (Beria et al., 2018)

4.4 Data Analysis

In this analysis section, the results of the water quantity and water quality analysis of chapter 4.2 and 4.3 are further analysed by means of the time-of-day analysis and by discussing the results of the isotopic mixing model. As a further matter, the results of the concentration-discharge relationship, correlation and principal component analysis are presented.

Time-of-Day Analysis

The normality check (see Table 22) of the discharge, the pH values, the temperature as well as the electrical conductivity (EC) show that all variables are not normally distributed since all the p-values are smaller than 0.05.

Table 22: Normality check of temperature, pH, electrical conductivity (EC) and discharge. These parameters are checked for normality by means of a Shapiro Wilk test.

Variable	p-value	Result
Temperature	$5.477 \cdot 10^{-09}$	not normal
pH	$3.238 \cdot 10^{-03}$	not normal
Electrical Conductivity (EC)	$6.677 \cdot 10^{-05}$	not normal
Discharge	$9.051 \cdot 10^{-07}$	not normal

As a consequence of the non-normally distributed data, a Wilcoxon test is performed in order to test the hypothesis of whether there is a significant difference between measuring the variables in the morning or in the afternoon.

The results of the hypothesis testing show, that there is no significant difference whether the values are measured in the morning or in the afternoon for the pH values, for the electrical conductivity as well as for the discharge values, whereas a significant difference can be identified when considering the temperature values.

Table 23: Results of statistical significance test for the time-of-day analysis. It was checked by means of a Wilcoxon significance test, if the time-of-day has a significant impact on the values of the temperature, pH, electrical conductivity (EC) and the discharge.

Variable	p-value	Result
Temperature	0.0003529	significant
pH	0.836	not significant
Electrical Conductivity (EC)	0.243	not significant
Discharge	0.2918	not significant

In the following plots, the relationship between the values measured in the morning and in the afternoon of the electrical conductivity, the pH value, the temperature as well as of the discharge are illustrated.

Electrical Conductivity (am) vs Electrical Conductivity (pm)

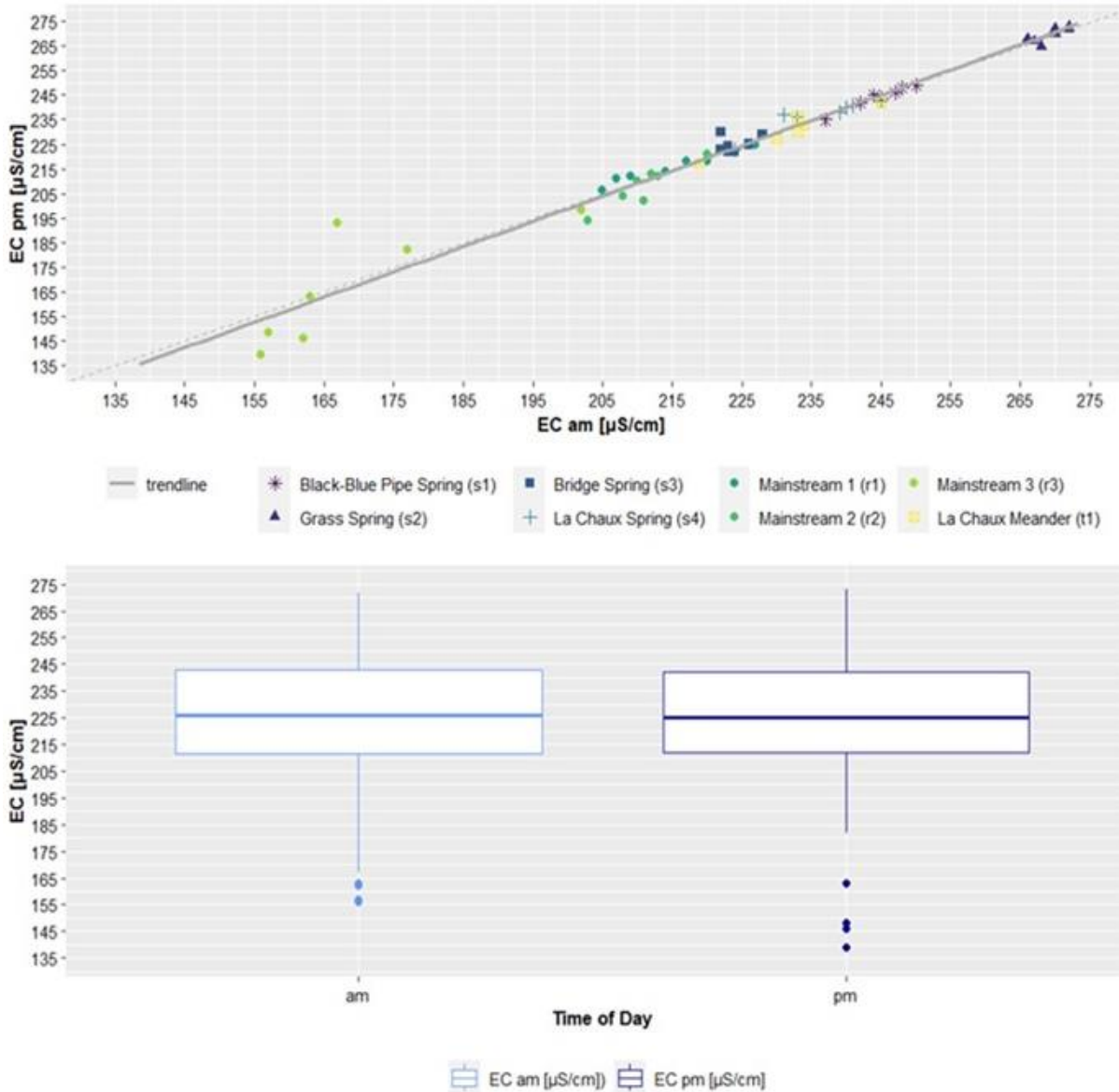


Figure 56: Time-of-day analysis of electrical conductivity (EC). The electrical conductivity, measured in the morning, is plotted against the electrical conductivity, determined in the afternoon (top), and in the boxplots, the electrical conductivity values are illustrated per time-of-day (bottom).

The trendline (see Figure 56) almost corresponds to the theoretical line, which indicates that the x value is equal to the y value, meaning that there is no difference between measuring the electrical conductivity in the morning (am) and in the afternoon (pm). In addition, most of the values are quite close to the trendline, which reinforces the result of the electrical conductivity independence of the time of the day. However, the values of the Mainstream 3 are more widely spread than the values of the other stations, highlighting that there is stronger time-of-day variations of the electrical conductivity values at the Mainstream 3. Besides, the Grass Spring has the largest electrical conductivity values, whilst the electrical conductivity values of the other stations are more closely to each other. When considering the boxplots of the electrical conductivity values, measured in the morning (am), and the ones, determined in the afternoon (pm), the median electrical conductivity values are almost identical. Finally, this graphical assessment highlights the finding of the hypothesis testing, namely that the electrical conductivity values are independent of the time of the day.

Outliers

All the outliers can be attributed to the Mainstream 3, measured during the first, second, third and the fourth sampling campaign.

pH (am) vs pH (pm)

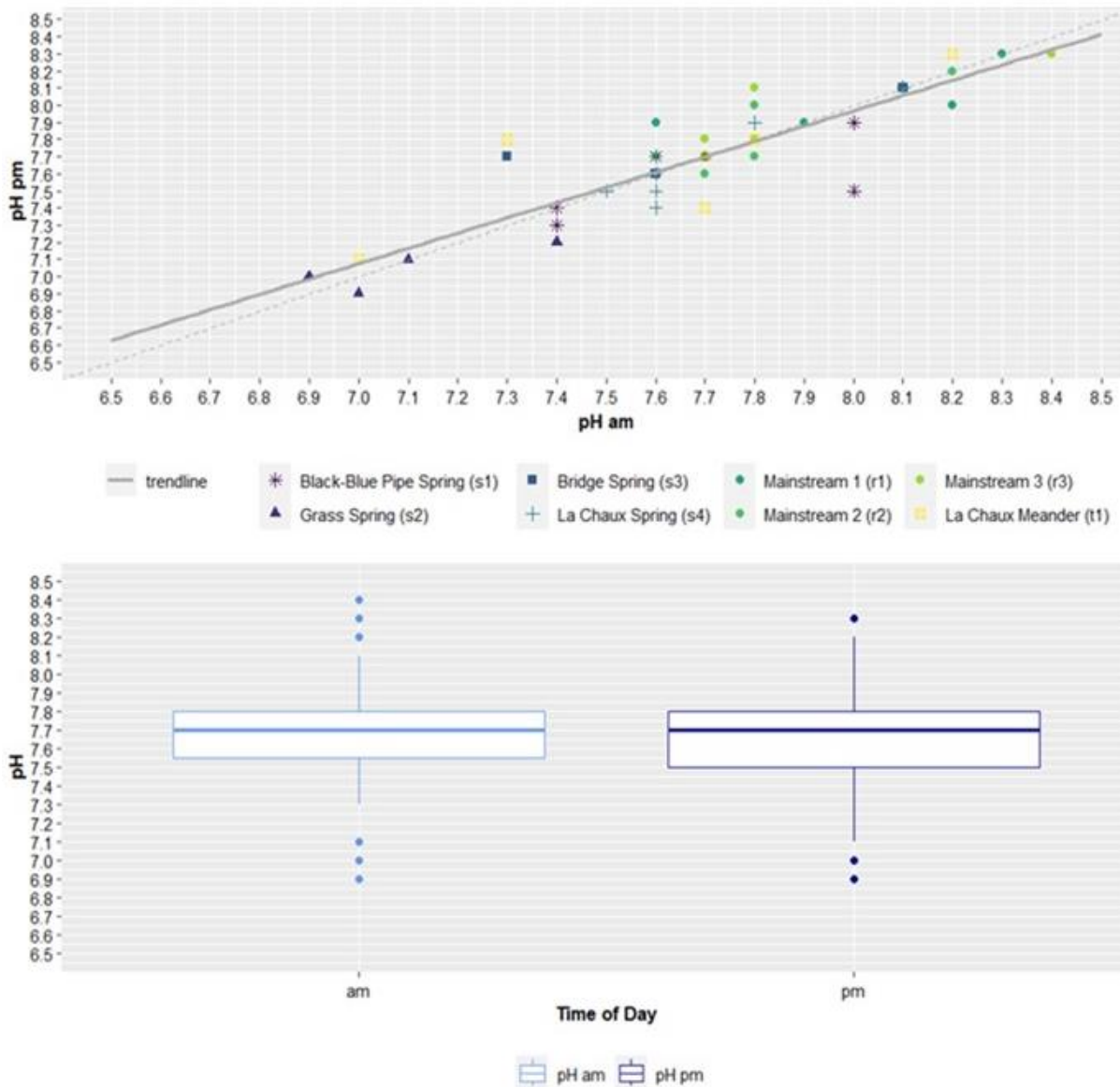


Figure 57: Time-of-day analysis of pH values. The pH values, measured in the morning, are plotted against the pH values, determined in the afternoon (top), and in the boxplots, the pH values are illustrated per time-of-day (bottom).

When considering the pH values, illustrated depending on the time of the day (see Figure 57), the trendline is quite close to the theoretical line and additionally, the median pH value, measured in the morning, is almost identical to the median in the afternoon. These observations highlight the result of the hypotheses testing, namely that the pH values are independent of the time of the day. However, the values are more widely spread around the trendline than they are in Figure 56, which, therefore, is an indicator for some diurnal variations, but no distinctive ones.

Outliers

The lower outliers, measured in the morning, are attributed to the Grass Spring, while the higher ones to stations along the mainstream as well as to the Bridge and the La Chaux Spring during the last sampling campaign. Additionally, the lower outliers, recorded in the afternoon, are pH values of the Grass

Spring, whereas the upper outlier of 8.3 is measured at the Mainstream 1 and the Mainstream 3 as well as at the La Chaux Meander during the last sampling campaign.

Temperature (am) vs Temperature (pm)

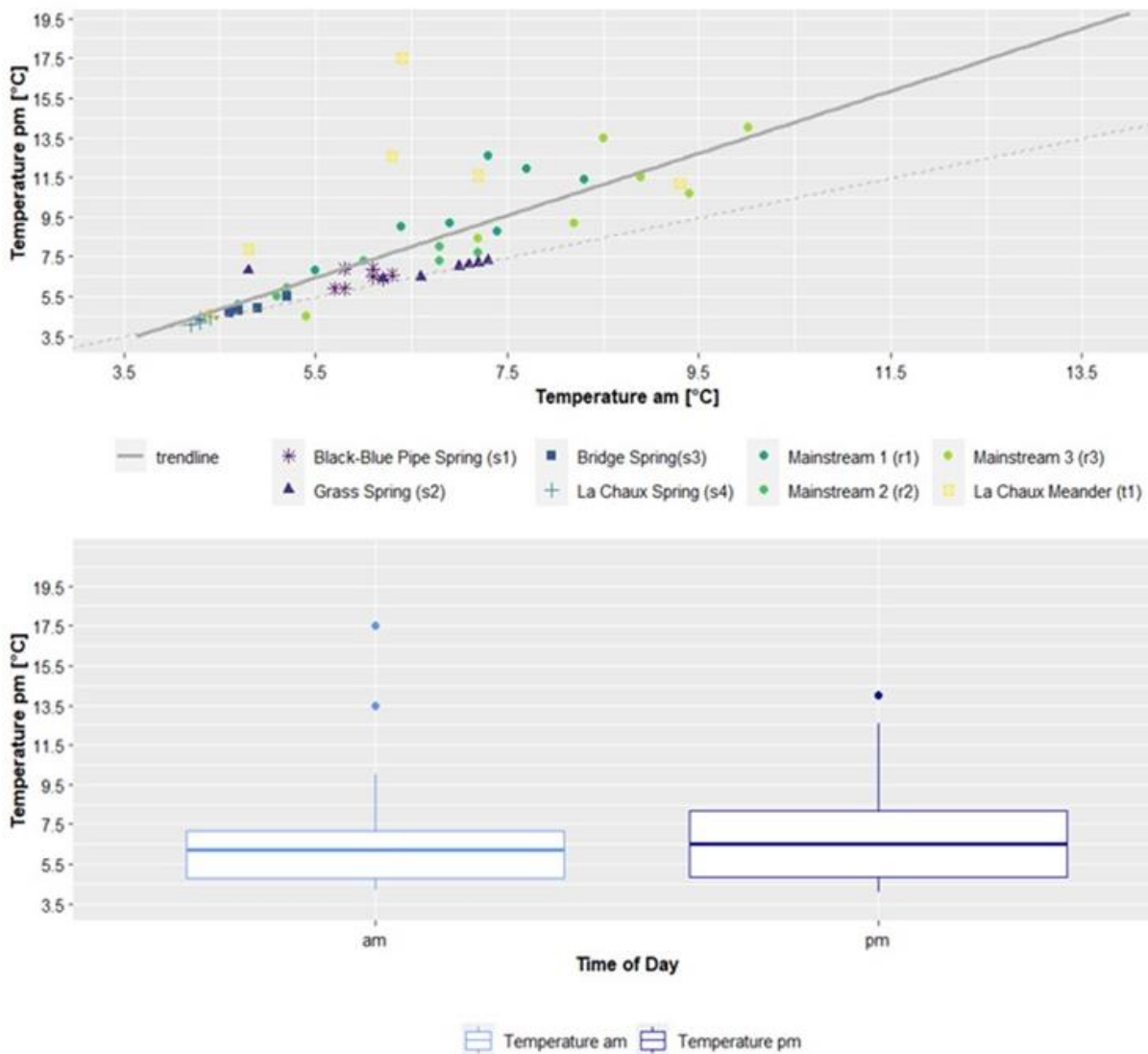


Figure 58: Time-of-day analysis of temperature. The temperature, measured in the morning, is plotted against the temperature, determined in the afternoon (top), and in the boxplots, the temperature is illustrated per time-of-day (bottom).

When considering the temperature values depending on the time of the day (see Figure 58), the trendline varies from the theoretical line, indicating that there is a difference visible. In particular, the temperature values, measured in the afternoon, are higher than they are in the morning. However, when having a closer look at the temperature distribution per sampling station, clear differences such as stronger variations at the stations along the mainstream than at the springs are noticed. Besides, the median temperature of the temperature values measured in the morning is quite close to the median of the temperature values measured in the afternoon, whereas the temporal variation is smaller among the values measured in the morning than in the afternoon.

Outlier

The highest outlier, recorded in the morning, is attributed to the La Chaux Meander and the second largest to the Mainstream 3 during the third sampling campaign. The outlier, measured in the afternoon, is recorded as well at the Mainstream 3 during the second sampling campaign.

Discharge (am) vs Discharge (pm)

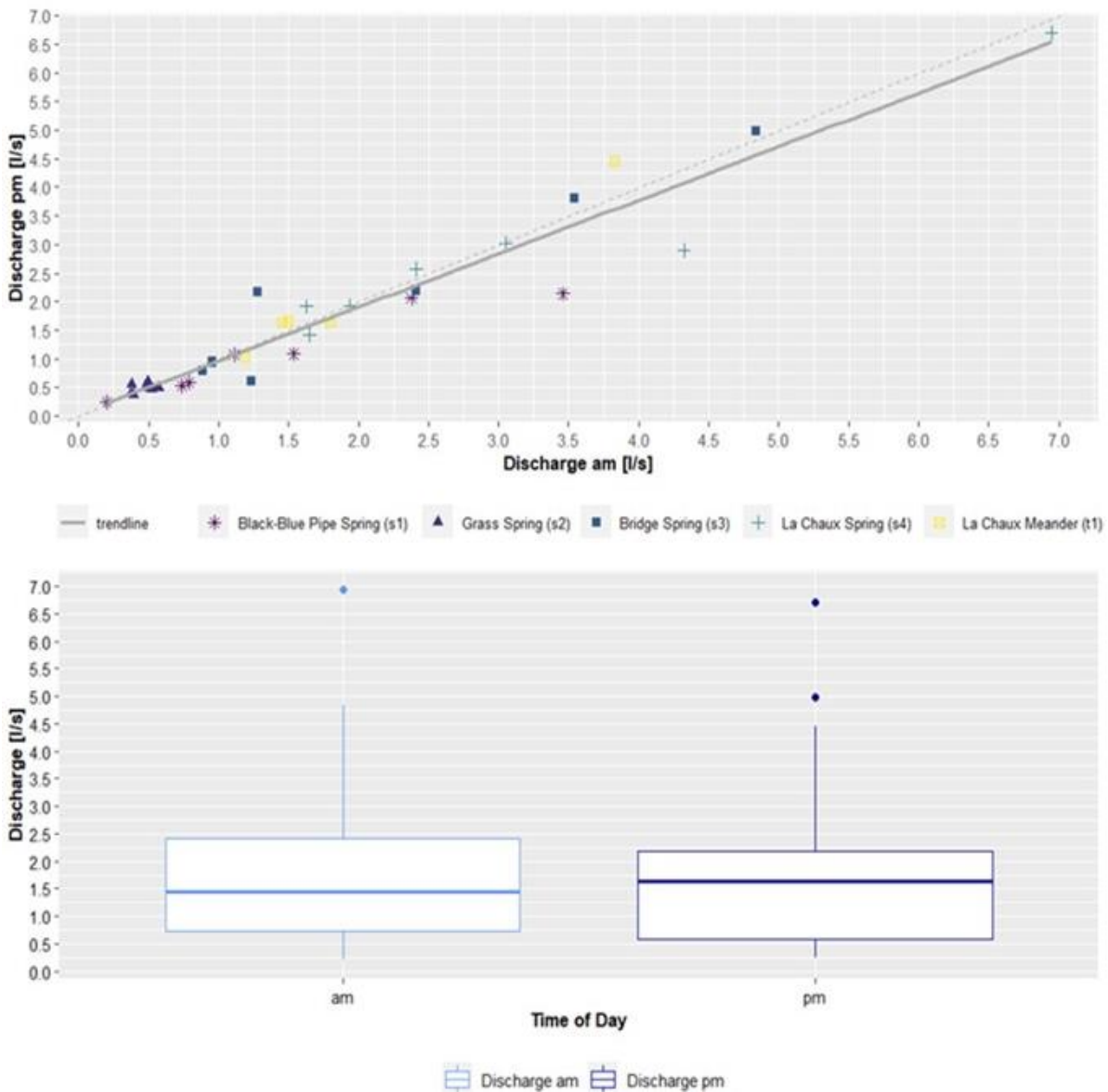


Figure 59: Time-of-day analysis of discharge. The discharge, measured in the morning, is plotted against the discharge, determined in the afternoon (top), and in the boxplots, the discharge values are illustrated per time-of-day (bottom).

When comparing the discharge values (see Figure 59), measured in the morning, with the ones in the afternoon, the trendline almost corresponds to the theoretical line. However, when having a deeper look at the trendline, it is noticed that it is slightly below the theoretical line at higher discharge values, indicating that the values measured in the morning are lower at some stations than they are in the afternoon. This observation is also made when analysing the boxplots, where the median of the discharge values, measured in the afternoon, are insignificantly higher than the median of the discharge values in the morning. Lastly, the visually assessed results correspond to the results of the hypotheses testing, highlighting that the discharge values are independent of the time of the day.

Outlier

The outlier, measured in the morning, as well as the higher one, measured in the afternoon, are attributed to the La Chaux Spring during the last sampling campaign, whereas the lower outlier, recorded in the afternoon, is measured at the Bridge Spring during the first sampling campaign.

Concentration-Discharge Analysis

When considering the results of the concentration-discharge analysis (see Table 24) of the first recession subperiod, chemostasis is the most frequent process, especially in case of the anions such as fluoride, chloride, nitrate, nitrite or phosphate, while sulphate shows at all sampling stations, apart from the La Chaux Meander, dilution processes, that is in contrast to the other anions. However, when considering fluoride, dilution happens at the La Chaux Spring as well as at the La Chaux Meander and in case of chloride, mobilization is recorded at the Bridge Spring and the La Chaux Meander. As a further matter, mobilization could be observed in case of nitrite at the La Chaux Meander. When considering the cations, dilution as well as chemostatic processes are identified, while the latter is showed by sodium as well as calcium. In addition, in case of ammonium and potassium dilution is determined at most stations, except at the Bridge Spring, where in case of ammonium chemostasis and when considering potassium mobilization is observed. At the outlet ammonium shows chemostatis. Finally, when considering magnesium, the Black-Blue Pipe Spring and the La Chaux Meander show dilution, while at the other stations chemostatis is determined.

Table 24: Results of concentration-discharge analysis of the first recession subperiod at the sampling stations. There are three different concentration-discharge patterns: dilution (red), mobilization (blue) and chemostasis (green), determined by plotting the mainstream data and the spring discharge respectively against the solute concentration. When the solute concentration decreases with increasing discharge, dilution happens; mobilization describes the relationship of increasing solute concentration with increasing discharge and when the solute concentration hardly changes with altered discharge rates, chemostasis occurs (Knapp et al., 2020).

	Black-Blue Pipe Spring	Grass Spring	Bridge Spring	La Chaux Spring	La Chaux Meander	Outlet
Fluoride	chemostasis	chemostasis	chemostasis	dilution	dilution	chemostasis
Chloride	chemostasis	chemostasis	mobilization	chemostasis	mobilization	chemostasis
Nitrate	chemostasis	chemostasis	chemostasis	chemostasis	chemostasis	chemostasis
Nitrite	X	X	X	X	mobilization	X
Phosphate	chemostasis	chemostasis	chemostasis	chemostasis	chemostasis	chemostasis
Sulphate	dilution	dilution	dilution	dilution	chemostasis	dilution
Sodium	dilution	chemostasis	chemostasis	chemostasis	chemostasis	chemostasis
Ammonium	dilution	dilution	chemostasis	dilution	dilution	chemostasis
Potassium	dilution	dilution	mobilization	dilution	dilution	dilution
Magnesium	dilution	chemostasis	chemostasis	chemostasis	dilution	chemostasis
Calcium	chemostasis	chemostasis	chemostasis	chemostasis	dilution	chemostasis

Mixing Model Analysis

In the following section, the results of the mixing analysis are presented, in particular, the proportion of rain is determined per sampling station as well as per sampling date.

Proportion of Rain per Sampling Site

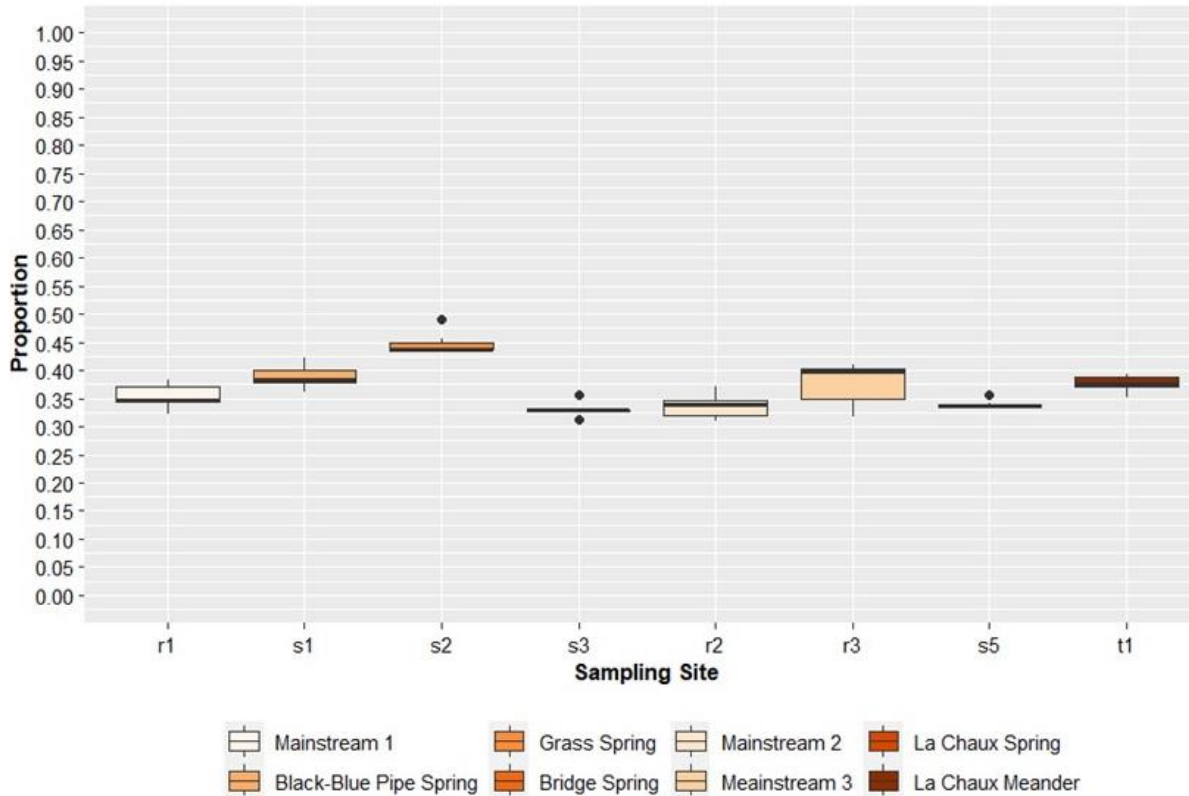


Figure 60: Boxplots of proportion of rain per sampling site over research period. The proportion of rain, determined by the isotopic mixing model (MixSIAR), during the research period from early July until early October 2022, is illustrated per sampling site in the Vallon de Nant catchment.

The sampling sites are ordered according to their elevation level, where the lowest lying sampling station, the Mainstream 1, is on the left side and the top station, La Chaux Meander, on the right side (see Figure 60). But this data does not reflect any elevation dependent pattern neither among the springs nor among the stations along the mainstream or when considering both springs and stations along the mainstream. However, the proportion of rain varies over the research period differently depending on the sampling station. The Grass Spring has the highest proportion of rain with a median value of almost 45%, followed by the Mainstream 3 of approximately 40%, while the Bridge Spring with a rain proportion of about 32% shows the lowest share. But very close to the median proportion of rain of the Bridge Spring are the median proportions of rain of the Mainstream 1, Mainstream 2 as well as of the La Chaux Spring, which all have median values in the range of 32% and 35%, while the Black-Blue Pipe Spring as well as the La Chaux Meander show slightly higher shares and thus, have median values of around 37%. In addition, the Mainstream 3 has the strongest temporal variation in the proportion of rain, while the La Chaux Spring and the Bridge Spring show hardly any temporal variation in the proportion of rain. The Grass Spring as well as the La Chaux Meander indicate a slightly stronger variation and finally, the Mainstream 1, the Mainstream 2 and the Black-Blue Pipe Spring show temporal variation to a similar moderate extent.

Outliers

All outliers are recorded during the last sampling campaign.

Research Significance Test

The results of the statistical significance test (Tukey HSD), assessing whether between two sampling stations a significant difference in the mean values of the proportion of rain exists, inter alia indicate that the proportion of rain, determined at the Grass Spring, is significantly different from all the other stations. In addition, the proportion of rain, measured at the Black-Blue Pipe Spring, is also significantly different from all stations, apart from the Mainstream 2, the Mainstream 3 and the La Chaux Meander. Besides, the Mainstream 3 is not significantly different from the La Chaux Meander, the Black-Blue Pipe Spring and the Mainstream 1.

Table 25: Results of the statistical significance test of the proportion of rain. The p-values of the proportion of rain between the different pairs of sampling stations are determined by the Tukey Honest Significant Differences (Tukey HSD) test.

Mainstream 1 (r1)								
Mainstream 2 (r2)	not significant							
Mainstream 3 (r3)	not significant	p<0.05						
Black-Blue Pipe Spring (s1)	not significant	p<0.001	not significant					
Grass Spring (s2)	p<0.001	p<0.001	p<0.001	p<0.001				
Bridge Spring (s3)	not significant	not significant	p<0.01	p<0.001	p<0.001			
La Chaux Spring (s4)	not significant	not significant	p<0.05	p<0.01	p<0.001	not significant		
La Chaux Meander (t1)	not significant	p<0.05	not significant	not significant	p<0.001	p<0.001	p<0.05	
	r1	r2	r3	s1	s2	s3	s4	t1

Proportion of Rain per Sampling Date

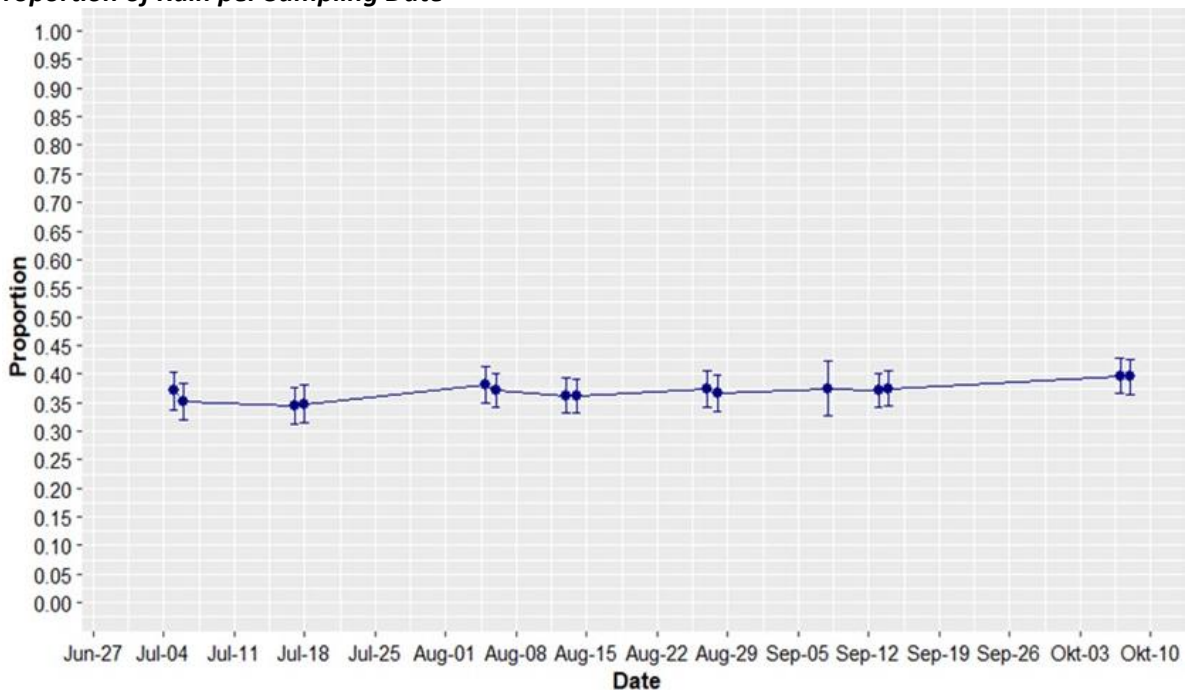


Figure 61: Proportion of rain per sampling date over research period in the Vallon de Nant catchment. The proportion of rain, determined by the isotopic mixing model (MixSIAR), is illustrated per sampling date over the research period from early July until early October 2022.

The proportion of rain indicated per date is the mean of all the stations and it varies slightly over the research period (see Figure 61). One can, for instance, observe a remarkable increase from mid-July

until early August, as well as one from mid-September until early October, whereas in between another small increase from mid-August until the end of August is noticed. As a further matter, a small decrease of the proportion of rain is observed from early July until mid-July as well as from early August until mid-August. Finally, slight variations during a sampling campaign are observed, while differences are more remarkable during the first, third as well as fifth sampling campaign.

Correlation Analysis - Springs

In this section, the results of the correlation analysis are presented, in particular, the significant correlations are extracted.

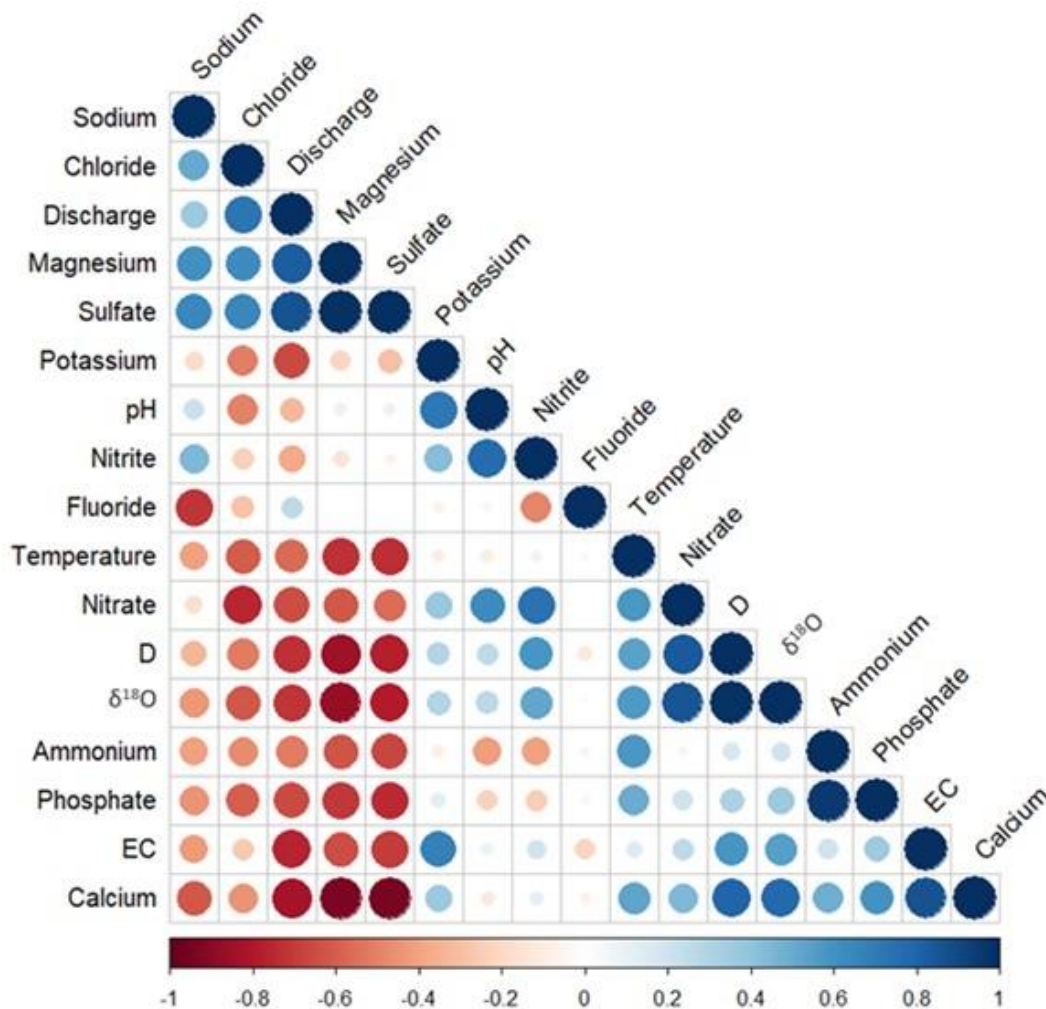


Figure 62: Correlation plot of water variables. In order to evaluate whether the water variables are linearly related among each other, correlation coefficients were determined in RStudio, while blue indicates positive correlations and red describes negative correlations.

Three correlation clusters among the ions are determined (see Figure 62), while they are positively correlated within such a cluster: calcium/phosphate (cluster 1) and ammonium/nitrate (cluster 2) as well as sulphate/magnesium/chloride/sodium (cluster 3). When analysing how these ion clusters are correlated, it can be observed that cluster 3 is negatively correlated with cluster 1 as well as with cluster 2, while cluster 2 is positively correlated with cluster 1.

When considering how these ions are correlated with the stable water isotopes, cluster 1 as well as cluster 2 are positively correlated with the stable water isotopes, while cluster 3 is negatively correlated with the stable water isotopes.

As a further matter, when analysing how these ion clusters are related to the discharge, cluster 3 is positively correlated with the discharge, while cluster 1 as well as cluster 2 are negatively correlated with the discharge.

In addition, cluster 1 as well as cluster 2 are positively correlated with the temperature and the electrical conductivity, but cluster 3 is negatively correlated with these parameters.

Finally, the stable water isotopes are negatively correlated with the discharge, but show a positive correlation to the temperature and to the electrical conductivity, while the discharge is negatively correlated with the temperature as well as with the electrical conductivity.

Significant Correlations

In Figure 63, the results of the significant correlation analysis with their corresponding correlation coefficients are illustrated, while in Table 26 the significant correlations are summarized.

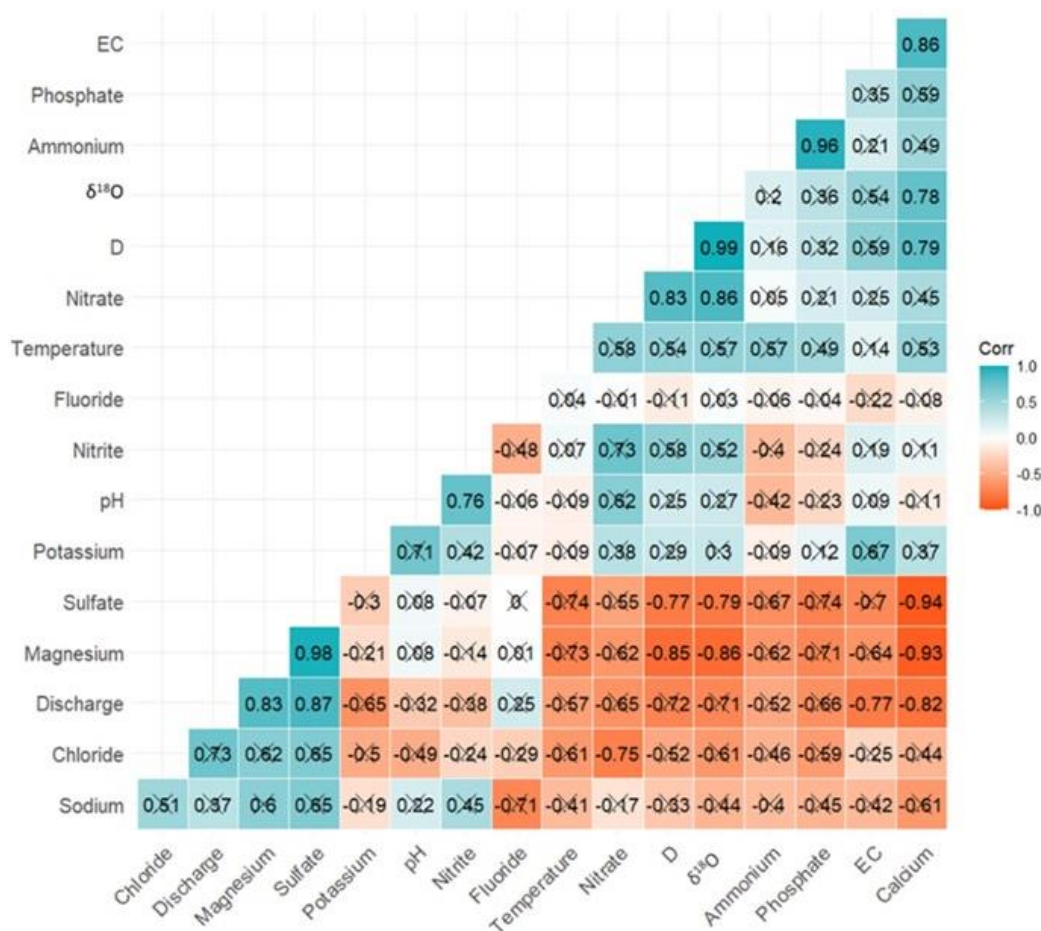


Figure 63: Correlation plot of water variables under consideration of significance level. In order to evaluate whether the water variables are significantly linearly related among each other, the water variables were tested for their significance level, while blue indicates positive correlations, red describes negative correlations and the cross highlights no significant correlations.

Table 26 shows that the discharge is significantly positively correlated with magnesium and sulphate and negatively correlated with the electrical conductivity as well as calcium. As a further matter, the heavy isotopes are significantly negatively correlated with magnesium as well as sulphate, but positively to calcium and nitrate. Finally, nitrite is significantly negatively correlated with the pH value, while nitrate is not, but with chloride.

Table 26: Summary of significantly correlated water variables. In order to evaluate whether the water variables are significantly linearly related among each other, the water variables were tested for their significance level.

Variable	Positive Correlation	Negative Correlation
discharge	magnesium, sulphate	electrical conductivity, calcium
magnesium	sulphate, discharge	calcium, $\delta^{18}\text{O}$, $\delta^2\text{H}$
sulphate	discharge, magnesium	calcium, $\delta^{18}\text{O}$, $\delta^2\text{H}$
pH	nitrite	
nitrate	$\delta^2\text{H}$, $\delta^{18}\text{O}$	chloride
ammonium	phosphate	
electrical conductivity	calcium	discharge
calcium	$\delta^2\text{H}$, $\delta^{18}\text{O}$, electrical conductivity	discharge, magnesium, sulphate
$\delta^{18}\text{O}$	nitrate, $\delta^2\text{H}$, calcium	magnesium, sulphate
$\delta^2\text{H}$	$\delta^{18}\text{O}$, nitrate, calcium	magnesium, sulphate

Principal Component Analysis

The number of principal components (PC) that explain at least 75% of the total variation, which was defined in chapter 3.5, is determined by means of the screeplot (see Annex B). The first two principal components explain 58.3% and then, together with the third and the fourth principal component the minimum boundary of 75% is slightly exceeded with a value of 77.4%. Thus, the first four principal components are considered in the following analysis.

PC1 vs PC2

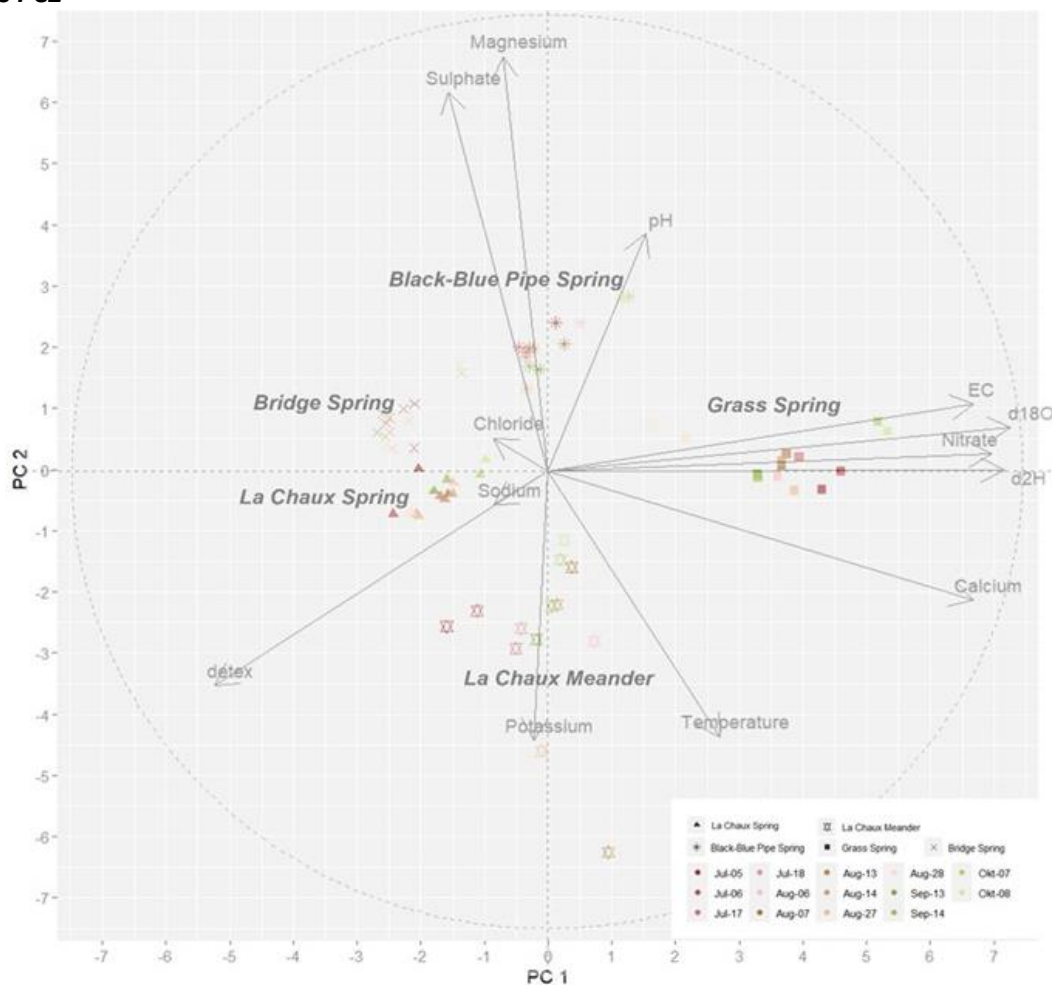


Figure 64: Principal Component 1 (PC 1) versus Principal Component 2 (PC 2) with sampling dates and sampling stations. The dimensionality is reduced by principal component analysis and thus, principal components, that contain the core information, are calculated by means of linear combinations of the original variables (Abdi and Williams, 2010).

$\delta^{18}\text{O}$, $\delta^2\text{H}$, nitrate and electrical conductivity contribute to a remarkable extent to PC1, since the arrows of these variables are almost parallel to the x-axis and since the length of the arrows is quite long, while magnesium, sulphate and potassium contribute to a considerable extent to PC2 (see Figure 64). Therefore, PC1 and PC2 describe much of the variability of these variables. In addition, calcium is also well represented by PC1, but to a lower extent. Similarly, the pH value as well as the temperature contribute to PC2, but also to a smaller extent. However, sodium and chloride are rather weakly represented by PC1 as well as by PC2. When considering the angles between the variables and thus, the correlation among the variables, it can, for instance, be noticed that $\delta^{18}\text{O}$, $\delta^2\text{H}$, nitrate and the electrical conductivity are strongly and positively correlated among themselves, since their angles are quite close to zero and their arrows point all in the same direction. But these variables are weakly correlated with magnesium and sulphate as well as potassium, since their angle is close to 90° or 270° respectively. Besides, they are strongly negatively correlated with sodium as well as to chloride, indicated by the angle of almost 180° and the opposite direction of the arrow. A strong negative correlation can also be identified between potassium and magnesium as well as between potassium and sulphate.

When taking the sampling stations and sampling dates into consideration, the datapoints are clustered per sampling station and not per sampling date. The Grass Spring is quite different from all the other stations, while the Bridge Spring is more similar to the La Chaux Spring than to the La Chaux Meander, whereas the cluster of the Black-Blue Pipe Spring is also closer to the Bridge Spring than to the Grass Spring. In addition, all the clusters are compact except the one of the La Chaux Meander, which is more widely spread. So, at the Grass Spring, in contrast to the La Chaux Spring, particularly the electrical conductivity values, the abundance of heavy isotopes as well as the concentration of nitrate and calcium are high and contribute to explaining the discharge rate, while at the La Chaux Spring all these variables are less expressed and thus, explain the discharge rate respectively. Another example is that at the Black-Blue Pipe Spring sulphate as well as magnesium concentrations are high and, therefore, contribute to explaining its discharge, while at the La Chaux Meander these variables are low, but potassium and the temperature are more expressed there.

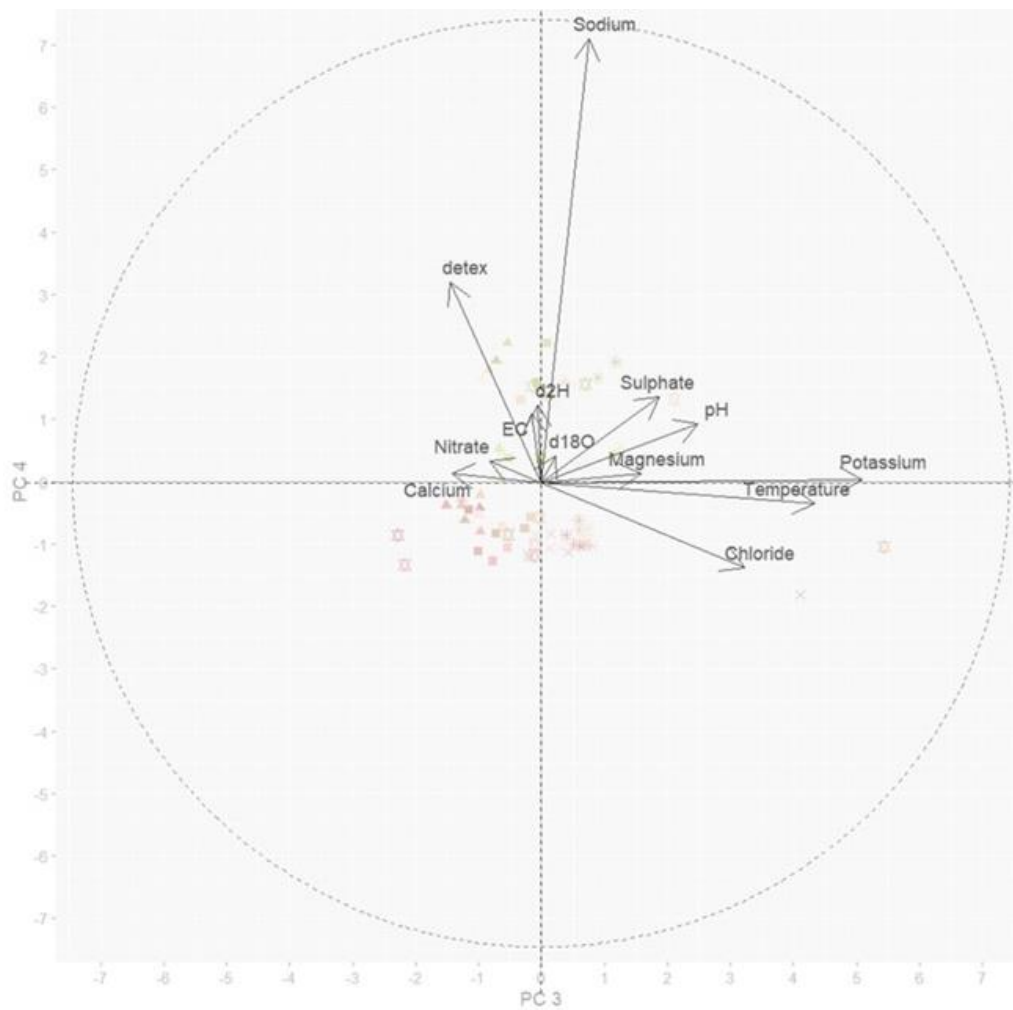
PC3 vs PC4

Figure 65: Principal Component 3 (PC 3) versus Principal Component 4 (PC 4) with sampling dates and sampling stations. The dimensionality is reduced by principal component analysis and thus, principal components, that contain the core information, are calculated by means of linear combinations of the original variables (Abdi and Williams, 2010).

Most of the variables are more weakly represented by PC3 and PC4 than they are by PC1 and PC2. However, magnesium and calcium contribute to PC3, since these arrows are quite parallel to the x-axis, but the length of the arrows is rather short (see Figure 65). In contrast, the temperature and potassium, which show a higher arrow length as well as an angle close to 0° or close to 180°, are represented by PC3 more strongly, while nitrate, pH and chloride also contribute to PC3, but to a lower extent due to their bigger angle to the x-axis. PC4 describes much of the variability of sodium, the electrical conductivity and the heavy isotopes, since these variables have the smallest angle to the y-axis and in case of sodium, the arrow is considerably long. Sulphate also contributes to PC4, but to a much lower extent. When considering the correlation among the variables and thus, having a closer look at the angles between the variables, one can, for instance, identify that there is a strong positive correlation between the temperature and potassium concentration, while they are rather weakly correlated with sodium or the heavy isotopes and additionally, the temperature as well as the potassium concentration are negatively correlated with the nitrate and calcium concentration. When considering the sampling stations and sampling dates, the spatial differences between the stations are less distinctive than they are in the first and second dimension, while the temporal variation is much more visible. For instance, the sodium concentration is higher in September and October than in July and August at most of the stations. Or the sulphate concentration is lower in July and August in comparison to September and October.

5 Discussion

In this section, the results (see chapter 4) are discussed in the context of the subquestions (see chapter 1.2) and therefore, they contribute to answering the main research question, in particular, to highlighting how the hydrochemical as well as the isotopic tracers are used to explain storage-discharge relationships of the springs in the Vallon de Nant over the summer recession period. This chapter is structured into five parts: the discussion of the meteorological conditions in the catchment (see chapter 5.1), the discussion of the water quantity variables (see chapter 5.2), the discussion of the water quality variables (see chapter 5.3), the synthesis (see chapter 5.4) and the limitations (see chapter 5.5).

5.1 Discussion of Meteorological Conditions in the Catchment

In this subchapter, it is explained how meteorological conditions have an impact on the discharge rate by the example of the discharge of the Avançon de Nant, measured at the outlet of the Vallon de Nant catchment (see chapter 4.1). In addition, the definition of the streamflow periods of the Avançon de Nant, particularly the recession period, introduced in chapter 4.1, are discussed.

Impact of meteorological conditions on discharge

Precipitation and temperature are fundamental variables that help interpret and understand the reasons behind the variations and the timing of discharge and are thus important to be considered. Since temperature has an impact on snowmelt, it is a key factor, according to Hayashi (2020), when explaining discharge variations in spring. However, he highlights that precipitation events are more relevant to explain discharge variations over the summer and fall time, whereas during winter time groundwater inputs are the key drivers for the discharge.

Two discharge peaks in early March as well as a discharge increase in May were, for instance, recorded at the outlet of the Avançon de Nant (see chapter 4.1). The increased discharge rates, however, occurred simultaneously with a temperature increase. So, due to the rising temperature in those months, snow melting was accelerated, leading to higher discharge rates. A more detailed evaluation of the discharge curve at the end of May shows that, as soon as temperature decreased, the discharge rate was slowed down, indicating that snow melting was then reduced. Therefore, the assumption that snowmelt is inter alia responsible for the increased discharge rate in May is based on the observation that in early April there were several precipitation events, when the temperature was low and thus indicating that snow must then have been accumulated. Additionally, the peaks of discharge correspond to the peaks of temperature, which is a clear indication for snowmelt. At the beginning of June, there was a series of precipitation events that led to several discharge variations and at the end of June there was a strong rise of discharge which can be explained by a strong precipitation event. Precipitation peaks in mid-July, end of August, mid-November and end-December can be clearly related to precipitation events. However, it remains unclear how this remarkable peak of discharge at the beginning of October occurred. But it can be identified that there was a series of precipitation events before, which definitely had an impact on the discharge, but may not fully explain this high discharge.

Discussion of Streamflow Periods

Cochand et al. (2019) explained (see chapter 1.1) that in Alpine catchments one talks about a high-flow period, describing the time in spring when the snowmelt has a strong impact on the discharge and the subsequent low-flow period, the so-called recession period, when groundwater maintains the streamflow. Michelon et al. (2023), who did profound research in the Vallon de Nant, defined streamflow periods based on discharge data for the years 2016-2018. So, in the following paragraphs, the definition of the streamflow periods, particularly of the recession period 2022 in the Vallon de Nant

catchment (see chapter 4.1), which ultimately lasts from 24th June to 30th September 2022, is discussed, compared to the streamflow periods of previous years and set into context of meteorological conditions.

In chapter 4.1, the melt period is identified to start in 2022 at a comparable timepoint as in the research years of Michelin et al. (2023), namely in mid-March, but it lasted until June, longer than it did in 2017 and 2018. The seasonal recession period started and ended in the research years of Michelin et al. (2023) at similar timepoints as it did in 2022. In order to obtain an understanding of why these periods are defined in this way, the meteorological conditions of the catchment in 2022 need to be considered, since the discharge is strongly linked with the consequences of precipitation events and temperature development.

The year 2022 started in Switzerland with a mild and dry winter (MeteoSwiss, 2023). Similarly, in the Vallon de Nant catchment, the temperature in the winter months until mid-April fluctuated between low positive and a slightly negative temperature, but towards mid-May a strong temperature increase was measured (see chapter 4.1). In the Vallon de Nant catchment, January was also dry when comparing it to the precipitation amount in February. In Switzerland there was little precipitation recorded in spring, in particular, in the western part of Switzerland (MeteoSwiss, 2023). The spring in the catchment started dry since there was hardly any precipitation recorded in March, whereas April and May were wetter. The early melt period was induced in mid-March, since there was a strong temperature increase, which accelerated the snow melting and thus, led to an increased discharge. This rise in temperature lasted until the beginning of May. The reason why this early melt period lasted a few weeks must have been the strong temperature variations within these weeks. There were, for instance, days when the temperature fell again below zero such as the cold spell at the beginning of April, which consequently slowed down the melting process. However, the temperature was positive without any exceptions from mid-April on. The melt period of 2022, lasting from the beginning of May until the end of June, occurred simultaneously to the high temperature rise in May and June. However, this melting period also included strong temperature fluctuations such as at the end of May as well as in early June, which also contributed to a reduced melting process and thus to a longer melting period.

According to MeteoSwiss (2023), summer 2022 was the second warmest summer since the beginning of measurements in 1864, and especially July was very dry, in particular, in the south western part of Switzerland, where severe dryness was observed, and additionally, it was the time, when the summer recession period started. So, based on the discharge data measured at the outlet in the catchment, the summer recession period is defined to start at the end of June and to last until the end of September. Once snowmelt is over, it does not contribute to discharge anymore. When considering the meteorological conditions in the Vallon de Nant, summer started warm and in mid-July a time period with a temperature between 17°C and 21°C, corresponding to the warmest time of the year, was recorded. Regarding the precipitation, several precipitation events were measured in June, whereas in the first half of July as well as of August hardly any rainfall was recorded, which was in contrast to their second halves, when some rain events were observed. The temperature from August until mid-September kept on fluctuating on a lower level than in July, but it was still warm.

The baseflow period 2023 started at the beginning of October 2022. In Switzerland, the autumn was warm but wet, particularly in the western part of Switzerland (MeteoSwiss, 2023). In the Vallon de Nant, October was warm and then in the following months the temperature fluctuated between a low positive and a slightly negative temperature until the end of the year. Throughout autumn as series of precipitation events was recorded, and thus it was quite wet apart from the first half of October in the catchment.

Despite the fact that 2022 was the warmest year since the beginning of the temperature measurements in 1864 and is also at some timepoints recorded exceptionally dry (MeteoSwiss, 2023), one cannot identify any remarkable consequences of these meteorological conditions on the definition of the streamflow periods, in particular, on the recession period, when comparing the periods of 2022 to the ones from Michelin et al. (2023). But when considering the Swiss Climate Change Scenarios (CH2018) for Switzerland, elaborated in details in chapter 2.2, the Vallon de Nant catchment, which is a high elevation catchment, will be hit by the consequences of climate change and, thus, will have an impact on the timing of the streamflow periods. Thus, the early melt period and the melt period respectively are assumed to occur earlier in time and may also last shorter than they do today, since the temperature is overall expected to rise and precipitation in winter will occur more often in form of rain and less snow will be accumulated (National Centre for Climate Services, 2018; Muelchi et al., 2021). The shift of the early melt period and the melt period have an impact on the timepoint of the recession period, which consequently will start earlier and thus last longer. In addition, evapotranspiration will be enhanced in that recession period. Finally, what is remarkable and clearly observable are strong precipitation events throughout all year in the catchment of the Vallon de Nant. Such events are expected to occur more frequently in the context of climate change as elaborated in chapter 2.2 (National Centre for Climate Services, 2018; Muelchi et al., 2021).

5.2 Discussion of Water Quantity Variables

In this section, the results of the discharge measurements at the springs, the comparison of the discharge pattern between the springs and the mainstream as well as the results of the recession time-scale analysis are discussed (see chapter 4.2).

Discussion of Discharge Analysis of the Springs

The results of the discharge analysis at the springs show that there is **spatial variation** between the sampling stations over the research period. In order to obtain an understanding of the spatial variation, the hydrological units of the springs (see chapter 2.1) need to be considered.

The La Chaux Spring and the La Chaux Meander, which have high discharge rates in comparison to the sampling stations of other hydrological units, are located on the western side of the catchment, which is primarily determined by hillslopes and pasture. In addition, the soils are of large depths and have high water storage capacities. These conditions as well as the fact that the slopes are not very steep are specifically beneficial for the existence of springs as well as for tributaries, which is concluded by Michelin et al. (2023), who identified a connection between low slopes and the occurrence of springs. The Grass and the Black-Blue Pipe Spring, which have the lowest median discharge, as well as the Bridge Spring are located in the riparian zone on the eastern part of the catchment. This unit generally consists of rough alluvial deposits, has high hydraulic conductivity and offers, according to Thornton et al. (2018), ideal conditions to store water.

However, based on the statistical significance test, highlighting that no statistically significant difference of the mean discharge between the sampling stations was noticed, apart from the pair La Chaux Spring/Grass Spring, it can be concluded that no spatial variation exists. But the data load is remarkably small, particularly, only 14 values per sampling station, for performing such a statistical significance test, and thus the result of the significance test needs to be treated with caution. Nevertheless, the statistical significance test indicated a significance between the Grass Spring, which has the lowest discharge, and the La Chaux Spring, where the highest discharge rate was determined. Finally, it can be concluded that there is a qualitatively observed spatial variation, but statistically no significant variation could be determined.

A **temporal variation** of the discharge at all the sampling stations apart from the Grass Spring is noticed, but to a different extent regarded over the whole research period. In the following paragraphs, the impact of precipitation on the discharge as well as the possibility, whether the time of the day, when the discharge measurement is performed, has an influence on the temporal variation, are discussed.

The discharge decreases from the first sampling campaign in early July until the fourth sampling campaign in mid-August at the La Chaux Spring, the Bride Spring and also slightly at the Grass Spring, when taking the discharge per sampling campaign into consideration. However, at the Black-Blue Pipe Spring and at the La Chaux Meander a decrease of the discharge is seen from early July towards mid-July and then the discharge increases again towards early August before it declines in mid-August. When considering the precipitation events, a series of precipitation events is recorded on some days before, but not immediately before the sampling campaigns. This observation leads to the assumption that the Black-Blue Pipe Spring as well as the La Chaux Meander are more sensitive to precipitation events than the other stations, and thus the water might be released from a shallower layer than at other stations or additional sources such as surface runoff might contribute to the discharge, which then explains why the discharge at these stations does not decrease equally fast as at other stations, but in a comparably delayed manner.

The results show, that from mid-August the discharge increases at all stations towards the end of August and then it decreases again towards mid-September, apart from the Black-Blue Pipe Spring, where it increases towards mid-September, before it increases again in early October, whilst the latter timepoint is not anymore part of the recession period. The discharge increase at all the stations from mid-August until the end of August can be related to a series of precipitation events with an event immediately before the sampling day, and thus this increase explains that all stations react to that precipitation event. But at the Black-Blue Pipe Spring the discharge does not decrease anymore until mid-September, which again confirms the assumption that the Black-Blue Pipe Spring cannot efficiently process the impact of precipitation events, since in the time span from end-August until mid-September another series of precipitation events is recorded. As a consequence, this finding again leads us to think that water from further sources than groundwater such as, for instance, soil water must contribute to the measured discharge. Then, the reason why the discharge increases that much at the beginning of October is unclear, since no precipitation data of the La Chaux weather station is available. But what the precipitation data of Sorniot-Lac Inférieur shows, is that there was a series of strong precipitation events at the end of September as well as a precipitation event on the second day of the sampling campaign, which must have had an impact on the discharge increase.

Finally, it needs to be considered that the measurements are snapshots and taken at a specific time of the day, which means once in the morning and once in the afternoon during a sampling campaign. So, in order to determine whether the time of the day has an impact on the discharge rate, a time-of-day discharge analysis was performed (see chapter 4.4), which however results in no significant difference between measuring the discharge in the morning or in the afternoon. Thus, one can exclude any diurnal variations, particularly that diurnal heating, which may lead to diurnal cycles of melt, have an impact on the discharge rates. If this was the case, the discharge measured in the afternoon would be significantly higher than in the morning due to an increasing temperature throughout the day.

Discussion of Mimicry Analysis between Springs and Mainstream

In order to gain an understanding of how the springs are connected to the mainstream, the springs discharge pattern is compared to the overall discharge as well as to the baseflow of the mainstream. In the following paragraphs, the results of the mimicry analysis between the springs and the overall discharge of the mainstream as well as its baseflow (see chapter 4.2) are discussed.

The mimicry analysis showed that the spatial variation, in particular, the assessment of in how many sampling campaigns a spring mimicked the discharge of the mainstream, is valuable for the overall mimicry analysis, while the temporal variation, in specific, the analysis of by how many stations the mainstream discharge was mimicked during a sampling campaign, more specifically indicates how well precipitation events are mirrored in the spring discharge in comparison to the discharge of the mainstream.

Since all the springs apart from the Grass Spring immediately reacted to precipitation events that occurred on the second sampling day of the fourth sampling campaign and neither the discharge of the mainstream nor its baseflow showed any reactions on that day, it can be concluded, despite the small data load, that the reaction time of headwaters to precipitation events is more immediate than the one of mainstreams. In addition, the results show that not all springs react the same after a series of precipitation events that occurred some days before, but not immediately before the sampling days. In particular, the overall discharge of the mainstream as well as its baseflow decrease and so does the discharge at the Black-Blue Pipe and at the Bridge Spring, while the La Chaux Spring, the Grass Spring and the La Chaux Meander show a discharge increase. This result lets us assume that precipitation must contribute to the discharge of the La Chaux Spring, Grass Spring and the La Chaux Meander to a larger extent and thus leading not only to an immediate but to a sustained increase in discharge due to an ongoing runoff.

Overall, the Black-Blue Pipe Spring as well as the Grass Spring mimic the discharge pattern of the mainstream the best, followed by the Bridge Spring, while the La Chaux Spring and the La Chaux Meander do the least. This result also indicates that water from further sources than groundwater such as the direct impact of precipitation or surface water may directly contribute to the measured discharge as they also do to the mainstream discharge. Nevertheless, to sum up, the discharge pattern of the mainstream is weakly reflected by the discharge pattern of the recorded springs during our sampling campaigns.

Therefore, the above-mentioned observations let us assume that other contributors need to be involved and need to remarkably contribute to the overall discharge of the mainstream and its baseflow. This assumption is enhanced when considering Figure 17. Since, when analysing the contribution of the monitored springs to the mainstream baseflow, their contribution is relatively modest, and thus other major sources such as further springs and tributaries must contribute to a much larger extent and consequently, control the mainstream baseflow. Additionally, the temporal evolution of the overall spring discharge contribution does not completely follow the temporal pattern most springs individually do. In particular, the contribution of the springs to the mainstream baseflow increases from July towards early August before it decreases again. This is the discharge pattern which the Black-Blue Pipe as well as the La Chaux Meander follow, while the other springs do not include such an increase but continue decreasing towards mid-August. This finding indicates that the mainstream baseflow varies temporarily differently than most of the springs do and therefore, the other contributors must vary differently than most of the recorded springs do.

Discussion of Recession Timescale Analysis: Mainstream

In chapter 4.2, the mainstream baseflow is analysed over the whole recession period. Since no continuous decrease of the baseflow was identified, similarly to the recession study performed in the Pescadero Creek, recession subperiods and their corresponding recession constants were calculated under the assumption that several different storages contribute to the mainstream baseflow at different moments over the recession period. In addition, the recession analysis, which *inter alia* includes the calculation of the recession constants, is based in this thesis specifically on inputs from Müller et al. (2022)'s paper (see chapter 3.4), and thus the recession constants of the Vallon de Nant catchments are discussed by means of their gained knowledge.

In the Vallon de Nant catchment, the recession constants of the mainstream baseflow increase from subperiod to subperiod, which indicates that the water storage-release rate becomes slower over the recession period. An explanation for the increase of the recession constant is, as already mentioned above, that with time passing different compartments of the Vallon de Nant catchment with different water storage-release rates may contribute to the mainstream baseflow. Müller et al. (2022) found in their study that surface-near landforms do not have recession constants of more than a few days and that flat aquifers usually have higher recession constants. So, based on Müller et al. (2022), it can be assumed that all the compartments, contributing to the mainstream baseflow, must be flat, since all calculated recession constants are quite high, and thus their water storage-release rates must be much slower. As a further matter, the main contributor to the mainstream baseflow in the first subperiod needs to come from a relatively superficial compartment of the aquifer, while the contributors to the mainstream baseflow in the other subperiods must come from much deeper compartments of the catchment. In addition, based on the different recession constants of the recession subperiods, it can be concluded that the storage capacity is the lowest in the first subperiod and the highest in the fourth. When taking the R^2 values into account, highlighting how robust the model is, it can be identified that especially the recession constant of the first subperiod as well as the one of the third subperiod is comparably robust, while there is much more uncertainty in the last subperiod, and thus it is then unclear where the water comes from.

In order to explain the baseflow increase in subperiod 3, precipitation data as well as the definition of the baseflow is considered. When considering the amount of precipitation during subperiod 3, a series of events is observed at the beginning of the period, at around 5th September, and then another one towards the end of the period, while in between no precipitation was recorded. Thus, these precipitation events must have an impact on the baseflow, despite the fact that it was assumed that the baseflow represents the groundwater contribution. So, this increase in discharge within the recession period reflects a weakness of the definition of the baseflow, which was defined by centring the lowest discharge over 7 days to midday of the reported day.

Discussion of Recession Timescale Analysis: Springs

A further step of the recession analysis is to analyse whether the springs show a similar discharge pattern within the subperiods previously defined by the mainstream baseflow pattern, while in case of the springs it was not differentiated between overall discharge and baseflow. So, the Bridge Spring, the Grass Spring and the La Chaux Spring also show this recession within the first subperiod, whereas the Black-Blue Pipe Spring as well as the La Chaux Meander show two recessions within the first subperiod.

The fluctuating behavior of the discharge within a short time at the Black-Blue Pipe Spring as well as at the La Chaux Meander, which result in two recessions, can be explained by the assumption that there might be water of other origins than groundwater such as precipitation and surface runoff that

contribute to the discharge. When considering the precipitation data, it can be identified that between the second and third sampling campaign, precipitation was recorded. So, this increase in discharge highlights a weakness of the definition of the spring baseflow, namely that the spring discharge does not completely correspond to its baseflow, but it also indicates that the Black-Blue Pipe Spring as well as the La Chaux Meander may be more strongly influenced by precipitation than the other stations are.

When considering the results of the calculation of the recession constants at the springs (see chapter 4.2), quite strong differences between the Grass Spring and the other springs are identified, while among the others also variabilities are observed, but to a smaller extent. These spatial differences in the recession timescale, represented by the recession constants, among the springs indicate that the individual compartments of the springs store and release water to different extents. For instance, the Grass Spring has a long recession constant indicating that it has a high storage capacity and thus, a rather slow storage-release rate, whereas the Black-Blue Pipe Spring as well as the La Chaux Meander have shorter recession constants, which highlight that their storage capacity is lower and thus, their storage-release rate faster. The Bridge as well as the La Chaux Spring have recession constants longer than the Black-Blue Pipe Spring, but remarkably shorter than the Grass Spring, which indicates that the Bridge as well as the La Chaux Spring have higher storage capacities than the Black-Blue Pipe Spring as well as than the La Chaux Meander and, consequently, also slower storage-release rates.

According to Müller et al. (2022), long recession constants indicate high storage capacity, and thus also a water release from rather deep layers in the compartment of the aquifer, since near surface landforms have recession constants of a few days. Therefore, based on the recession constants determined at the springs, the Black-Blue Pipe Spring as well as the La Chaux Meander release water from relatively superficial compartments, while the Bridge and the La Chaux Spring from comparably deep compartments. However, the Grass Spring must release water from a completely different, specifically from a much deeper part of the aquifer compartment, since the recession constant is remarkably longer than the ones of the other springs. Furthermore, the discharge of the Black-Blue Pipe Spring as well as the discharge of the La Chaux Meander are not necessarily predominantly determined by groundwater, but also by waters from other origins such as, for instance, by soil water due to their comparably low recession constants. When considering the discharge of the La Chaux Spring, it is assumed that the impact of groundwater on its discharge is less overshadowed by waters of different origins.

5.3 Discussion of Water Quality Variables

In this chapter, the results of chapter 4.3, in particular of the electrical conductivity, pH value and temperature measurements as well as of the hydrochemical and isotopic analysis, are discussed. The key processes were introduced in Table 21 (see chapter 4.3). As a further matter, it is explained how the ions are related to the discharge pattern as well as the proportion of rain at the individual stations is discussed in order to gain a more profound understanding of how ions and isotopes can serve as hydrological tracers and thus create a fundament for answering the main research question in chapter 5.4.

Electrical Conductivity

The electrical conductivity reflects, according to Pellerin et al. (2008), the mineral composition of water and the variable is used to differentiate between different origins of water and additionally, to make conclusions about its flow path.

When considering the results of the electrical conductivity values, the springs have higher and thus significantly different electrical conductivity values than the mainstream. This finding indicates that the

mainstream particularly contains surface water, which is less minerally enriched than the water, that is released at the springs. In addition, at the springs the spatial variation of the electrical conductivity values is larger than the temporal variation, in particular, the electrical conductivity at the Grass Spring is the highest and significantly different from all other stations, while the electrical conductivity values of the other springs lie closer together, but are still significantly different in most cases. The observation of Michelin (2022), who found in his study that the electrical conductivity value of the mainstream is lower than the one measured at the springs, corresponds thus to our finding. Furthermore, high electrical conductivity values indicate, according to Michelin (2022), relatively high residence time of the water in the subsurface, small flowing rates or extended flowing paths. Since the springs have lower flowing rates, which is reflected in their discharge, the residence time of the water in the subsurface is higher, and thus the water of the springs is minerally more enriched than the water in the mainstream. The finding that the Grass Spring has particularly high electrical conductivity values, therefore, indicates that this relationship is specifically pronounced. However, when considering the electrical conductivity isolated from other variables, it can be assumed that the springs have in comparison to the mainstream a higher share of groundwater, which is due to its exposure to the ground, that is minerally more enriched, while the mainstream has a higher share of surface water and is, therefore, more diluted.

Michelon (2022) explains in his paper that when an incline of the electrical conductivity is observed at the springs over the recession period, water from deeper flow paths starts heavily contributing to the discharge. As a consequence, the mainstream is then also less diluted by shallow water. However, the considered springs show a rather constant electrical conductivity over the recession period. But when considering the evolution of the electrical conductivity values at the stations along the mainstream, particularly, at the Mainstream 3, the values increased over the recession period, which finally is an indication that the contribution of water from deeper layers rose and the contribution of water from more shallow layers as well as the snowmelt contribution decreased as explained above by Michelin (2022). As a further matter, small temporal variations in the mainstream such as the light decrease from mid-July towards early August, which corresponds to the time when a series of precipitation events occurred, were recorded. Hayashi (2004) explains that precipitation usually contains the lowest number of solids, and, therefore, the rain inputs, which were recorded then, must be the reason for the decline of the electrical conductivity values, since the water became more diluted by those precipitation events. Finally, the time-of-day analysis has showed that there is no significant difference between measuring the electrical conductivity in the morning or in the afternoon, and thus any diurnal variations can be excluded, particularly diurnal heating, which may lead to diurnal cycles of melt, otherwise the electrical conductivity would be significantly higher in the morning than in the afternoon.

Temperature

The key result of the temperature measurement is that the spatial variation is more distinctive than the temporal variation when considering the springs, while when taking the temperature at the stations along the mainstream into consideration, temporal variation can be clearly observed.

Reasons for such temporal variations are the time-of-day dependency of the temperature, which is identified in the time-of-day analysis to be significant and the fact that surface water is more exposed to solar radiation, which consequently is responsible for heating up the water. However, the La Chaux Meander also shows temporal as well as diurnal variation, indicating that groundwater contributes to a smaller extent to its water release, while the La Chaux and the Bridge Spring hardly and the Grass and Black-Blue Pipe Spring to a slightly higher extent show temporal variation, indicating that the groundwater contribution is larger at the springs than it is at the La Chaux Meander. The Black-Blue Pipe Spring is the spring which shows the largest diurnal variation, which indicates that surface water

must contribute to a certain extent to the water, released at the Black-Blue Pipe Spring, but its contribution is definitely smaller than at the La Chaux Meander, since the temporal as well as the diurnal variations are much smaller. In addition, when considering the temperature at the Mainstream 3, it can be identified that this station shows the highest temperature as well as the strongest diurnal variation. This observation can be explained by the comparably large width of the streambed and the low water level, which lead to a faster warming but also to quicker cooling with changed solar radiation compared to the Mainstream 2, where the water level is higher.

Aside from the exposure to the surface or the depth of the water flowing path, the amount of total dissolved solids in the water also has an impact on the temperature. Nelson (2002) explains, as elaborated in chapter 3.5, that a higher water temperature can indicate a higher amount of total dissolved solids. When considering the spatial distribution of the individual springs, the Grass Spring has the highest median temperature among the spring, and thus, based on the relationship described by Nelson (2002), it is the station with the largest number of dissolved solids, in contrast to the La Chaux as well as to the Bridge Spring, which therefore have the lowest amount of total dissolved solids. In addition, Nelson (2002) explained that temperature variations can also be attributed to inflow from the surface, which, however, could not be considered in our temperature data. Finally, when considering the continuous temperature data, the temperature at the springs hardly changed over time, but some noise was recorded. One reason for the recorded noise is logger displacement by animals like, for instance, the temperature peak at the Bridge Spring or also the first peak at the La Chaux Meander. Another factor, which is responsible for noise, is the low water level at the springs, which led to the situation that not the whole HOBO logger was in the water for a limited time until its position was readjusted.

pH value

Nelson (2002) explained, as elaborated in chapter 3.5, that the lower the pH value is, the more H^+ ions are present in the water, which then may accelerate the weathering process, resulting in higher mineral concentrations of certain ions. When considering the results of the pH measurements at the springs, the median pH value of the Grass Spring is much lower as well as significantly lower than the median pH value of the other springs, which are all on quite a similar level. Based on that key finding, it can be concluded that the water at the Grass Spring must contain the largest number of dissolved solids. In addition, this finding is an indication that the water of the Grass Spring must have a different origin than the water of the other springs.

The results of the pH measurements show that the spatial variation is more remarkable than the temporal variation. The impact of rain, which is according to Berner and Berner (1987) acidic, cannot directly be seen in a pH decline at the stations and is thus not responsible for any temporal variation. Apart from the Grass Spring, where the pH value declined from the second to the third sampling campaign, since in this time period a series of precipitation events was recorded. Additionally, the time-of-day analysis shows that no significant difference between measuring the pH value in the morning or in the afternoon is noticed. Additionally, the remarkable increase of the pH value towards the last sampling campaign needs to be considered with caution, since it was determined by means of a different instrument and therefore, the instruments might be calibrated differently as well as the accuracy of measurements might differ from the previous one. Furthermore, I did not know that the pH instrument that I used needed to be calibrated before every measurement in the field in order to guarantee an optimal accuracy of measurement and as a consequence, this lack of knowledge led to measurement inaccuracies which are consequently expressed inter alia in temporal variations of the pH value.

Ions

In the following paragraphs the results of the hydrochemical analysis of chapter 4.3 as well as of the concentration-discharge analysis are discussed. The origins of the ions are highlighted and potential reasons for the spatial as well as temporal variations of the ion concentration are given by taking the background information of chapter 3.5 into consideration and by comparing the findings to the results of Knapp et al. (2020). However, since neither any further geological investigations nor any in-depth research about the exact geological conditions of the sampling stations were performed, the discussion below elaborates assumptions about the origins of the ions and their variation in the Vallon de Nant catchment. In addition, the hydrochemical analysis, performed with the collected data of the Vallon de Nant, and particularly, the discussion of the concentration-discharge analysis is tightly leant on the study of Knapp et al. (2020), who performed a two-year study in the Erlenbach catchment, which is situated on an elevation that reaches from 1100 to 1655m.a.s.l.

Before discussing the results on the level of the individual ions, it needs to be highlighted that in the lab a measurement error happened, which was unfortunately discovered at a later timepoint in the research process and, thus, could not be eliminated. In particular, when determining the ion concentration of the water samples of the fifth and sixth sampling campaign by means of the ion chromatography, the tube was not properly rinsed after the individual measurements. As a result, the determined concentrations at those dates are slightly distorted, but only to a limited extent, since the deviations from the standards are only little. However, this measurement error might be responsible for causing some temporal variation, as elaborated in the paragraphs below.

Fluoride, which is part of the upper crust, is naturally found in low concentration in the waters and its concentration strongly varies depending on the small-scale geological as well as chemical conditions (Qian et al., 1999). These low concentrations can also be determined at the different stations in the Vallon de Nant catchment, while there is a spatial variation of the fluoride concentration, indicating locally different geological and chemical conditions. As a further matter, according to Podgorski and Berg (2022), the pH value has an impact on the fluoride concentration. But in the Vallon de Nant catchment, the remarkable decrease of the fluoride concentration towards late August until mid-September does not correspond to a decrease of the pH value, even the opposite, since one can observe at some stations a pH value increase. Finally, the measurement error that happened in the lab, as elaborated above, needs inter alia to be responsible for this decrease.

We learnt that **chloride** (see chapter 3.5) particularly enters the water by dissolution of salts as well as by weathering of soils and rocks (Berner and Berner, 1987). When considering the results of the temporal as well as spatial variation analysis in chapter 4.3, the spatial variation is little pronounced, which is in contrast to the temporal variation. Thus, the chloride abundance as well as the conditions for weathering chloride must be similar between the different sampling stations. Having a closer look at the chloride increase at the end of August, it does not seem to be probable that at all the stations the conditions have changed that strongly and consequently cause such an increase of the concentration. As a result, it needs to be assumed that the measurement error, that happened in the lab, is responsible for this concentration increase. In addition, Knapp et al. (2020) write in their paper that chloride particularly enters the system in the Erlenbach catchment by atmospheric inputs, specifically by precipitation. Besides, they add that the chloride concentration strongly varies over their research time due to variations in the extent of the atmospheric inputs. Based on the findings of Knapp et al. (2020), precipitation might be a key contributor of chloride in the Vallon de Nant catchment since the spatial variation is little, and thus precipitation contributes to a similar extent over the whole catchment as well as temporal variation over the research time is visible, which can also indicate that the origins may

vary over time, specifically at some timepoints, when the chemical weathering is stronger than the atmospheric inputs or vice-versa.

Nitrite is a product of biological weathering processes, and thus, according to Lingle (2013), it often appears as an intermediate product of nitrification as well as of denitrification processes. At the considered stations in the Vallon de Nant, nitrite is not measured through the whole research period at every single sampling station. When considering the temporal variation of nitrite, which is much more pronounced than the spatial variation, it can be observed that through July and early August, hardly any nitrite is recorded, while towards the end of the research period, nitrite is measured again. In addition to the biological inputs, atmospheric deposition of nitrite might also be responsible for the observed temporal variation. However, the strong increase of nitrite towards the end of August might be a bit exaggerated due to the measurement error, but nevertheless nitrite could be detected.

Lingle (2013) explains that **nitrate** primarily has its origin in nitrification as well as in nitrogen fixation processes and thus enters the water by biological weathering. In addition, we learnt that due to the fact that nitrate is negatively charged, it can be easily washed out since it cannot well attach to the negatively charged clay particles in the soil (Lingle, 2013). When considering the results of the hydrochemical analysis in chapter 4.3, there is neither a remarkable spatial nor temporal variation visible, with the exception of the Grass Spring, that has in comparison to the other stations a significantly higher nitrate concentration. Based on that finding, it can be assumed that near the Grass Spring, which is embedded in a grassy pasture, the biological activity is high, and thus much ammonium is transformed to nitrate and additionally, much nitrogen is fixed, resulting in the formation of nitrate. Ultimately, due to the fact that nitrate is negatively charged, it then can be easily washed out. In addition, Knapp et al. (2020) mentioned that in the Erlenbach catchment nitrate primarily enters the system by atmospheric inputs, but also by biological inputs such as in form of manure, and identified temporal variation, which may indicate, similarly to chloride, a variation of sources that contribute depending on the timepoint to a different extent or simply a variation in the extent of the atmospheric input. But they also highlight that this varying concentration of nitrate, which is an important nutrient for plants, can also be caused by the nutrient shift from the soil to the plants. However, no remarkable temporal variation is observed in the Vallon de Nant catchment, with the exception of the strong increase through September towards October at the Grass Spring. That was the time, when cows were grazing there, and thus their manure must also have an impact on the nitrate concentration in the water. Finally, concerning the origin of nitrate, it can be assumed, also based on Knapp et al. (2020), that nitrate is added in the Vallon de Nant catchment by biological as well as atmospheric inputs.

The accumulation of **phosphate** in the water happens due to weathering processes of phosphate minerals such as apatite. The results of the hydrochemical analysis have showed that neither any remarkable spatial nor any temporal variation is identified with the exception of the time period between early and mid-August. Precipitation is also a source of phosphate and when having a closer look at the precipitation data, precipitation events are recorded before both sampling campaigns, which might have a direct impact on the phosphate concentration.

Sulphate is accumulated in the water, according to Berner and Berner (1987), by weathering of sedimentary rocks that include minerals such as pyrite, gypsum or anhydrite. When considering the results of the spatial as well as the temporal variation analysis of the sulphate concentration, the sulphate concentration is the largest at the Black-Blue Pipe Spring and the lowest at the La Chaux Meander. Based on the spatial variation of the sulphate concentrations, it can be concluded that the share of sedimentary rocks must vary among the different sampling stations, in particular, that the Black-Blue Pipe Spring must have a higher amount of sulphate input from the surrounding sedimentary rock than, for instance, the Grass Spring, which has the lowest sulphate concentration. The extent of temporal

variation depends on the sampling station and is more pronounced at the Black-Blue Pipe and the Grass Spring as well as at the Mainstream 3, while at the other stations the temporal variation is more limited. The geographic location of the Mainstream 3 is assumed to be responsible for this temporal variation, since it is located in an area where water from different origins as well as from different locations in the catchment is collected, which ultimately contributes to variations of the sulphate concentration over time. Knapp et al. (2020) observed that the sulphate concentration of the stream water is lower than the concentration in the groundwater. However, when comparing the sulphate concentration of the springs with the one of the mainstream, measured in the Vallon de Nant catchment, the difference between streamwater and groundwater cannot be observed, specifically the Grass Spring has lower concentrations than the stations along the mainstream.

Schilling (2002) explained, as presented in chapter 3.5, that **ammonium** is the product of nitrogen fixation as well as of nitrogen mineralization, and thus ammonium enters the water by biological weathering. As a further matter, Harrison (2003) mentioned that the temperature as well as the pH value have an impact on the ammonium abundance, in particular, neutral or acidic as well as warm conditions support high ammonium concentrations. The results of the ammonium concentration over time as well as the variation between the stations showed that there is hardly any variation visible, apart from the fact that the La Chaux Meander as well as the Mainstream 3 have at some points over time higher ammonium values than the other stations. Based on these results, it can be assumed that not particularly the pH value or the appropriate temperature are the explanation for this finding, since the variation is very little, but that at the La Chaux Meander the biological weathering is in comparison to the other stations more pronounced. Besides, the observed temporal variation may also be an indication that ammonium is contributed by the atmosphere to the system. When explaining the ammonium concentration at the Mainstream 3, it needs to be emphasized that this sampling station is embedded in a surrounding, where water from a series of different origins is collected, while the concentration at the other stations along the mainstream with lower elevations is more diluted.

Calcium accumulates in the groundwater due to geological weathering. Saha et al. (2019) explain that particularly the weathering of carbonate rocks such as limestones and the dissolution of minerals like calcic-plagioclase feldspars or pyroxene lead to the calcium input. In addition, Berner and Berner (1987) added, as presented in chapter 3.5, that due to the fact that calcium is heavily enriched in the sedimentary rocks, it is the ion that is the most abundant one in the water. When considering the results of the calcium concentration analysis in the Vallon de Nant catchment, it can be clearly seen, aside from the fact that calcium is indeed the ion with the highest concentration among all the investigated ions, that the spatial variation is more pronounced than the temporal variation. In particular, the springs have higher calcium concentrations than the mainstream, while specifically the Grass Spring shows a significantly higher concentration compared to the other sampling stations. Based on these findings, the calcium abundance in the bedrock is assumed to be either larger or the conditions for calcium weathering are more appropriate at the Grass Spring, while at the stations along the mainstream the water is more diluted, which must be responsible for the lower concentrations. When comparing these results to Knapp et al.'s (2020) findings, who found that the calcium concentration of groundwater is almost identical to the concentration of the stream water or even larger, it can be concluded that the calcium concentration in the Vallon de Nant catchment is lower in the mainstream than at the springs.

Potassium accumulates, according to Saha et al. (2019), in the groundwater due to geological weathering of minerals such as potassium feldspar, biotite or clay minerals. In addition, they highlight that due to the fact that potassium is often part of primary minerals, and thus not weathered before, its weathering process is not very efficient. However, when considering the results of the temporal as well

as of the spatial analysis of the potassium concentration in the Vallon de Nant, neither any remarkable spatial nor any temporal variation can be identified. The Mainstream 3 has the highest potassium concentration, which can also be explained by the diverse water inputs in that area, especially from springs and tributaries, but also due to weathering within the stream, similarly to Knapp et al. (2020), who assigned in their study the origin of potassium in the surface water to geological weathering. But they also highlight that potassium has its origin from atmospheric inputs, since it temporarily varies strongly over the research period, indicating that the extent of atmospheric potassium inputs varies over time. However, when considering the results in the Vallon de Nant catchment, neither a remarkable spatial nor a temporal variation is observed, and thus both origins are assumed to have an impact on the potassium abundance.

Magnesium enters the groundwater by geological weathering processes of minerals such as amphiboles, biotite or olivine (Berner and Berner, 1987; Saha et al., 2019). When considering the results of the hydrochemical analysis, a spatial variation, which is more expressed than the temporal variation, is observed. The Black-Blue Pipe Spring as well as the Bridge Spring have the significantly highest magnesium concentration, while the La Chaux Meander shows the lowest concentration. Based on this finding, the amphibole amount of the bedrock of the Black-Blue Pipe as well as of the Bridge Spring is assumed to be higher due to the stronger weathering rate of magnesium, while in case of the La Chaux Meander the magnesium content of the bedrock must be lower or the water must be more diluted in comparison to the other stations, which is, for instance, assumed when considering the Mainstream 3. When comparing the results to Knapp et al. (2020), who observed that the magnesium concentration of the mainstream is lower than the one of the groundwater, it can be identified that in the Vallon de Nant catchment the magnesium concentration of the springs is higher than the concentration in the mainstream, and thus these observations correspond with the findings of Knapp et al. (2020).

Sodium is primarily accumulated by geological weathering. Saha et al. (2019) as well as Berner and Berner (1987) explained, as elaborated in chapter 3.5, that due to weathering of silicate minerals such as plagioclase or feldspar an increased sodium concentration in the water can be identified as well as due to the dissolution of halite. When considering the results of the sodium analysis in the catchment, hardly any spatial variation is noticed, while a temporal variation is observed, particularly from mid-August towards mid-September. Thus, the sodium abundance as well as the conditions for sodium weathering are comparable between the stations. This strong increase of the sodium concentration can also be explained by the measurement error that occurred. Besides, it is mentioned in chapter 3.5 that in case of a correlation between chloride and sodium, halite can be assumed to be a key contributor of sodium and chloride. So, since we can identify a similar pattern between chloride and sodium, one can therefore assume that halite is in the Vallon de Nant catchment a remarkable contributor of sodium as well as of chloride, while hardly any correlation between chloride and potassium can be noticed, indicating that sylvite does hardly contribute to the potassium as well as to the chloride concentration. Finally, when comparing the results of the sodium concentrations, measured in the Vallon de Nant, to the findings of Knapp et al. (2020), who determined a difference of the sodium concentration between groundwater and the mainstream, no remarkable difference can be observed.

The geological, atmospheric as well as biological inputs of the ions and ultimately, the origins of the ions, namely bedrock, atmosphere or soil, of the Vallon de Nant as well as of the Erlenbach catchment are summarized in Table 27. However, when defining the origins of the ions, it needs to be emphasized that a series of different sources contribute to the ion abundance and that the contribution of such an input may vary spatially, which is especially the case when considering the geological input. Knapp et al. (2020) elaborated that groundwater varies strongly in its geochemical composition depending on where in the catchment the groundwater is sampled, since the weathering of the bedrock as well as

the corresponding conditions vary over the whole catchment. Besides, the hydrochemical analysis allows us to identify the solutes that are most prominently represented in the waters. Independent on the sampling stations, sulphate as well as calcium are the most abundant ones and have the biggest impact on the electrical conductivity. When comparing these key contributors to the ones of Knapp et al. (2020), a difference can be noticed, namely that in case of Knapp et al. (2020) calcium as well as magnesium are most prominently represented, while the latter contributor could be measured to a minor extent at the sampling stations in the Vallon de Nant catchment. Therefore, it can be concluded that the geological conditions must be different between the Vallon de Nant catchment and the Erlenbach catchment, since sulphate as well as magnesium enter the water by geological inputs.

Table 27: Origin of ions in the Vallon de Nant (VdN) and the Erlenbach catchment (Erlenbach C.). The ions are attributed to their corresponding input, while it is differentiated between geological, atmospheric and biological input and based on these inputs the origin of the ions is defined, namely bedrock, atmosphere or soil.

Ion	Geological Input (bedrock)	Atmospheric Input (atmosphere)	Biological Input (soil)
Fluoride	VdN		
Chloride	VdN	VdN, Erlenbach C.	
Nitrite		VdN	VdN
Nitrate		VdN, Erlenbach C.	VdN, Erlenbach C.
Phosphate	VdN	VdN	
Sulphate	VdN, Erlenbach C.		
Ammonium		VdN	VdN
Calcium	VdN, Erlenbach C.		
Potassium	VdN Erlenbach C.	Erlenbach C.	
Magnesium	VdN, Erlenbach C.		
Sodium	VdN, Erlenbach C.		

Concentration-Discharge Analysis

Knapp et al. (2020) explained in their paper, that the ions that have the origin as well as some chemical characteristics in common show comparable concentration-discharge relationships. Thus, after having investigated the sources of the ions, the concentration-discharge relationship of these categories is determined. Based on that approach, which is introduced by Knapp et al. (2020), the concentration-discharge relationships of the ions, recorded at the springs as well as at the outlet of the Vallon de Nant catchment, are discussed. Besides, since the concentration-discharge relationship of the individual ions is quite consistent with all the stations (see chapter 4.4), the spatial variation is less discussed, but more the individual concentration-discharge relationship of the ions.

As explained by Knapp et al. (2020), dilution particularly occurs in situations, when the abundance of the ion is limited or when the concentration of the ion is diluted by water that has a smaller or equal concentration of the corresponding ion. Such a dilution behavior, which describes the process, when the ion concentration increases with decreasing discharge, could in the study of Knapp et al. (2020), who investigated stream water, strongly be observed for ions that have their origin in groundwater such as calcium, magnesium, sodium or sulphate and to a smaller extent for potassium, which, however, also has its origin aside from the groundwater also in the atmosphere. When considering the results of the Vallon de Nant catchment, dilution is particularly observed for sulphate, potassium and ammonium, while the latter ion has its origin in the soil or in the atmosphere and the former two ions in groundwater. So, these ions must have the lowest concentration when the discharge is the highest.

Furthermore, when discussing dilution processes, Knapp et al. (2020) explained that environmental factors such as temperature or wetness, which are summarized as seasonality indicators, need to be considered. They, for instance, found that ions, which have their origins in the groundwater, show positive correlation with these seasonality indicators, particularly showing less negative concentration-discharge relationships under the condition of warmer temperature as well as of higher dryness, which means that the dilution is less pronounced, and thus the ions are more concentrated in the water. So, when considering the temperature as well as the precipitation data of the Vallon de Nant catchment over that time, this finding of Knapp et al. (2020) is assumed to be the explanation, why magnesium, sodium or calcium have showed in the Vallon de Nant catchment chemostatic behavior instead of dilution, which would be expected as they have their origin in the groundwater. In addition, differences between the springs could be determined, particularly the Black-Blue Pipe Spring as well as the La Chaux Meander show dilution behavior, and thus the abundance of these ions must be limited in the corresponding compartment of the catchment.

When considering the ions that enter the system through atmospheric inputs such as chloride, potassium or nitrate, Knapp et al. (2020) could observe that these ions do not show such a clear pattern as the groundwater solutes show, and thus they could observe all three patterns such as dilution, chemostasis and mobilization, but in particular chemostasis and mobilization. In the Vallon de Nant catchment, particularly nitrite, nitrate, ammonium as well as eventually also phosphate, potassium and chloride might be added by atmospheric inputs and all these ions with the exception of ammonium and potassium, as discussed above, show to a large majority of the stations chemostatic as their dominant concentration-discharge relationship, while occasionally at some springs mobilization could be determined. Knapp et al. (2020) highlighted that the relative moisture has a strong impact on the ions such as chloride, potassium or nitrate, which have their origin, determined in the study performed in the Erlenbach catchment, from the atmosphere. Based on that, they could observe that the higher the relative moisture is, the more dilution processes occur and vice versa, the lower the moisture is, the more mobilization behavior is observed. This relationship occurs, according to Knapp et al. (2020), due to the fact that under lower moisture conditions the evapoconcentration in the soil is more pronounced.

Taking the findings of Knapp et al. (2020) into consideration as well as the warm and relatively dry conditions during the research period in the Vallon de Nant catchment, potassium, chloride as well as nitrite showed mobilization at some stations in the catchment, and thus this finding corresponds to their result. However, mobilization can rarely be noticed at the stations, only when considering the concentration-discharge relationship of chloride at the Bridge Spring and the La Chaux Meander or the one of potassium as well as at the Bridge Spring. In addition, nitrite at the La Chaux Meander also shows mobilization. Mobilization, which is the process where the ion concentration decreases with decreasing discharge, is, according to Knapp et al. (2020), due to the washing out of ions from the soil. In this context, Knapp et al. (2020) explained that precipitation events generally have an impact on the concentration-discharge relationship of some ions, such as potassium, chloride and nitrate, but they highlight that no clear concentration-discharge pattern can be manifested, since their relationship really depends on the event. This observation, however, was not made in the Vallon de Nant catchment.

Finally, in most cases, when considering the concentration-discharge relationships at the springs as well as when investigating the processes per ion, chemostasis is observed, which indicates that the ion concentration is not changed with altered discharge rates. Potential reasons for such a behavior can, according to Knapp et al. (2020), be that the solute abundance is not limited in its origin. But, the attribution of a chemostatic behavior to a solute can also overshadow light mobilization as well as dilution processes and the fact of overshadowing either dilution or mobilization is also reinforced by a

low data density, which is the case and, thus, needs to be considered, when discussing concentration-discharge relationships of the solutes in the Vallon de Nant catchment over the summer recession period.

Isotopes

In chapter 3.5, it was elaborated that $\delta^2\text{H}$ as well as $\delta^{18}\text{O}$ are stable water isotopes, which are heavier, but much less abundant in nature than the lighter isotopes ^1H or ^{16}O and additionally, that the isotopic composition is indicated by delta values, describing to which extent the isotopic composition of a water sample is different from the V-SMOW standard (Yoshimura, 2014; Galewsky et al., 2016). Generally, the more negative a value is, the smaller is the number of heavy isotopes in the sample and thus the higher is the isotopic depletion. In the following paragraphs, the results of the isotopic analysis of chapter 4.3 as well as of the mixing analysis are discussed by taking the background information of chapter 3.5 into consideration and by comparing the results to some findings of Michelon (2022), who also did isotopic analysis of springs as well as of the mainstream.

Spatial Variation of Isotopic Composition

When considering the results of the isotopic analysis of chapter 4.3, the $\delta^2\text{H}$ as well as the $\delta^{18}\text{O}$ values show temporal and spatial variation. What is particularly remarkable is that the Grass Spring is significantly the least depleted in $\delta^2\text{H}$ as well as in $\delta^{18}\text{O}$, while the water at the Bridge Spring is most depleted in $\delta^2\text{H}$ as well as in $\delta^{18}\text{O}$. The isotopic depletion of the La Chaux Spring and the Mainstream 1 as well as of the Mainstream 2 is similar to the one of the Bridge Spring, but not significantly different. The median $\delta^2\text{H}$ as well as $\delta^{18}\text{O}$ compositions of the Mainstream 3, the Black-Blue Pipe Spring and the La Chaux Meander are also close together and thus not significantly different, but less enriched than the Grass Spring but more than the other stations. Michelon (2022) came in his study to similar results, despite the fact that he sampled several different stations. He also found that the sampling stations show comparable median isotopic compositions with the exception of the Grass Spring that also shows much higher median isotopic values.

When discussing the spatial variation, the varying isotopic compositions might be assumed to be the result of different fractionation processes. When water changes its phase such as in evaporation or condensation processes, fractionation occurs, resulting in an altered composition of stable isotopes. Beria et al. (2018) explain that evaporation, for instance, is a kinetic process, where the liquid phase is more enriched in heavy isotopes than the gaseous phase. In addition, they highlight that temperature has an impact on the fractionation processes and they particularly point out that the higher the temperature is, the weaker is the condensation level and thus the lower the fractionation. Therefore, at a warmer temperature evaporation is more pronounced than condensation is.

Since the Grass Spring is the least depleted in the considered stable isotopes among the considered stations, it is assumed, based on the explanations of Beria et al. (2018), that evaporation generally happens there to a larger extent than at the other stations. The median $\delta^2\text{H}$ as well as $\delta^{18}\text{O}$ compositions of the Bridge Spring as well as of the La Chaux Spring are in about the same range as the Mainstream 1 and the Mainstream 2, indicating that at these stations lower evaporation must occur than it does at the Grass Spring, while the median $\delta^2\text{H}$ as well as $\delta^{18}\text{O}$ compositions of the Mainstream 3, the Black-Blue Pipe Spring and the La Chaux Meander are also close together, assuming a moderate evaporation in comparison to the Grass Spring. As a further matter, it is highlighted by Beria et al. (2018) that such a kinetic effect is more strongly pronounced when considering $\delta^2\text{H}$ values than $\delta^{18}\text{O}$ values, since the HD^{16}O isotopes show a lower weight than the H_2^{18}O water isotopes. This fact can also be observed in the results of the isotopic analysis of the collected water samples in the Vallon de Nant catchment. The collected water samples are all much more depleted in ^2H than they are in ^{18}O , which

is explained by the fact that ^2H is lighter than ^{18}O and thus tend to enter the gaseous phase than the ^{18}O does. However, these findings are only based on the comparison of the median isotopic composition of the sampling stations. Thus, in order to gain a deeper understanding whether kinetic processes are responsible for the spatial variation of the isotopic compositions, $\delta^2\text{H}$ is plotted against $\delta^{18}\text{O}$ (see Figure 53). So, aside from the relationship between $\delta^2\text{H}$ and $\delta^{18}\text{O}$ and potential fractionation processes, also the spatial distribution of the isotopic depletion level, which corresponds to the above-mentioned explanations, can be observed.

When analysing the relationship between $\delta^2\text{H}$ and $\delta^{18}\text{O}$, it can also be analysed how the datapoints are scattered around the Local Meteoric Water Line (LMWL). The determined isotopic compositions of the water samples follow the LMWL, indicating that the current local conditions of the Vallon de Nant still correspond to the conditions of 2019, when the LMWL was defined by Mächler et al. (2021). However, the LMWL shows a larger intercept, but a smaller slope than the Global Meteoric Water Line (GMWL) does. When considering the slope of the LMWL, Araguás-Araguás et al. (2000) highlighted that areas with a LMWL of a slope smaller than 8 are, for instance, regions where d-excess values of precipitation slightly vary seasonally or where a strong evaporation in summer is observed. In contrast, LMWL of a slope larger than 8 can, according to Araguás-Araguás et al. (2000), be recorded in regions, where the water vapour comes from different regions depending on the season, resulting in strong seasonal variations in the isotopic composition as well as in the deuterium excess (d-excess) values. Having a closer look at the slope of the LMWL of the Vallon de Nant, it is identified to be slightly lower than 8, namely 7.82, and therefore, according to Araguás-Araguás et al. (2000), the Vallon de Nant is a region, which tends to have distinctive evaporation in summer as well as a seasonally varying isotopic composition of precipitation. The intercept of the LMWL indicates that the deuterium excess (d-excess), which is, according to Beria et al. (2018), often used to identify whether fractionation happens under equilibrium or kinetic conditions and, thus, determine whether evaporation or condensation occurs, slightly higher. However, deuterium excess values in the range of 10 to 11 indicate stable conditions (IAEA, 2006). Aron et al. (2021) highlighted that the extent of deuterium excess depends on the relative humidity as well as on the temperature. In particular, they noticed that the higher the temperature is, the lower is the deuterium excess in the liquid phase, while the higher the relative humidity is, the lower is the deuterium excess in the gaseous phase. So, the slightly larger intercept of the LMWL, namely 10.47, highlights that the deuterium excess is a bit more expressed in the Vallon de Nant than it is in case of the GMWL. So, when taking the findings of Aron et al. (2021) into account, it can be assumed that due to the higher deuterium excess values the relative humidity is slightly higher and the temperature lower compared to the global average expressed by the GMWL.

When considering the median d-excess values of the different sampling stations separately, the Grass Spring as well as the Black-Blue Pipe Spring are identified to be the stations that have the significantly lowest d-excess values, while all the other stations show median values in a similar range and are in most cases not significantly different. Similarly, Michelon (2022) found in his study that the water samples, which were collected at springs as well as at stations along the mainstream in the Vallon de Nant catchment, show median d-excess values that are similar to those of rain and are thus lower than the d-excess values for snow. However, since the Grass Spring as well as the Black-Blue Pipe Spring are the two stations, which deviate the least from the GMWL, they are more similar to the global average than the other stations. In addition, Michelon (2022) elaborated that the d-excess values of soil water are even lower than they are for rain or snowmelt due to evaporation processes of the vegetation as well as of the soil, also known as secondary evaporation. Therefore, when considering the lower d-excess values and the explanations of Michelon (2022), it can be assumed that soil water is a severe contributor to the discharge of the Black-Blue Pipe as well as of the Grass Spring.

When analysing how the datapoints are scattered around the LMWL, the datapoints follow the LMWL quite accurately, but nevertheless some deviations are noticed. Most of the datapoints of the Grass Spring and the Black-Blue Pipe Spring are scattered slightly below the LMWL, which is also indicated by the lower d-excess values, while most of the datapoints of the La Chaux Spring as well as of the La Chaux Meander are located either above or on the LMWL. Beria et al. (2018) highlighted that values that differ from this LMWL may indicate evaporation, sublimation or other processes that occur under kinetic conditions. But, since such nonequilibrium processes lead to different ^2H and ^{18}O abundances in the two phases, a new slope has to be defined, as explained by Beria et al. (2018) in order to show the altered relationship. In particular, since the ^2H is the lighter stable isotope than the ^{18}O , the $^1\text{H}^2\text{H}^{16}\text{O}$ stable water isotope is more enriched in the gaseous phase than $^1\text{H}^1\text{H}^{18}\text{O}$, which is more present in the liquid phase. Therefore, due to the higher abundance of the heavy oxygen isotopes in the water, the slope of the evaporation line is smaller than the one of the LMWL.

However, in the plot which illustrates the relationship between $\delta^2\text{H}$ and $\delta^{18}\text{O}$ (see Figure 53) no kinetic process such as evaporation can be identified. Therefore, the assumption, which is based on the comparison of the individual isotopic compositions of the sampling stations, that evaporation is responsible for the spatial variation of the isotopic depletion level cannot be seen in the plot that illustrates the relationship between $\delta^2\text{H}$ and $\delta^{18}\text{O}$. In contrast, it can be clearly identified that the datapoints follow the LMWL quite accurately and additionally, the intercept of the LMWL, indicating the d-excess, also highlights stable conditions. Therefore, not kinetic processes explain the spatial variation, but much more the origin of the water, which also plays a role when explaining the finding that the Grass Spring has such a different isotopic composition to the other stations, needs to be considered. In particular, Michelon (2022) explained this result regarding the Grass Spring by the assumption that the Grass Spring might store water from a low lying subcatchment of a small size and not from the rock faces, which are located closely to the Grass Spring.

Another point, which is highlighted by Michelon (2022), is that the electrical conductivity in combination with the isotopic analysis can serve as an indicator for identifying the origin of the water, namely by determining how old the investigated water is. By means of the isotopic composition it can be differentiated between “old” and “new” water, while Taylor et al. (2002) explain that the former describes water before precipitation events such as groundwater, soil water or surface water and the latter defines the water that is added to the system by precipitation such as snow, rain as well as by snowmelt. The more isotopically depleted the water is, the higher is the snowmelt contribution, since, according to Ala-aho et al. (2017), snow and snowmelt respectively are isotopically more depleted than rain is due to the fact that the temperature is lower when condensation happens. Therefore, young water has rather low electrical conductivity, since it has a higher snowmelt contribution than older water and additionally, young water has, according to Michelon (2022), a lower subsurface residence time and thus also shows a lower number of dissolved ions. Based on this relationship, the age of the monitored springs of the Vallon de Nant catchment can be assessed. The Grass Spring has the highest electrical conductivity and contains therefore the oldest water with the smallest snowmelt contribution, while the Bridge Spring has the lowest electrical conductivity and is therefore the youngest water with the highest snowmelt contribution, which is also reflected in its largest isotopic depletion. Finally, in order to assess the snow contribution to the individual spring discharge, the mixing analysis is performed, as discussed below.

Temporal Variation of Isotopic Composition

When having a closer look at the potential reasons for the temporal variation of the isotopic composition, precipitation is assumed to have an impact on the observed temporal variation of the isotopic composition. Beria et al. (2018) explained that the heavy isotopes are rained out first, and thus, with

time passing, the precipitation shows a lower abundance of heavy isotopes. So, the isotopic depletion is reduced after precipitation events. This relationship is observed when considering the reduction of the isotopic depletion towards early October, when a series of precipitation events is recorded before the water samples are collected. In addition, another isotopic depletion reduction is observed at all the stations, apart from the Grass Spring, but specifically pronounced at the stations along the main-stream, towards early August. When having a closer look at the precipitation data, a series of precipitation events is observed before the sampling dates.

Beria et al. (2018) explained that temperature as well as elevation have an impact on the isotopic composition of precipitation, while the isotopic composition of precipitation varies depending on the elevation level, where it is formed. The higher the elevation is, the higher is, according to Beria et al. (2018), the isotopic depletion of the precipitation, which is described by the isotopic lapse rate. Regarding the temperature, they explain that when precipitation is formed under warmer conditions, the precipitation is less depleted in heavier isotopes than under cooler conditions due to the fact that the fractionation factors decline with an incline of the temperature. Beria et al. (2018) mentioned that reasons for this elevation dependent lapse rate are, aside from the lower cloud condensation temperature at higher elevation levels, also orographic effects, which reinforce the condensation process and thus lead to an incline of precipitation with higher elevation levels. Furthermore, they highlighted that an isotopic depletion of rain is also observed over the time period of a precipitation event, which means that the heavy isotopes are preferentially rained out first. However, in this study the isotopic composition of precipitation was not analysed, but Michelin (2022) investigated in his studies the isotopic depletion of rain in the Vallon de Nant and he could determine a lapse rate of 0.84‰/100 m for $\delta^2\text{H}$ and one of 0.128‰/100 m for $\delta^{18}\text{O}$ and he also set the values into relation to the isotopic lapse rates determined for Switzerland and could identify that these values correspond to about 50% of these rates.

The results of Michelin (2022) show a temporal variation of the isotopic composition at the springs over the defined streamflow periods but also over the research years. Thus, there is no general temporal pattern that can be seen over the years. However, the investigated springs of this thesis do not show the same extent of temporal variation, but from an overall perspective, the springs are either isotopically enriched or stay on the same level over the summer recession period primarily due to rainfall, which was also observed by Michelin (2022) in his study.

Due to the fact that the sampling stations of Michelin (2022) vary in their isotopic composition over the recession period to a different extent, he assumes that when the isotopic composition increases slowly over the recession period, the water is stored in a big reservoir or that the water storage reservoir is not well permeable resulting in slower flowing rates. Vice versa, when the isotopic composition increases fast over the recession period, he assumes that the water storage reservoir is well permeable resulting in higher water flowing rates. Based on the qualitative assessment of how fast the isotopic composition of the monitored sampling stations increase over time, it can clearly be observed that it increases slowly at the La Chaux Spring as well as at the Bridge Spring, therefore indicating that the water is stored in a relatively big reservoir or that the reservoir is weakly permeable for the water, while at the Black-Blue Pipe Spring as well as the Grass Spring the isotopic composition increases the fastest in comparison to the other stations and therefore, indicating a comparably small reservoir or a reservoir that is well permeable. The La Chaux Meander which is geographically quite closely situated to the La Chaux Spring, however, shows a different pattern, namely a faster increase than the La Chaux Spring and thus indicating that the water is stored in a smaller reservoir than the water from the La Chaux Spring.

Mixing Analysis

In order to assess the snow as well as the rain contribution to the individual spring discharge, the mixing analysis is performed per sampling station as well as per sampling date (see chapter 4.4). In the following paragraphs, these findings are discussed and complete the above-mentioned explanations.

When considering the proportion of **rain per sampling date**, one can identify hardly any changes when comparing the proportion of rain from the beginning of the research period to the proportion of the end, but within the research period there are some variations in the proportion of rain visible such as an increase in the rain proportion from mid-July towards early August as well as from mid-September towards early October. As a further matter, the proportion of rain is always smaller than the proportion of snowmelt. So, the observation that the proportion of rain increases at these specific timepoints in August as well as towards October corresponds to the above-discussed assumption that rain events must be responsible for the observed temporal variation, which is also reflected in the isotopic enrichment of $\delta^2\text{H}$ and $\delta^{18}\text{O}$ at the sampling stations. In addition, the fact that the proportion of rain hardly changes over the research period, and thus the fraction of snowmelt does not decrease, indicates that the contribution of meltwater is constant over the whole research period.

In chapter 4.4, the proportion of **rain** is observed to vary **per sampling station**. The Grass Spring shows the highest median proportion of rain over the research period, followed by the Black-Blue Pipe Spring as well as the La Chaux Meander, while lower rain proportion contributions at the Bridge Spring and at the La Chaux Meander are noticed. Based on these findings, it can be assumed that the water at the Grass Spring as well as at the Black-Blue Pipe Spring flows on a relatively shallow path, while the water of the Bridge as well as of the La Chaux Spring on a deeper path due to the observation that the proportion of rain is larger at the Grass as well as at the Black-Blue Pipe Spring than it is at the other stations. Michelon (2022) came in case of the Grass Spring to a comparable result. He namely assumed that based on the isotopic composition as well as on the measured electrical conductivity and the temperature values, that the water must flow quite close to the surface and finally, that precipitation must contribute to a large extent.

As already elaborated above, snow has at all stations the larger share of the collected water samples than rain has. Based on that finding, snow must have a dominant impact on the groundwater recharge at the springs. This pattern is particularly expressed at the higher lying springs such as the La Chaux Spring or at the Bridge Spring, but the strong contribution of snow is also reflected in the streamflow. The observation that snow fundamentally contributes to groundwater recharge as well as to the maintenance of the streamflow in the Vallon de Nant catchment corresponds to the findings of Beria et al. (2018), who emphasize that such a pattern is particularly pronounced in high-elevation catchments.

5.4 Synthesis

In order to discuss how the different tracers can be used to explain storage-discharge relationships at the springs in the Vallon de Nant catchment and thus to answer the main research question, the results of the correlation analysis as well as the principal component analysis (see chapter 4.4) are considered and put into context with the findings of the subquestions elaborated above.

A significantly negative correlation between **discharge** and **electrical conductivity**, indicating that the higher the discharge is, the lower is the electrical conductivity, is observed. This finding can be explained as follows: When a high discharge is recorded, the flowing rate of the water is faster, and thus the residence time of the water in the subsurface is lower, which consequently leads to an overall lower concentration of ions in the water. For instance, as explained in details in the electrical

conductivity section above, the electrical conductivity of the springs is higher than the one of the mainstream, which also corresponds to the lower discharge rates at the springs. As a further matter, measuring the electrical conductivity, for instance, in the mainstream over the recession period has also showed to be a tracer in order to identify whether water is stored in comparably deep or shallow layers. Since in case of an increase of the electrical conductivity over time, water from deeper layers start contributing to the discharge, which was particularly noticed at the Mainstream 3.

A weak negative correlation between **pH** value and **discharge** can be identified. Therefore, using the pH value as a tracer for discharge analysis has showed not to be meaningful for determining any storage-discharge relationships at the springs in the Vallon de Nant catchment. However, the pH value can give indication about the conditions under which water is stored as explained by Nelson (2002), highlighting that the lower the pH is, the more solids are dissolved, which was particularly observed at the Grass Spring, having a significantly different pH value, but a high electrical conductivity value, which, therefore, indicates a high number of dissolved solids in the water.

The correlation analysis shows that the **temperature** is negatively correlated with the **discharge**, in particular, the higher the discharge is, the lower is the temperature, which can particularly be noticed at the springs. In order to understand the relationship between discharge and temperature, the electrical conductivity values need to be considered as well, since Nelson (2002) explained, as discussed in the temperature section of this chapter, that high water temperatures indicate high amounts of total dissolved solids, which, therefore, is reflected in higher electrical conductivity values. However, in my data there is only a weak positive correlation between temperature and the electrical conductivity. Nevertheless, the analysis has showed that temperature in combination with the electrical conductivity can serve as tracers for discharge analysis. Since the springs with the highest median electrical conductivity such as the Grass Spring or the Black-Blue Pipe Spring, indicating relatively low discharge, are also the stations with a higher median temperature and consequently, the water must be released from comparably shallow areas.

There are differences of an ion abundance depending on the **discharge** rate, which can be identified in the analysis of the concentration-discharge relationships and which are consequently also reflected in the different correlation behavior of the ions. Based on these findings, three ion clusters are defined (see chapter 4.4), while positive correlations are noticed within such a cluster: **Cluster 1** includes calcium and phosphate, which are both ions that are the product of geological weathering processes, and thus their origin is defined in the groundwater. Additionally, since calcium and phosphate are positively correlated, it can be assumed that particularly the weathering of calcium-phosphate is distinctive. As a further matter, ammonium and nitrate, which are the product of biological weathering processes as well as of atmospheric inputs, are considered in **cluster 2**. **Cluster 3** includes magnesium, chloride, sulphate and sodium, which are all ions that are products of geological weathering processes and therefore, their origin is also defined in the groundwater, while chloride can also be added to the system by atmospheric inputs. Since chloride is positively correlated with sodium, chloride as well as sodium are assumed to have their origin *inter alia* from halite weathering. So, a positive correlation between cluster 3 and the discharge is identified, while the discharge is negatively correlated with cluster 1 and cluster 2. Based on that finding, the ions of cluster 3 are assumed to be more easily washed out than the ions of cluster 1 and 2, which may be the reason why these ions are more abundant in water of high discharge rates. When considering the concentration-discharge relationships it would be expected that the ions of cluster 1 and 2 show dilution processes, since the higher the discharge is, the lower is their concentration. However, when analysing the results at most stations the ions show chemostatic behavior except for the ammonium for which dilution is determined at most of the sampling stations. In contrast, for the ions of cluster 3 mobilization is expected to be the main concentration-

discharge relationship, since the ions show higher concentrations at higher discharge rates. But in most of the cases chemostasis is observed and mobilization can only be noticed in isolated cases for chloride as well as for sodium, while even dilution is recorded for sulphate at most of the stations. So, some contradictions between the correlation and the concentration-discharge analysis are noticed, but it needs to be highlighted that for performing a deep concentration-discharge analysis more data should be available, which, however, is profoundly elaborated in the limitation section (see chapter 5.5) below.

The correlation analysis of the **discharge** and the **heavy isotopes** such as $\delta^2\text{H}$ and the $\delta^{18}\text{O}$ has showed that they are negatively correlated with discharge, which can be inter alia explained by the findings of the mixing analysis, as discussed above. There, it could be identified that the higher the discharge is, the lower is the electrical conductivity and thus the higher is the amount of snowmelt, which is more depleted than rain, and consequently the higher is the contribution of water from comparably deeper layers, which can specifically be observed at the La Chaux Spring or at the Bridge Spring.

Storage-Discharge Characteristics of the Springs

In the following paragraphs, the relationships explained above as well as the results of the principal component analysis (see chapter 4.4), which highlight the key tracers that describe the individual spring discharge characteristics, are applied and additionally, the results of the recession analysis are taken into consideration, in order to qualitatively discuss the different storage-discharge characteristics of the springs in the Vallon de Nant catchment.

The analysis of the water quality variables suggest that the water stored and released by the **Black-Blue Pipe Spring** as well as the **Grass Spring** in comparison to the other stations is relatively shallow groundwater as well as it consists of a certain amount of soil water due to the fact that the isotopic depletion in heavy isotopes is lower, and thus the proportion of rain is higher, indicating a shallower water flowing path. As a further matter, these stations show a warmer water temperature, which also highlights that the depth of the water pathway is not that deep. Then, the electrical conductivity is higher at these stations, indicating higher residence time of the water in the subsurface as well as smaller water flowing rates, which is also reflected in the low median discharge rates. In addition, under consideration of the ions of the first and second cluster, that are negatively correlated with the discharge and thus more abundant in low discharge areas, the Grass Spring, for instance, has the highest median calcium as well as nitrate concentration in comparison to the other stations, while the sodium concentration, which is positively correlated with the discharge, is the lowest at the Grass as well as at the Black-Blue Pipe Spring. Therefore, high calcium and nitrate, but low sodium concentrations indicate rather low discharge rates.

The analysis of the recession constants indicates that the water at the Black-Blue Pipe Spring must be stored in comparably shallow layers due to the short recession constant, indicating a small storage capacity, which corresponds to the result of the analysis of the water quality variables, which also showed that the water must flow through a rather shallow water flowing path. As a further matter, the two recessions within the first subperiod let us assume that not particularly only groundwater contributes to the recorded discharge, but potentially also precipitation and surface runoff. This finding is enhanced when considering the mimicry analysis between the mainstream and the Black-Blue Pipe Spring, showing that the discharge pattern of the mainstream, is mimicked best among all the sampling stations by the Black-Blue Pipe Spring. These factors indicate that the groundwater proportion on the recorded discharge is limited although high storage capacity is expected, since the Black-Blue Pipe Spring is part of the riparian zone that has, according to Michelon et al. (2023), a high hydraulic conductivity. In contrast, Michelon (2022) highlighted in the context of the evolution of the isotopic

composition over the recession time that a small increase of the isotopic composition, particularly, a slight isotopic enrichment over the recession period, indicates a small water reservoir, which is the case at the Black-Blue Pipe Spring.

When considering the long recession constant of the Grass Spring, indicating a large storage capacity in rather deep layers and a slow storage-release rate, it can be identified that this large storage capacity corresponds to the characteristics of its hydrological units, which particularly has a high groundwater storage. However, there is a contradiction between the findings of the water quality analysis, indicating a water release from comparably shallow layers, and the recession analysis, highlighting a water release from deep layers.

In order to explain this contradictory result, it needs to be taken into consideration that the Grass Spring is situated close to an artificial water catchment. Regarding the community of Bex, this artificial water catchment is not a capped spring, but it collects water, that is released by a spring with no specific location somewhere on the bottom of the scree cone. This spring must, however, be close to the artificial catchment since, according to the community of Bex, it particularly collects water that emerges at different points on the bottom of the alluvial scree cone. Then, the water is collected by a simple tube and stored in the artificial catchment, which, however, shows, according to the Community of Bex, a limited storage capacity. Therefore, the water that is not collected by the artificial catchment due to a full storage but nevertheless still released by the unknown spring is assumed to flow partly on superficial, partly on shallow water flowing paths down the pasture and therefore, the Grass Spring must represent an outflow of this water. So, the measured discharge corresponds to groundwater, indicated by its constant discharge rate and its longer recession constant, with surface water characteristics, since the discharge is not measured directly at the unknown spring and thus, the water must flow through shallow water paths, as elaborated in the isotopic analysis, and is therefore released at the Grass Spring. As a further matter, it is assumed that surface runoff has a minor extent on the Grass Spring discharge due to hardly altered discharge patterns after precipitation events. Besides, when considering the surrounding of the Grass Spring, which is embedded in a flat and muddy surrounding, where much of the water seems to be stored in the vegetation, the surface runoff, therefore, is not focused on the Grass Spring outlet but widely spread.

The analysis of the water quality variables suggests that the water released by the **Bridge as well as by the La Chaux Spring** is from deeper layers in comparison to the other stations due to the fact that the isotopic depletion in heavy isotopes is higher, and thus the proportion of rain is lower. In addition, these stations show a cool water temperature, which highlights that the depth of the water pathway is deeper. But when considering the median electrical conductivity, mixed signals are observed. The Bridge Spring shows a lower median electrical conductivity, which indicates a lower residence time of the water in the subsurface as well as a higher water flowing rate, that is also reflected in the higher discharge rates. However, the electrical conductivity of the La Chaux Spring is comparably high, almost on the level of the Black-Blue Pipe Spring, but the median discharge is not low, as might be expected, but it even is the highest. Thus, other factors such as different bedrocks or higher rates of geological weathering must be responsible for the higher electrical conductivity values. When taking the results of the hydrochemical analysis into account, in particular the ions of the first and second cluster, the Bridge Spring, for instance, shows the lowest calcium concentration and the La Chaux Spring the lowest nitrate concentration in comparison to the other stations. Sodium from the third cluster, which is positively correlated with the discharge, has the highest concentration at the La Chaux Spring and also a relatively high concentration at the Bridge Spring. Therefore, low calcium and nitrate, but high sodium concentrations indicate comparably high discharge rates.

The analysis of the recession constants suggests that the water at the Bridge as well as at the La Chaux Spring is stored in relatively deep layers, since the recession constants are longer than at the Black-Blue Pipe Spring, but still shorter than at the Grass Spring. Thus, the storage-release rate is comparably slow, indicating a relatively high capacity, which is in contrast to the Black-Blue Pipe Spring. So, the findings of the recession analysis correspond to the findings of the water quality analysis. In addition, the long recession constants also reflect the characteristics of the corresponding hydrological units of the La Chaux Spring as well as of the Bridge Spring, namely that high storage capacities can be expected. But the impact of precipitation can also be noticed at these springs, but to a lower extent and finally, the mainstream discharge pattern is weakly mimicked by the springs. All the aspects highlight that the groundwater must contribute to a larger amount to the discharge of the Bridge and the La Chaux Spring than water from other origins.

The analysis of the water quality variables does not clearly indicate whether the water is released from shallow or deep layers at the **La Chaux Meander**. The proportion of rain, determined in the mixing analysis, indicates that the La Chaux Meander is the station with the third largest proportion of rain. However, the comparably low median electrical conductivity as well as the quite high median discharge rate suggest that the water is released from deeper layers, while the comparably low isotopic depletion as well as the warm temperature give indications for shallow water. Based on these findings, it is assumed that water contributing to the tributary discharge comes from different origins, in particular, from shallow as well as deep sources. When taking the results of the hydrochemical analysis into account, in particular the ions of the first and second cluster, which are negatively correlated with discharge, the La Chaux Meander has similar low median calcium concentration as the La Chaux Spring and strongly lower nitrate concentration than the Grass Spring. In addition, the La Chaux Meander shows a similar sodium concentration to the Bridge Spring as well as the La Chaux Spring, while sodium, which is part of the third cluster, is positively correlated with the discharge.

5.5 Limitations

The key limitation of this thesis is the lack of data, particularly of the spring discharge over the research period. More data would, therefore, support to gain a more profound understanding of the storage-discharge characteristics at the springs. The limitations related to this little amount of discharge data as well as some other limitations are elaborated in more details in the following paragraphs.

Since the **precipitation data** of the La Chaux weather station is incomplete over the research time, and thus additional precipitation data of Sorniot Lac-Inférieur, which is a MeteoSwiss weather station of a comparable elevation to the La Chaux weather station, is considered, there is no authentic picture of the precipitation situation over time in the Vallon de Nant catchment. Therefore, the missing precipitation data is a major limitation of the performed study as exact precipitation data would particularly be important when analysing how springs specifically react to precipitation events, and thus contribute to gaining a more profound understanding of the specific discharge patterns.

In contrast to the discharge data of the mainstream, there is no continuous **discharge data** recorded at the springs, and thus the collected discharge data represents a limited picture of the discharge pattern at the springs over the research time. Therefore, measuring the discharge at the springs in smaller and more regular time intervals would definitely be beneficial in order to gain a deeper understanding of spring discharge patterns over the recession period. Furthermore, in case of precipitation, its impact on the spring discharge is only recorded if rain fell at the time of the day when the discharge was measured, but in case of precipitation events at a later timepoint of the day, no data is collected, which, however, is in contrast to the discharge data of the mainstream that corresponds in this paper to mean daily values and, therefore, includes precipitation events of the whole day. The lack of spring discharge data is also present in the analysis of how the mainstream discharge is mimicked by the springs. The investigation is only based on some isolated discharge measurements at the springs and then it is assessed whether the spring discharge increased, decreased or stayed equal during a sampling campaign. Then, this pattern is compared to the mainstream discharge and its baseflow pattern. So, in order to make a more fundamental mimicry analysis, more data needs to be considered.

In addition, the results of the **statistical significance analysis**, which was performed for all water quality variables as well as for the discharge, must be treated with caution since there is very little data for doing such statistical significance tests.

When considering the calculation of the **recession constants** in this paper, there are a few limitations that need to be considered. Since the calculation of the alpha value and consequently also of the recession constant is only based on discontinuous discharge measurements at the springs without taking any topographic or geological indicators into account, the analysis of the water origin has limited meaning. Besides, in a further study, it should not be assumed that the spring discharge directly corresponds to the baseflow, since the results of this study have showed that in most cases precipitation and surface runoff also contribute to the measured discharge, however, to a different extent. Therefore, the spring baseflow should be calculated, but in order to do so, continuous or at least more discharge measurements should be performed at the springs.

In the context of the **concentration-discharge relationship analysis** Knapp et al. (2020) highlighted that in order to make substantial conclusions about concentration-discharge relationships, and thus, to gain an understanding of how these ions are stored and released, an extended research period with regular sampling is fundamental. Due to a limited amount of ion concentration data, the determination of chemostasis might overshadow other processes such as dilution and mobilization.

Regarding the **isotopic analysis**, it would be beneficial to determine the isotopic data of rain as well as of groundwater in order to make a specific comparison of the different isotopic composition in the Vallon de Nant catchment and additionally, allow to determine, based on the isotopic composition, the main contributors to the springs discharge more accurately.

Finally, another limitation of this study is the **timing of the research**. I started with my measurements in early July, but for further summer recession studies, I suggest starting with research already in June in order not to miss the start of the recession period and furthermore, I recommend making measurements until October in order to identify the end of the recession period.

6 Conclusion

The aim of this study was to investigate how specific tracers such as ions, stable isotopes as well as electrical conductivity, pH and temperature values can be applied in order to gain an understanding of storage-discharge patterns of specific springs in the Vallon de Nant catchment over the time period July until early October 2022, including the summer recession period.

Water samples were taken, salt dilution measurements were performed and pH, temperature and electrical conductivity values were determined at the springs in the field. The ion concentration as well as the isotopic composition of the collected water samples were afterwards determined. Then, recession constants were defined per spring in order to gain an understanding of the storage-release rate of the individual springs. As a further matter, the proportion of rain and snow was determined by means of an isotopic mixing model analysis. By means of the tracers as well as of the calculated recession constants storage-discharge characteristics were defined per spring:

- Low depletion in heavy isotopes and thus higher proportion of rain, high electrical conductivity values, which result in higher residence time of the water in the subsurface as well as in smaller water flowing rates, and warm temperatures indicate a shallow water flowing path. Additionally, high calcium and nitrate concentrations, but a low sodium concentration give indication for a comparably shallower water storage and slower discharge pattern. The recession analysis, which has showed relatively low recession constants, describing a fast storage-release rate and thus a small storage capacity, corresponds at the Black-Blue Pipe Spring to the tracer analysis and finally, the recession analysis also indicates a shallow water storage.
- The opposite of the above-mentioned relationships indicates deep water flowing paths. Regarding the hydrochemistry, one could particularly observe at the La Chaux Spring and the Bridge Spring that low calcium and nitrate, but high sodium concentration indicates a comparably deeper water storage and faster discharge pattern. Additionally, the recession analysis, which has showed relatively long recession constants, describing a slow storage-release rate and thus a high storage capacity, corresponds at the La Chaux Spring and the Bridge Spring to the tracer analysis and finally, the recession analysis also indicates a deeper water storage.
- At the Grass Spring and the La Chaux Meander the analysis of the tracers was only partly coherent with the recession analysis, since in the former case an artificial water catchment has an impact on its storage-discharge pattern and the latter station is a tributary, indicating several different water origins. So, in such cases the angle needs to be opened and more factors need to be considered.

This work contributed to identifying storage-discharge characteristics of some isolated springs in the Vallon de Nant catchment of 2022, but for gaining a more profound understanding of how groundwater storage can buffer by climate change induced alterations in the storage-discharge pattern of headwaters, further in-depth research of headwaters, specifically at springs, needs to be done. However, for future research in the Vallon de Nant catchment, it would particularly be valuable to study the storage-discharge pattern through all streamflow periods and not only during a fixed time range, such as, for instance, during the recession period, since the storage-discharge pattern varies seasonally, and is thus a dynamic process, enforced by the consequences of climate change. As a further matter, having a solid data base is fundamental for making valuable conclusions, so it would be beneficial to continuously measure the discharge at the springs. Specifically, since the stable water isotopes as well as the

electrical conductivity have showed to be valuable tracers for storage-discharge analysis, these water quality variables should also be determined on a regular basis. In addition, the concentration-discharge analysis has showed that measuring the ion concentration of the sulphate, calcium, sodium, magnesium and potassium, which have their origin in groundwater, on a regular basis, also contributes to the understanding of the discharge pattern over time. Additionally, since the storage-discharge characteristics of a spring is strongly linked to the geological conditions of the aquifer compartment, it would be interesting to make geological investigations of the different compartments of the springs, which then also allows setting the recession constants into a wider context. Finally, analysing a higher number of springs within a hydrological unit would also allow to draw conclusions on the storage-release pattern of springs within such a hydrological unit and gain a larger picture of the storage-discharge pattern within the catchment of the Vallon de Nant.

7 References

- Abdi, H. and Williams, L.J. (2010). Principal component analysis. John Wiley & Sons, 2, 433-459. <https://doi.org/10.1002/wics.101>
- Ala-aho, P., Tetzlaff, D., McNamara, J.P., Laudon, H., Kormos, P., Soulsby, Ch. (2017). Modeling the isotopic evolution of snowpack and snowmelt: Testing a spatially distributed parsimonious approach. *Water Resources Research*, 53, 5813–5830. <https://doi.org/10.1002/2017WR020650>
- Anderson, M.P. (2005). Heat as a Ground Water Tracer. *Groundwater*, 43(6), 951-968. <https://doi.org/10.1111/j.1745-6584.2005.00052.x>
- Aneja, V.P. and Cooper, W.J. (1989). Biogenic Sulfur Emissions: A Review. *ACS Symposium Series*. <https://pubs.acs.org/doi/pdf/10.1021/bk-1989-0393.ch001>
- Araguás-Araguás, L., Froehlich, K., Rozanski, K. (2000). Deuterium and oxygen-18 isotope composition of precipitation and atmospheric moisture. *Hydrological Processes*, 14, 1341-1355. [https://doi.org/10.1002/1099-1085\(20000615\)14:8<1341::AID-HYP983>3.0.CO;2-Z](https://doi.org/10.1002/1099-1085(20000615)14:8<1341::AID-HYP983>3.0.CO;2-Z)
- Aron, Ph.G., Levin, N.E., Beverly, E.J., Huth, T.E., Passey, B.H., Pelletier, E.M., Poulsen, Ch. J., Winkelstern, I. Z., Yarian, D.A. (2021). Triple oxygen isotopes in the water cycle. *Chemical Geology*, 565, 1-23. <https://doi.org/10.1016/j.chemgeo.2020.120026>
- BAFU. (2021). Auswirkungen des Klimawandels auf die Schweizer Gewässer. Hydrologie, Gewässerökologie und Wasserwirtschaft. *Umwelt-Wissen*, 2101, 1-134. <https://www.bafu.admin.ch/bafu/de/home/themen/wasser/publikationen-studien/publikationen-wasser/auswirkungen-des-klimawandels-auf-die-schweizer-gewaesser.html> (02.04.2023).
- Beria, H., Larsen, J.R., Ceperley, N.C., Michelon, A., Vennemann, T., Schaepli, B. (2018). Understanding snow hydrological processes through the lens of stable water isotopes. *WIREs Water*, 5, 1-23. <https://doi.org/10.1002/wat2.1311>
- Berner, E.K., Berner, R.A. (1987). *The Global Water Cycle: Geochemistry and Environment*. Prentice-Hall, Inc., Englewood Cliffs, New Jersey.
- Brutsaert, W. and Lopez, J. P. (1998). Basin-scale geohydrologic drought flow features of riparian aquifers in the southern Great Plains. *Water Resources Research*, 34, 223-240. <https://doi.org/10.1029/97WR03068>
- Ceperley, N., Michelon, A., Escoffier, N., Mayoraz, G., Boix Canadell, M., Horgby, A., Hammer, F., Antoniazza, G., Schaepli, B., Lane, S., Rickenmann, D., and Boss, S. (2018). *Salt gauging and stage-discharge curve, Avançon de Nant, outlet Vallon de Nant catchment*. Zenodo. [data set], <https://doi.org/10.5281/zenodo.1154798>
- Cochand, M., Christe, P., Ornstein, P., Hunkeler, D. (2019). Groundwater Storage in High Alpine Catchments and Its Contribution to Streamflow. *Water Resources Research*, 55, 2613-2630. <https://doi.org/10.1029/2018WR022989>
- Constantz, J. (1998). Interaction between stream temperature, streamflow, and groundwater exchanges in alpine streams. *Water Resources Research*, 34, 1609–1615.

- Doummar, J., Kassem, A. H., Gurdak, J. J. (2018). Impact of historic and future climate on spring recharge and discharge based on an integrated numerical modelling approach: Application on a snow-governed semi-arid karst catchment area. *Journal of Hydrology*, 565, 636-649. <https://doi.org/10.1016/j.jhydrol.2018.08.062>
- Frisbee, M. D., Phillips, F. M., Campbell, A. R., Liu, F., Sanchez, S. A. (2011). Streamflow generation in a large, alpine watershed in the southern Rocky Mountains of Colorado: Is streamflow generation simply the aggregation of hillslope runoff responses? *Water Resources Research*, 47, 1-18. <https://doi.org/10.1029/2010WR009391>
- Fuss, C.B.; Driscoll, Ch.T., Campbell, J.L. (2015). Recovery from chronic and snowmelt acidification: Long-term trends in stream and soil water chemistry at the Hubbard Brook Experimental Forest, New Hampshire, USA. *JGR Biogeosciences*, 120, 2360-2374. <https://doi.org/10.1002/2015JG003063>
- Galewsky, J., Steen-Larsen, H.Ch., Field, R.D., Worden, J., Risi, C., Schneider, M. (2016). Stable isotopes in atmospheric water vapor and applications to the hydrologic cycle. *Reviews of Geophysics*, 54, 809-865. <https://doi.org/10.1002/2015RG000512>
- Gees, A., Gertsch, J., Schenk, J., Weingartner, R. (1995). Abflussmessung nach dem Verdünnungsverfahren: Verbesserung der Messung. «wasser, energie, luft – eau, énergie, air», 87, 203-206.
- Grolemund, G. and Wickham, H. (2011). Dates and Times Made Easy with lubridate. *Journal of Statistical Software*, 40(3), 1-25. <https://doi.org/10.18637/jss.v040.i03>
- Gunarathna, M.H.J.P, Kumari, M.K.N., Nirmanee, K.G.S. (2016). Evaluation of Interpolation Methods for Mapping pH of Groundwater. *IJLTEMAS*, 5(3), 1-5.
- Harrison, J.A. (2003). *The Nitrogen Cycle: Of Microbes and Men*. Visionlearning. <https://www.visionlearning.com/en/library/Earth-Science/6/The-Nitrogen-Cycle/98> (01.05.2023).
- Hayashi, M. (2004). Temperature-Electrical Conductivity relation of water for environmental monitoring and geophysical data inversion. *Environmental Monitoring and Assessment*, 96, 119-128. <https://doi.org/10.1023/B:EMAS.0000031719.83065.68>
- Hayashi, M. (2020). Alpine Hydrogeology: The Critical Role of Groundwater in Sourcing the Headwaters of the World. *Groundwater*, 58(4), 498-510. <https://doi.org/10.1111/gwat.12965>
- Hendriks, M.R. (2010). *Introduction to Physical Hydrology*. Oxford University Press.
- Hornberger, G.M., Wiberg, P.L., Raffensperger, J.P., Eshleman, K.N. (1998). *Elements of Physical Hydrology*. The Johns Hopkins University Press.
- IAEA. (2006). *Isotopes in Environmental Studies. Aquatic Forum 2004*. <https://www.iaea.org/publications/7404/isotopes-in-environmental-studies-aquatic-forum-2004> (05.05.2023).
- Jachens, E.R., Rupp, D.E., Roques, C., Selker, J.S. (2020). Recession analysis revisited: impacts of climate on parameter estimation. *Hydrology Earth System Sciences*, 24, 1159-1170. <https://doi.org/10.5194/hess-24-1159-2020>, 2020

- Kassambara, A. (2023). *rstatix: Pipe-Friendly Framework for Basic Statistical Tests*. R package version 0.7.2. <https://CRAN.R-project.org/package=rstatix> (28.06.2023).
- Knapp, J.L.A., von Freyber, J., Studer, B., Kiewiet, L., Kirchner, J.W. (2020). Concentration-discharge relationships vary among hydrological events, reflecting differences in event characteristics. *Hydrological System Sciences*, 24, 2561-2576. <https://doi.org/10.5194/hess-24-2561-2020>
- Kiewiet, L., von Freyberg, J., van Meerveld, I. (2019). Spatiotemporal variability in hydrochemistry of shallow groundwater in a small pre-alpine catchment: The importance of landscape elements. *Hydrological Processes*, 33, 2502-2522. <https://doi.org/10.1002/hyp.13517>
- Kiewiet, L., van Meerveld, I., Stähli, M., Seiber, J. (2020). Do stream water solute concentrations reflect when connectivity occurs in a small, pre Alpine headwater catchment? *Hydrology and Earth System Sciences*, 24, 3381-3398. <https://doi.org/10.5194/hess-24-3381-2020>
- Kohler, U. and Luniak, M. (2005). Data inspection using biplots. *The Stata Journal*, 5 (2), 208-223. <https://doi.org/10.1177/1536867X050050020>
- Le, S., Josse, J., Husson, F. (2008). FactoMineR: An R Package for Multivariate Analysis. *Journal of Statistical Software*, 25(1), 1-18. <https://doi.org/10.18637/jss.v025.i01>
- Likens, G. E. and Butler, Thomas J. (2019). *acid rain*. Encyclopedia Britannica. <https://www.britannica.com/science/acid-rain/Effects-on-lakes-and-rivers> (21.06.2023).
- Lingle, D. (2013). *Origin of High Levels of Ammonium in Groundwater, Ottawa County, Michigan* [Master's Thesis]. ScholarWorks@WMU. https://scholarworks.wmich.edu/masters_theses/442 (23.04.2023).
- Mächler, E., Salyani, A., Walser, J.C., Larsen, A., Schaepli, B., Altermatt, F., Ceperley, N. (2021). Environmental DNA simultaneously informs hydrological and biodiversity characterization of an Alpine catchment. *Hydrology and Earth System Sciences*, 25, 735-753. <https://doi.org/10.5194/hess-25-735-2021>
- MeteoSwiss (2023). *Klimabulletin Jahr 2022*. <https://www.meteoschweiz.admin.ch/service-und-publicationen/publikationen/berichte-und-bulletins/2022/klimabulletin-jahr-2022.html> (02.04.2023).
- Meybeck, M., Green, P., Voïroïsmarty, C.J. (2001). A new typology for mountains and other relief classes: An application to global continental water resources and population distribution., *Mountain Research and Development Journal*, 21(1), 34 -45.
- McMahon, T.A. and Nathan R.J. (2021). Baseflow and transmission loss: A review. *WIREs Water*, 8(4), 1-30. <https://doi.org/10.1002/wat2.1527>
- Michelon, A., Benoit, L., Beria, H., Ceperley, N., Schaepli, B (2021a). Benefits from high-density rain gauge observations for hydrological response analysis in a small alpine catchment. *Hydrology and Earth System Sciences*, 25, 2301-2325. <https://doi.org/10.5194/hess-25-2301-2021>

- Michelon, A., Ceperley, N., Beria, H. (2021b). *Short description of the Vallon de Nant research site* [working document]. Zenodo. <https://www.zenodo.org/record/4432226#.ZEFK4HZBxPZ> (07.08.2022).
- Michelon, A. (2022). *Hydrological processes analysis in a high Alpine catchment: the case of the Vallon de Nant* [PhD thesis, University of Lausanne]. SERVAL. serval-BIB_0C61AF7447303
- Michelon, A., Ceperley, N., Beria, H., Larsen, J., Schaepli, B., Venneman, T. (2022). 2707 water samples from Vallon de Nant analyzed for stable water isotopes (dD, d17O, d18O) and electric conductivity [Data set]. Zenodo. <https://doi.org/10.5281/zenodo.7540709> (20.03.2023).
- Michelon, A., Ceperley, N., Beria, H., Larsen, J., Vennemann, T., Schaepli, B. (2023): Hydrodynamics of a high Alpine catchment characterized by four natural tracers, *Hydrology and Earth System Sciences*, 27 (7), 1403-1430. <https://doi.org/10.5194/hess-27-1403-2023>
- Muelchi, R., Rössler, O., Schwanbeck, J., Weingartner, R., Martius, O. (2021). River runoff in Switzerland in a changing climate – runoff regime changes and their time of emergence. *Hydrology and Earth System Sciences*, 25, 3071-3086. <https://doi.org/10.5194/hess-25-3071-2021>
- Müller, T., Lane, S.N., Schaepli, B. (2022). Towards a hydrogeomorphological understanding of proglacial catchments: an assessment of groundwater storage and release in an Alpine catchment. *Hydrology and Earth System Sciences*, 26, 6029-6054. <https://doi.org/10.5194/hess-26-6029-2022>
- National Centre for Climate Services. (2018). *CH2018 – Climate Scenarios for Switzerland, Technical Report*. <https://www.nccs.admin.ch/nccs/en/home/climate-change-and-impacts/swiss-climate-change-scenarios.html> (02.04.2023).
- Nelson, D. (2002). *Natural variations in the composition of groundwater*. Drinking Water Program, Oregon Department of Human Services.
- Neuwirth, E. (2022). *RColorBrewer: ColorBrewer Palettes. R package version 1.1-3*. <https://cran.r-project.org/web/packages/RColorBrewer/index.html> (25.04.2023).
- New Zealand Government. (2023). *Chloride in groundwater*. <https://www.es.govt.nz/environment/water/groundwater/chloride-in-groundwater> (31.05.2023).
- Onset (2023). *HOBO Pendant Temperature/Light 64K Data Logger*. HOBO. <https://www.onset-comp.com/products/data-loggers/ua-002-64/> (25.04.2023).
- Ou, J. (2021). *colorBlindness: Safe Color Set for Color Blindness. R package version 0.1.9*. <https://cran.r-project.org/web/packages/colorBlindness/index.html> (31.05.2023).
- Pellerin, B.A., Wollheim, W.M., Feng, X., Vörösmarty, Ch. J. (2008). The application of electrical conductivity as a tracer for hydrograph separation in urban catchments. *Hydrological Processes*, 22 (12), 1810-1818. <https://doi.org/10.1002/hyp.6786>
- Podgorski, J. and Berg, M. (2022). Global analysis and prediction of fluoride in groundwater. *Nature Communications*, 13, 1-9. <https://doi.org/10.1038/s41467-022-31940-x>

- Prakash, J., Agrawal, S.B., Agrawal, M. (2023). Global Trend of Acidity in Rainfall and its impact on plants and soil. *Journal of Soil Science and Plant Nutrition*, 23, 398-419.
<https://doi.org/10.1007/s42729-022-01051-z>
- Qian, J., Susheela, A.K., Mudgal, A., Keast, G. (1999). Fluoride in water: An overview. *Unicef WATER-front*, 13, 11-13.
- Rau, G.C., Andersen, M.S., McCallum, A.M., Roshan, H., Acworth, R.I. (2014). Heat as a tracer to quantify water flow in near-surface sediments. *Earth-Science Reviews*, 129, 40-58.
<https://doi.org/10.1016/j.earscirev.2013.10.015>
- R Core Team (2022): R: A language and environment for statistical computing. R Foundation for Statistical Computing, Vienna, Austria. <https://www.r-project.org/> (25.04.2023).
- Rogerson, P.A. (2015). *Statistical Methods for Geography: A Student's Guide*. SAGE Publications.
- Saha, S., Selim Reza, A.H.M., Roy, M.K. (2019). Hydrochemical evaluation of groundwater quality of the Tista floodplain, Rangpur, Bangladesh. *Applied Water Science*, 9, 1-12.
<https://doi.org/10.1007/s13201-019-1085-7>
- Schaffner, M., Pfaundler, M., Göggel, W. (2013). Fließgewässertypisierung der Schweiz. Eine Grundlage für Gewässerbeurteilung und -entwicklung. *Umwelt-Wissen*, 1329, 1-63. www.bafu.admin.ch/uw-1329-d (31.05.2023).
- Schilling, K.E. (2002). Occurrence and Distribution of Ammonium in Iowa Groundwater. *Water Environment Research*, 74 (2), 177-186. <https://doi.org/10.2175/106143002X139893>
- Stock, B.C. and Semmens, B.X. (2016). *MixSIAR GUI User Manual. Version 3.1*. Zenodo. <https://zenodo.org/record/1209993#.ZEfPB3ZBxPY> (25.04.2023).
- Stock B.C., Jackson A.L., Ward E.J., Parnell A.C., Phillips D.L., Semmens B.X. (2018). Analyzing mixing systems using a new generation of Bayesian tracer mixing models. *PeerJ*, 6, e5096.
<https://doi.org/10.7717/peerj.5096>
- Swisstopo. (2023). <https://www.swisstopo.admin.ch/de/karten-daten-online/karten-geodaten-online/kartenviewer.html> (31.05.2023).
- Tallaksen, L.M. (1995). A review of baseflow recession analysis. *Journal of Hydrology*, 165, 349-370.
[https://doi.org/10.1016/0022-1694\(94\)02540-R](https://doi.org/10.1016/0022-1694(94)02540-R)
- Taylor, S., Feng, X., Williams, M., McNamara, J. (2002): How isotopic fractionation of snowmelt affects hydrograph separation. *Hydrological Processes*, 16, 3683-3690.
<https://doi.org/10.1002/hyp.1232>
- Thornton, J.M., Mariethoz, G., Brunner, Ph. (2018): A 3D geological model of a structurally complex Alpine region as a basis for interdisciplinary research. *Scientific Data*, 5, 1-20.
<https://doi.org/10.1038/sdata.2018.238>

- Tutmez, B., Hatipoglu, Z., Kaymak, U. (2006). Modelling electrical conductivity of groundwater using an adaptive neuro-fuzzy inference system. *Computers & Geosciences*, 32, 421-433.
<https://doi.org/10.1016/j.cageo.2005.07.003>
- Viviroli, D., Dürr, H. H., Messerli, B, Meybeck, M., Weingartner, R. (2007). Mountains of the world, water towers for humanity: Typology, mapping, and global significance. *Water Resources Research*, 43, W07447. <https://doi.org/10.1029/2006WR005653>
- Wernli, H.R. (2007): Abflussmessung mittels Tracerverdünnung – Pumpmethode mit Pockefluorimeter. *Hydrologie und Wasserbewirtschaftung*, 51, 1-8.
- Wernli, H.R. (2011): *Einführung in die Tracerhydrologie. Hydrologisches Praktikum*. 1-152.
- Wickham, H. (2016). *ggplot2: Elegant Graphics for Data Analysis*. Springer-Verlag New York.
- Wickham, H., Seidel, D. (2022). *Scales: Scale Functions for Visualization. R package version 1.2.1*.
<https://cran.r-project.org/web/packages/scales/index.html> (25.04.2023).
- Wickham, H.; Francois, R., Henry, L., Müller, K., Vaughan, D. (2023). *dplyr: A Grammar of Data Manipulation, R package version 1.1.1*. <https://cran.r-project.org/web/packages/dplyr/index.html> (25.04.2023).
- Xylem. (2020). EXO User Manual: Advanced Water Quality Monitoring Platform.
<https://www.yisi.com/file%20library/documents/manuals/exo-user-manual-web.pdf>
(31.05.2023).
- Yoshimura, K. (2014). Stable Water Isotopes in Climatology, Meteorology and Hydrology: A Review. *Journal of the Meteorological Society of Japan*, 93 (5), 513-533.
<https://doi.org/10.2151/jmsj.2015-036>
- Zecharias, Y. B., Brutsaert, W. (1988). Recession Characteristics of Groundwater Outflow and Base Flow From Mountainous Watersheds. *Water Resources Research*, 24, 1651-1658.

Acknowledgements

This Master project would not have been possible without the support of several people, whom I would like to thank from the bottom of my heart. I would like to express my special thanks to Dr. Natalie Ceperley, who supported me during my Master thesis with encouraging advice, support and huge commitment. Besides, I would like to thank a lot Prof. Dr. Bettina Schaepli for making it possible to write my Master thesis in her research group. Furthermore, a big thank you goes to my friends and family, who spent the long field days in the Vallon de Nant with me, supported me performing the measurements and encouraged me during tough times. And finally, many thanks to Peter Leiser, Maarika Bischoff and René Nussbaumer, who introduced me to the lab and field work.

Online Access

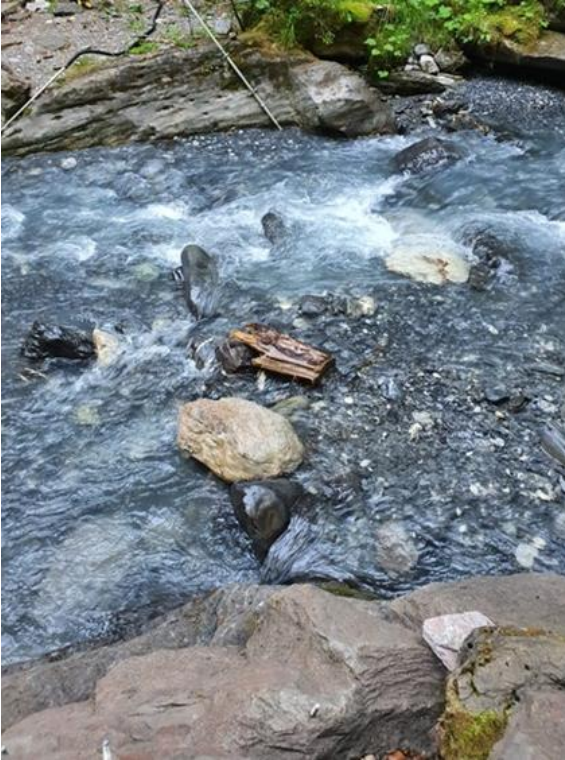
All data collected over the course of this thesis is available on Zenodo. This thesis and accompanying data should be referenced as:

DOI: [10.5281/zenodo.8112455](https://doi.org/10.5281/zenodo.8112455)

Annex A - Pictures and Coordinates of Sampling Stations

Mainstream 1/Outlet (1190m.a.s.l.)

46.25301, 7.10954



Mainstream 2 (1461m.a.s.l.)

46.23171, 7.10231



Mainstream 3 (1554m.a.s.l.)

46.22332, 7.09756



Black-Blue Pipe Spring (1268m.a.s.l.)

46.24828, 7.10664



Grass Spring (1281m.a.s.l.)

46.24760, 7.10642



Bridge Spring (1465m.a.s.l.)

46.23167, 7.10235



La Chaux Spring (1730m.a.s.l.)

46.22194, 7.09238



La Chaux Meander (1780m.a.s.l.)

46.22565, 7.09163



Annex B – Data Acquisition

Collection of Water Samples

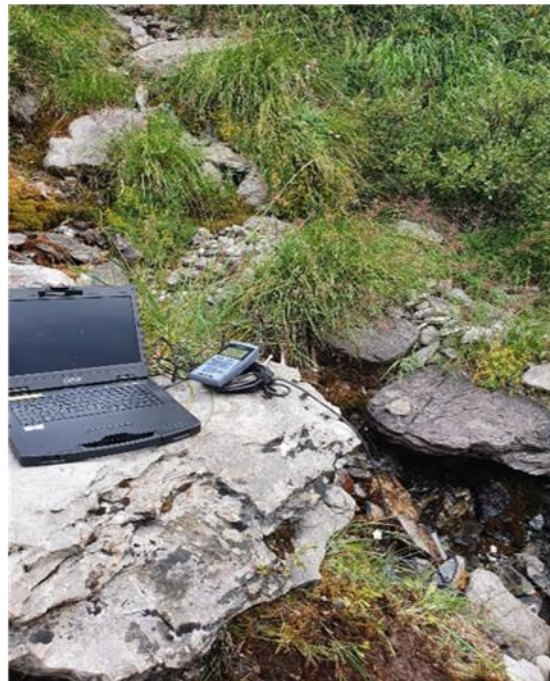


The water samples were taken in duplicate by a 20ml vial at each sampling station.

Electrical Conductivity, pH and Temperature Measurement



The pH value was measured by a pH-meter (WTW pH330i; Xylem Inc., Washington DC, United States) (left) and the temperature as well as the electrical conductivity by the WTW Portable Conductivity meter (Profiline Cond 3310; Xylem Inc., Washington DC, United States) (right).

Salt Dilution Method

Determining amount of salt (left) and installation of electrical conductivity probe in the streambed (right). After having calculated the amount of salt and the mixing section, the probe was installed, the background electrical conductivity was determined and then the measurement could be started.

Long Term Water Temperature Measurements

Temperature loggers (HOBO Pendant Temperature/Light 64K Data Loggers; Onset, Bourne, United States of America) were installed at the springs, the tributary and Mainstream 3 in order to measure the water temperature in a 10minute interval over the whole research period.

Water Quality Measurements by the EXO2 Sonde

The EXO2 Sonde (EXO2 Multiparameter Sonde; YSI, Yellow Springs, United States) measures several water quality variables simultaneously and records the values over a predefined time period after having situated it into the water.

Determination of Ion Concentration

The concentration of a series of ions is determined by the ion chromatography machine (Dionex Aquion Ion Chromatography System; Thermo Fisher Scientific, Waltham, United States) in the lab at the Institute of Geography at the University of Bern.

Determination of Isotopic Composition

The L2140-I Isotope and Gas Concentration Analyzer (Picarro, Inc.; Santa Clara, California, USA) was used to determine the isotopic composition of water samples in the lab at the Institute of Geography at the University of Bern.

Annex C - Additional Results

Metadata of Sampling Campaigns

Sampling Campaign	Sampling Date	Daily Sum of Precipitation [mm]	Mean Daily Temperature [°C]	Mean Daily Discharge [m ³ /s]
1	5 July	0	12.22	0.5387
1	6 July	0	12.40	0.5060
2	17 July	0	17.47	0.4082
2	18 July	0	19.83	0.4007
3	6 August	0	14.80	0.3739
3	7 August	0	12.71	0.3080
4	13 August	0	16.01	0.2718
4	14 August	3.30	14.22	0.2611
5	27 August	0	12.84	0.2867
5	28 August	0	13.67	0.2702
6	13 September	0	18.24	0.2531
6	14 September	16.76	14.15	0.2719
7	7 October	0	10.51	0.6832
7	8 October	0	8.57	0.6521

Correlation Categories

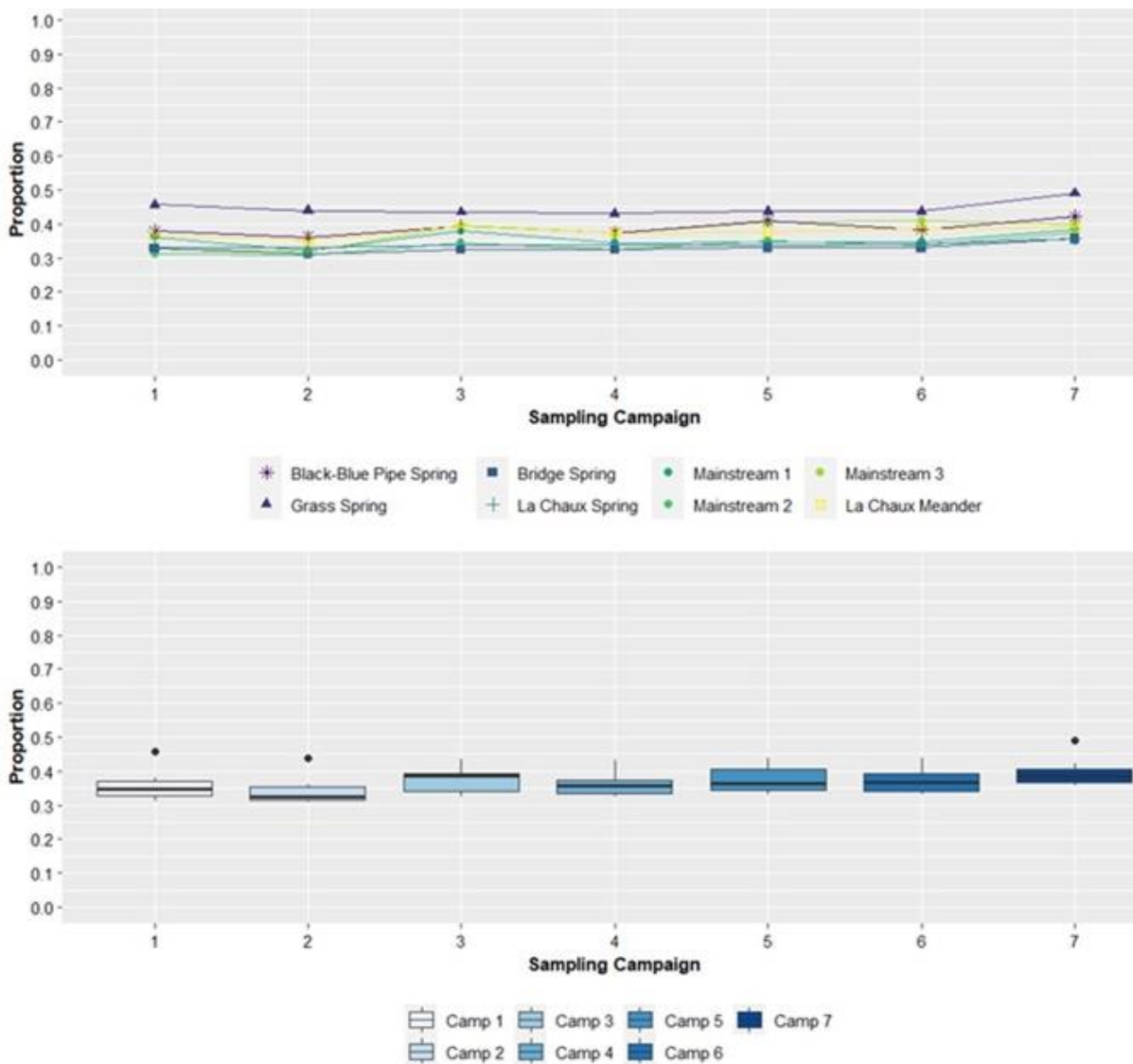
In the following table the variables are attributed to their corresponding correlation category, while red expresses a negative and blue a positive correlation.

variable	very strongly correlated (0.8-1)	strongly correlated (0.6-0.79)	moderately correlated (0.4-0.59)	weakly correlated (0.2-0.39)	very weakly correlated (0-0.19)
Sodium		Magnesium, Sulphate, Fluoride, Calcium	Chloride, Nitrite, Temperature, ¹⁸ O, Ammonium, Phosphate, EC	Discharge, pH, Deuterium	Potassium, Nitrate
Chloride		Discharge, Magnesium, Sulphate, Temperature, Nitrate, ¹⁸ O, Phosphate	Potassium, pH, Deuterium, Ammonium, Calcium, Sodium	Nitrite, Fluoride, EC	
Discharge	Magnesium, Sulphate, Calcium	Potassium, Nitrate, Deuterium, ¹⁸ O, Phosphate, EC, Chloride	Temperature, Ammonium	pH, Nitrite, Fluoride, Sodium	
Magnesium	Sulphate, Calcium, Deuterium, Discharge, ¹⁸ O	Temperature, Nitrate, Ammonium, Phosphate, EC, Chloride, Sodium		Potassium	pH, Nitrite, Fluoride

variable	very strongly correlated (0.8-1)	strongly correlated (0.6-0.79)	moderately correlated (0.4-0.59)	weakly correlated (0.2-0.39)	very weakly correlated (0-0.19)
Sulphate	Discharge, Magnesium, Calcium	Temperature, ¹⁸ O, Deuterium, Ammonium, Phosphate, EC, Chloride, Sodium	Nitrate	Potassium	pH, Nitrite, Fluoride
Potassium		pH, EC, Discharge	Nitrite, Chloride	Nitrate, D, ¹⁸ O, Magnesium, Sulphate, Calcium	Fluoride, Temperature, Ammonium, Phosphate, Sodium
pH		Nitrite, Nitrate, potassium	Ammonium, chloride	Deuterium, ¹⁸ O, Phosphate, Discharge, Sodium	Fluoride, Temperature, EC, Calcium, Magnesium, Sulphate

variable	very strongly correlated (0.8-1)	strongly correlated (0.6-0.79)	moderately correlated (0.4-0.59)	weakly correlated (0.2-0.39)	very weakly correlated (0-0.19)
Nitrite		Nitrate, pH	Fluoride, Deuterium, ¹⁸ O, Ammonium, Potassium, Sodium	Phosphate, Discharge, Chloride	Temperature, EC, Calcium, Sulphate, Magnesium
Fluoride		Sodium	Nitrite	EC, Discharge, Chloride	Temperature, Nitrate, Deuterium, ¹⁸ O, Ammonium, Phosphate, Calcium, pH, Potassium, Sulphate, Magnesium
Temperature		Sulphate, Magnesium, Chloride	Nitrate, Deuterium, ¹⁸ O, Ammonium, Phosphate, Calcium, Discharge, Sodium		EC, Fluoride, Nitrite, pH, Potassium
Nitrate	¹⁸ O, Deuterium	Nitrite, pH, Magnesium, Discharge, Chloride	Temperature, Sulphate, Calcium	Phosphate, EC, Potassium	Ammonium, Sodium, Fluoride
Deuterium	¹⁸ O, Magnesium, Nitrate	Calcium, Discharge, Sulphate	EC, Temperature, Nitrite, Chloride	Phosphate, Sodium, Potassium, pH	Fluoride, Ammonium
δ¹⁸O	Magnesium, Nitrate, Deuterium	Calcium, Chloride, Discharge, Sulphate	EC, Sodium, Temperature, Nitrite,	Ammonium, Phosphate, Potassium, pH	Fluoride
Ammonium	Phosphate	Magnesium, Sulphate	Calcium, Sodium, Chloride, Discharge, pH, Nitrite, Temperature	EC, ¹⁸ O	Nitrate, Potassium, Fluoride, Deuterium
Phosphate	Ammonium	Discharge, Magnesium, Sulphate	Calcium, Sodium, Temperature, Chloride	EC, pH, Nitrite, Nitrate, ¹⁸ O, Deuterium	Potassium, Fluoride
EC	Calcium	Discharge, Magnesium, Sulphate, Potassium	Sodium, ¹⁸ O, Deuterium	Chloride, fluoride, Nitrate, Ammonium, Phosphate	pH, Nitrite, Temperature
Calcium	Discharge, Magnesium, Sulphate, EC	Sodium, ¹⁸ O, Deuterium	Chloride, Temperature, Nitrate, Ammonium, Phosphate	Potassium	pH, nitrite, fluoride,

Mixing Analysis: Proportion of Rain per Sampling Campaign



In addition to the previously described spatial variation such that the Grass Spring has the highest proportion of rain or that the other stations' median proportions of rain are more closely together one can clearly see when analysing the boxplots that the spatial variation is different depending on the sampling campaign. The proportion of rain is rather constant at the Bridge and the La Chau Spring over the Research Period. For instance, there is more variation in the proportion of rain within the **third** and the **fifth** sampling campaign indicating that the proportion of rain varies then more strongly between the individual sampling stations than within other sampling stations. Having a closer look at the third sampling campaign one can identify that in contrast to the second sampling campaign, where all the stations along the mainstream as well as the La Chau and the Bridge Spring are approximately at the same level, the proportions of rain at all the stations along the mainstream increase, whereas the proportion of the Bridge and the La Chau Spring is still on approximately the same level as it used to be in the second campaign. Regarding the spatial variation in the fifth sampling campaign one can see that in contrast to the fourth campaign, where the La Chau Meander, the Black-Blue Pipe Spring as well as Mainstream 3 were all on the same level, the proportions of rain at the Black-Blue Pipe Spring and at Mainstream 3 increase, whereas the proportion of rain at the La Chau Meander is more or less on the same level.

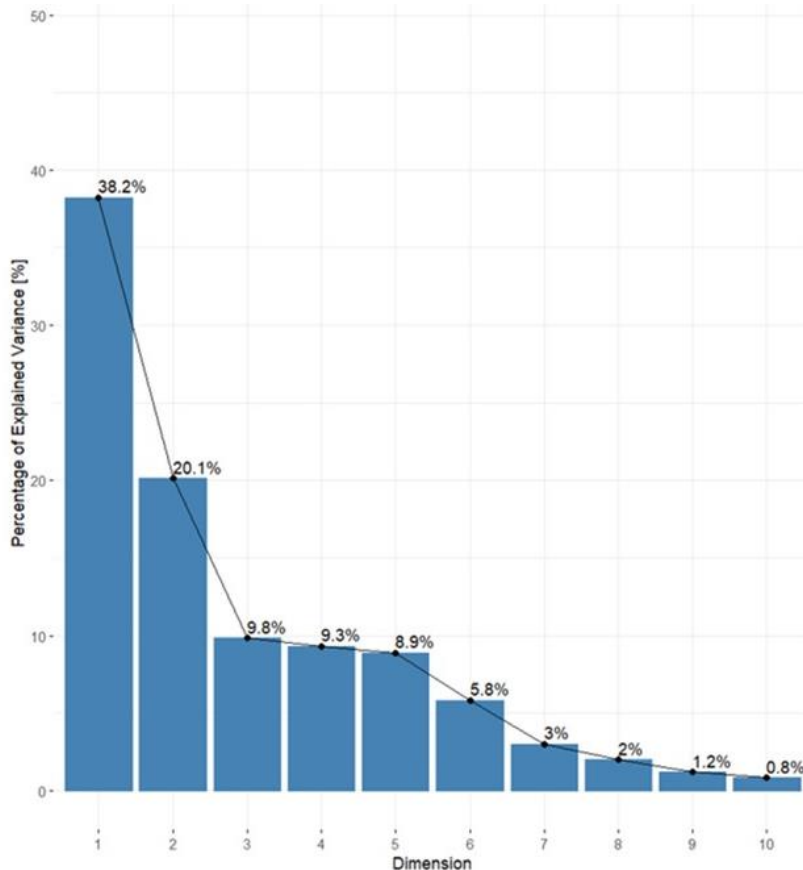
When considering the temporal variation of the proportion of rain per sampling campaign one can see that the median proportion of rain varies to a limited extent. But, before the median proportion increases towards the third sampling campaign, there is a decrease of the proportion of rain from the first towards the second sampling campaign. While the median proportion of rain determined in the second sampling campaign is the lowest, is the median proportion during the third sampling campaign the highest one over the whole research period. Then, the median proportion of rain is rather constant from the fourth to the sixth sampling campaign, whilst another increase in the seventh sampling campaign can be identified.

Outlier

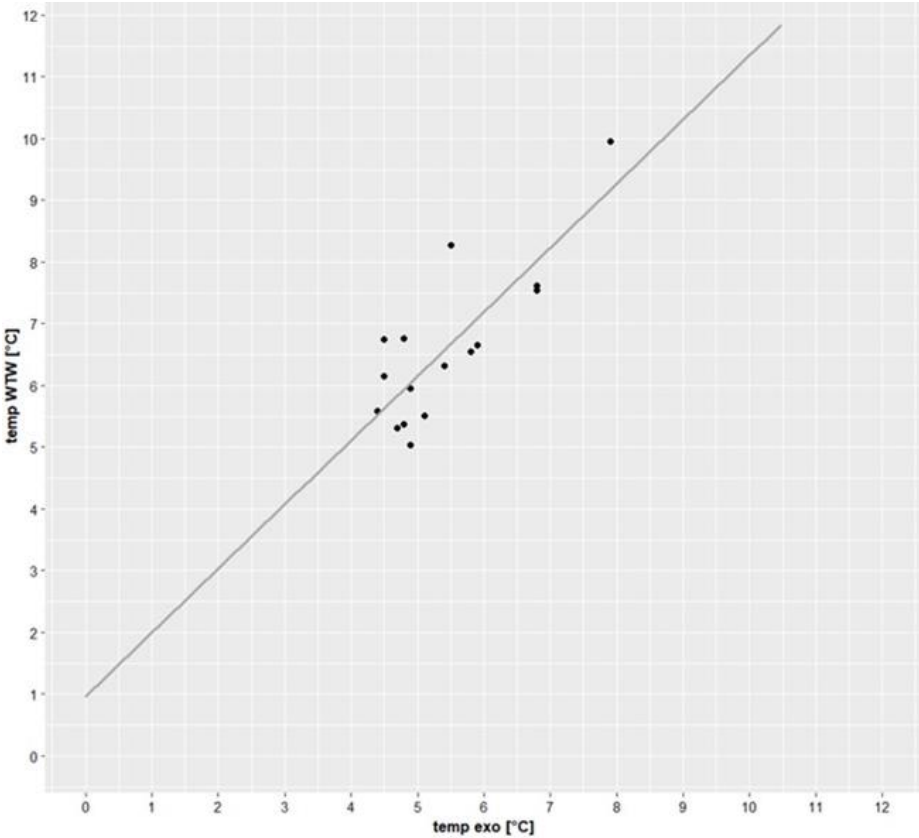
After having compared the outliers with the data, one can identify that all these values are recorded at the Grass Spring.

Screplot for Principal Component Analysis

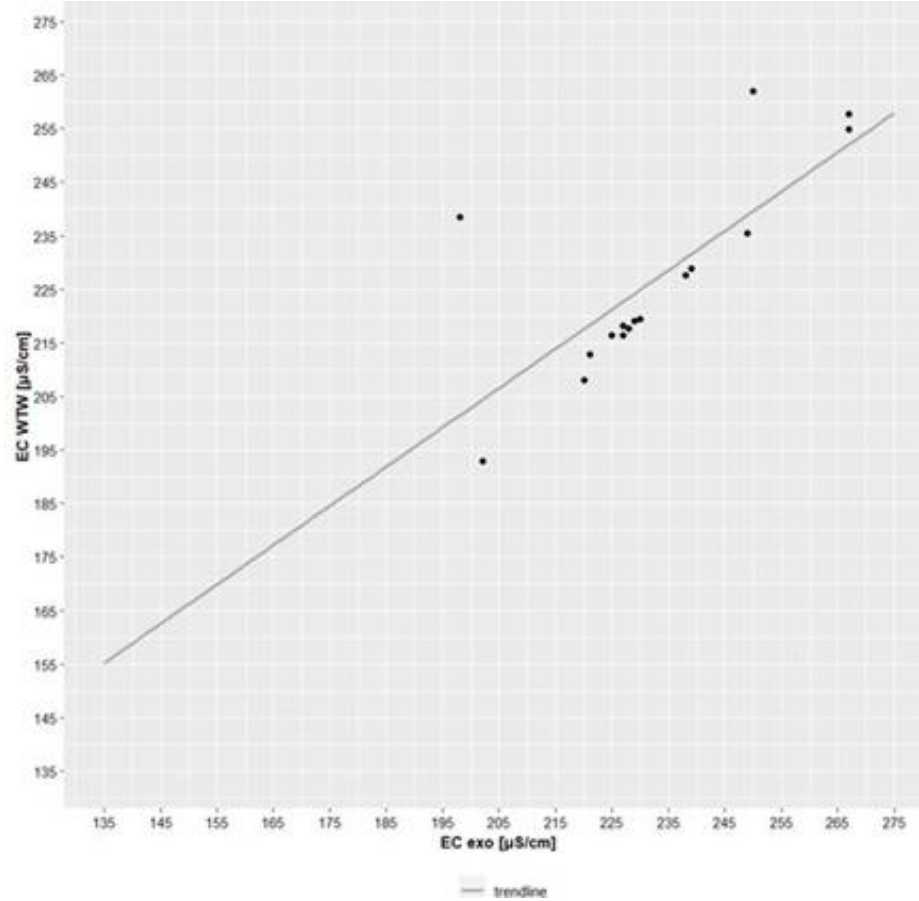
This screplot is used in order to determine the number of principal components that need to be considered in order to explain at least 75% of the total variation. Therefore, the first four principal components need to be taken into account.



Temperature WTW versus Temperature EXO2



Electrical Conductivity WTW versus Electrical Conductivity EXO2



Declaration of consent

on the basis of Article 30 of the RSL Phil.-nat. 18

Name/First Name: Sabina Kurmann

Registration Number: 16-710-618

Study program: Msc Climate Sciences

Bachelor Master Dissertation

Title of the thesis: Storage-Discharge Characteristics of Headwaters by Tracer Analysis: A Case Study in the Vallon de Nant Catchment over the Summer Recession Period 2022

Supervisor: Prof. Dr. Bettina Schaefli
Dr. Natalie Ceperley

I declare herewith that this thesis is my own work and that I have not used any sources other than those stated. I have indicated the adoption of quotations as well as thoughts taken from other authors as such in the thesis. I am aware that the Senate pursuant to Article 36 paragraph 1 litera r of the University Act of 5 September, 1996 is authorized to revoke the title awarded on the basis of this thesis.

For the purposes of evaluation and verification of compliance with the declaration of originality and the regulations governing plagiarism, I hereby grant the University of Bern the right to process my personal data and to perform the acts of use this requires, in particular, to reproduce the written thesis and to store it permanently in a database, and to use said database, or to make said database available, to enable comparison with future theses submitted by others.

Zug, 6th July 2023

Place/Date

Signature 